N° d'ordre :

REPUBLIQUE ALGERIENNE DEMOCRATIQUE & POPULAIRE

MINISTERE DE L'ENSEIGNEMENT SUPERIEUR & DE LA RECHERCHE SCIENTIFIQUE

UNIVERSITE DJILLALI LIABES
FACULTE DES SCIENCES EXACTES
SIDI BEL ABBÈS

THESE DE DOCTORAT DE 3ème CYCLE

Présentée par

BOUBCHIR Mohammed Abdeldjallil

Domaine : *Science de la matière*
Filière : *Physique*
Spécialité : *Physique des Milieux Condensés*

Intitulé

Développement massive de nouveaux matériaux par l'approche ab-initio couplé au datamining

Soutenue le……
Devant le jury composé de :

Président : *TADJER Abdelkader*	*Professeur, U.SBA*
Examinateurs : *SAHRAOUI Tahar*	*Professeur, U.Blida*
HARMEL Meriem	*MCA, U.USTO,Oran*
Directeur de thèse : *AOURAG Hafid*	*Professeur, U.Tlemcen*
Co-Directeur de thèse : *BOUHAFS Bachir*	*Professeur, U.SBA*

Année universitaire 2021-2022

Remerciment

The work reported in this thesis was done at Djillali Liabes University's Faculty of Exact Sciences' Modeling Laboratory and Simulation in Materials Sciences (LMSSM).
First and foremost, I thank my God ALLAH, who is constantly with us in good times and bad.
I want to thank the lecturer from the bottom of my heart. I appreciate Professor AOURAG Hafid for the honor of being my supervisor, and I thank him for the faith he has placed in me, as well as for providing me with all of the required resources, without which I would not have been able to complete my work and calculations.
I would like to express my gratitude and deep appreciation to my co-supervisor Professor. BOUHAFS Bachir, who has directed me during these five years and for his wise advice on the treatment of my thesis subject I would like to express my sincere thanks to the members of the jury of this thesis: Professor TADJER Abdelkader, who agreed to chair the jury of this thesis, as well as to Professor SAHRAOUI Tahar and doctor HARMEL Meriem for having agreed to examine my research work.
Prof. ZAOUI Ali and Dr. CHEKROUN Mohamed Zohir, for their invaluable technical and scientific assistance as well as enrichment talks that greatly aided me in writing my thesis, and Dr. ATTOUCHE Mohamed for his mastery of the LATEX program, I would like to express my gratitude to them.
I'd like to thank Dr. ILES Amine, the director of the SMRIS technical platform, for the design and production of prototypes, as well as everyone else who assisted me in this effort in any manner.

Didicate

Idedicate this thesis to
To my dear parents,
may god protect them inshallah .
who constantly watch over me with his prayers,
its guidance and ongoing support.
My dearest grand Mother.
May God Almighty protect her and grant her a long and better life.
Has the memory of the paternal grand Mother
may god welcome him into his vast paradise.
To my dearest uncle ***Pr:AOURAG Hafid*** *qmay god protect him inshallah.*
To my dearest brothers ***Rachid*** *and sister* ***Fatima Zohra****.*
To the whole family ***BOUBCHIR*** *and* ***AOURAG****.*
To all my friends ***Dr CHEKROUN Mohamed Zohir****,* ***BOUBLENZA Djamel Eddine*** *and* ***HAMMEM Abdelwaheb****.*
thank you.

CONTENTS

LIST OF FIGURES

LIST OF TABLES

CHAPTER 1

PEROVSKITES, INVERSE-PEROVSKITES AND DOUBLE HALIDE PEROVSKITES

1.1 Introduction

Perovskite was first described around 1830 by the geologist Gustav Rose, its name comes from that of Lev Aleksevich Von Perovsky, a Russian mineralogist.

Originally, it was a precious mineral, a calcium titanate $CaTiO_3$ with a simple cubic structure, but the term perovskite today refers to a set of compounds all having the same ABX_3 atomic arrangement, where A is the largest cation, B the smallest and X the anion. This anion can be oxide, fluoride and, in a few cases, chloride, bromide, iodide, sulphide or hydride.

The perovskite-type structure occupies a very predominant place in the ternary systems known as ABX_3. This is due not only to its wide occurrence, but also to a series of interesting and useful properties related to this structural type.

1.2 Generality about the perovskite structure

Ideal perovskites have the general formula ABX_3 where cations A are typically larger than cations B and similar in size to anions X (Figure1.1).

Perovskites, having an ideal structure, adopt the space group ($Pm\overline{3}m$) belonging to the cubic system.where the atoms A occupy the vertices of the cube, the atoms B the centre and the oxygen atoms O the faces (figure1.1) In this structure, cations A represents

a cation of large radius with a coordination number 12,cubo-octahedral (e.g. Ba, Ca, Pb, Rb, Sr, Na, K. O is the oxygen ion surrounded by 2 cations B and 4 cations A.

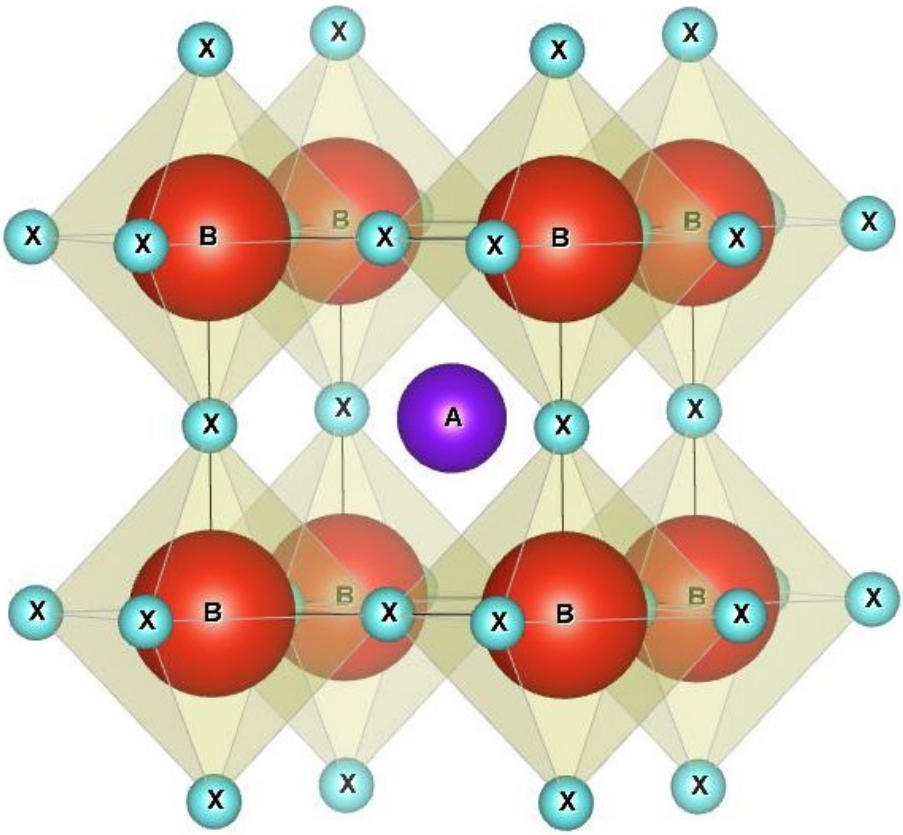

Figure 1.1: The perovskite structure.

1.2.1 Distortions of the ideal structure

The ideal structure is rarely found. Most often we find distorted shapes, in which the symmetry is lowered by the rotation of the BO_6. octahedrons.

The ideal perovskite-type phases of $Pm\bar{3}m$ symmetry are non-polar. Polar phases belong to lower symmetry systems. Indeed, their meshes present light and varied deformations of quadratic, orthorhombic or even rhombohedral type, due to a very weak deformation corresponding to a settling of the oxygen octahedra with decentration of the "B" ion which occurs in certain directions privileged by the symmetry elements of the new crystalline system, see the following figure (figure1.2):

* the 3 axes of order 4 (L4) in the quadratic phase.

* the 6 axes of order 2 (L2) in the orthorhombic phase.

* the 4 axes of order 3 (L3) in the rhombohedral phase.

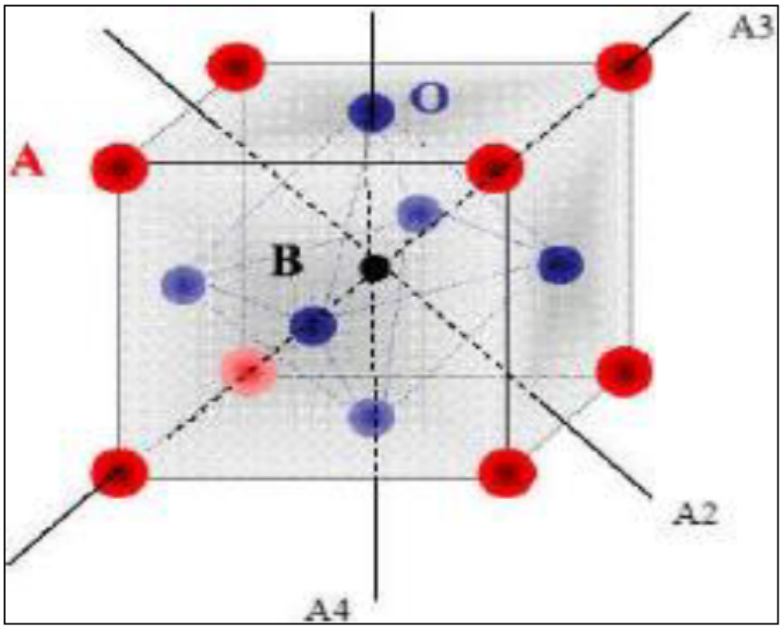

Figure 1.2: Directions of the deformations due to the displacement of the B-ion in the octahedron. [1]

These B-ion shifts are due to a significant change in the interatomic binding forces, in particular an increase in the covalency of the B-O bonds. The settlement of the oxygen octahedron framework occurs when the size of the A ions does not allow the filling of all the free space corresponding to the cubo-octahedral site. The distance A-O is then made as small as possible by pivoting the octahedron around its centre of gravity and moving it relative to the ion A [1].

1.3 Stability conditions of a perovskite structure

The stability of the perovskite structure depends essentially on two factors:

1.3.1 Ionicity and bonding

The difference in electronegativity between the ions of an ABO_3 perovskite structure provides insight into the stability of the structure [2].

Perovskite structures will be all the more thermally stable the more pronounced the ionic character of the cation-anion bonds. The ionicity of the bonds can be calculated by the following formula:

$$\bar{\chi} = \frac{\chi_{A+O} + \chi_{B+O}}{2} \tag{1.1}$$

Where χ_{A+O} and χ_{B+O} are the electronegativity differences between cations A and anions B and the associated oxygen.

The perovskite structure is all the more stable as the bonds involved have a strong ionic character.

It should be noted that in our case, we use of ionic radii. In fact, for many cations as well as anions, the Shannon and Prewitt ion radii values represent a model of hard spheres that does not take into account all the factors that influence them such as the distortion of coordination polyhedra, the presence of gaps, the covalence of the bonds or their metallic character. The relevant quantities in this situation are rather the interatomic distances obtained by crystallographic analysis of the compound.

The perovskite structure ABO_3 is likely to host a large number of elements of the Mendeleev classification at sites "A" and "B" since A^{m+} is a cation of the alkaline earth or transition metal family, and B^{n+} is a cation of the transition metal or rare earth metal family. In order to form an oxide with a perovskite structure, a given (A^{m+}, B^{n+}) couple must satisfy a number of speculations.

On the one hand, the sum of the oxidation numbers m and n of the cations must be equal to +6, so that the charge of the compound is globally zero, on the other hand, the congestion of the ions in the structure implies that the ion radii of the cations are in agreement with the geometry of the perovskite lattice. The smaller cation B^{n+} is placed at the apex of a cube whose anions O^{2+} occupy the centre of the edges and the cation A^{m+} the centre of the cube. The coordinations of the O^{2+} and B^{n+} ions are then 6 while the A^{m+} cation is placed in the octahedral cube cavity in coordination 12.

In addition to structural asymmetries, perovskites can deviate from the ideal structure

by exhibiting ionic and electronic structural defects, which is the cause of a large number of conduction (insulating, ionic conduction, electronic semi-conduction or superconduction), piezoelectric and ferroelectric, ferromagnetic and magnetoelectric properties. resistivity and catalysis of reactions at medium and high temperatures [11].

1.3.2 The Goldschmidt Factor

The flexibility of the perovskite structure lends itself to a wide variety of applications, depending on the choice of atoms at the A and B sites. Especially the relationship between the lengths of the A-O and B-O sub-grids plays an important role in determining the properties of these materials. This relationship is often characterized by Goldschmidt's tolerance factor (t) [3] . In the ideal structure, where the atoms touch each other, the distance B-O is equal to $a/2$ ("a" is the cubic cell parameter) while the distance A-O is $a/\sqrt{2}$ giving rise to this relationship between the ion radii: $r_A + r_O = (r_B + r_O)\sqrt{2}$. However, in ABO_3 compounds, this equality is not exactly obeyed. The Goldschmidt tolerance factor(1.2) measures the deviation from the ideal situation of compact stacking of atoms and gives an idea of the stability of the perovskite structure as a function of the radii of the A, B and O ions[1]

$$t = \frac{(R_A + R_O)}{\sqrt{2} * (R_B + R_O)} \tag{1.2}$$

A list of the ions that form most perovskites, together with their ion radii, is given in (Table1.1)and some perovskites and their tolerance factors are shown in (Table1.2).

site of cation A	Ionic radius(Å)for $O^{2+}/[12]^a$	site of cation B	Ionic radius(Å)for $O^{2+}/[6]^b$
Bi^{3+}	1.11	Ti_{4+}	0.605
Na^{+}	1.32	Nb^{5+}	0.64
Ca^{2+}	1.35	Fe^{3+}	0.645
Sr^{2+}	1.44	Ta^{5+}	0.68
Pb^{2+}	1.49	Zr^{4+}	0.72
Ba^{2+}	1.6	Sc^{3+}	0.73
K^{+}	1.6	Pb^{4+}	0.775

Table 1.1: The most common cations forming the oxides of perovskite structure and their ionic radii. Ion radius taken from Ref. [4]. a : Coordination 12; b: Coordination 6.

[1]This is the radius of an ion in an ion crystal, where the ions are packed together until their outermost orbitals are in contact.

perovskite oxide	Tolerance factor t
$BiScO_3$	0.874
$BiFeO_3$	0.913
$SrZrO_3$	0.942
$PbZrO_3$	0.943
$CaTiO_3$	0.946
$NaNbO_3$	0.972
$PbTiO_3$	1.001
$SrTiO_3$	1.001
$BaTiO_3$	1.063
$KTaO_3$	1.085
$KNbO_3$	1.090

Table 1.2: Some perovskite compounds and their tolerance factors (calculated according to reference [5])

1.3.3 Deviations from ideality

For an ideal structure, the value of Goldschmidt's factor, "t" , is the unit: in the case of $SrTiO_3$ for example, t = 1.00. Experimentally, the perovskite structure is considered stable for $0,88 \leq t \leq 1,05$. This range therefore allows for variations in composition, particularly in the cations used. It is, however, only a geometric indicator and in no way guarantees that a compound with a tolerance factor t within this range will or will not adopt a perovskite structure. This is particularly the case for bismuth perovskites: compounds such as $BiGaO_3$, $BiAlO_3$ our $BiScO_3$ can only be obtained by synthesis under pressure, even if they have a tolerance factor in the perovskite formation range (Table1.3) [6, 7].

This can be explained by the assumption made when calculating the Goldschmidt factor,consisting in saying that ions are ideal spheres having the ion's radius as their radius. However, in the case of bismuth III, it is known that the existence of a non-binding doublet ns^2 does not make it possible to verify this hypothesis.

Compounds	$BiGaO_3$	$BiAlO_3$	$BiScO_3$
Goldschmidt Factor	0.97	1.02	0.92

Table 1.3: Goldschmidt factors obtained from bismuth perovskites

Depending on the value of "t" , structural modifications can be observed in relation to the ideal cubic structure :

1. If t > 1, cation A fills the cubo-octahedral cavity while cation B is smaller than the octahedral site in which it is located. The latter moves in its cavity to reduce

the length of some B-O bonds and decrease its coordination. This situation is generally conductive to the emergence of an polar and ferroelectric structure. This is particularly the case for $BaTiO_3$ and $PbTiO_3$ compounds.

2. If t < 1, cation B fills the octahedral cavity while cation A is smaller than the cubo-octahedral cavity. In this case, a rotation of the octahedrons can be observed, thus minimizing the A-O distances. Cation A can then possibly move out of the centre of its cavity. This is the case of $BiFeO_3$ for which a rotation of the octahedrons and a displacement of the cations A and B are observed simultaneously.
   The resulting structures may be polar or non-polar. This case is therefore not the most favourable for ferroelectricity. In the case of $SrTiO_3$ for example, the decrease in the degree of symmetry of the structure at low temperature, quadratic below $+168°C$ with octahedron rotation, leads to a non-ferroelectric compound [8]. The associated deformation is then purely ferroelastic and non-ferroelectric.

In both cases, the symmetry of the perovskite is lowered and a deformation of the structure is observed compared to the prototype structure. The possible deformations were described by Glazer in 1972 [9] in a classification of the different possible octahedral. He counted 23 rotation systems.

To identify them, he set up a specific symbolic notation in which the three main directions of the cubic prototype mesh are the axes of rotation.

The letters a, b and c are associated respectively with the rotations around these axes. In the case of a rotation of equal amplitude along several axes, the letter is repeated: for example, "aaa" is noted as a system where all rotations are identical. An exponent is assigned to each letter, describing the alternation of rotations from one octahedron layer to the next.

A "0" is used when there is no rotation along the considered axis, a "+" when the octahedrons rotate in phase (i.e. the octahedrons of layers n and n+1 have the same direction of rotation) and a "-" when the octahedrons rotate in anti-phase (i.e. the direction of rotation of layers n and n+1 is different).(Figure1.3)

For example, an $a^0b^+c^+$ type notation corresponds to no rotation along the "a" axis, to rotations in phase according to "b" and in antiphase according to "c". In the case of $NaNbO_3$ ($a^0b^+c^0$), there is no rotation along the "a" and "c" axes and a rotation in phase along the "b" axis.

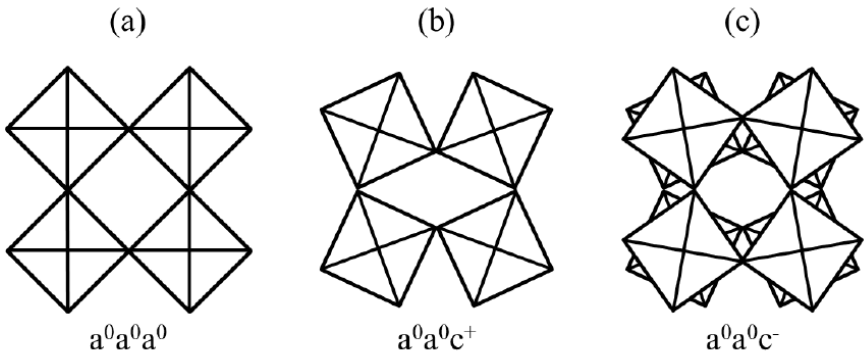

Figure 1.3: (a) Unswivelled octahedra; (b) Octahedra swivelled in phase according to |0.0.1|; (c) Octahedra swivelled in anti-phase according to |0.0.1|. [9]

More recently, Howard and Stockes [10]have reduced the number of systems to 15, taking into account the fact that some of them lead to a symmetry higher than that required by the corresponding space group. They also established that there were group/sub-group relationships, shown in Figure1.4.

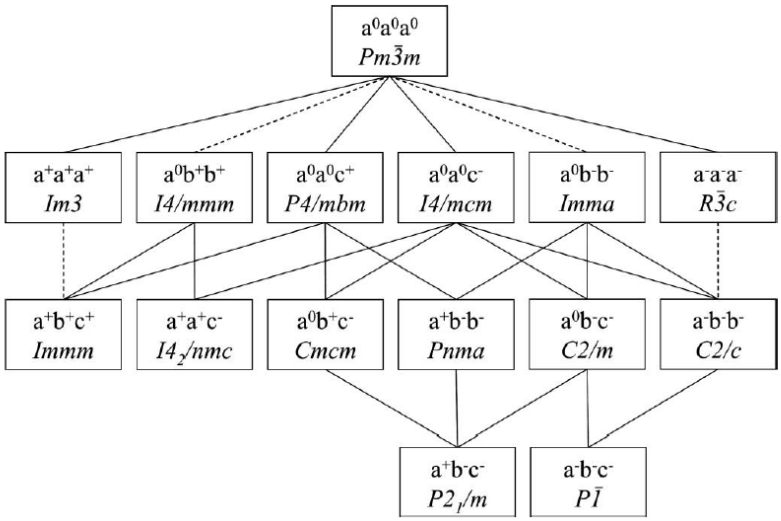

Figure 1.4: Representation of group/subgroup relations of octahedron rotations in perovskites. The dotted lines represent phase transitions necessarily of first order [10]

1.3.4 Polar properties and point groups

The polar properties of materials are directly related to their crystal structure and thus to their space group. Depending on their symmetry, they can exhibit different behaviours such as piezoelectricity, pyroelectricity or ferroelectricity. The relationships between the

point group and the properties are shown in Figure1.5.

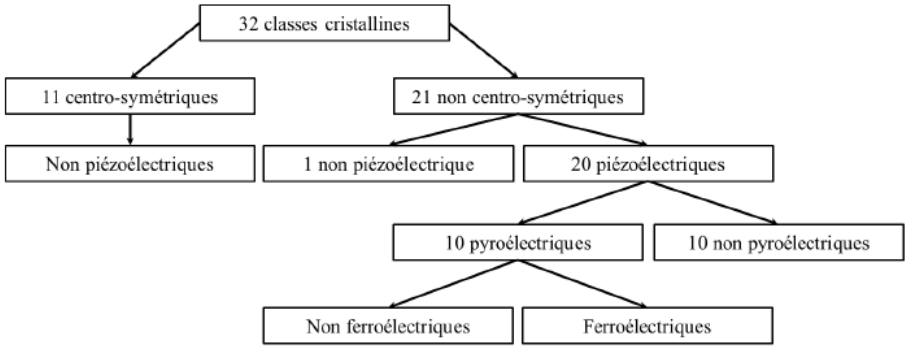

Figure 1.5: Relationship between crystal classes and electrical properties

Of the 32 existing crystal classes, 11 are centrosymmetric, i.e. they have a centre of symmetry. In this case, the material does not exhibit piezoelectricity. The remaining 21 point groups are non-centrosymmetric but only 20 of these groups are piezoelectric. Group 432 has no piezoelectric properties since all its piezoelectric coefficients are zero.Of these 20 point groups, 10 are pyroelectric and only some of these compounds will exhibit ferroelectric properties.

The piezoelectricity

It is a phenomenon corresponding to the appearance of loads and therefore of polarization under the influence of mechanical stress. This is the direct piezoelectric effect. The inverse piezoelectric effect corresponds to the deformation of a material under an electric field.

This property is only observed in crystals belonging to a non-centrosymmetric class.

The pyroelectricity

Some piezoelectric compounds have a permanent dipole moment in the absence of an external electric field. Thus, there is spontaneous polarization on a macroscopic scale. These materials are called pyroelectric. Structurally, this property translates into a polar axis in the mesh, according to which the spontaneous polarization (noted P_s) of the material is directed. P_s evolves with temperature and it is possible to characterize these

materials by their pyroelectric coefficient "p":

$$p = +\frac{dP_s}{dT} \tag{1.3}$$

This property disappears at a phase transition temperature called the Curie point. Above this temperature, the polar order no longer exists and the material's behaviour is therefore of the paraelectric type. It is then governed by a Curie-Weiss type law:

$$\chi = \frac{C}{T + T_C} \approx \varepsilon^{'} \tag{1.4}$$

with χ the dielectric susceptibility, C the Curie constant, T the temperature and T_C the Curie-Weiss temperature.

The Ferroelectricity

Ferroelectrics are pyroelectric materials for which the direction of polarization can be reversed by the application of an electric field, the value of which is higher than that of the coercive field Ec. (Figure1.6)A simple definition of ferroelectricity could therefore be :

A ferroelectric crystal is a crystal which has a spontaneous polarization which can be reversed under the action of an electric field and can be represented by a hysteresis cycle.

This type of cycle is characteristic of ferroic materials in general (ferroelectric, ferromagnetic or ferroelastic). This cycle implies a remanent character of the polarization once the electric field is cut off ($\pm P_r$) as well as a maximum value of the polarization for high fields: the saturation polarization P_s.

Finally, the main characteristics of a ferroelectric material are the presence of: a hysteresis cycle P(E), a remanent polarization P_r, which decreases with temperature and is associated with a long-distance polar order, and a peak on the curve $\varepsilon^{'}(T)$ at Curie temperature, corresponding to the ferroelectric/paraelectric phase transition.

The antiferroelectricity

In antiferroelectric materials, as in ferroelectric materials, there is a displacement of the cations relative to the centre of their cavity. However, if these displacements are all in the same direction in the case of ferroelectric materials, this is not the case for antiferro-

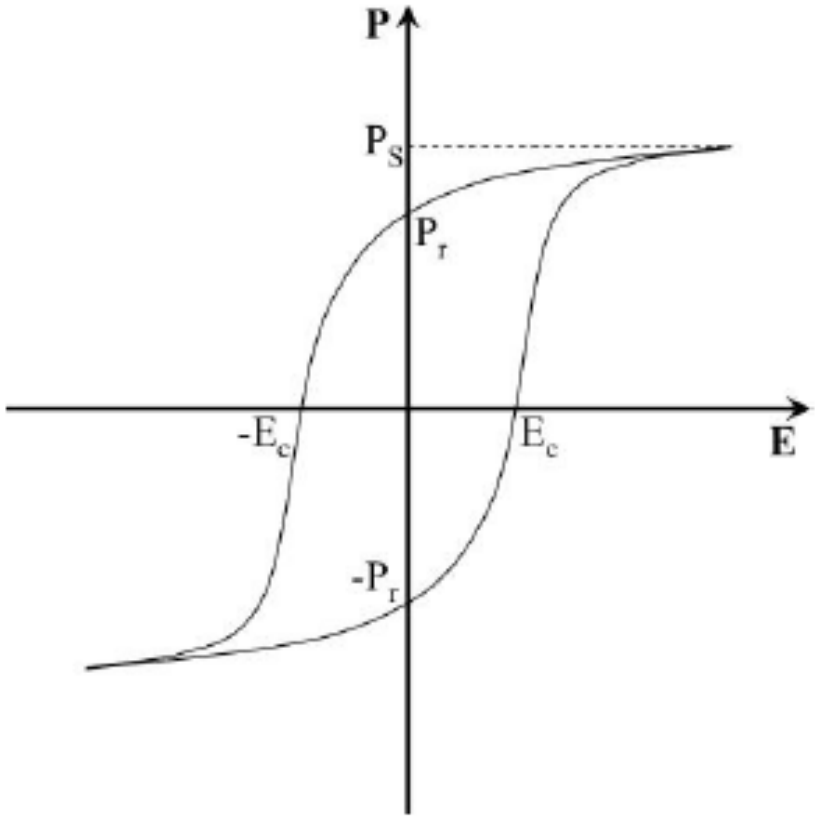

Figure 1.6: Hysteresis cycle of a ferroelectric material

electric compounds: there is therefore for each cationic displacement its opposite within the mesh. The mesh will therefore necessarily be non-polar.

This ordering is similar to that observed for ferroic materials with a magnetic order, which are antiferromagnets, hence by extension the name antiferroelectric.

Antiferroelectric materials, such as ferroelectric materials, have a behavior non-linear as a function of the electric field. However, the polarization of these material is cancelled after the field is removed (Figure1.7). The observed double loop is characteristic of antiferroelectric materials.

1.4 The different Perovskite structures

there are several Perovskite structures which are stable according to the materials and their lattice parameters and their properties among these structures we find:

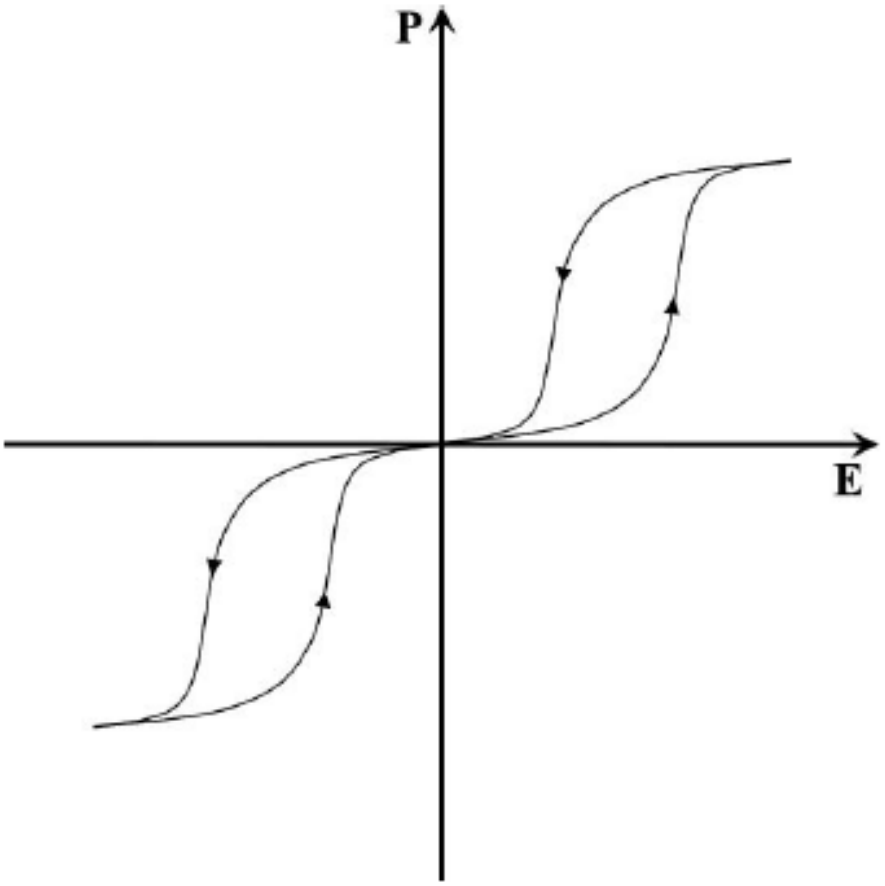

Figure 1.7: Hysteresis cycle of an antiferroelectric material [16]

1.4.1 Tetragonal perovskite

The best known example of a tetragonal perovskite is probably the form of ferroelectric $BaTiO_3$ at room temperature, with a = 3,994Å, c = 4,038Å. In this case the TiO_6 octahedra are slightly distorted (a Ti-O bond at 1.86Å, four at 2.00Åand a longer one at 2.17Å). Barium is coordinated, by four oxygen at 2.80Å, four at 2.83Å and four at 2.88Å. In the iso type$PbTiO_3$, the TiO_6 polyhedra are more twisted than in $BaTiO_3$, this may be related to the power polarization and the ion radius of Pb (II), this has been often discussed in systems containing this cation [12].

1.4.2 Rhombohedral Perovskite

In several materials, the cubic mesh can have a small deformation with rhombohedral symmetry. If this deformation does not widen the unit mesh, it is possible to index it to the unit mesh containing one or two unit formulae respectively with rhombohedral angles

$\alpha \sim 90°$ $\alpha \sim 60°$. However, the anions are usually displaced as required by the larger unit mesh with $\alpha \sim 60°$. Examples of rhombohedral perovskites are $LaA1O_3$, $PrA1O_3$, $LaNiO_3$ et $LaCoO_3$.

$LaCoO_3$ has the rhombohedral structure at room temperature, but at elevated temperatures it undergoes two interesting phase transitions to another phase Rhombohedral (R3c to R3), wherein the trivalent cobalt is ordered to have an alternation of the (111) planes with high-spin and low-spin of Co (III) ions. Above of $937°C$, a second transition occurs, wherein space group R_3 is maintained but the angle changes abruptly from $60.4°$ to $60.0°$. [13].

1.4.3 Orthorhombic Perovskite

The $GdFeO_3$ structure is probably the most illustrative of all perovskites. orthorhombic distortions. Its space group is Pbnm and the mesh parameters are: a = 5.346Å , b = 5.616Å and c = 7.666Å . These parameters are related to the pseudo cubic mesh a' by:$a \sim b \sim \sqrt{2a'}$ and $c \sim 2a'$.

In this structure the octahedrons of FeO_6 are distorted and tilted [14]. Moreover the polyhedron GdO_{12} is severely distorted, showing coordinations (8 + 4). Other materials adopting this distorted orthorhombic structure are $NaUO_3$, $NaMgF_3$, $LaYbO_3$ and a large number of lanthanide compounds of the type $LaCrO_3$, $LaGaO_3$, $LaFeO_3$, $LaMnO_3$, $LaRhO_3$, etc

Figure1.8 is a stereographic view of the structure clearly showing its three-dimensional character.

1.4.4 Monoclinic and triclinic perovskite

Single meshes ($BiMnO_3$, $BiScO_3$) monoclinic or ($AgCuF_3$ et $CsPbI_3$, $PbSnO_3$, $BiCrO_3$, etc.) triclinic have been reported in several cases. However, in many cases, these meshes were found to be pseudo meshes of a true multiple lattice. For example; $GdFeO_3$-type phases were frequently classified on the basis of a monoclinic pseudo lattice with $a \sim b \sim a'$ and $\beta \sim 90°$.

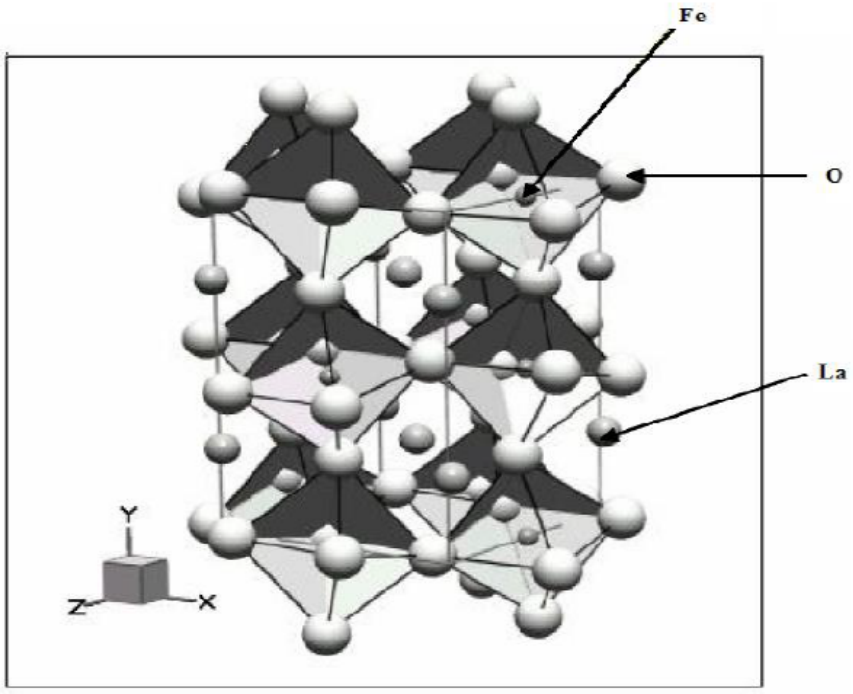

Figure 1.8: Stereographic view of the $LaFeO_3$ structure. [14]

1.5 Stoichiometric aspects of the perovskite structure :

For simple ABO_3 oxide systems, the following classification can be made, based on cationic valences:

$$[1+5] = A^1B^5O_3$$

$$[2+4] = A^2B^4O_3$$

$$[3+3] = A^3B^3O_3$$

Only these three types cover a wide range of compounds. However, a large number of other possibilities arise when we consider mixed cation structures of the type: $A_{1+x}A'_xBO_3$. The following are also possible: $AB_{1+x}B'_xO_3$, $A_{1+x}A'_xB_{1+y}B'_yO_3$, $A_2BB'O_9$, etc...

1.6 Defects in the perovskite structure

Defects in perovskite materials can result from cation deficiency in the sites of A or B as well as from insufficient and/or excess oxygen.

Before detailing this point, a general overview of point defects in crystals will be necessary [15].

Description of defects in the crystals

In crystallography, point defects are defects in the organization of the crystals which only concern isolated nodes.

Point defects

In the simple case of an AB ordered crystal we can describe several types of defects which are shown on (figure1.9).

* **Vacancy:** it is the absence of an atom. For example, a cationic vacancy therefore has a negative charge in the crystal.

* **Interstitial:** The presence of an atom in the lattice between atoms. The presence of a foreign atom between the atoms of the lattice is called interstitial solid solution.

* **Substitution :** The presence of a foreign atom in place of a lattice atom is called a substitution solid solution.

* **Electrical charge defect:** A crystal site has a negative charge (free electron) or more positive charge (electron hole) than other sites of the same type.

* **Anti-site defects:** If the crystal is an ordered crystal, i.e. formed of several types of atoms with a strict chemical alternation; then there can be anti-site defects, i.e. atoms that are well at a node of the lattice but break the chemical regularity.

Association of point defects

* **Schottky defect:** represents a combination of an anion gap and a cation gap in ionic crystals.

* **Frenckel defect:** an atom leaves its normal position and moves into an interstitial position.
  In the case of an ionic crystal, only cations can do this, because they are more smaller than the anions.

*** Clusters of defects:** There may be more complex combinations of defects, called clusters or complexes.

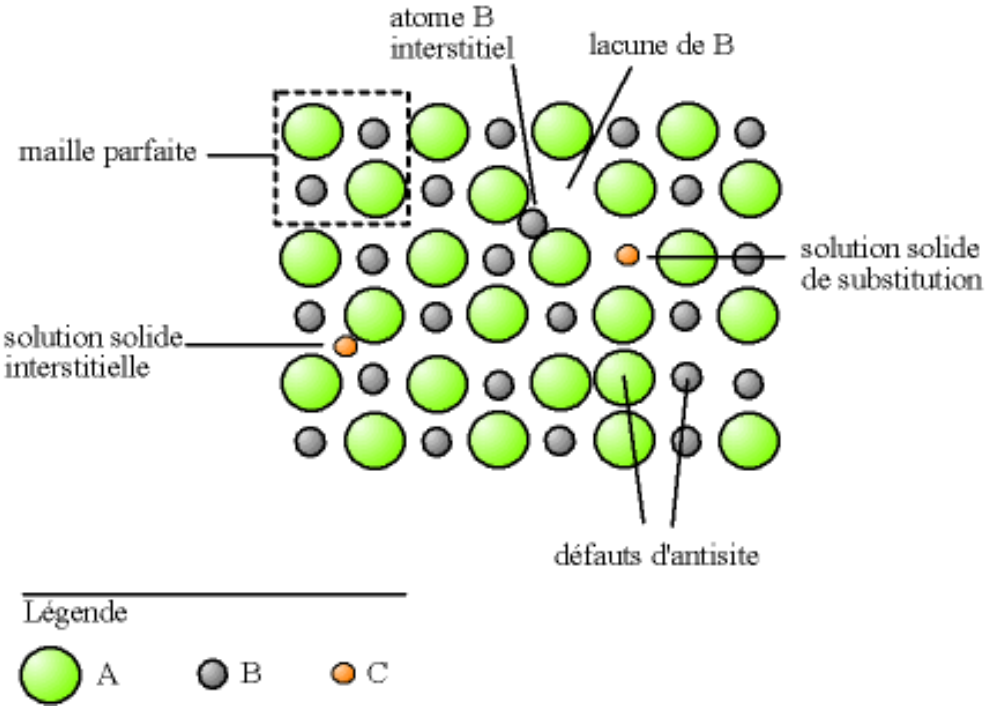

Figure 1.9: Example of point defects in an AB ordered crystal

Point defect representations

The Krager and Vink notation is used to represent point defects in the crystals. The notation describes :

- The chemical nature of the species (gap, atom, ion).
- The position of the species (in insertion in such crystallographic site, interstitial).
- The relative charge of the defect.

A one-off defect is thus noted X_Y^C

*** X:** is the chemical nature, V for a gap, e for a free electron.

*** Y:** the position, either the name of the atom or ion it replaces, or i for interstitial .

*** C:** the relative charge, an apostrophe ' for a negative relative charge, a point . for a positive relative charge, nothing or a cross x for a neutral charge.

Mechanism of defect diffusion

Atoms are always stirring in place. When the temperature becomes high, the atoms move enough to be able to get out of their housing and move around, this phenomenon is called diffusion.

Gap mechanism : If a site is unoccupied, a nearby atom can jump to that site, causing a gap to appear at the site it has just left. Gap conservation: This is called gap migration and/or atom migration, but the behaviours are not identical.

Interstitial mechanism: An interstitial atom jumping from interstitial site to interstitial site is a point defect whose successive jumps are uncorrelated. This is the direct interstitial mechanism. It is typical of atoms that are normally in interstitial solution. A variant of this mechanism is possible, if the located atom can be in a substitutional and interstitial position: it is the indirect interstitial mechanism.

1.7 General information on inverse-perovskites

1.7.1 The inverse-Perovskite structure

AXM_3 compounds crystallize in the cubic space group Pm3m (No. 221) in the International Crystallography Tables and belong to the class of materials called inverse-perovskites (Figure1.10). The atoms "A" occupy the vertices of the cubic lattice, "X" is in the centre of the lattice and the atoms of "M" are located at the centres of the faces of the lattice. Wyckoff atomic positions are : A: 1a (0, 0, 0); X: 1b (1/2, 1/2, 1/2); M: 3c (1/2, 1/2, 0). Thus, in the unit cell, the "C" atom is surrounded by six "M" atoms to form an octahedral cage generating a three-dimensional network of M_6 octahedrons.

1.7.2 The properties of inverse-Perovskites

Inverse perovskite compounds exhibit a variety of physicochemical properties, as do perovskites. As an example; insulating compounds which are described by a large gap and this is the case of oxygen-based inverse perovskites A_3BO (with "A" an alkaline earth: Ca, Sr, Ba and "B" an element of column IV: Si, Ge, Sn, Pb), nitrogen-based semiconductor-type inverse perovskites A_3BN (with "A" : Mg, Ca, Sr, Ba and "B" an element from column V: P, AS, Sb, Bi) without forgetting metals as in the case of A_3BN with A a rare earth or alkaline earth and B an element from columns III and IV, and especially superconductors as in $MgCNi_3$. Interesting mechanical and magnetic properties appear in inverse-perovskites based on carbon and nitrogen, such as the compounds

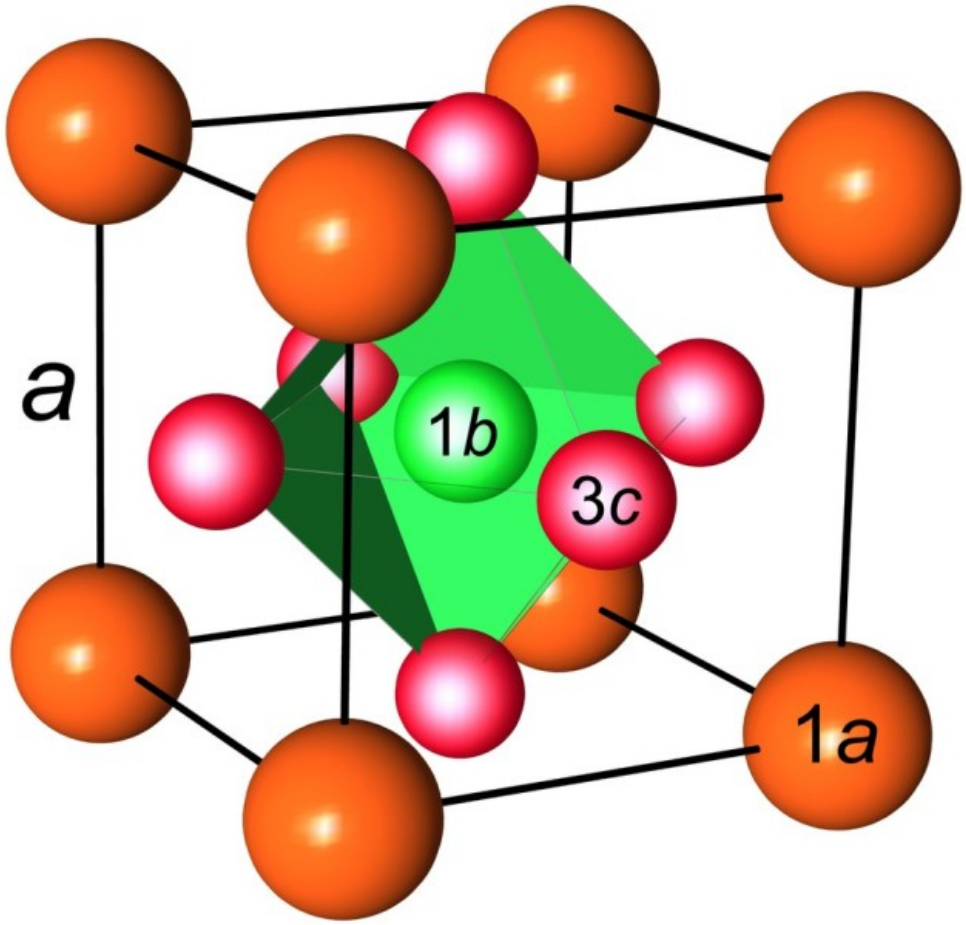

Figure 1.10: The inverse Perovskite structure AXM_3. [26]

$MC(Mn, Fe)_3$ with M = Al, Ga, In, Ge and the d-metals, and some nitrides (example: $GaNMn_3$ and $SnNFe_3$). These are magnets that represent ferromagnetic, antiferromagnetic, or a more complex magnetic arrangement and undergo a magnetic phase change under the effect of temperature [30].

In general, the stability and high hardness of this inverse-perovskite structure are very important from a technological point of view, which makes them makes it useful in high-temperature environments, for cutting tools, and in the hard coating applications.

After the discovery of superconducting properties in the inverse-perovskite compound $MgCNi_3$ [17], inverse-perovskites have become an attractive and growing area of research. Intermetallic inverse-perovskites, which are closely related to $MgCNi_3$, have been the subject of intense investigations both for the search for new superconductors and for a better understanding of the interaction between superconductivity and magnetism.

Indeed, superconductivity is a new criterion that describes one material to another [31]. This state is characterized by a combination of electrical and magnetic properties under the effect of temperature. The main characteristic of superconductivity is based on the complete absence of resistivity in the passage of an electric current, resulting in a current flow without losses due to the Joule effect, without forgetting the effect of perfect diamagnetism or the Meissner effect, which also represent another fundamental property for superconductivity.

Superconducting elements have been developed to modernize the field of renewable energies and electrical energy storage systems. Indeed, generators wind turbines to store kinetic energy in levitating flywheels [32], have integrated superconducting bearings into their manufacturing processes. Superconducting inductance is also considered for storing electrical energy in magnetic form without energy conversion, as an example; superconducting inductance (SMES: Superconductor Magnetic Energy Storage) stores electrical energy in the magnetic field produced by the flow of an electric current in a coil of superconducting material.

1.8 Double Halide perovskites

Over the last years, the family of double halide perovskite compounds with general formula A_2BX_6 have been identified as one of the most promising materials in photovoltaic and light-emitting devices [33–40].

Since the existence of few theoretical model on this family limits their synthesis and study to a labor-consuming trial and error approach. As a result, only about 1600 distinct double halide perovskites has been reported in the literature. However, according to the last prediction more than 90.000 compounds may have these perovskite structure [41]. It is meaning that nowadays only 1.8% of all perovskites are known.

The question which remains is how many double halide perovskite compounds are left to discover?

Fig.1.11 illustrates ABX_3 and A_2BX_6 perovskite structures, A represents (K, Cs, TI, Rb); B represents the tetravalent cation; and X represents halogens (F, Cl, Br, I). Relative to regular perovskite, double perovskite has 50% periodic vacancies on the $[BX_6]$ octahedrons positions. For this reason, they are called vacancy-ordered perovskites. These are similar to ordered perovskites, but the B-site cation is partially replaced with a va-

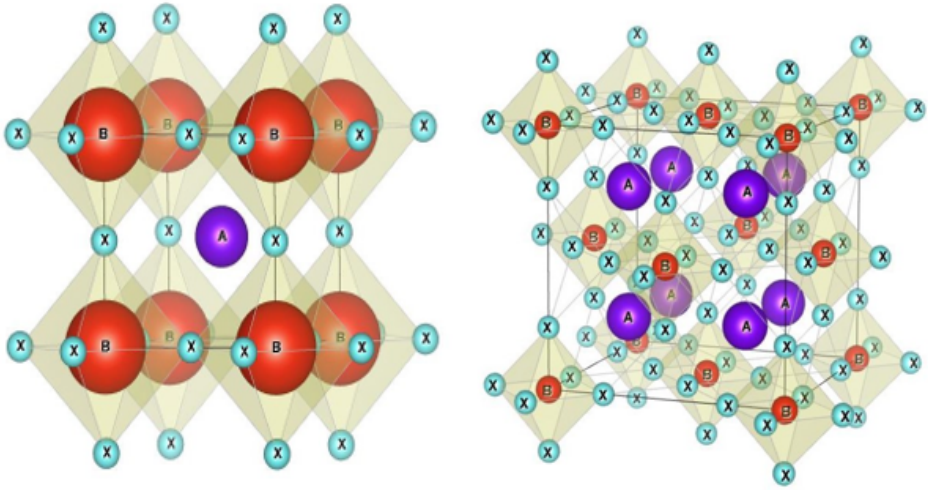

Figure 1.11: The unit cell structure of a) ABX_3 perovskite, b) A_2BX_6

cancy, it requires the doubling of the formal oxidation state of the remaining half. Thus, if the B site metal is selected from group 4 of the periodic table (e.g. Ge, Sn, Pb), the perovskite ABX_3 compound will contain the B metal in its formal lone pair oxidation state, with electronic configuration "ns", whereas in the A_2BX_6 analogue the metal will adopt its formal group oxidation state, with configuration "ns0". It is known that the ideal perovskite structure is cubic with the larger A-site cations located at the corners of the cube, the B-site ions at the body center, and the oxygen ions at the centers of the faces. Whereas the double cubic perovskite belongs to the Fm3m group, with each of its unit cells containing four formula units. Looking at its coordinate geometry, the cation A is positioned at (0.25, 0.25, 0.25), the B cation is located at the origin (0, 0, 0), and the halogen ion X occupies (x ,0, 0), with x being different for each structure.

BIBLIOGRAPHY

[1] S. C. Miller and W. F. Love, *"Tables of Irreducible Representations of Space Groups and Co-representations of Magnetic Space Groups"*, Pruett.Boulder, Col., 1967.

[2] L. Pauling,*"The chemical bond"*, vol. 152. Cornell University Press Ithaca, 1967.

[3] V. M. Goldschmidt,*"Geochemistry"*, Oxford Univ. Press, Oxford, 1958.

[4] R. D. Shannon and C. T. Prewitt, *"Effective ionic radii in oxides and fluorides"*, Acta Cryst.B 25, 925, 1969.

[5] http ://www.me.utexas.edu/ benedekgroup/ToleranceFactorCalculator/home

[6] Y. Inaguma, *" High-pressure synthesis and ferroelectric properties in perovskitetype* $BiScO_3$*and*$PbTiO_3$*solid solution"*, J. Appl. Phys., vol. 95, no 1, p.231, 2004.

[7] A. A. Belik and al.,*" High-Pressure Synthesis, Crystal Structures, and Properties of Perovskite-like* $BiAlO_3$ *and Pyroxene-like* $BiGaO_3$*"*, Chem. Mater., vol. 18, no 1, p.133-139, 2006.

[8] J. M. Kiat et T. Roisnel,*" Rietveld analysis of strontium titanate in the Müller state"*, J. Phys. Condens. Matter, vol. 8, no 19, p. 3471-3475, 1996.

[9] A. M. Glazer, *" The classification of tilted octahedra in perovskites"*, Acta Crystallogr. B, vol. 28, no 11, p. 3384-3392, 1972.

[10] C. J. Howard et H. T. Stokes, *" Group-Theoretical Analysis of Octahedral Tilting in Perovskites"*, Acta Crystallogr. B, vol. 54, no 6, p.782-789, 1998.

[11] D.M.Smyth,*"Defects and structural changes in perovskite systems: from insulators to superconductors"*, Cryst. Latt. Def. Amorph. Mater,, vol.18, no1-3, p.355-375, 1989.

[12] E.J.Baran , P.J.Aymonino, An.Asoc.Quim.Argent. vol.56, no.11, 1968.

[13] P.M.Raccah, J.B.Goodenough, Phys.Rev. vol.155, no.932, 1967.

[14] S.Geller , E.A.Wood, Acta Crystallogr,vol.593, no. 9, 1956.

[15] O.MDller , R.Roy, *"The Major Ternary Structural Families"*, Springer, New York, 1974.

[16] Tan,X.,and Al,*"The antiferroelectric-Ferroelectric phase transition in lead-containing and lead-free perovskite ceramics"*.Journal of the American ceramic society,2011,94,(12).

[17] T. He, O. Huang, A.P. Ramirez, Y. Wang, K.A. Regan, N. Rogado, M.A. Hayward,M.K. Haas, J.S. Slusky, K. Inumara, H.W. Zandbergen, N.P. Ong, and R.J. Cava,*"Supraconductivity in non oxide perovskite* $MgCNi_3$*"*Nature, vol.411, pages 54 - 56, 2001.

[18] P.M. Singer, T. Imai, T. He, M.A. Hayward, and R.J. Cava,*"*^{13}C *NMR Investigation of the Superconductor* $MgCNi_3$ *up to 800 K"* Phys. Rev. Lett. vol.87, 2001.

[19] W.S. Kim, E.O. Chi, J.C. Kim, H.S. Choi, and N.H. Hur,*"close correlation among lattice spin,and charge in the manganese-based anti-perovskite material"* Solid State Commun. vol.119, page.507-510, 2001.

[20] K. Kamishima, T. Goto, H. Nagakawa, N. Miura, M. Ohashi, N. Mori, T. Sasaki, and T. Kanomara,*"Giant magnetoresistance in the intermetallic compound* Mn_3GaC*"* Phys. Rev. B, vol.63, 2000.

[21] E.O. Chi, W.S. Kim, and N.H. Hur,*"Nearly zero temperature coefficient of resistivity in antiperovskite compound* $CuNMn_3$*"* Solid State Commun, vol 120, page.307-310, 2001.

[22] E.O. Chi, W.S. Kim, N.H. Hur, and D. Jung,*"New Mg-based antiperovskites* $PnNMg_3$ *(Pn=As, Sb)"* Solid State Commun, vol.121, page.309-312, 2002.

[23] M. Uehara, A. Uehara, K. Kozawa, and Y. Kimishima,*"New Antiperovskite-Type Superconductor* ZnN_yNi_3*"* J. Phys. Soc. Jpn. vol. 78, 2009.

[24] Z.Q. Mao, M.M. Rosario, K.D. Nelson, K.Wu, I.G. Deac, P. Schiffer, Y. Liu, T. He, K.A. Regan, and R.J. Cava,*"Experimental determination of superconducting parameters for the intermetallic perovskite superconductor* $MgCNi_3$*"* Phys. Rev. B , vol.67, 2003.

[25] A.F. Dong, G.C. Che, W.W. Huang, S.L. Jia, H. Chen, and Z.X. Zhao,*"Synthesis and physical properties of $AlCNi_3$"* Physica C. vol.422, page.65-69, 2005.

[26] M.S. Park, J.S. Giim, S.-H. Park, Y.W. Lee, and E.J. Choi,*"Physical properties of $ZnCNi_3$: comparison with superconducting $MgCNi_3$"* Supercond. Sci. Technol. vol.17, 2004.

[27] P. Tong, Y.P. Sun, X.B. Zhu, and W.H. Song,*"Strong spin fluctuations and possible non-Fermi-liquid behavior in $AlCNi_3$"*, Phys. Rev. B, vol. 74, 2006.

[28] P. Tong, Y.P. Sun, X.B. Zhu, and W.H. Song,*"Synthesis and physical properties of antiperovskite-type compound $In_{0.95}CNi_3$"* Solid State Commun. vol. 141, 2007.

[29] W.H. Cao, B. He, C.Z. Liao, L.H. Yang, L.M. Zeng, and C. Dong,*"Preparation and properties of antiperovskite-type nitrides: $InNNi_3$ and $InNCo_3$"* J. Solid State Chem. vol. 182, 2009.

[30] V.V. Bannikov, I.R. Shein, A.L. Ivanovskii*"Structural, elastic and electronic properties of superconducting anti-perovskites $MgCNi_3$, $ZnCNi_3$ and $CdCNi_3$ from first principles"*Physica C:Superconductivity and its Applications. Vol. 468, 2008.

[31] L.M. FALICOV,*"Superconductivity: a brief introduction to its phenomenology and theories"* IEEE Journal of Quantum Electronics. vol. 25, 1989.

[32] M.Minami, S. Nagaya, H. Kawashima,*"A trial manufacturing of 1k Wh flywheel with high temperature superconducting magnetic bearing for energy storage system"*.IEE Japan, vol 120, no 10, 2000.

[33] Q. Sun, W.-J. Yin, S.-H. Wei, J. Mater. Chem. C., 2020 , 8, 12012-12035.

[34] M.R. Linaburg, E.T. McClure, J.D. Majher, Chem. Mater., 2017, 29 , 3507-3514.

[35] M. Tsuyama, S. Suzuki, J. Phys. Soc. Japan., 2019, 88, 104802.

[36] A.A. Dotsenko, V.I. Vovna, V. V. Korochentsev, A.G. Mirochnik, O.L. Shcheka, T. V. Sedakova, V.I. Sergienko, Inorg. Chem., 2019, 58, 6796-6803.

[37] T. Zhang, Z. Cai, S. Chen, ACS Appl. Mater. Interfaces., 2020, 12, 20680-20690.

[38] D. Han, T. Zhang, M. Huang, D. Sun, M.-H. Du, S. Chen, APL Mater., 2018, 6, 084902.

[39] Z. Li, Q. Xu, Q. Sun, Z. Hou, W.J. Yin, Adv. Funct. Mater., 2019, 29, 1807280.

[40] M.M.S. Karim, A.M. Ganose, L. Pieters, W.W. Winnie Leung, J. Wade, L. Zhang, D.O. Scanlon, R.G. Palgrave, Chem. Mater., 2019, 31, 9430-9444.

[41] M.R. Filip, F. Giustino, Proc. Natl. Acad. Sci., 2018, 115, 5397-5402.

CHAPTER 2

DATA AND BIGDATA

2.1 Data

2.1.1 introduction

The data is only a basic raw material.Yet its collection and processing can lead to knowledge understood as information established at the level of scientifically accepted provisional truth and to knowledge understood as what each of us constructs from interactions with our environment. To speak of data then evokes numeric or alphanumeric, coded, machine-readable information for the purpose of recording, processing, storage and communication. The codification, fixing and transmission of information are a series of ancient operations, which are at the origin of the development of writing, commercial exchanges, accounting, taxation, money, transport and science. Observation of the structure of scientific revolutions [1] suggests that they often follow the same course: data collection undermines the dominant scientific theory, which goes into crisis before being replaced by a new theory, a framework that is better able to explain problematic data.

The best example remains the work of the Danish astronomer Tycho Brahe [2] who, advocating a return to observation, was the first to collect an extensive mass of data that allowed him to establish a capable mapping of the sky and to make correct predictions about the movements of the stars. In this 16th century work, the problem of data is already present: the massive collection of data and the processing of these data allow robust predictions to be made.

2.1.2 Datafication: coded, fixed and transmissible data

Datafication is more than just measuring or transforming reality into data that can be collected and analyzed. It is the perception that there is more value in large volumes of data than in small volumes of data. This being said, even if Brahe and others can be presented as examples of this movement, datafication remains until the 20th century something rare. The recent development of computer technology changes this, by making it possible to simplify, speed up and massify datafication. data collection and processing.

Data is, by definition, coded, fixed and transmissible information. The data requires coding, which allows both its collection and its reconciliation with other data formulated in the same repository. For example, a date of birth has a format, and can be compared with another date of birth. The data is fixed: the data must be equal to itself, otherwise its collection and processing become impossible. Two distinct birth dates cannot be one data that changes: they are two data. Finally, the data is transmissible! This means that it can be stored, entrusted to a recording system, for immediate or later processing.

Digital data is data that has been stored in a computer system (and not on paper, for example). This definition, because of its simplicity, is of a great extension and makes it possible to designate very different realities! Digital data can be created and not collected, even though, most often, digital data is used to refer to data that has been collected.

2.1.3 The different kind of data

There are three types of data: quantitative data, qualitative data, known data and useful data.

Quantitative data

Quantitative data are data that can be measured (size, weight . . .) or marked (temperature,pressure . . .) [3] Examples of quantitative physical properties: Melting point, (for example, iron melts at a temperature of $1535°C$), boiling point, density, viscosity, solubility, electrical conductivity, thermal conductivity. . .

Qualitative Data

Qualitative data are data to which a value or characteristic cannot be assigned. Examples of qualitative physical properties: Colour, texture, taste, odour, condition and ductility. Some consider any data that cannot be qualified as quantitative to be qualitative by default.

Known and useful data

The data of interest to a statistician correspond to objects or events that appear, change, represent the present and then the past. In addition, new elements appear in a more or less hidden and obvious way, which would require knowledge.

As a result, existing and known data may cease to provide useful information, while information may have emerged that is useful or even essential, but is not yet understood and therefore known by the statistical analyst. The stock of available data often needs to be dynamically renewed [4].

2.1.4 Challenges

Databases have taken an important place in computer science, particularly in the field of management. The study of databases has led to the development of specific concepts, methods and algorithms, in particular for managing data in secondary memory (i.e. hard disks).

Thus, tomorrow's databases will have to be capable of managing several tens of terabytes of data, geographically distributed on an Internet scale, by several tens of thousands of users in a changing operating context (we do not know how to control or predict communication speeds between sites very well) or even on volatile nodes. In high-energy physics, it is predicted that a single experiment will produce about one petabyte of data per year.

Since it is unlikely that disk technology will be available to store this amount of information on a single disk, databases have moved towards distributed architectures which allow, for example, potentially executing several input/output instructions at the same time on different disks and thus dividing the total execution time by an order of magnitude.

2.2 Notion of Big data

2.2.1 Introduction

Big Data represents a significant evolution of the company's technological models. The Big Data phenomenon is radically changing the way data is managed, as it introduces new issues regarding the volume, speed of transfer and type of data. It allows the adaptation of technologies and business strategies by providing critical information for

targeted and optimized actions, and offers the possibility to access new business opportunities and better control incoherent risks. Moreover, it is likely to transform the modern enterprise as we know it today. Here is the obvious conclusions we can draw from this:

- Big Data addresses the real needs of the market with a new technological breakthrough.
- While most companies are in the research phase, many models for using Big Data have emerged.
- While data integration is essential to the processing of Big Data, data quality and data governance remain major concerns.
- Big Data's projects will leave the sphere of experimentation to become a strategic asset for the company.
- Development tools are needed to increase the adoption of these new technologies and thus reduce the need for highly skilled developers. All major infrastructure and database vendors are beginning to introduce Big Data solutions to the market.

2.2.2 The Big Data notion

Big Data is a concept that is very difficult to define precisely, since the very notion of big in terms of data volume varies from one company to another. It is not defined by a set of technologies, on the contrary, it defines a category of techniques and technologies. It is an emerging field and as we seek to learn how to implement this new paradigm and exploit its value, the definition is changing. Yet while it may be ambiguous, many experts are convinced that entire sectors of industry and markets will be reached and others created as these capabilities enable new products and functionalities that were previously unimaginable.

As the expression indicates, Big Data is characterized by the size or volume of the information. But other attributes, such as the speed and type of data, are also to be considered. As far as type is concerned, big data is often attached to unstructured or semi-structured content, which can represent a die for traditional relational storage and computing environments. Unstructured and semi-structured data is everywhere: web content, twitter posts or free format customer comments. Speed refers to the speed with which information is created. Thanks to these new technologies, it is now possible to analyze and use the large amount of data provided by web site log files, social network opinion analysis, and even streaming video and environmental sensors. This allows us to take advantage of a strategic vision that has been impossible until now.

2.2.3 The 3 V's of Big Data

These new sources of data are characterized by what is commonly referred to as the 3 V's [5]:

V for Volume

with an annual increase of more than 50%, the volume of data available is growing exponentially. Since the cross-referencing of these data is the basis of the relevance of the information generated, the volume of data is explosive.

V for Variety

to the diversity of formats (Text, Photo, Video, Sound, Technical Log...) is added a wide variety of internal and external suppliers, objects or people . . The variety also relates to the possible uses associated with a raw data (for example, the same file generated on a telephone set can be used to create a text file [speech-text application] or to sample the voice for later voice recognition).

V for Vitesse

In addition to the rapid obsolescence of some of these data from real time and social media (behavioural data or data expressing a feeling), there is also the need to integrate other data as quickly as possible in order to generate fresh information.

This brings us to a first clarification. There are two major families of Big Data projects. The one that deals with real-time data and the one that works without that constraint. These two families of projects involve different approaches, different technical architectures, different tools and different data.

2.2.4 More than the 3 V; the 5 V

In addition to this classical characterization, 2 other V's have been added which seem important to us:

V for Veracity

the data from the central applications of the information system are limited in number but controlled in terms of consistency and quality level. On the other hand, public data relating to the expression of feelings or behaviour can be abundant but subject to prisms or distortions. In the use that will be made of them, it will be necessary to be able to

neutralize these phenomena without modifying the original data. The management of the criteria of veracity of the manipulated data is therefore an induced characteristic of the Big Data project. The reliability of the data has become an essential criterion.

V for Value

While it is difficult to judge a priori the value of basic data, it makes sense to focus on integrating data sources that are likely to generate information with proven added value. However, be careful not to fall into a simplistic scheme: a data source without internal use may have a monetisable value for a partner. Another data source can be a priori without value and prove to be a carrier of a discriminating signal in the context of a rapprochement.

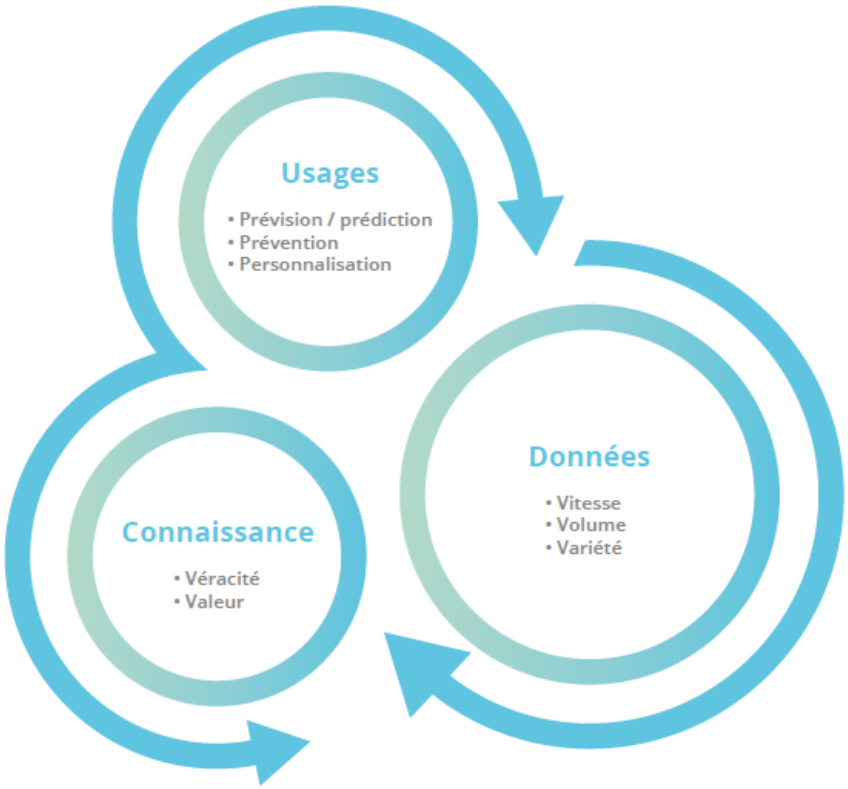

Figure 2.1: Big Data is more than the descriptive 3 V's. We can add 2 additional V's to qualify the data and, last but not least, the 3 P's that describe the destination of the Big Data. [6]

2.2.5 In addition to the 5 V, the 3 P

In addition to this 3V approach, which has become 5, useful but very descriptive, we can shed additional light in terms of the destination of Big Data through what we have

called the 3P's: P:Prediction, P:Personalisation and P: Prevention, which highlight in an original way the role played by Big Data in certain particularly relevant cases of use.

2.2.6 Data, information, knowledge and wisdom... What difference, what's the value?

The difference between data, information, knowledge and wisdom has been well codified by Russell Acko [7], a system theorist and professor of organizational change, who has classified content as it is interpreted by the human mind into five different categories:

1. the data: which is placed at the level of the symbol .
2. information: refers to data that can be processed in such a way as to become useful; provides answers to the following questions <who, what, where and whe>
3. knowledge: which relates to information and data processing by the human mind; knowledge answers the question "how".
4. understanding: i.e. taking into account the "why".
5. Wisdom: the ultimate step, the result of the assessment of understanding.

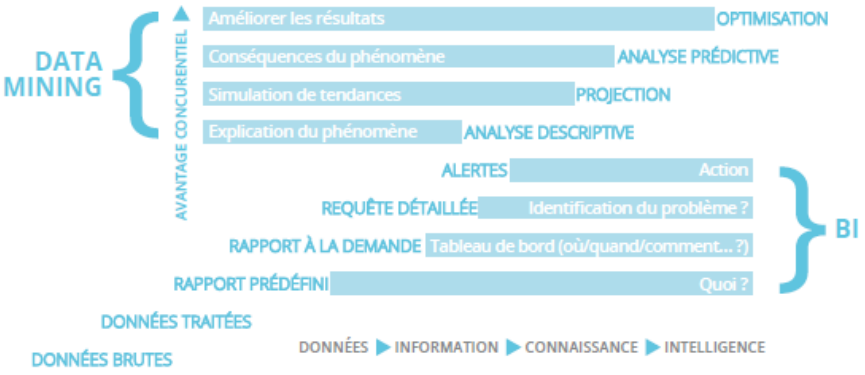

Figure 2.2: Big Data is perfectly suited to Acko's theory of data and information. [7]

2.2.7 Conclusion

Big data volumes are driving a significant evolution in the company's technology models, providing access to new business opportunities and better control of risks. Big Data

represents a significant opportunity, but also poses specific challenges. These include a relatively new set of technologies that are rather complex to grasp, with no tools to encourage their adoption and development. Big Data addresses these challenges, allowing users to easily link and analyze data from disparate systems to help drive and improve business performance.

BIBLIOGRAPHY

[1] Thomas Khun,*"The structure of scientific revolutions"*, Ed. Flammarion, coll. Champs, 1962.

[2] Tycho Brahe(1546-1601), is a Danish astronomer. He takes great care in the manufacture and development of his instruments, which allow him to collect a considerable amount of data.

[3] Introduction to the Statistical Method, Albert Monjallon, Bookstore Vuibert Paris 1963.

[4] J.D. Warnier, op.cit.

[5] http://blogs.gartner.com/doug-laney/othersclaiming gartners volume,velocity,variety,construct for bigdata

[6] http://fr.blog.businessdecision.com/3v-opportunites-big-data/

[7] http://www.systems thinking.org/dikw/dikw.htm

[8] http://drewconway.com/zia/2013/3/26/the datascience venn diagram

CHAPTER 3

DATA PROCESSING METHODS

3.1 introduction to data mining

Data mining is a process of exploration and analysis of large volumes of data in order to make them more understandable and to discover significant correlations, i.e. classification and prediction rules whose most common ultimate purpose is to help in decision making.

Data mining is a knowledge production process. In terms of traditional philosophical logic[1], data mining consists in producing judgments (all people are "x", the average of the "y" of people is worth so much, etc.). This is the step of describing and understanding the data) and reasoning rules (if all people are "a" then they will be "b": this is the modeling step that allows prediction).

Datamining then proposes to use a set of algorithms from various scientific disciplines (statistics, artificial intelligence, database) to build models from data, i.e. to find interesting patterns according to criteria set at the beginning, to extract from these data a maximum of useful knowledge.

3.2 Principal Component Analysis (PCA)

3.2.1 introduction

Principal Component Analysis PCA is one of the oldest factorial methods. It was developed by Karl Peason (1901) and integrated into statistics by Harold Hotelling (1933)

[1] THIRY Philippe, Notions of Logic, De Boeck University, 1996.

[1]. It is used when one observes on "n" individuals, "p" quantitative variable $X_1, X_2, ...X_p$ presenting multiple links that one wants to analyze. These observations are grouped in a rectangular table (matrix) "X" having "n" rows (individuals) and "p" columns (variables).

These data may be derived from a sampling procedure or from the observation of an entire population. The representations of the units make it possible to see if there is a structure, not known a priori, on this set of units. Similarly, the representations of the variables make it possible to study the structures of linear links. on all the variables under consideration. Thus, we will look to see whether we can distinguish between groups in all units by looking at which units look alike, those that stand out from the others, and so on. For the variables, we will look for those that are which are highly correlated with each other, those which, on the contrary, are not correlated with each other [2], and so on.

Finally, as with any descriptive method, conducting a PCA is not an end in itself. The PCA will be used to gain a better understanding of the data being worked on, to possibly detect values, and will help to formulate hypotheses that will need to be investigated using models and inferential statistical studies. Representations provided by the PCA can also be used a posteriori to illustrate certain results for research purposes.

3.2.2 Objective

PCA aims to reduce the often very large amount of data in an array of data represented algebraically as a matrix and geometrically as a point cloud.

PCA consists of the study of the projections of the points of this cloud on an axis (factorial or principal axis), plane or hyperplane judiciously determined.

Mathematically, the best fit of the cloud would be obtained by vector subspaces.

3.2.3 Data Table

The data are the measurements made on "n" units $u_1, u_2, ..., u_i, ...u_n$. The "p" quantitative variables that represent these measurements are$v_1, v_2, ..., v_j, ...v_p$.
The table of raw data from which the analysis will be made is marked "X" and has the following form:

$$X = \begin{array}{c} \\ u_1 \\ u_2 \\ . \\ u_i \\ . \\ u_n \end{array} \begin{array}{c} \begin{array}{cccccc} v_1 & v_2 & \cdots & v_j & \cdots & v_p \end{array} \\ \begin{pmatrix} x_{11} & x_{12} & \cdots & x_{1j} & \cdots & x_{1p} \\ x_{21} & x_{22} & \cdots & x_{2j} & \cdots & x_{2p} \\ . & . & \cdots & . & \cdots & . \\ x_{i1} & x_{i2} & \cdots & x_{ij} & \cdots & x_{ip} \\ . & . & \cdots & . & \cdots & . \\ x_{n1} & x_{n2} & \cdots & x_{nj} & \cdots & x_{np} \end{pmatrix} \end{array}$$

Each unit can be represented by the vector of its measurements on the "p" variables.

$${}^tU_i \begin{bmatrix} x_{i1} & x_{i2} & \cdots & x_{ij} & \cdots & x_{ip} \end{bmatrix} \text{ which results in } U_i \begin{bmatrix} x_{i1} \\ x_{i2} \\ . \\ x_{ij} \\ . \\ x_{ip} \end{bmatrix}$$

So U_i is a vector of $\mathfrak{R}^p$
... Similarly, each variable can be represented by a vector of $\mathfrak{R}^n$ whose components are the values of the variable for the "n" units :

$$V_j \begin{bmatrix} x_{1j} \\ x_{2j} \\ . \\ x_{ij} \\ . \\ x_{nj} \end{bmatrix}$$

To get an image of all the units, we place ourselves in an affine space by choosing as origin a particular vector of $\mathfrak{R}^p$ for example the vector whose all coordinates are zero. Then, each unit will be represented by a point in this space. The set of points representing the units is traditionally called the cloud of individuals.

By doing the same in $\mathfrak{R}^n$, each variable can be represented by a point in space. corresponding affine. The set of points that represent the variables is called cloud of variables.

We can see that these spaces are generally larger than 2 or even 3, so we cannot visualize these representations. The general idea of factorial methods is to find a system of axes and planes such that the projections of these clouds of points on these axes and

planes make it possible to reconstruct the positions of the points in relation to each other, i.e. to have images with as little distortion as possible.

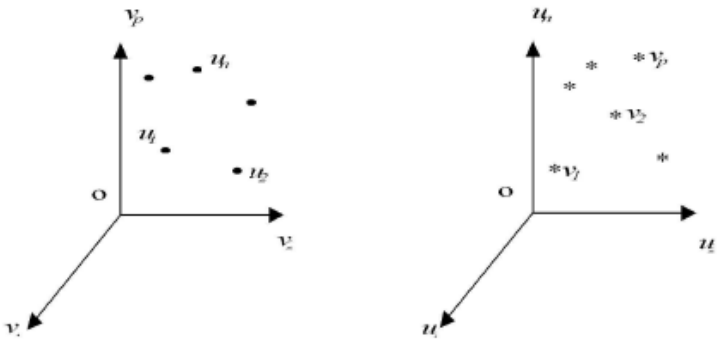

Figure 3.1: the point clouds after the deformation

3.2.4 Choice of a distance

To make a geometric representation, a distance between two points in space must be chosen. The distance used by the PCA in the space where the units are represented is the classical Euclidean distance. The distance between two units u_i and $u_{i'}$ is equal to :

$$d^2(u_i, u_{i'}) = \sum_{j=1}^{p} (x_{ij} + x_{i'j})^2$$

With this distance, all the variables play the same role and the axes denoted by the variables constitute an orthogonal base. At this distance a scalar product is associated between two vectors :

$$< \overrightarrow{ou_i}, \overrightarrow{ou_{i'}} >= \sum_{j=1}^{p} x_{ij} x_{i'j} = {}^t U_i U_{i'} \tag{3.1}$$

and the norm of a vector :

$$\|\overrightarrow{ou_i}\|^2 = \sum_{j=1}^{p} x_{ij}^2 = {}^t U_i U_i \tag{3.2}$$

We can then define the angle α between two vectors by its cosine :

$$\cos(\alpha) = \frac{< \overrightarrow{ou_i}, \overrightarrow{ou_{i'}} >}{\|\overrightarrow{ou_i}\| \|\overrightarrow{ou_{i'}}\|} = \frac{\sum_{j=1}^{p} x_{ij} x_{i'j}}{\sqrt{\sum_{j=1}^{p} x_{ij} \sum_{j=1}^{p} x_{i'j}}} = \frac{{}^t U_i U_{i'}}{\sqrt{{}^t U_i U_i^t U_{i'} U_{i'}}} \tag{3.3}$$

3.2.5 Choice of the origin

The point "o" corresponding to the vector of all-zero coordinates is not necessarily a satisfactory origin, because if the coordinates of the points of the cloud of individuals are

large, the cloud is distant from this origin. It seems more judicious to choose an origin linked to the cloud itself: the center of gravity of the cloud [3]. To define this center of gravity, a weighting system for the units must be chosen :
$\forall i = 1, ..., n$ $p_i =$ unit weight u_i such as $\sum_{i=1}^{n} p_i = 1$. By definition the center of gravity is defined as the point such that :

$$\sum_{i=1}^{n} p_i \overrightarrow{Gu_i} = \overrightarrow{0} \tag{3.4}$$

For the PCA we choose to give the same weight $\frac{1}{n}$ to all individuals.
The center of gravity "G" of the cloud of individuals is then the point whose coordinates are the mean values of the variables:

$$G = \begin{pmatrix} \frac{1}{n}\sum_{i=1}^{n} x_{i1} \\ \vdots \\ \frac{1}{n}\sum_{i=1}^{n} x_{ij} \\ \vdots \\ \frac{1}{n}\sum_{i=1}^{n} x_{ip} \end{pmatrix} = \begin{bmatrix} x_{.1} \\ \vdots \\ x_{.j} \\ \vdots \\ x_{.p} \end{bmatrix}$$

Taking "G" as the origin, as shown in the following figure, is then equivalent to working on the table of centered data :

$$X_c = \begin{bmatrix} x_{11} + x_{.1} & \cdots & x_{1j} + x_{.j} & \cdots & x_{1p} + x_{.p} \\ \vdots & & \vdots & & \vdots \\ x_{i1} + x_{.1} & \cdots & x_{ij} + x_{.j} & \cdots & x_{ip} + x_{.p} \\ \vdots & & \vdots & & \vdots \\ x_{n1} + x_{.1} & \cdots & x_{nj} + x_{.j} & \cdots & x_{np} + x_{.p} \end{bmatrix}$$

and the vector of the centered coordinates of the unit u_i is :

$$U_{ci} = \begin{bmatrix} x_{i1} + x_{.1} \\ x_{i2} + x_{.2} \\ \vdots \\ x_{ij} + x_{.j} \\ \vdots \\ x_{ip} + x_{.p} \end{bmatrix}$$

that of the centered coordinates of the variable v_j is :

$$V_j = \begin{bmatrix} x_{1j} + x_{\cdot j} \\ \vdots \\ x_{ij} + x_{\cdot j} \\ \vdots \\ x_{nj} + x_{\cdot j} \end{bmatrix}$$

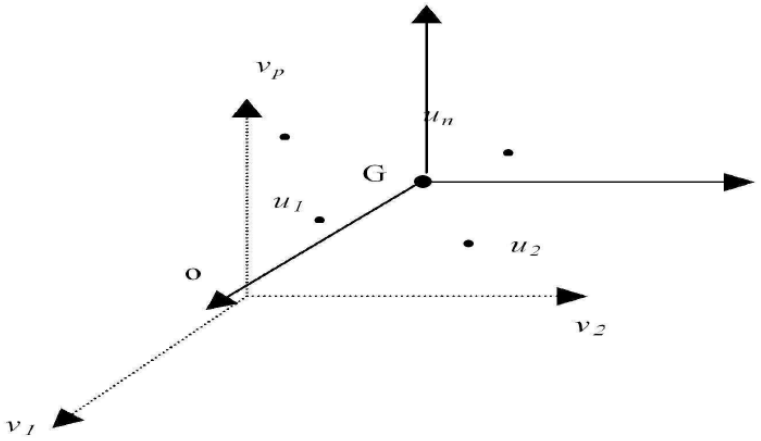

Figure 3.2: original choice

3.2.6 Identification of the PCA model

Let $x(k) = [x_1, ..., x_m]^T$ a vector of observations of "m" random variables. Note $\overline{x}$ the vector corresponding to the mean of the observations of "X" and $\sum$ the covariance matrix of these "m" observations. The estimation of the parameters of the PCA model is summarized in an estimation of the eigenvalues and eigenvectors of the covariance matrix $\sum$ Since the covariance matrix $\sum$ is square with dimension $m \times m$ is symmetrical, we can, according to the linear algebra, verify a relation of type :

$$P^t \sum P = L \tag{3.5}$$

Where "L" is a diagonal matrix and "P" is an orthonormal matrix [7]. The diagonal elements of $L = \{\lambda_1, ..., \lambda_m\}$ are the eigenvalues of the covariance matrix $\sum$ while the column vectors of $P = [P_1, P_2, ..., P_m]$ are the eigenvectors of $\sum$ The eigenvalues λ_i can

be obtained by solving the characteristic equation

$$Det(\sum +\lambda.I) = 0 \tag{3.6}$$

Where $Det(.)$ is the determinant of a square matrix.
For the "m" eigenvalues. Knowing the eigenvalues λ_i , we can deduce the eigenvectors of the covariance matrix by the solution of :

$$(\sum +\lambda_i I)P_i = 0 \tag{3.7}$$

We can then write:

$$\sum p_i = p_i\lambda_i, i = 1, ..., m \tag{3.8}$$

The "m" unit eigenvectors p_i of the covariance matrix $\sum$ represent the "m" orthogonal directions in the data space in which the variances of the projections t_i of the data are maximum (figure3.3).

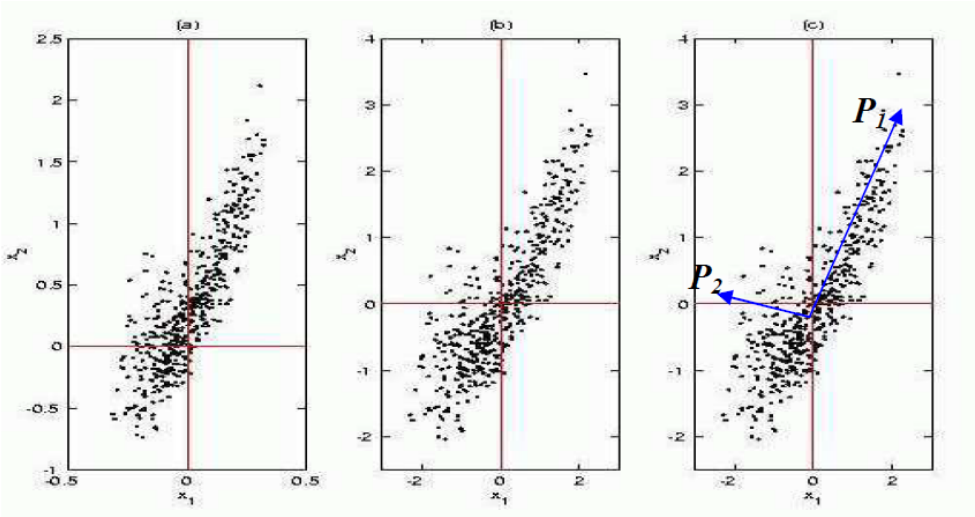

Figure 3.3: Conduct of a Principal Component Analysis. (a) Input distribution. (b) Centering and reduction of this distribution. (c) Both main axes, corresponding to the eigenvectors of the distribution covariance matrix [6] .

In this eigenvector space, the principal components t_i of the data vector "x" are defined by :

$$t_i = p_i^T x = x^T pi \tag{3.9}$$

These are referred to as principal components and are statistically uncorrelated.
The matrix transposition of the type projection relationships 3.9 provides the analytical

expression of the principal component analysis of the data vector "x" :

$$t = P^T x \tag{3.10}$$

where P^T represents the optimal projection matrix of the data in the sense of principal component analysis [9] [7] .
The new variables t_i obviously have a mean of zero and they have a variance given by λ_i(eigenvalue of $\sum$). The column vectors "pi" of "P" are orthonormal because they are orthogonal and of module units $\parallel P \parallel^2 = p^T.p = 1$ (figure3.2). Therefore, if we use these vectors to obtain the principal components, as shown in equation3.9, we will obtain principal components which are uncorrelated and of equal variance to the eigenvalues of the covariance matrix $\sum$.
Finally, we point out that we can have a measure of variability explained by each of the principal components using the vectors transformed according to [8]:

$$Var\{t_i\} = p_i^T \sum p_i = \lambda_i, i = 1, ..., m \tag{3.11}$$

Equation3.11 reveals that the eigenvalues of the covariance matrix $\sum$ represent the variances of the t_i projections of the data on the directions represented by the eigenvectors $p_i (i = 1, ..., m)$ and can be used to indicate the percentage variability of the characteristics represented by each of the main components.

In conclusion, the direction in which the variance of the projection of the data vector "x" is maximum is represented by the eigenvector p_i corresponding to the maximum eigenvalue λ_i . The second factorial axis makes the variance maximum while being orthogonal to the first. More generally [9], the vector subspace of dimension "l" which ensures maximum dispersion of the observations is denied by an orthonormal base formed by the "l" eigenvectors corresponding to the largest "l" eigenvalues of the matrix $\sum$.

3.2.7 Data compression

The practical interest of Principal Component Analysis lies in the reduction of data representation dimensions or more simply data compression.

Indeed, this technique makes it possible to characterize the orthogonal directions of a data space carrying the maximum amount of information in the sense of maximizing the projection variances. The amplitude of the eigenvalues of the covariance matrix $\sum$ of the data quantifies for each of these directions the quantity of encoded information [7] .

Denote by $\lambda_1, ..., \lambda_m$ the "m" non-negative eigenvalues of the covariance matrix $\sum$ checking $\lambda_1 > \lambda_2 > ... > \lambda_m$. The direction of the data space materialized by the eigenvector p_1 associated with the largest eigenvalue λ_1 is the richest in information. Conversely, the eigenvector direction p_m associated with the smallest eigenvalue λ_m is the one with the minimum information [6] .

Recall that any data vector "x" can be represented by the linear combination of the "m" eigenvectors $p_i (i = 1, ..., m)$ of the covariance matrix $\sum$, weighted by main components $t_i = p_i^T x$ "x". The estimation of a data vector "x" from its associated principal component vector t is trivial. To do this, he knew how to multiply each member of equation3.10 by "P" to the right, and the result is :

$$X = Pt = \sum_{i=1}^{m} t_i p_i \tag{3.12}$$

It is therefore possible to reduce the size of the data representation by retaining from the expansion3.12 only the terms $t_j p_j (j = 1, ..., l)$ associated with the $l (< m)$ largest eigenvalues λ_j . The estimate $\widehat{x}$ of a data vector "x" is then described by the reduced expression [9] :

$$\widehat{x} = \sum_{j=1}^{l} t_j p_j = \sum_{j=1}^{l} (p_j^T x) p_j \tag{3.13}$$

The data are thus encoded via the "l" main components $t_1, ..., t_l$ with the highest variances, compared to the "m" descriptive values $x_1, ..., x_m$ initially required.

note: Eigenvalues are not directly involved in the reduced data representation. Their usefulness is limited to the selection of the relevant 'l' main components, whose respective variances they reflect.

The loss of information induced by the reduction of the representation dimension of each data vector "x" is measured by the difference e between its exact representations3.12 and approached3.13:

$$e = x + \widehat{x} = \sum_{i=l+1}^{m} t_i p_i \tag{3.14}$$

The $(m + l)$ principal components$t_i (i = l + 1, ..., m)$ from which the reconstruction error "e" of a data vector is evaluated, are associated with the lowest eigenvalues. It is therefore quite obvious that data compression preserves the information all the better as the eigenvalues are low. The sum of the $m + l$ eigenvalues the loss of the minimum

amount otherwise quantified. of quadratic information averaged over the data set.

$$\varepsilon[e^T e] = \sum_{i=l+1}^{m} Var[t_i] \tag{3.15}$$

The "l" eigenvectors $p_1, ..., p_l$ involved in the reduction of the data representation dimension are referred to as principal vectors. They characterize the subspace of optimal data projection called sub-main space.

3.2.8 Average equity value

This rule consists in taking into account only those components for which the eigenvalue is greater than the arithmetic mean of all eigenvalues [9].

In particular, if one works on the reduced centred data, this amounts to neglecting the components whose variance is less than the unit($\frac{1}{m} trace(\sum) = 1$)

In the case of the PCA model calculated from the covariance matrix $\sum$,the arithmetic mean of the eigenvalues is given by$\frac{1}{m} trace(\sum)$

3.2.9 conclusion

as a conclusion for the PCA method the principle of principal component analysis.

The basic idea is to reduce the size of the data matrix, retaining as much as possible the variations present in the initial data set. This reduction will only be possible if the initial variables are not independent and have non-zero correlation coefficients between them.

These initial variables are transformed into new variables, called principal components. They are obtained by linear combinations of the above and are ordered and uncorrelated.

3.3 Partial Least Squares Regression (PLS)

3.3.1 introduction

Historically PLS regression, the result of the NIPALS algorithm initially developed by Wold (1966) [10]and described in detail by Tenenhaus (1998) [11], has already been

successfully extended to generalized linear models by Bastien et al.(2005) [12] and to Cox models by Bastien (2008) [13].

Many industrial, physical, chemical and economic problems can be described in the form of a regression model, where we have "X" variables that we can more or less influence and "Y" variables that we can only observe.

The objective is then to describe the relationships between "Y" and "X", in the absence of a theoretical model. The problem is that the number of "X" variables is often very large compared to the number of observations. Partial Least Squares Regression (PLS) is a data analysis method specifically designed to study this type of problem.

3.3.2 Presentation

PLS regression is therefore an extension of the multiple linear regression model. In its simplest form, a linear model specifies the (linear) relationship between a dependent variable (or variables) "Y" and a set of predictor variables "X" such as :

$$Y = b_0 + b_1 X_1 + b_2 X_2 + \cdots + b_p X_p$$

where the b_i are the regression coefficients.

So, for example, we can estimate (predict) a person's weight based on height or gender. Linear regression can be used to estimate the coefficients regression from a sample of data measuring height and weight, respectively. and observing the gender of individuals.

In many data analysis problems, the estimation of the linear relationship between two variables is adequate to describe the observed data and to make good forecast for new observations.

The multiple regression model has been extended in several ways to fit the more sophisticated data analysis problems. It therefore serves as a basis for many multivariate methods such as discriminant analysis, principal component regression (PCR) and canonical correlation.

PLS regression is a recent technique that generalizes and combines the characteristics principal component analysis and multiple regression.

It is particularly useful when there is a need to predict a set of variables dependent from a very large set of explanatory variables (predictors) that can be very highly correlated with each other.

PLS is therefore a method for building prediction models when the factors are many and very collinear.

3.3.3 Objective of PLS

The PLS regression for the linear model applies to the field of application where there are few observations on highly correlated variables and in very large numbers, this is the pathological case of linear regression, where the usual methods do not work ("n" being very small one cannot tend towards infinity).

3.3.4 Approaches to get around the problem of multi-collinearity

There are several approaches to get around the problem of multi collinearity among the approaches we will choose the PLS method it is a factorial method.

The factorial methods

We're downsizing. We construct a small number of synthetic variables (latent variables or principal components) that are linear combinations of the natural variables (they summarize these natural variables).

PLS regression ("Partial Least Squares")

With factorial methods, one obtains "k" latent variables, placed in the matrix $C_{n\times k}$ for PCA, and one obtains $\widehat{y} = P_c Y$. Now if $k = rang(X)$, we will have $Im(C) = Im(X)$, that is to say the uncorrelated latent variables form a base of $Im(X)$ and I find exactly the linear regression:

$$P_c = P_X$$

and

$$\widehat{Y}_{PLS} = \widehat{Y}_{PCR} = \widehat{Y}_{OLS}$$

The idea of PLS regression is therefore to take the latent variables most correlated with "Y" and project them.

3.3.5 The PLS linear method

Principle Basic model

As in multiple linear regression, the main purpose of PLS regression is to construct a linear model

$$Y = XB + E$$

or $B_{p\times c}$ c regression coefficients $E_{n\times c}$ noise term for the model.

Usually the variables in "X" and "Y" are centered by subtracting their mean, and reduced by dividing by their standard deviation. Principal component regression and PLS regression both produce score factors as linear combinations of the original predictor variables, such that there is no correlation between the score factors used by the predictive regression model.

For example, suppose that we have a data set for response variables "Y" and a large number of predictor variables "X", some of which are very strongly correlated. A regression using factor extraction for this type of data calculates the factor matrix score $T = XW$ for a matrix of appropriate weight "W" and then we consider the linear regression model $Y = TQ + E$ where "Q" is a matrix of regression coefficients for "T" and "E" an error term. Once the "Q" is calculated, the above regression model is equivalent to $Y = XB+E$ where $B = WQ$ which can be used as a predictive regression model.

To establish the model, the PLS regression produces a matrix of weights $W_{p\times c}$ for "X" such that $T = XW$, i.e. the columns of "W" are vectors of weights for the columns of "X" producing the corresponding matrix of score factors $T_{n\times c}$. These weights are calculated in such a way that they maximize the covariance between the response and the corresponding score factors.

3.3.6 The method

The PLS method is a linear regression method of "c" response variables on "p" explanatory variables all measured on the same "n" individuals. The tables of observations, noted respectively "Y" and "X", of dimensions $n \times c$ and $n \times p$, are assumed centred and possibly reduced with respect to the weights $(p_1; \cdots; p_n)$. One notes $D = diag(p_1; \cdots; p_n)$ the diagonal matrix of the weights.

Note $E_0 = X$ and $F_0 = Y$ the tables centered and reduced in the sense of "D" which is

generally equal to $\frac{1}{n}I_n$. The method proceeds by successive steps allowing the calculation of the main components. Note "A" is the total number of steps, i.e. components indexed by $k = 1; \cdots; A$.

3.3.7 The PLS model

Updating formulas result in the writing of linear models:

$$X = E_0 = \sum_{k=1}^{A} \widehat{X}_k + E_A = \widehat{X}_A + E_A$$

$$Y = F_0 = \sum_{k=1}^{A} \widehat{Y}_k + F_A = \widehat{Y}_A + F_A$$

where $\widehat{X}_k = P_{tk}E_{k+1}$ and $\widehat{y}_k = P_{tk}F_{k+1}$ are the partial models of row 1. $\widehat{X}_A$ is the approximation of "X" with an E_A error, the same for $\widehat{Y}_A$.
The updating of the variables and the non-correlation of the components lead to write more simply the partial models: $\widehat{X}_k = P_{tk}X$ and $\widehat{y}_k = P_{tk}Y$. The non-correlation of the components allows on the one hand the decomposition of the total variance.

$$var(Y) \sum_{j=1}^{c} var(Y^j) = \sum var(\widehat{Y}_k) + var(F_A)$$

as far as the answers are concerned. On the other hand, it leads to the final writing of PLS models according to the components.

$$\widehat{Y_A} = P_{TA}Y$$

$$\widehat{X_A} = P_{TA}X$$

which implies that the PLS model is linear in the initial explanatory variables.

$$\widehat{Y_A} = X\widehat{\beta_A}$$

3.3.8 Conclusion

PLS regression brings the statistician closer to the researcher in modeling problems.

In general, the researcher wishes to keep all the data in his model,important variables while obtaining consistent regression equations. When, in multiple regression, there is

multi-colinearity and/or a large number of variables explanations in relation to the number of observations, the most common solution consists of exclude explanatory variables by step-by-step methods.

PLS regression allows in these situations to retain all the explanatory variables while obtaining a consistent regression equation.

BIBLIOGRAPHY

[1] H. Hotelling*"Analysis of a complex of statistical variables into principal components"*,Journal of Educational Psychology, 1933, 24, 417- 441.

[2] I.T. Jolliffe*"Principal component analysis"*,Springer-Verlag, New York, 1986.

[3] C. Duby, S. Robin *"Principal component analysis"*,Departement O.M.I.P 2006.

[4] Lindsey Smith*" A tutorial on Principal Component Analysis"*, 2002.

[5] S. Wold, K. Esbensen, P. Geladi,*"Principal component analysis "*,Chemometrics and Intelligent Laboratory Systems 1987, 2, 37-52.

[6] P. Teppola, S. Mujunen, P. Minkkinen, T. Puijola, P. Pursiheimo,*"Principal component component analysis"*,Chemometrics and Intelligent Laboratory Systems, 1998, 44, 307-317.

[7] L. Ferre*"Selection of components in principal component analysis : A comparaison of methods"*, Computational Statistics and Data Analysis, 1995, 669-682.

[8] J.V. Kresta, J. F MacGregor, T.E. Marlin,*"Multivariate statistical monitoring of process operating performance"*,Chemometrics Engineering, 1991, 69, 35-47.

[9] S. Valle and al,*"Selection of the number of principal components : The variance of The reconstruction error criterion with a comparison to other methods"*,Industrial and Engineering Chemestry Research, 1999, 38, 4389-4401.

[10] H.Wold,*"Estimation of principal component and related models by iterative least squares"*, Academic Press, New York, 1966, 391-420.

[11] M.Tenenhaus,*"The regression PLS : Theory and Pratique"*,Technip, Paris, 1998.

[12] P.Bastien,V.Esposito Vinzi, and M.Tenenhaus,*"Pls generalised linear regression"*,Computational Statistics and Data Analysis, 2005, 48(1), 17-46.

[13] P.Bastien,*"Deviance residuals based PLS regression for censored data in high dimensional setting"*,Chemometrics and Intelligent Laboratory Systems, 2008, 91(1), 78-86.

CHAPTER 4
RESULTS AND DISCUSSION

4.1 Oxide perovskites

4.1.1 introduction

this chapter concern oxide perovskite compounds with general formula ABO_3. It is well known that perovskite structure can tolerate extensive modifications with regard to composition, where it is possible to substitute the A and/or the B-site cations of the perovskite ABO_3 to develop a particular property such as conductivity, catalytic activity. This leads to numerous substances which are considered to be potentially interesting. However, the difficulties inherent in the prediction of systems with valuable properties.

The question which remains is how many oxide perovskites are left to discover?

Therefore, interesting oxide perovskites may be hidden among the large variety of oxide perovskites, that have never been tested, where finding them would require a tremendous effort and a time-consuming experimental work.

The perovskite structure has the general formula ABX_3. The ideal perovskite structure is cubic with the larger A-site cations located at the corners of the cube, the B-site ions at the body center, and the oxygen ions at the centers of the faces. (figure4.1)

Since the determination of lattice constant, it's not so easy, whether to be measured using X-ray, electron or neutron diffraction techniques, or with advanced high-performance computing techniques based on first-principles quantum mechanics. Recently, some empirical models were established that can predict lattice constant of perovskite from selected atomic properties of their constituent elements [2, 3].

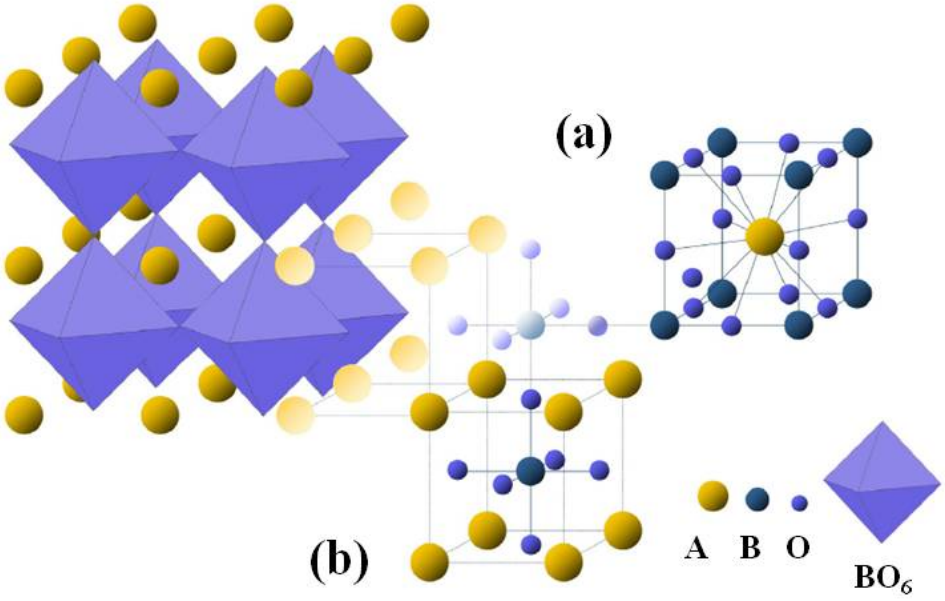

Figure 4.1: Different representations of a perovskite structure. With A ion situated in the centre of the cube (a), or with B ion situated in the centre of the cube (b). It is also shown the threedimensional union of a BO6 octahedra. [1]

Jiang,and al [2] predicted the following equation:

$$a = 1.8836(r_B + r_X) + 1.4898\frac{r_A + r_X}{\sqrt{2}(r_B + r_X)} + 1.2062 \tag{4.1}$$

on the other hand Ye,Chenzhou and al [3] he found for ideal perovskite this linear relation:

$$a_0 = 0.3166r_A + 1.422r_B + 0.1708\chi_A + 0.0562\chi_B + 0.0066(Z_B + Z_A) + 2.706 \tag{4.2}$$

where the r_A, r_B, χ_A, χ_B are ionic radii for atoms "A,B" and electronegativityfor atoms "A,B". However, we should be very attentive to the coordination number of A, B and X, as it has been reported by Moreira et al. [4], since we may obtain an incorrect expression for the prediction of the lattice parameter and the tolerance factor as a function of the ionic radius.

Moriera and al [4], corrected the above equation, with this new relationship.

$$a_{pred} = 2\beta(r_B + r_X) + \gamma t + \delta \tag{4.3}$$

where the β,γ and δ are empirical coefficients for determining the lattice constants of cubic perovskites by Jiang and al [2].

Therefore, a prediction of a robust model of lattice constant in cubic perovskite ABO_3 on the basis of the atomic radius of the different species is crucial.

4.1.2 Determination of the lattice parameter

In this thesis we re-examine the correlation between ionic radii and the lattice constant, and a new empirical relation is derived for oxides perovskite compounds.

Knowledge of the ionic radii of the elements is the most important parameter in the determination of the stability of perovskite structures. Several sets of radii have been published (e.g. by Goldschmidt [5], Zachariasen [6], Pauling [7], Ahrens [8], Shannon [9–11]) and differ from each other sometimes by more than 10%. We know that the ionic radii are strongly dependent on its coordination number and, therefore, upon its near neighborhood structure. In this study, Shannon [11] ionic radii are used, where the B-cations are coordinated by 6 X-anions (CN=6), while the A-cations have a coordination number equal to 12 (CN=12). The X-anions are coordinated by 2 A-cations (CN=2), although it is known that an oxygen deficiency influences the coordination number and, therefore, the ionic radii.

On the basis the partial least square method (PLS) [12–22] we will re-examine the relationship between the lattice parameter and the different ionic radii of oxide perovskites. Several empirical models were established that can predict lattice constant of perovskites from selected atomic properties of their constituent elements. Among them that developed by Li et al. [23, 24], which allows one to predict the lattice constant of cubic perovskites by using the known ionic radii and the electronegativities of the cations and anion.

Partial least squares regression (PLS regression) is a statistical method that bears some relation to principal components regression; instead of finding hyperplanes of minimum variance between the response and independent variables, it finds a linear regression model by projecting the predicted variables and the observable variables to a new space.

The prediction was performed on the basis of the databases of (table5.1), named as the test set. Using PLS, we connected the matrix X of predictor variables with the matrix Y of predicted (response) variables. The SIMPLS algorithm and leave-one-out method were used for cross validation in PLS. In other words, without any information on structural properties of the perovskites in the test set (table5.1), it was possible to predict these quantities using the prediction model for the training set (experimental and theoretical lattice constants available in the literature). The predicted model for oxide perovskites is:

$$a = 2.145 + 0.519r_A + 1.675r_B \tag{4.4}$$

The correlation coefficient is about 87%.If we include the electronegativities in the models, we obtain the following equation:

$$a = 1.448 + 0.384r_A + 1.176r_B + 0.111E_A + 0.021E_B \tag{4.5}$$

The correlation coefficient is 84%.

We notice that the model without the electronegativities are more precise.

The correlation coefficient between the literature reported values of "a"and the values obtained from the above equation is more than 95%.

However, before we can apply the (equation4.4) to a set of unknown compounds, it was first tested on our training data set. (Figure.4.2) shows predicted against calculated values of "a", for the training set. The values predicted for the test set are in good agreement with the training set (table5.2) and are more accurate than those of the other calculated models, and demonstrates the robustness of the analysis using the training dataset (table5.1). Based on these results, we may embark on completing our analysis of property prediction for all combinations of new oxide perovskites based on our predicted model. While this new database shows promise, the ultimate challenge is to develop a validation test for some of these predictions, whether or not the design of any of these combinations could be designed experimentally.

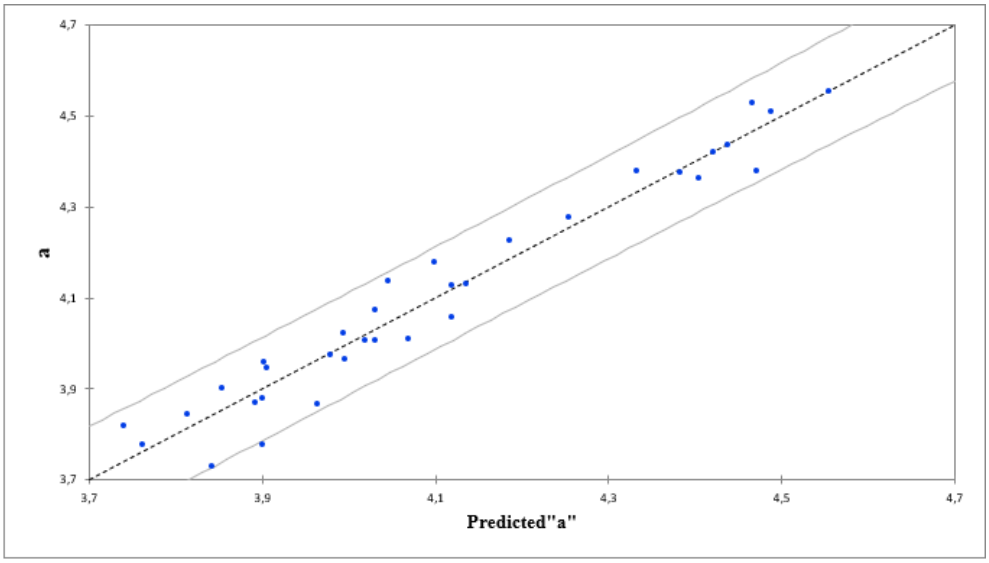

Figure 4.2: PLS results for the predicted lattice constants versus the measured one for perovskites

This model is further tested for more than 892 recently reported or hypothetical perovskite compounds, which are not used in the PLS's model development. The results are presented in (table5.3), we notice an excellent agreement with the recently reported data in literature when available. Among these 892 perovskites, the cations can have oxidation states $A^{+}B^{5+}$ (Na, K), $A^{2+}B^{4+}$ (Ca, Ba, Sr, Cd, Pb), or $A^{3+}B^{3+}$ (Pr, Er, Dy, Bi..).

We may conclude until now, that we have developed a datamining approach for predicting a new oxide perovskites. However, we are not able to predict whether the formation of any combinations of these compounds is possible or not?

4.1.3 structural stability of oxide perovskites

For perovskites structures (ABX_3) Goldschmidt et al. [5] have introduced the concept of tolerance factor "t" which is a measure of the fit of the A-site cation to the cubic corner sharing octahedral network. In a cubic perovskite twice the B-X bond length is the cell edge and twice the A-X bond length is equal to the face diagonal. The tolerance factor is introduced to evaluate the stability of the perovskites, and indicated that the cubic perovskite structure could be maintained for 0.95< t <1.04. Whereas, if t>1.05 the compound will crystallize in hexagonal structure, and if 0.75<t<0.9 it will adopt an orthorhombic structure. If t<0.75 the compound is not a perovskite. However, there are other factors (e.g., temperature, atmosphere) which affect the crystal structure of a material, are not considered in the calculation of the tolerance factor.

The tolerance factor as proposed by Goldsmith is, given by:

$$t = \frac{(r_A + r_X)}{\sqrt{2}(r_B + r_X)} \tag{4.6}$$

Where r_A, r_B and r_X are ionic radius of ions A, B and X respectively.

However, different authors have mentioned, that the tolerance factor is a necessary but not a sufficient condition for the formation of these systems [23–30]. A first approach suggested by these authors is to include in the discussion the values of the octahedral factor $\mu = r_B/r_X$. The lowest limit of the octahedral factor for cubic perovskite formation is 0.414 and the highest value of cubic perovskites is 0.6785. However, for the octahedron MX_6 the value of the ratio r_M/r_X is ranging from 0.414 to 0.732.

Although the (t, μ) variation provides a good qualitative picture, the quantitative relationship between perovskites stability and t or μ has never been reported, and the un-

derlying fundamental issues are unclear. The main question would, is there any trend for perovskite stability? Is t or μ a good quantitative descriptor for the structural stability?

Recently Travis et al. [31] demonstrate that tolerance factor based on these Shannon radii fails to accurately predict the stability of some perovskite compounds.

Therfore, a good stability descriptor should not only provide quantitative guidance in experiments to stabilize these structures but also their thermodynamics stability which a key parameter for searching new emerging stable perovskites through massive calculations and several experimental syntheses.

We have noticed through the literature an important number of data have been produced for the stability of perovskites . However, not only is the creation of data whether through calculation or experiment important, but a way to analyze the data in a comprehensive and robust manner is also necessary, as it has been illustrated by several authors [32–55]. Despite its thoroughness and objectivity, their work did not reveal any new interesting oxide perovskites .

Therefore, the aim of this part is to analyze large amounts of data of oxide perovskites, understanding the correlations among their various properties, and using these correlations to better understand the underlying physics of perovskite by utilizing a multivariate analysis. Additionally, the number of properties required to describe the formability may be reduced to a minimum number so that the problem of creating sufficient amounts of data and analyzing this data is reduced. Data mining is employed in this work in order to fully uncover inter-correlations in the data. Additionally, the mathematical relationship between descriptors have be studied. Based on these relationships we have then developed models, which can be accurately extended to new data so that a virtual system can be fully described with limited data. The data mining method used here is principal component analysis (PCA) [12–22], which is a powerful statistical approach for the analysis of materials properties and has been used to address a variety of physics and materials science issues.

We develop here an approach for selecting and evaluating the formability of cubic oxide perovskites on the basis of the PCA technique. For this purpose, we have selected an initial data set of 34 oxide perovskites, each with 9 predictor variables.

The data was collected from the literature [32–55] and are listed in (table5.1).

PCA is used to assess the correlation between each of the descriptors input into the regression analyses and the stability of the compounds. The results of these analyses can then be compared with the predictive models to understand the physics and limitations of the models. The PCs do not necessarily have an obvious physical meaning, but rather are a combination of descriptors which explain the largest variation in the data. The advantage of PCA is that, since each PC uniquely captures the effect of a certain combination of relevant descriptors, typically a few PCs are sufficient for describing a system.

The first analysis done, was to examine if in our case the PCA captures the differences between the different perovskites? The resulting scores plot of this analysis is shown in (Figure. 4.3) For this analysis (Figure. 4.3), the sign of each principal component has only relational meaning. We notice that PC1(F1) captures 56.28% of the variance, whereas PC2(F2) captures 25.28%. The two PCs together capture ~ 82% of the variance of the data in (Table5.1). Therefore, a dataset of n-dimensions (9 initial descriptors in this case) can be reduced to a few dimensions (2 PCs) while capturing ~ 82% of the original information. The reduction in dimensionality makes trends and correlations, which are hidden in the data, become easily visualized and described in PC space as can be seen in (Figure.4.3).

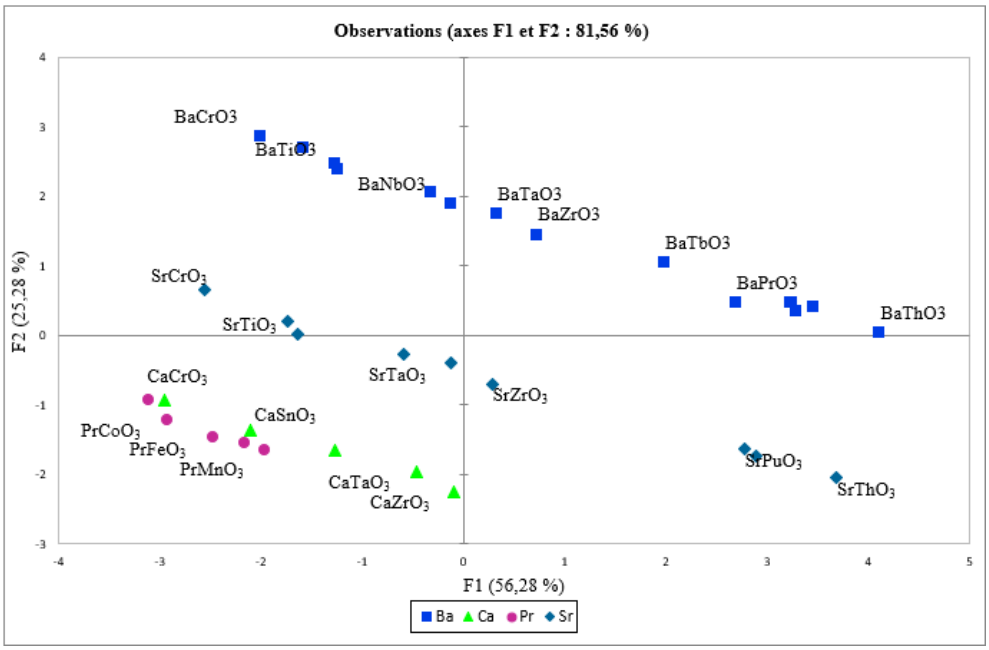

Figure 4.3: PCA score (F1-F2) plot for oxide perovskites from a dataset of table5.1.

As an interesting observation, perovskites ABO_3 with the same A-cation but a differ-

ent element B-cation are placed very close together in the score plot.

From this figure, it appears four important clustering, one (which we will refer to cluster1 which includes perovskites (A=Ba), cluster2 which corresponds (A=Sr), cluster3 (A=Ca) and cluster 4 (A=Pr). It seems that PC1 in going from the bottom to the top is the same as going from the bottom to the top in the periodic table. Whereas, PC2 in going from the left to the right is the same trend as in the periodic table. $BaThO_3$ has the most positive PC1 value of all compounds, while $CaCrO_3$ has the most negative PC1 value. On the other hand, $BaCrO_3$ has the most positive PC2 value and $CaZrO_3$ has the lowest PC2 value. We notice from (table5.1), that $BaCrO_3$ has the lowest t, whereas $SrThO_3$ has the highest one. We display on (Figure.4.4) the variation of tolerance factor t versus the octahedral factor μ for the 34 perovskites, it look like a mirror image of (Figure.4.3). Therefore, the PC's clearly describe the behavior of the tolerance factor for perovskite compounds.

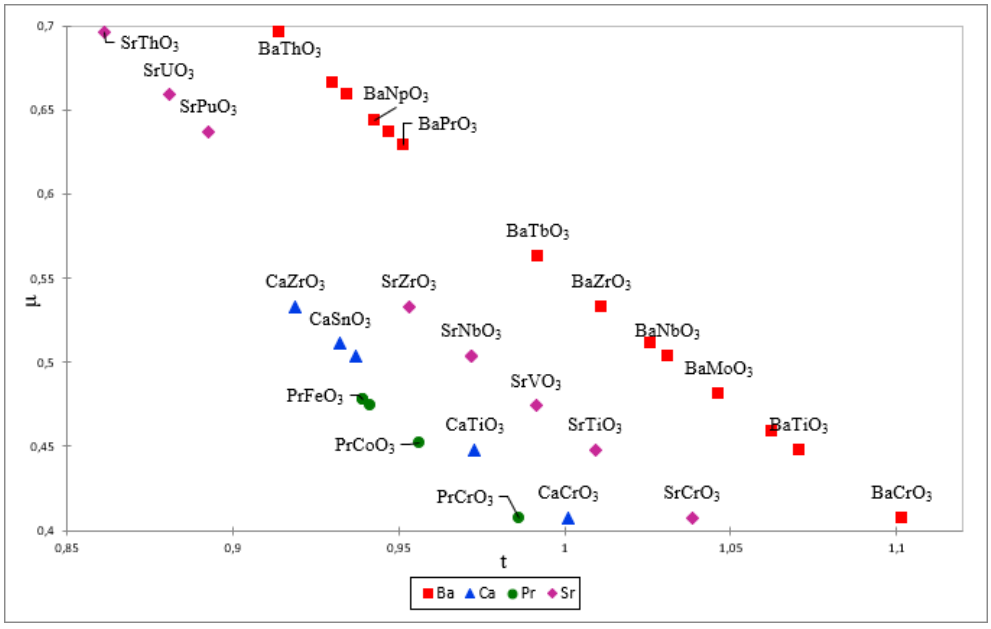

Figure 4.4: The variation of the tolerance factor versus the octahedral factor for the oxides of (table5.1).

One the other hand, the loadings plot corresponds with the scores plot but represents the variance among descriptors. (Figure.4.5) shows the loadings plot corresponding with the samples shown in (Figure.4.3). The axes of the scores plot and loadings plot are the same so the information in the plots can be compared directly. The angles between the vectors tell us how characteristics correlate with one another. When two vectors are close, forming a small angle, the two variables they represent are positively correlated. If they

meet each other at $90°$, they are not likely to be correlated. When they diverge and form a large angle (close to $180°$), they are negative correlated.

Thus, from (Figure.4.5), we notice that r_A and r_B are inversely correlated to E_A and E_B, respectively. That means if the ionic radii increase, the electronegativity decreases. We observe, that μ is inversely correlated to "t".

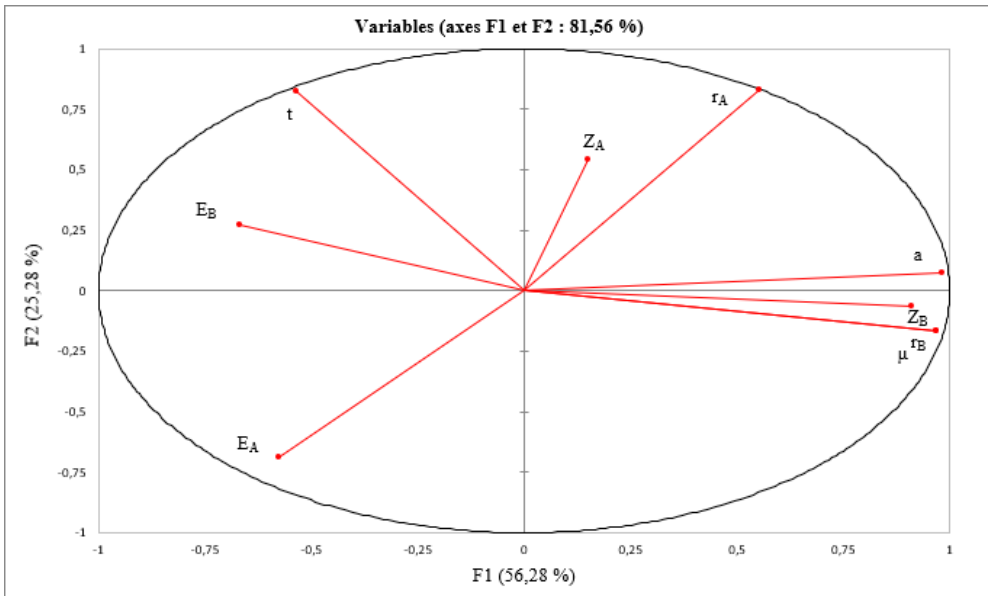

Figure 4.5: PCA loading (F1-F2) plot for oxide perovskites from a dataset of (table5.1 1).

Since, the relative impact of each descriptor in a loading score is identified by measuring the absolute distance from the origin, we display below the different PC's equations as derived from the eigenvalue analysis:

$$\begin{aligned} PC1 = {} & 0.981a + 0.552r_A + 0.970r_B + 0.578E_A \\ & + 0.667E_B + 0.15Z_A + 0.912Z_B + 0.534t + 0.970\mu \end{aligned} \tag{4.7}$$

$$\begin{aligned} PC2 = {} & 0.072a + 0.831r_A + 0.169r_B + 0.688E_A + 0.270E_B + 0.543Z_A \\ & + 0.067Z_B + 0.823t + 0.169\mu \end{aligned} \tag{4.8}$$

The impact of the descriptors is increased as its distance from the origin is increased. We note from equations 4.7 and 4.8 that for PC1, the weighting coefficients for (a, r_B, Z_B, and μ) are the more important descriptors ($\sim 0,9$), whereas for PC2 (t and r_A) have the highest weighting ($\sim 0,8$).

Reducing the complexity of the choice and limiting the number of compounds potentially interesting for valuable applications are a reason to look for an empirical prediction

of perovskites structural parameters.

Thus, to evaluate the formability of the 892 predicted perovskites, we have calculated their tolerance factors on the basis of the Goldschmidt tolerance factor and their octahedral factor, the results are also displayed on (table5.3).

As we know the cubic perovskite structure could be maintained for 0.95 <t < 1.04. As t decreases from 1, the perovskite structure deforms towards structures with lower coordination for A. When it is slightly less than unity a rhombohedral distortion usually results. When t is near the lower limit (0.75) for perovskite-type structure formation,the distortions lead to a larger orthorhombic unit cell. When the A ion is very large ($t > 1$) the distortions of the perovskite structure led to closely related polytypic phases. However, the limiting values of t may differ depending upon the set of ionic radii employed. The set of ionic radii proposed by Shannon [9] is commonly used.

Then, according to (table5.3), we may identify the corresponding crystal structure of the different perovskite compounds according to the value of their tolerance factor.

We have plotted on (Figure.4.6) the variation of the tolerance factor versus the octahedral factor. From these predicted 892 compounds, we have identified 181 cubic perovskites since their 0.95<t<1.04 and 0.414<μ <0.6785, among 867 possible perovskites.

Even if several approach using different criterion approach has been developed to examine the formability of perovskites [23–30]. When we compare the results of these authors [23, 24], we notice several anomalies as it has been reported by Moriera et al. [4]. Therefore, there are still more to do on the formability of perovskites.

In this work, will extend our study to a new improved tolerance factor (τ) proposed by Bartel et al [29]. τ has the form:

$$\tau = \frac{r_X}{r_B} + n_A(n_A + \frac{r_A/r_B}{ln(r_A/r_B)}) \tag{4.9}$$

where n_A is the oxidation state of A.

Bartel tolerance factor distinguished between perovskites and nonperovskites with an accuracy of 92%, compared to only 74% accuracy for the Goldschmidt tolerance factor.

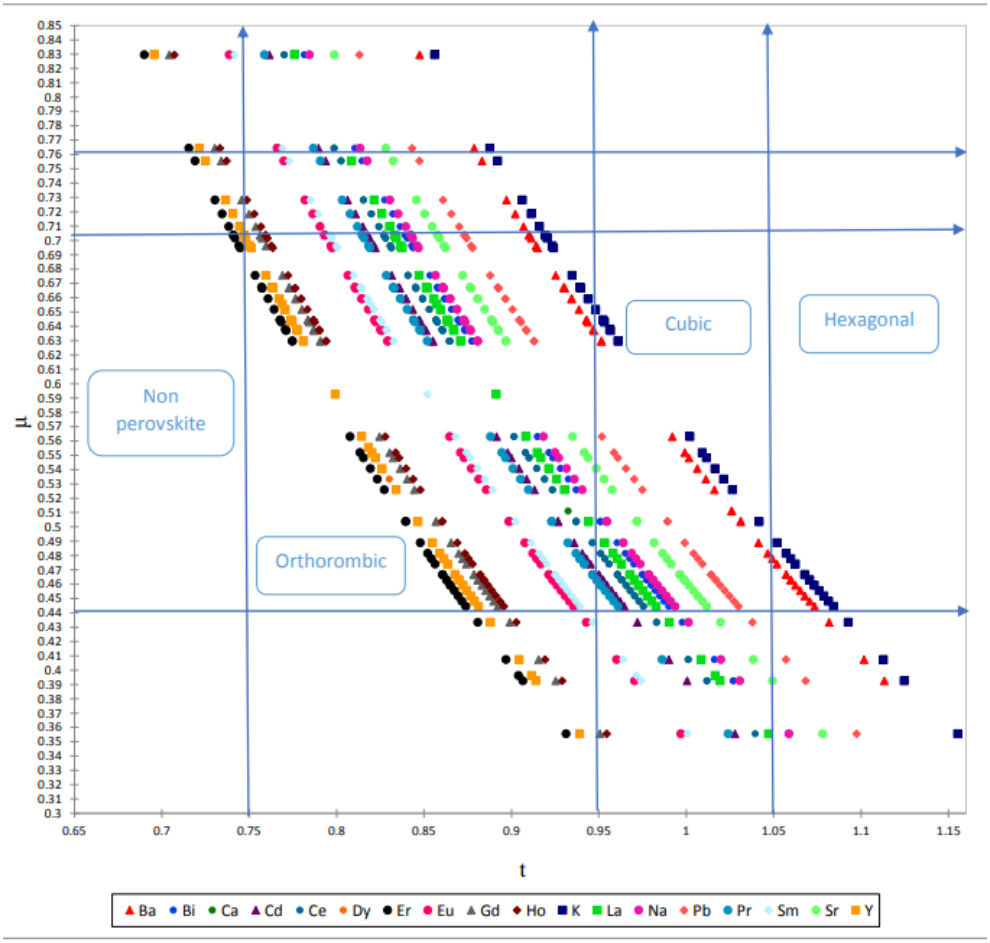

Figure 4.6: The variation of the tolerance factor versus the octahedral factor for the oxides of (table5.3)

We display on (Figure.4.7) the resulting scores and loading plots of (table5.1) including the corresponding values of τ. We notice that PC1(F1) captures 55.42% of the variance, whereas PC2(F2) captures 25.74%. We notice that the PCA clearly distinguish between the oxidation states of the perovskites cation-A (n_A=3 (Pr) and n_A=2 (Ca, Sr and Ba)) (Figure.4.7) when compared with those of (Figure.4.3).

On (Figure.4.8), we have plotted the variation of the improved tolerance factor τ versus the octahedral factor μ for the 892 hypothetical perovskite compounds. Since, according to Bartel et al [29] , when t<4.18 indicates perovskite. We identify 154 possible cubic perovskite compounds as displayed in (Figure.4.8).

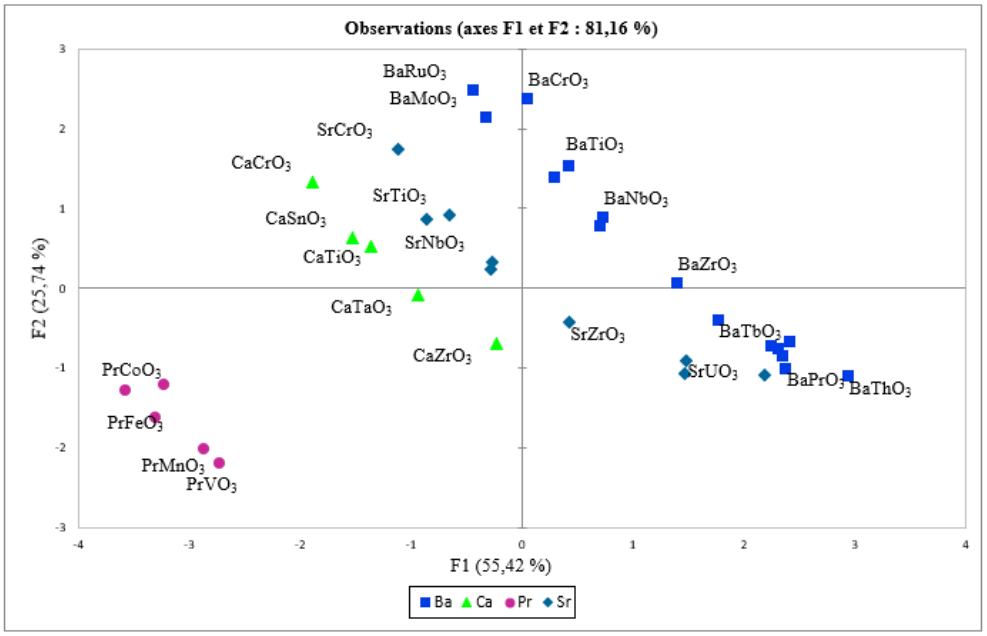

Figure 4.7: PCA score (F1-F2) plot for oxide perovskites from a dataset of (table5.1) including the improved tolerance factor τ.

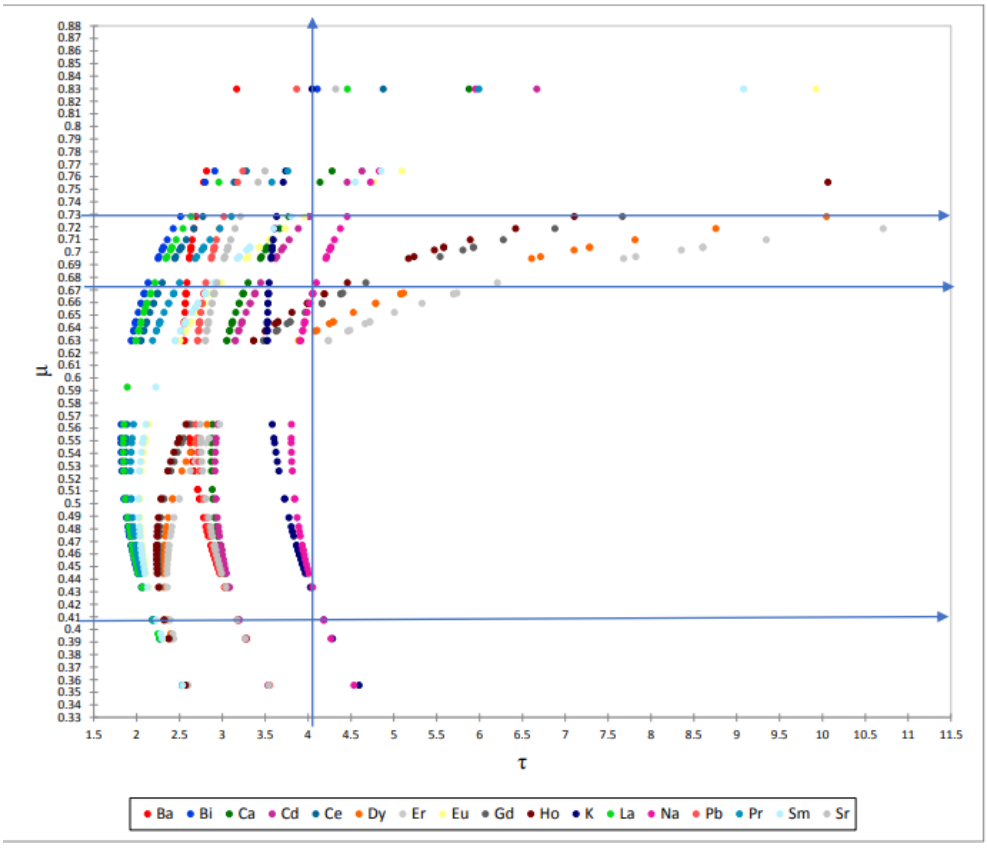

Figure 4.8: : The variation of the improved tolerance factor τ versus the octahedral factor for the oxides of table5.3.

4.1.4 Thermodynamic stability of oxide perovskites

Unfortunately, relatively little attention has been given to the thermodynamic properties of these perovskites. The thermodynamic phase stability of perovskite oxides is investigated on the basis of the work of Sun et al. [56].

Sun et al. [56] identified an interesting correlation between the thermodynamic stability and the descriptor $(t + \mu)^{\eta}$, where η is the atomic packing fraction (APF). Their results showed that APF is an important factor. The η factor has never been considered in previous studies for the formability of perovskites, η is calculated as:

$$\eta = (V_A + V_B + 3V_X)/a^3 \tag{4.10}$$

On the basis of the high-throughput DFT results of the decomposition energy (ΔH_D) as reported by Sun et al [56] (table5.4), we have determined by using the PLS method the variation of ΔH_D with $(t + \mu)^{\eta}$. The equation for our predicted decomposition energies is:

$$\Delta H_D = +3889.18 + 3055.5(t + \mu)^{\eta} \tag{4.11}$$

The correlation coefficient between the values of (table5.4) and the values obtained from the above equation is more than 75%. This equation gives the right sign for ΔH_D, and seems to be more reliable than those equations given by Sun et al [56].

We extend the calculation of ΔH_D to our 892 compounds using equation4.11. We deduce as a first approximation 572 thermodynamically stable perovskites among the 892 perovskites $(\Delta H_D < 0)$ as shown in (table5.5).

Therefore, we conclude that even if we have identified the formability of 867 perovskites, only 572 are thermodynamically stable.

4.2 inverse perovskites

4.2.1 introduction

the inverse Perovskites the type ABX_3 is a cubic crystal structure with divalent or trivalent cation atoms (A) at the cube corner sites, transition metal atoms (X) at face-centered positions, and the nonmetal atoms (B) in the body-centered position (Carbon or Nitrogen). In effect the inverse perovskite is an ordinary perovskite where the heavy metal atoms have exchanged positions with the nonmetal atoms within the unit cell.

Thus, in this chapter we re-examine the correlation between ionic radii and the lattice constant, and a new empirical relation is derived for inverse perovskites compounds. Since the chemical bonds in inverse perovskites represent an intermediate state between ionic (heteropolar) and covalent (homopolar) bond formation, we will not use the Shannon radii values, but the data taken from the crystal-maker web site [57], based on an empirical system of unified atomic-ionic radii, which is suitable for describing anion-cation contacts in ionic structures. The data were derived by the comparison of bond lengths in over 1200 bond types in ionic, metallic, and covalent crystals and molecules based on the work of J.C. Slater [58, 59], and Clementi et al. [60], in order to demonstrate if these values of the radii give a more robust lattice parameter model.

4.2.2 determination of lattice parameter

In this work, the relationships between the lattice parameter (a) and the radii of A-site, B-site and X-site and the respective electronegativities are calculated by the using the partial least square method (PLS) for perovskites and inverse perovskites alone [12–22].

Partial least squares regression (PLS regression) is a statistical method that bears some relation to principal components regression; instead of finding hyperplanes of minimum variance between the response and independent variables, it finds a linear regression model by projecting the predicted variables and the observable variables to a new space.

The prediction was performed on the basis of the databases of (table5.6), named as the test set. Using PLS, we connected the matrix X of predictor variables with the matrix Y of predicted (response) variables. The SIMPLS algorithm and leave-one-out method were used for cross validation in PLS. In other words, without any information on structural properties of the perovskites and inverse perovskites in the test set (Table5.6), it was possible to predict these quantities using the prediction model for the training set (exper-

imental and theoretical lattice constants available in the literature). The predicted models for inverse perovskites are:

$$a = 0.233 + 0.372r_A + 0.568r_B + 2.02r_X \tag{4.12}$$

The correlation coefficient between the literature reported values of "a" and the values got from the above equation is more than 95%.
If we include the electronegativities in the models, we obtain the following equation for inverse perovskites:

$$a = 0.041 + 0.53r_A + 0.254r_B + 2.02r_X + 0.102E_A + 0.026E_B + 0.032E_X \tag{4.13}$$

The correlation coefficient is 90%.

Before we can apply the equations 4.12 and 4.13 to a set of unknown compounds, it was first tested on our training data set. (Figure.4.9) shows predicted against calculated values of "a", for the training set. The values predicted for the test set are in good agreement with the training set (table5.7). Once again (Figure.4.9) demonstrates the robustness of the analysis using the training dataset (Table5.6). Based on these results, we may embark on completing our analysis of property prediction for all combinations of new inverse perovskites based on our predicted models. While this new database shows promise, the ultimate challenge is to develop a validation test for some of these predictions, whether or not the design of any of these combinations could be designed experimentally.

This model is further tested for more than 264 recently reported or hypothetical inverse perovskites compounds, which are not used in the PLS's model development. The results are presented in (table5.8), we notice an excellent agreement with the recently reported data in literature when available.

We have developed a datamining approach for predicting a new inverse perovskites. However, we are not able to predict whether the formation of any combinations of these compounds is possible or not?

4.2.3 structural stability

Reducing the complexity of the choice and limiting the number of compounds potentially interesting for valuable applications are a reason to look for an empirical prediction

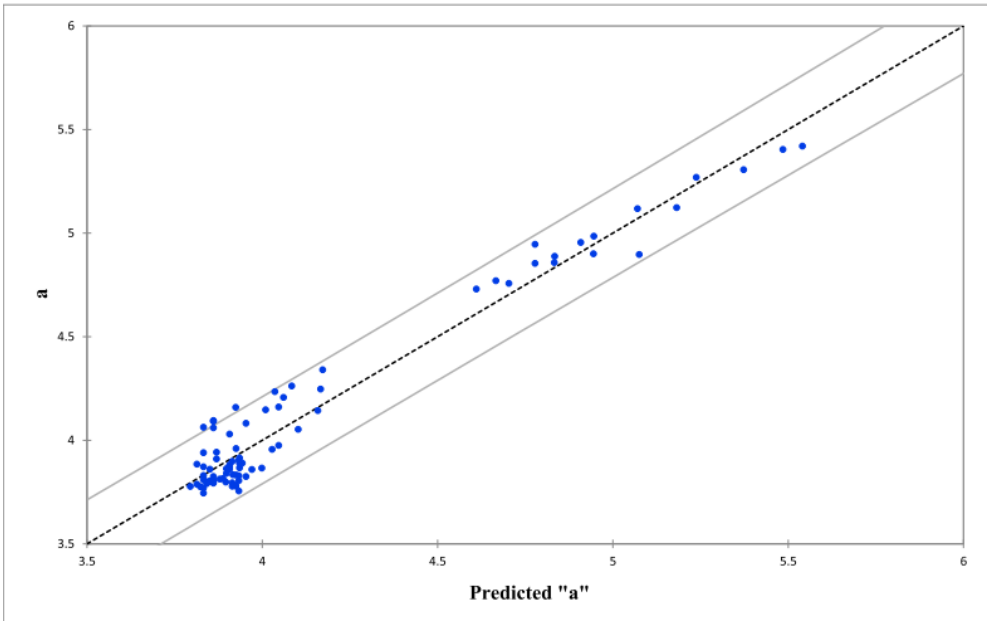

Figure 4.9: PLS results for the predicted lattice constants versus the measured one for inverse perovskites

inverse perovskites structural parameters. Here, we are interested in the evaluation of the geometrical factors. Thus, to evaluate the stability of the inverse perovskites, we have calculated the tolerance factors of the predicted perovskites and inverse perovskites compounds on the basis of the Goldschmidt tolerance factor, the results are displayed on (table5.8).

As we know the cubic perovskite structure could be maintained for 0.95 $<t<$ 1.04. As t decreases from 1, the perovskite structure deforms towards structures with lower coordination for A. When it is slightly less than unity a rhombohedral distortion usually results. When t is near the lower limit (0.75) for perovskite-type structure formation, the distortions lead to a larger orthorhombic unit cell. When the A ion is very large ($t > 1$) the distortions of the perovskite structure lead to closely related polytypic phases. So what about the inverse perovskite?

The initial data set contains 125 perovskites and inverse perovskites, each with 11 predictor variables. The data was collected from the literature [61–89] and are listed in (table5.6). The first analysis done, was to examine if the PCA captures the differences between perovskites and inverse perovskites? The resulting scores plot of this analysis is shown in (Figures.4.10). The objective of the present analysis is to use the present knowledge about perovskites and inverse perovskite to determine the formability of these compounds. PCA is used to assess the correlation between each of the descriptors in-

put into the regression analyses and the stability of the compounds. The results of these analyses can then be compared with the predictive models to understand the physics and limitations of the models. The PCs do not necessarily have an obvious physical meaning, but rather are a combination of descriptors which explain the largest variation in the data.

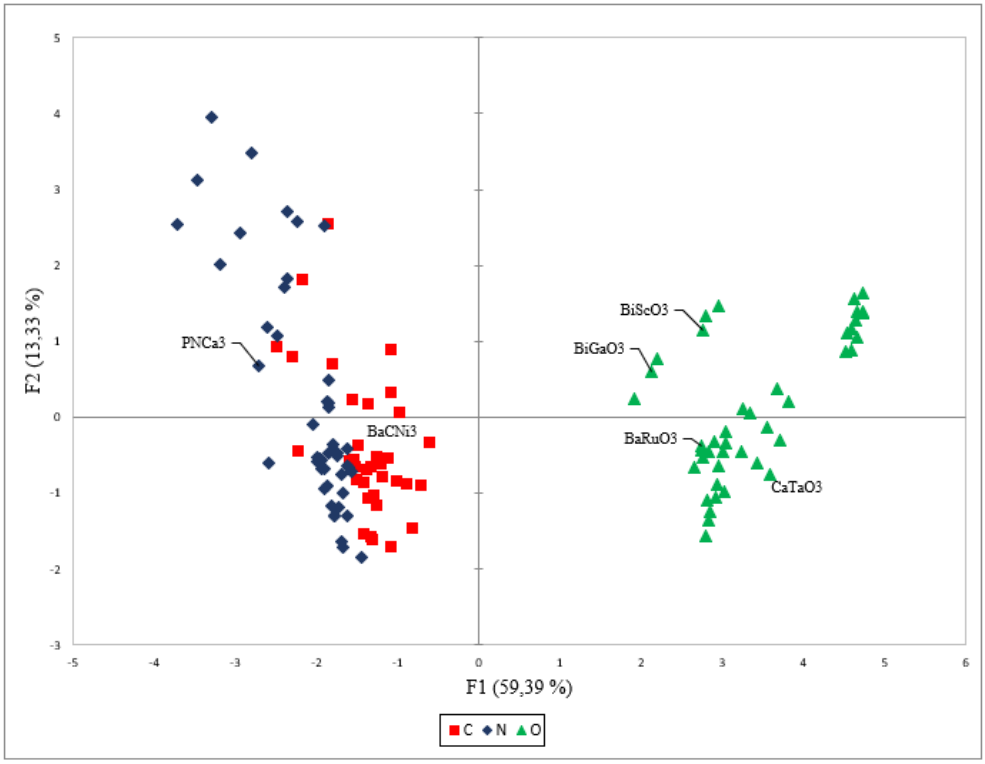

Figure 4.10: PCA Scores (PC1-PC2) plot for perovskites and inverse perovskites from a dataset.

The advantage of PCA is that, since each PC uniquely captures the effect of a certain combination of relevant descriptors, typically a few PCs are sufficient for describing a system. We notice that PC1(F1) captures 59,39% of the variance, whereas PC2(F2) captures 13,33%. (Figure.4.11) display the score plot of PC1 versus PC3, we notice that PC3 captures 11,27% of the variance. From these figures, it appears two important clustering, one (which we will refer to cluster1) which includes perovskites (positive values of F1) and cluster2 which corresponds to the inverse perovskites (negative F1). Therefore, the PCA's clearly distinguish between perovskites and inverse perovskites. In the other hand in zooming cluster 1 or cluster 2, we observe different groups. We may then refer to some subgroups with the same atom A or X.

The loadings plot corresponds with the scores plot but represents the variance among descriptors. (Figure.4.12) shows the loadings plot corresponding with the samples shown

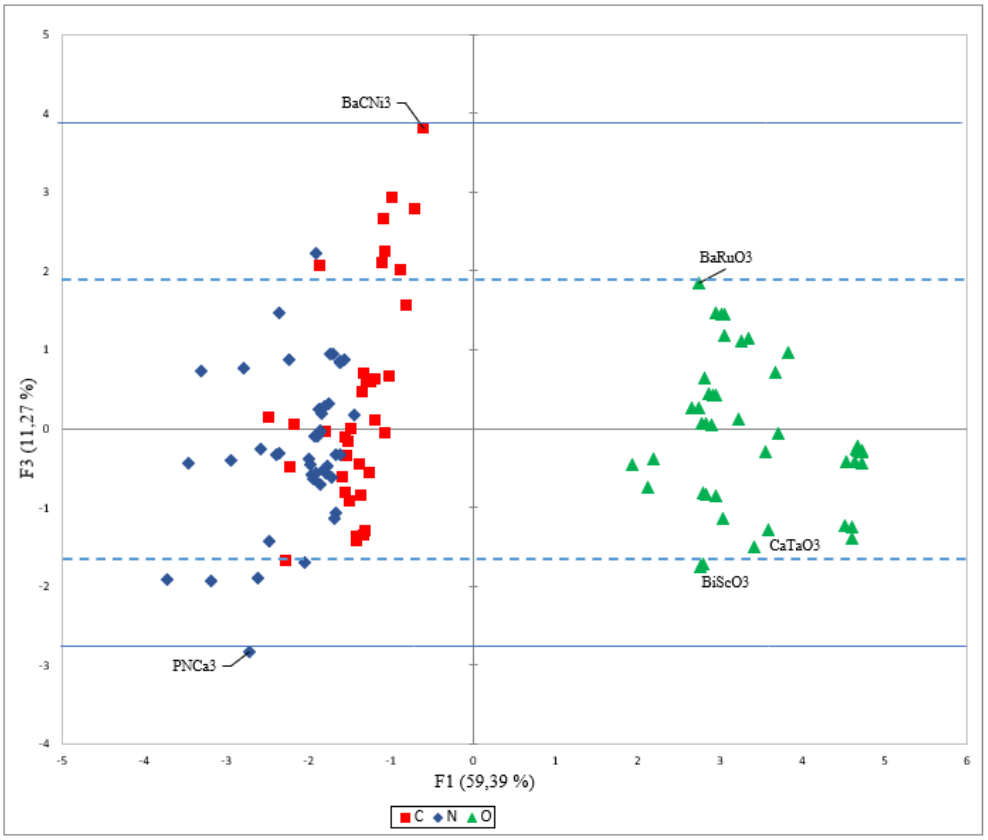

Figure 4.11: PCA Scores (PC1-PC3) plot for perovskites and inverse perovskites from a dataset.

in (Figure.4.10). The axes of the scores plot and loadings plot are the same so the information in the plots can be compared directly. It is well known that properties with similar PC values are highly correlated, while inverse PC values indicate inverse correlations. It's known also that properties near the origin are not important, whereas those far from the origin are the more dominant. We notice from (figure.4.11), that the lattice constant is the more dominant parameters. Where the corresponding loading plot for PC1-PC3 (figure.4.13) shows that t is the mode dominant parameter, whereas the lattice parameter plays a minor role.

We expect then, that the lattice parameter "a" is a complicated function of r_A, r_B, r_X and the values of the different electronegativities. It is therefore important to know how the cation size (X) influences the value of the lattice parameter, which can provide guideline for the doping ion selection. As we observe on Figure1b, the electronegativities and the atomic radius are on opposite direction, this means that if the atomic radius increases the electronegativity decreases, and also r_x and both r_A and r_B behaves inversely.

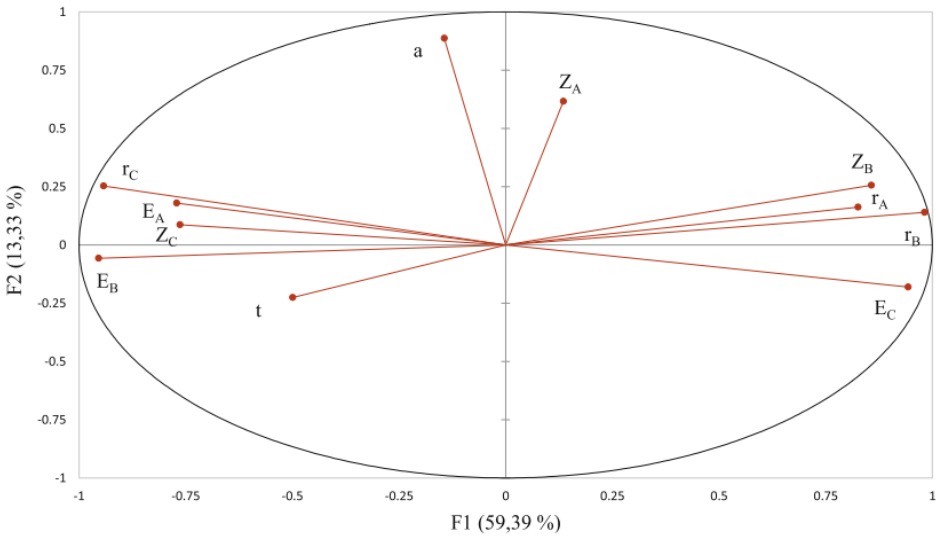

Figure 4.12: The PCA (PC1-PC2) loadings values for perovskites and inverse perovskites from a dataset.

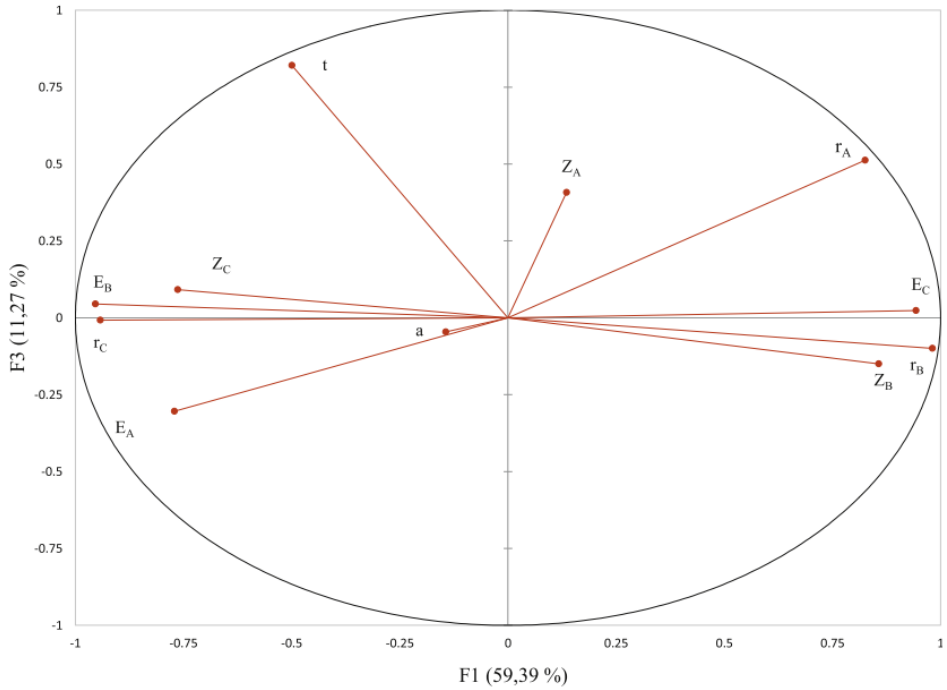

Figure 4.13: The PCA (PC1-PC3) loadings values for perovskites and inverse perovskites from a dataset.

The PC equations as derived from the eigenvalue analysis yielded:

$$PC1 = +0.56a + 0.323r_A + 0.384r_B + 0.369r_X + 0.302E_A + 0.373E_B + 0.369E_X + 0.195t + 0.053Z_A + 0.335Z_B + 0.299Z_X \quad (4.14)$$

$$PC2 = +0.732a + 0.133r_A + 0.115r_B + 0.209r_X + 0.148E_A + 0.048E_B + 0.149E_X + 0.186t + 0.508Z_A + 0.211Z_B + 0.071Z_X \quad (4.15)$$

$$PC3 = +0.041a + 0.460r_A + 0.09r_B + 0.007r_X \\ +0.273E_A + 0.04E_B + 0.021E_X + 0.737t + 0.366Z_A + 0.135Z_B + 0.082Z_X \quad (4.16)$$

Note that for PC1, the weighting coefficients for $r_A, r_B, r_X, E_A, E_B, E_X, Z_B$ and Z_X are the same (~ 0.3) and shown on (figures.4.12 and 4.13). For PC2, "a" have the highest weighting (0.732), whereas for PC3, t has the largest one (0.737).

So, we expect that PC1-PC2 classify the compounds according to their lattice constant, whereas, PC1-PC3 will classify the compounds according to their tolerance factors and may give an insight on the formability of the perovskites and inverse perovskites.

We have plotted on (figure.4.14) the variation the lattice parameter versus the tolerance factors, we notice that the inverse perovskite compound with the largest tolerance factor is $BaCNi_3$, and that with le lowest one is $PNCa_3$. Whereas for perovskite compounds, the largest one is $BaRuO_3$, and the lowest one is $BiScO_3$. The trends shown in (figure.4.14), is clearly observed on the PCA's score plot as shown by the horizontal lines (dashed line for perovskites, and full line for the inverse perovskite. So, from to PCA results of (figure.4.11) and on the basis of (figure.4.14), we notice that may deduce the formability all perovskites according to their position on the score plot PC1-PC3.

Although the (t, μ) variation provides a good qualitative picture, the quantitative relationship between perovskite or inverse perovskite stability and t or μ has never been reported, and the underlying fundamental issues are unclear. The main question would, is there any trend for perovskite stability? Is t or μ a good quantitative descriptor for the stability? A good stability descriptor should not only provide quantitative guidance in experiments to stabilize these structures but also be a key parameter for searching new emerging stable perovskites or inverse perovskites through massive calculations and several experimental syntheses. Sun et al. [56] identified an interesting correlation between the thermodynamic stability and the descriptor $(t + \mu)^{\eta}$, where η is the atomic packing fraction (APF). Their results showed that APF is an important factor. The η factor has never been considered in previous studies for the formability of perovskites or inverse perovskites, η is calculated as:

$$\eta = (V_A + V_B + 3V_X)/a^3 \quad (4.17)$$

Based on the work of Sun et al. [56] we extend this approach to our perovskite compounds. In (figure.4.16) we display the variation of t versus η. We know that in the rigid sphere model, higher η usually leads to more stable structures. We notice a clear separation be-

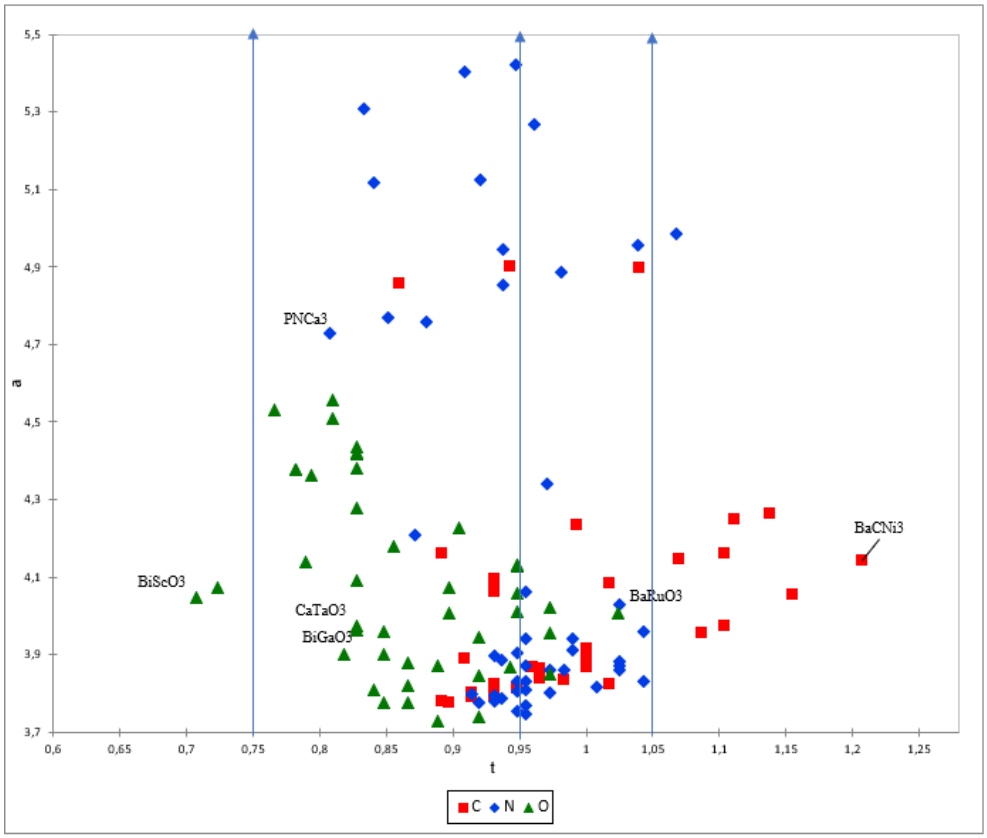

Figure 4.14: The variation of the tolerance factor versus the lattice constant of some perovskites and inverse perovskites.

tween a different compound according the A-cation, and it seems those with a Ba-cation have greater η and those with a Bi-cations have the smallest η. Whereas, on (figure.4.17) we draw the variation of $(t+\mu)^{\eta}$ versus t, we observe a nearly linear correlation. When compare the results of (figure.4.15) with those of (figure.4.17), we may conclude that the descriptor $(t+\mu)^{\eta}$, may provide direct guidance for precise control of chemical composition towards stable perovskites. Therefore, this descriptor opens a way for quantitatively describe perovskite stability instead of qualitatively tolerance factor t, or octahedral factor μ. When we compare the values for all our oxide perovskites with those of Li et al. [90], we notice that all the compounds having their 1.117<$(t+\mu)^{\eta}$<1.38 are perovskites. We conclude that just with one criterion we could decide on the formability of perovskite structures. We expect that that those with a cubic structure are 1.32<$(t+\mu)^{\eta}$<1.429.

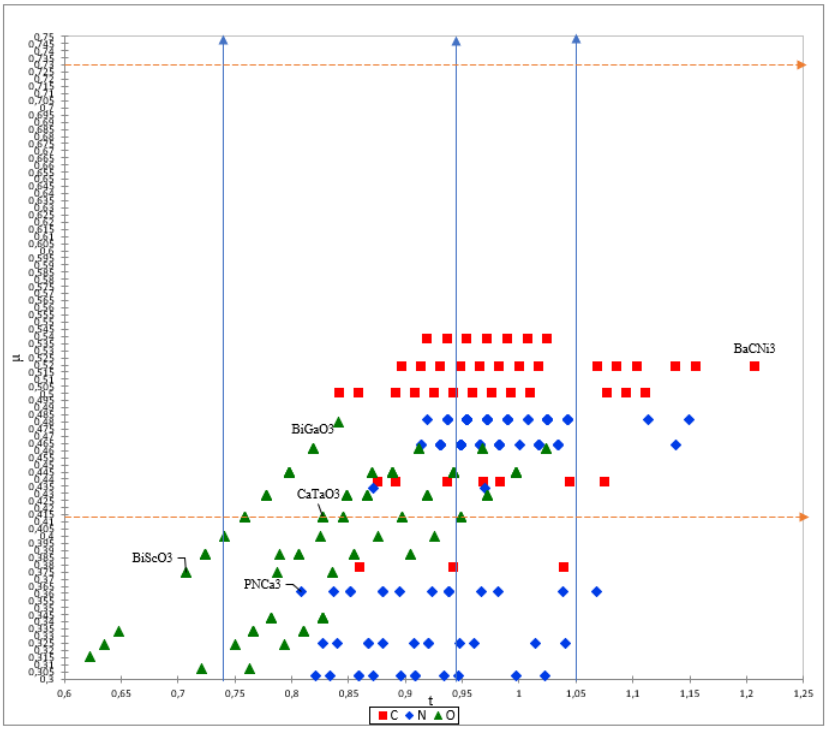

Figure 4.15: The variation of the octahedral factor μ versus the tolerance factor of some perovskites and inverse perovskites.

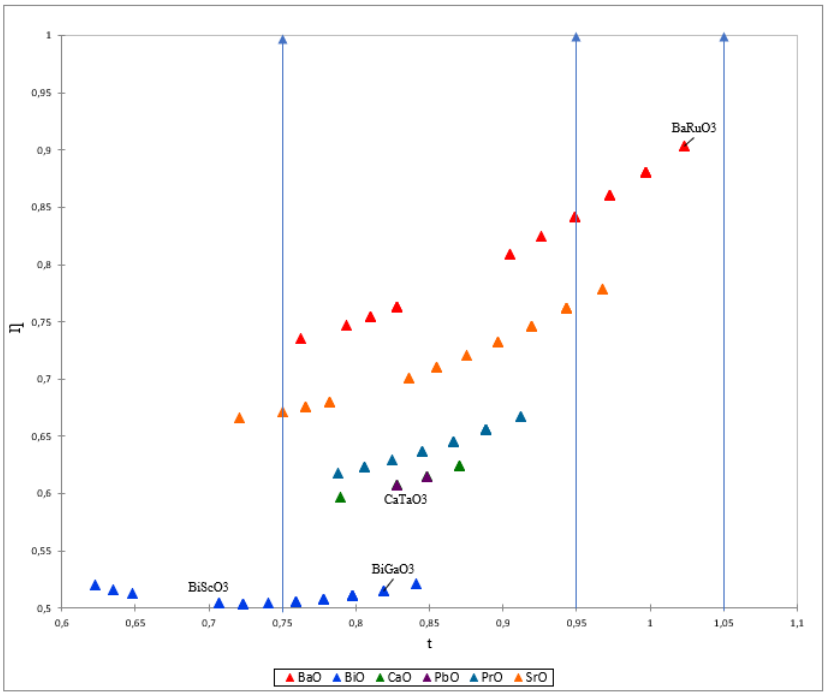

Figure 4.16: The variation of the atomic packing fraction η versus the tolerance factor of some perovskites and inverse perovskites.

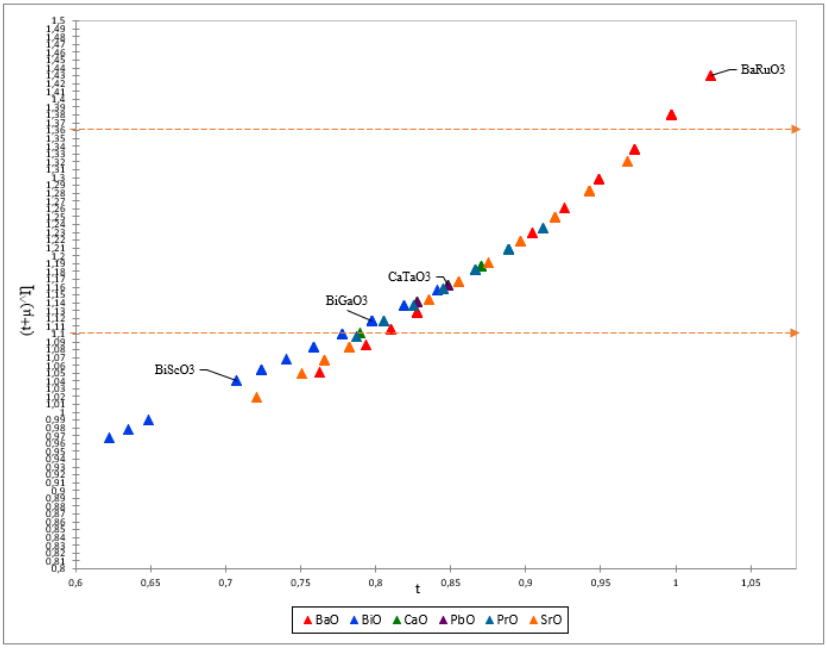

Figure 4.17: The variation of $(t+\mu)^{\eta}$ versus the tolerance factor of some perovskites and inverse perovskites.

4.3 the Ionic Conductivity in Oxide Perovskites

4.3.1 Structural identification of ionic conductor

Despite an intensive amount of research study on solid oxide electrolytes, the development of a universal selection criteria for the identification of high conductivity solid oxide electrolytes has not as yet been reported. Previously-proposed descriptors for oxygen migration in perovskites include Kilner critical radius [91–94], Goldschmidt tolerance factor [5], volumetric factors [91], crystal structure ideality [95], oxygen vacancy formation energy [96, 97], and metal oxygen bond strength [98], both average [91]and related to vacancy trapping [99].

This thesis is an attempt to predict new oxide perovskites solid electrolytes by using empirical crystallographic criteria as described in the introduction. One criterion frequently cited for achieving high ionic mobility in solid electrolytes, is the maintain a cubic structure. Since in going from cubic to another structures, the number of crystallographic equivalent sites decreases. Among the others crystallographic criteria, is the critical radius (R_C), which is the narrowest passage through which the oxygen ion can migrate along the crystal. The greater the value of the critical radius, the smaller the migration activation energy. Larger critical radii can be achieved by increasing r_B and/or reducing r_A.

From the calculated values of the critical radii of 892 oxide perovskites (see table. 5.3), we can identify those where the oxygen ions can migrate more readily which generally leads to the enhancement in ionic conductivity. We notice that for the oxides with A= Bi, Ba, Sr, the highest values of R_c are for $AAcO_3$ and $ALaO_3$ and the lowest are for $AMnO_3$ and $ACrO_3$. This we expect that the oxides of the types $ALaO_3$ or $ACrO_3$ should have a high ionic conductivity. On the other hand, for the families, where A=La, Pr, the largest R_c are for $LaNdO_3$ and $LaPrO_3$, and the smallest are for $PrNiO_3$ and $LaMnO_3$.

One the other hand the lattice free volume (V_L) is another important criterion as suggested by Cook et al [91, 107], since a larger free volume provides more space for the mobile ions to move more easily and therefore reduces the activation energy for anion migration. Hayashi et al. [100] introduced the notion of specific free volume (V_S).

It should be noted also from PCA results (Fig. 4.18 and 4.19), based on the initial data set of 34 oxide perovskites, each with 13 predictor variables (table5.9), that the tolerance factor t is inversely correlated to R_C, there is also no correlation between R_C and V_S (Since V_S is perpendicular to R_C). Then, although the free space will increase with increasing sizes of the A and B, we should in the same time maintain $t = 1$. Consequently, the critical radius will anyhow decrease (table. 5.9).

When the specific free volume becomes larger, the tolerance factor becomes smaller (table. 5.9). The decrease of the tolerance factor means that the deformation from the cubic lattice becomes larger. When a larger ion is introduced in the B site, the specific free volume becomes large and the tolerance factor becomes smaller. A large specific free volume is desirable in order to obtain larger oxygen ion mobility.

On the other hand, the binding energy, for a given A ions decreased linearly with the increase of the tolerance factor. Thus, the increase of the tolerance factor will lower the interactions of B-O-B bond and may promote the formation of oxygen vacancies at the surface [101].

Clearly a balance would have to be made between all these geometrical parameters for minimizing parasitic electronic conductivity and those conditions favoring high ionic mobility. So, in order to minimize the electronic conductivity, we must take into account that this conductivity is a results of multiple valence states cations (such as Mn, V, Cr..)

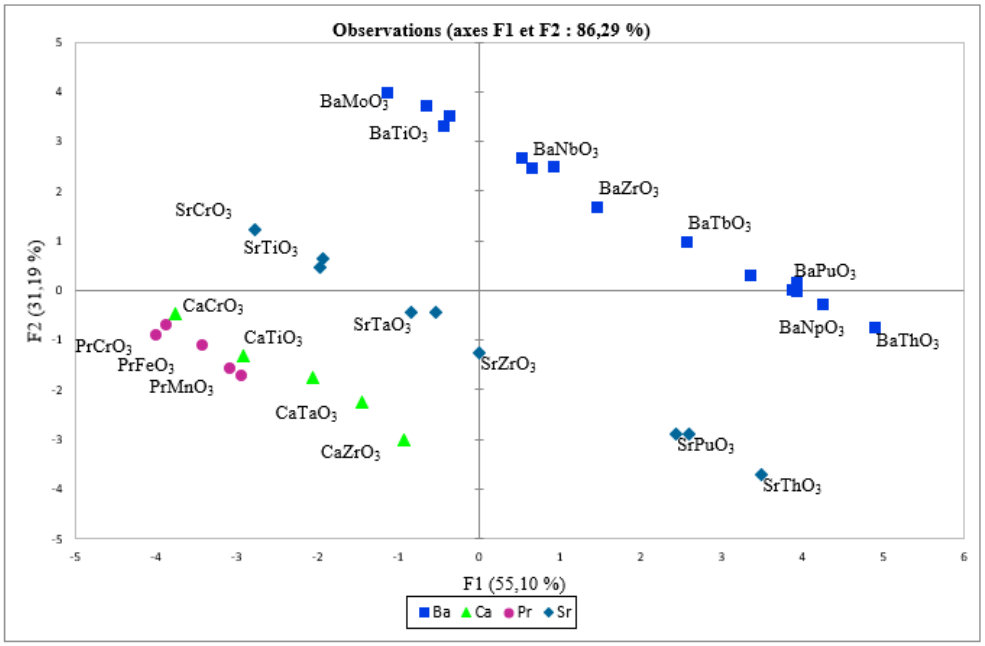

Figure 4.18: PCA score (F1-F2) plot for oxide perovskites from a dataset of table5.6 including 13 descriptors

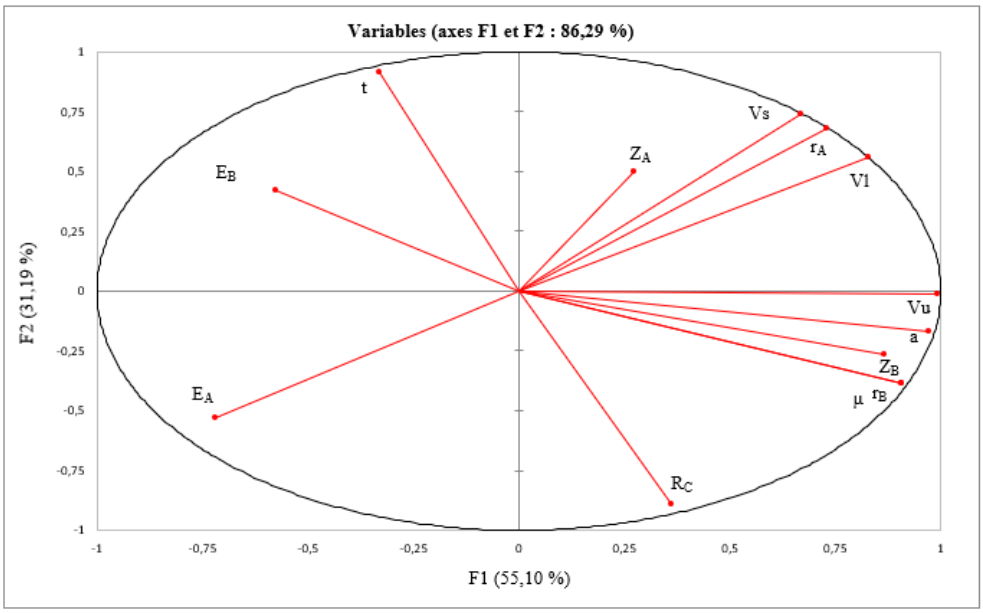

Figure 4.19: PCA loading (F1-F2) plot for oxide perovskites from a dataset of table5.6 including 13 descriptors.

with a small energy differences between valence states. Therefore, we remove from (table. 5.3) all perovskites with these cations such as Mn, V, Cr... On the other hand, we should avoid cation or non-oxygen anion conduction, by the fact that cationic conduction is usually due to univalent ions (alkali metals, Ag) and we have to exclude also halogens which promote non-oxygen anion conduction. We know, that ionic conduction is to some

degree a function of ion size, it can be inhibited by avoiding all small cations or anions of low valence. Therefore, the potential candidates as solid oxide electrolytes should have a large polyvalent cation which are not easily reduced (such as Ba, Bi). Based on all these assumptions we propose on (table. 5.10), the potential candidates as ionic conductors.

4.3.2 Empirical models of the Activation and Migration Energies

It is known that the activation energy of oxygen migration decreases with oxygen lattice bonding energy. Several authors have also shown that perovskite solid electrolytes are also capable of proton transport, as it has observed in perovskite compounds based on $BaCeO_3$, $SrCeO_3$, $BaZrO_3$, and $CaHfO_3$. The activation energy for proton conduction is smaller and proton conductivity is larger in the crystal with a larger lattice parameter [102].

On the other hand, oxygen vacancy formation energy has also been proposed as a descriptor for oxygen diffusion [96, 97, 103]. The results of Mayeshebi and al [104] show that oxygen vacancy formation energy correlates strongly with oxygen migration barrier. While, they suggested that the correlation between migration and vacancy formation energy can be understood physically by the fact, that lower oxygen vacancy formation energy indicates that it is easier to break cation bonds with oxygen, which is a necessary part of the process for migrating an oxygen atom from one position to another. In (table5.11) we display the results of Mayeshebi along with the geometrical other parameters. On the basis of (tables. 5.10 and 5.11), we will try to correlate these geometrical parameters to the oxygen transport in perovskites, through the vacancy content and low oxygen migration barrier. As they are the dominant factors leading to fast vacancy-mediated oxygen transport in perovskites.

We have analyzed the results of Mayeshebi and al [104]. by using the principal component analysis. The resulting scores plot of this analysis is shown in (Fig.4.20). We notice that PC1(F1) captures 44,30% of the variance, whereas PC2(F2) captures 38,39%. The two PCs together capture ~ 83% of the variance of the data in (Table5.11). The reduction in dimensionality makes trends and correlations, which are hidden in the data, become easily visualized and described in PC space as can be seen in (Fig.4.20).

As an interesting observation, perovskite ABO_3 with the same A-cation but a different element B-cation are placed very close together in the score plot (groups of La, Pr, Y). (Fig.4.21)shows the loadings plot corresponding with the samples shown in (Fig.4.20). Thus, from (Fig.4.21), we notice that R_c are inversely correlated to t, The same behavior

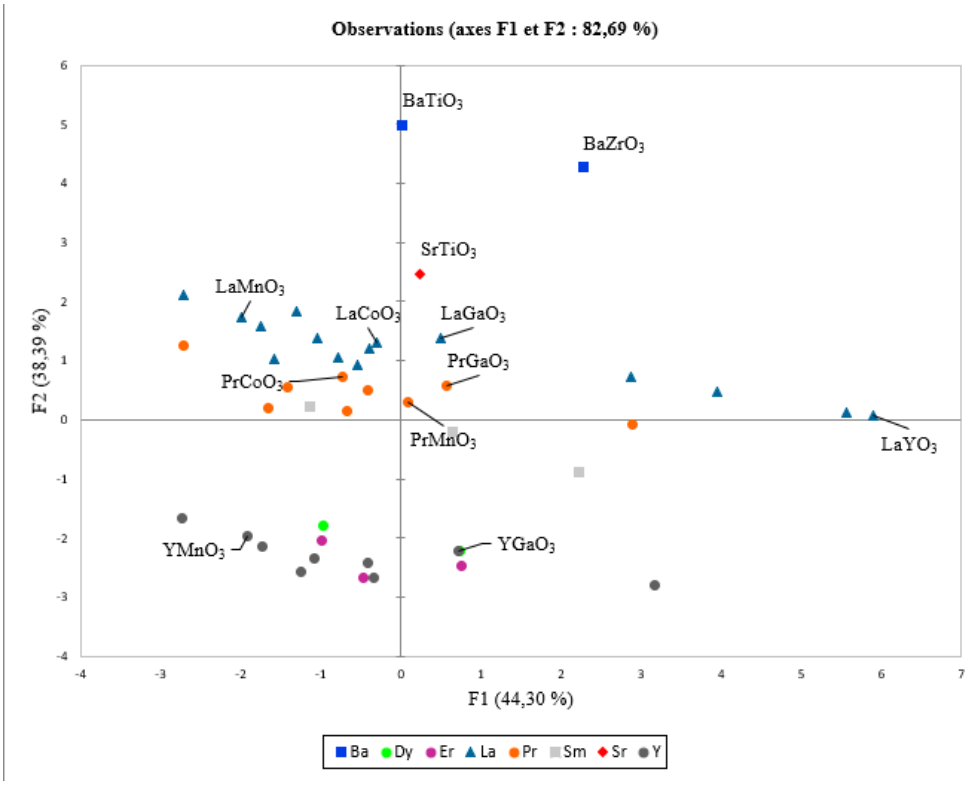

Figure 4.20: PCA score (F1-F2) plot for oxide perovskites from a dataset of table5.11.

is observed for the oxygen migration barrier O_M and the oxygen vacancy formation energy O_B and "a", that means if the lattice constant increases, the O_M decreases and O_B increases. On the other hand, as r_B increases O_B increases and O_M decreases.

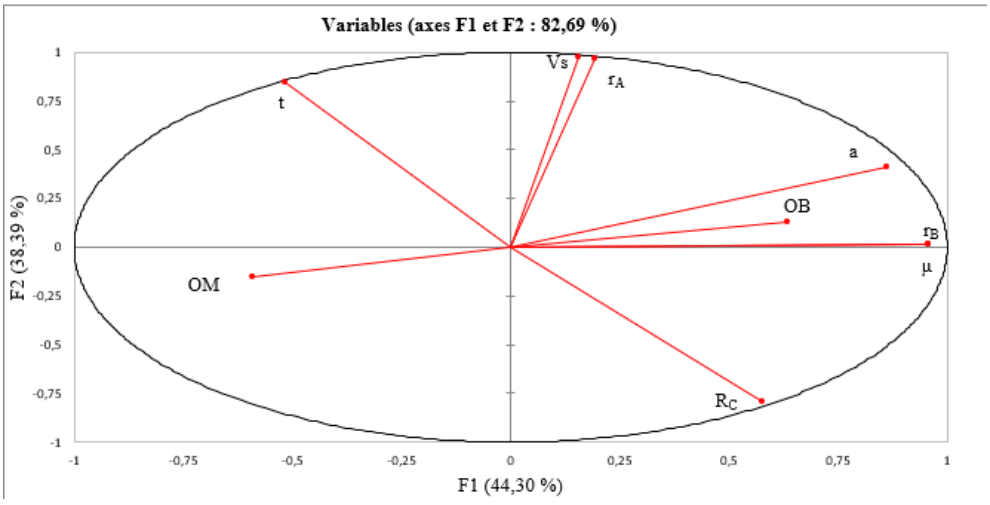

Figure 4.21: PCA loading (F1-F2) plot for oxide perovskites from a dataset of table5.11.

In order to determine the relationships between the oxygen migration barrier O_M and the oxygen vacancy formation energy O_B and the radii of A-site, B-site we use the partial

least square method (PLS) for the perovskites of (table5.11). The predicted model for different groups according whether with the same A-cation or the same B-cation are given by the following equation: For ($BaTiO_3$, $BaZrO_3$, $SrTiO_3$)

$$O_M = +0.468 + 0.964r_A + 0.226r_B + 0.139O_B \tag{4.18}$$

The correlation coefficient between the reported values of Mayeshebi and the values obtain from the above equation is 100%. For the group with the same Y-cation, the equation is:

$$O_M = +2.9E^{+3} + 4.89E^{+2}r_B + 0.27O_B \tag{4.19}$$

The correlation coefficient between the reported values of Mayeshebi and the values obtained from the above equation is 82.39%.

Therefore, through these results we confirm the reported close relationship between the oxygen migration barrier O_M and the oxygen vacancy formation energy O_B as suggested by Mayeshebi and al [104].

Furthermore, we have also search for a relationship between O_M,O_B and the geometrical parameters ($t, R_c and V_s$) for the La and Pr perovskites group according to the series of B-cations. Then, when applying the PLS approach for the series of $LaInO_3$,$LaPbO_3$, $LaRuO_3$, and $LaYO_3$ (transition elements of the 4th line of the periodic table, we obtain the following equations):

$$O_M = 14455.25 + 12209.67t + 9507.89R_C + 1349.07V_S \tag{4.20}$$

$$O_B = +30567.01 + 25825.58t + 20113.2R_C + 2856.06V_S \tag{4.21}$$

The correlation coefficient between the reported values of Mayeshebi et al. [104] and the values obtained O_M the above equations is 100%.

Based on these equations we can predict the O_M and O_B for the all-other remaining transition elements of the 4th line of the periodic table. The results are given in (table. 5.12).

In order to extend our analysis, we have depicted the work of Richter et al [105] and that of Islam [106]. Islam have calculated the migration energies E_M on a series of La compounds ($LaGaO_3$, $LaMnO_3$, $LaCoO_3$, $LaYCO_3$) as displayed on (table. 5.13), although as he said, direct comparison may not be straightforward since the observed

values show significant variation. On the basis of their computed migration energies of (table. 5.13), we have applied a PLS approach in order to define a relationship between these energies and the different anionic radius. The resulting equation is:

$$E_M = +2.77E^{+2} + 1.32r_B \tag{4.22}$$

The correlation coefficient between the reported values of Islam [106] and the values obtained from the above equation is 66%.

This model is used to predict migration energies of other La-based oxide perovskite. The results are presented in (table. 5.14), we notice an excellent agreement with the recently reported data in literature when available. On the basis of these equations, we may anticipate on the prediction of migration energies of other La-based oxide perovskites.

Whereas, Richter et al. [105] show that the conductivity increases with increasing temperature and increasing In-content in Pr-Sr-based perovskites leads to an increasing activation energy (E_a). We know that higher conductivity is associated with lower activation energies and vice versa. However, there is no explanation for this correlation between conductivity and activation energy. On the basis of their measured activation energies of $PrMnO_3$, $PrInO_3$ and $SrMnO_3$, we have again used the PLS technique in order to find a relationship between these energies and the ionic radii of Pr, Sr, Mn and In. The resulting equation is:

$$E_a = +1.118 + 0.664r_A + 0.959r_B \tag{4.23}$$

The correlation coefficient between the reported values of Richter et al. [105] and the values obtained from the above equation is 100%. From this equation may predict the activation energies of other Pr based oxide perovskites. The results are displayed in (table5.12).

Based on the PLS's models (tables. 5.13 and 5.14) from the works of Mayebeshi et al [104], Islam [106] and Richter et al [105], we will try to correlate their results of the activation or the migration energies with t and R_c. We display in (Fig.4.22, 4.23, 4.24, 4.25, 4.26, 4.27, 4.28, 4.29, 4.30, 4.31 8-10), the variation of t and R_c for different oxide perovskites according to their raw position on the periodic table. For the results of Richter, for the perovskites based on Pr and Sr, we notice from (Fig.4.22, 4.23, 4.24, 4.25, 4.26, 4.27), that the activation energy decreases as the tolerance factor tends to 1, whereas it increases as the critical radius R_c increases. Since, higher conductivity is associated with lower activation energies, we may expect that $PrMnO_3$ should have a highest ionic

conductivity and $PrBiO_3$ the lowest one (table. 5.15). Whereas, for the results for those of Islam as displayed on (Fig.4.28, 4.29, 4.30), we notice that the migration energy increases as the tolerance factor decreases, and it decreases as the critical radius increases. The highest migration energy is for $LaBiO_3$ and the lowest is for $LaCoO_3$. Finally, for the Mayeshebi work the corresponding results are displayed on (Fig.4.31), there is no observable correlation between the migration energies and t or R_c. We may conclude, that despite different works on high ionic conductivity of oxide perovskites a relationship between activation energy and the crystallographic criterion has never been theoretically investigated, and the underlying fundamental issues are unclear. The only issues in order to predict a possible high ionic conductor are empirical and based on mining the different available data.

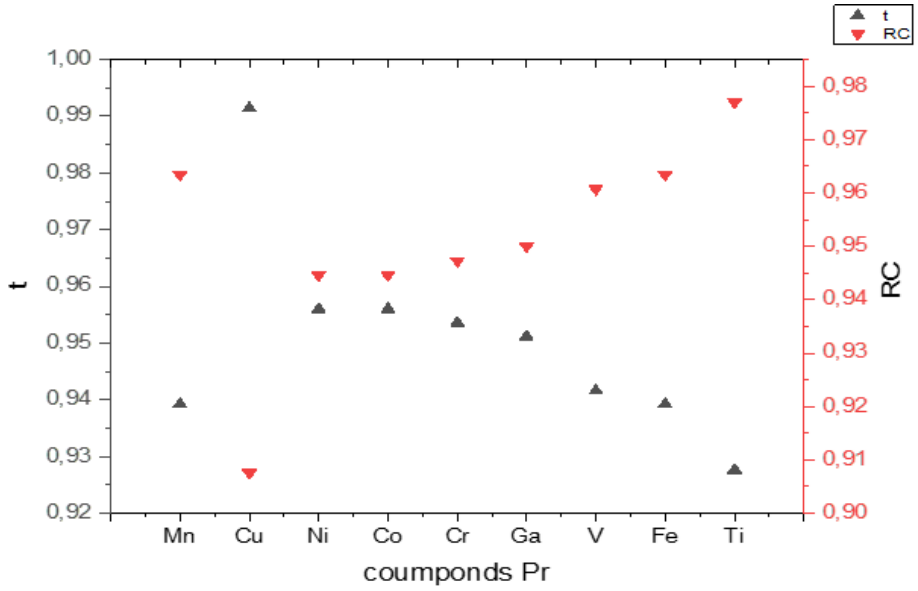

Figure 4.22: the variation of tolerance factor "t" and the critical radius "Rc" for the "Pr-Based perovskites of 3rd raw of the periodic table".

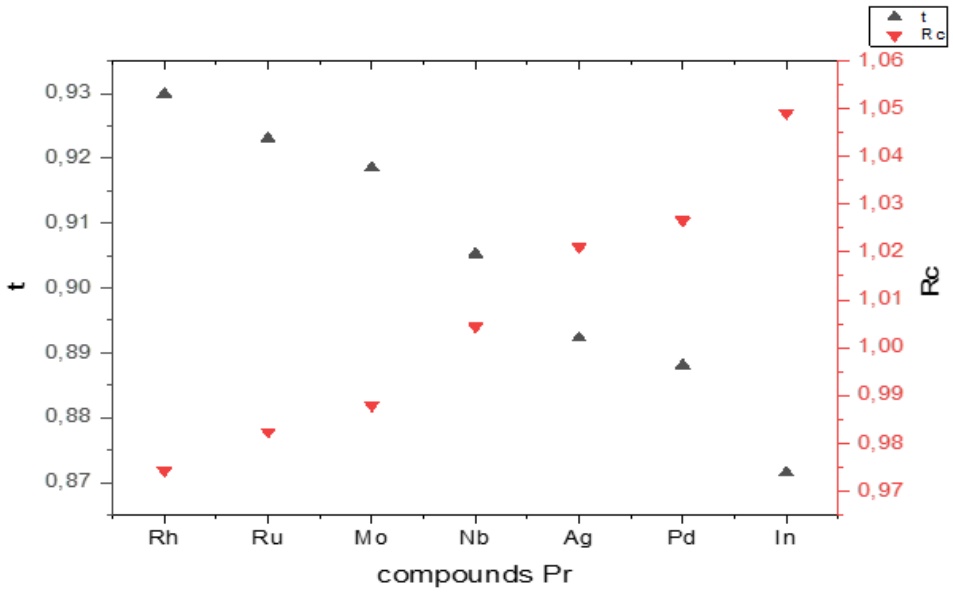

Figure 4.23: the variation of tolerance factor "t" and the critical radius "Rc" for the "Pr-Based perovskites of 4th raw of the periodic table"

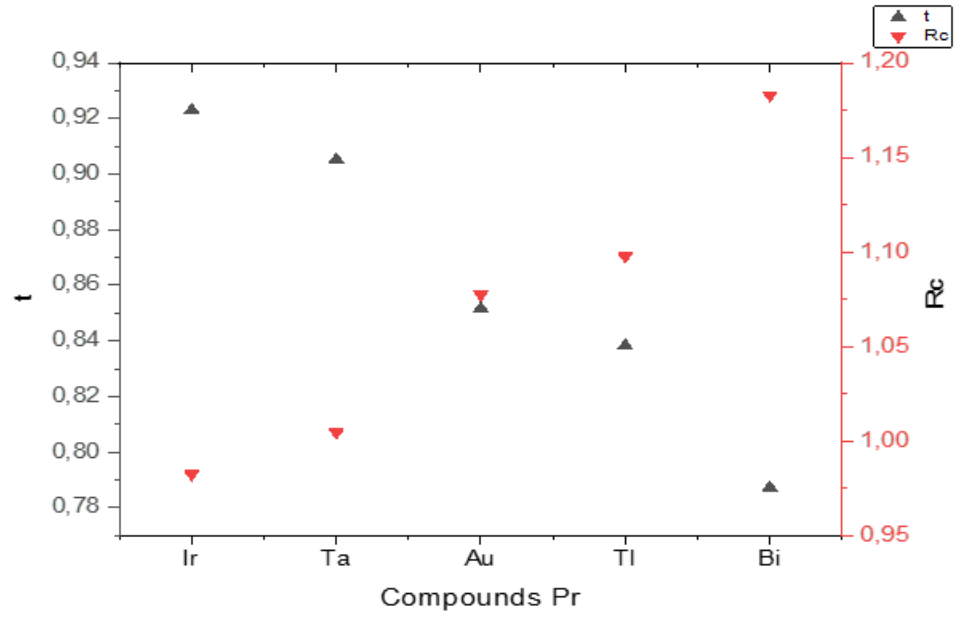

Figure 4.24: the variation of tolerance factor "t" and the critical radius "Rc" for the "Pr-Based perovskites of 5th raw of the periodic table".

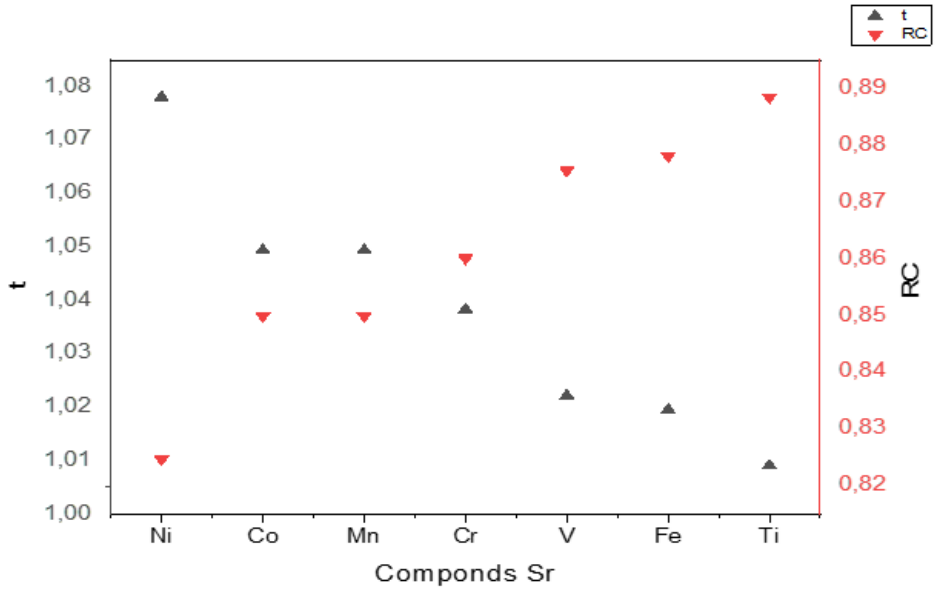

Figure 4.25: the variation of tolerance factor "t" and the critical radius "Rc" for the "Sr-Based perovskites of 3rd raw of the periodic table"

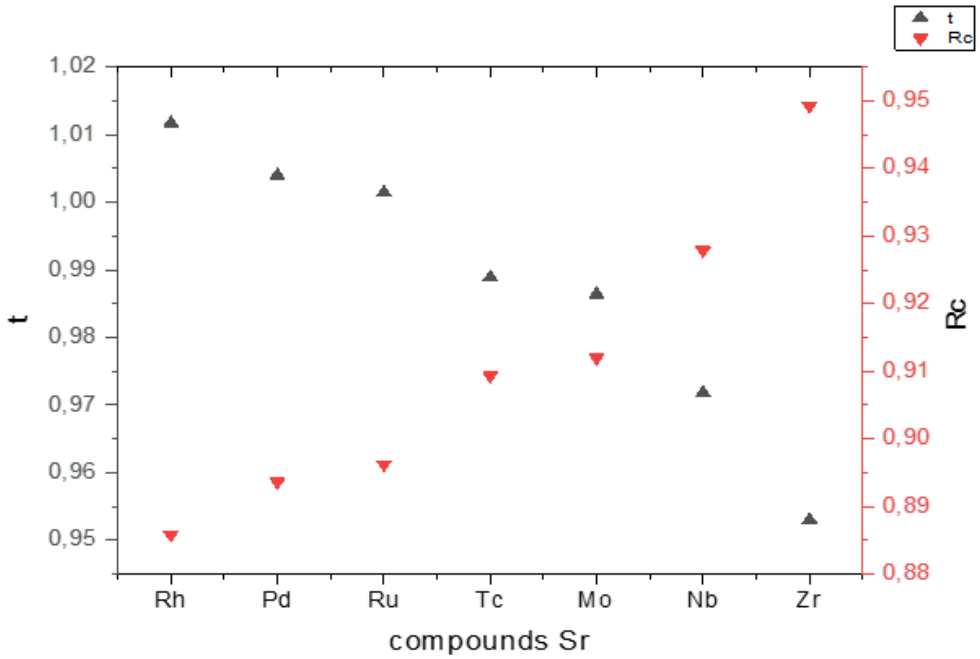

Figure 4.26: the variation of tolerance factor "t" and the critical radius "Rc" for the "Sr-Based perovskites of 4th raw of the periodic table".

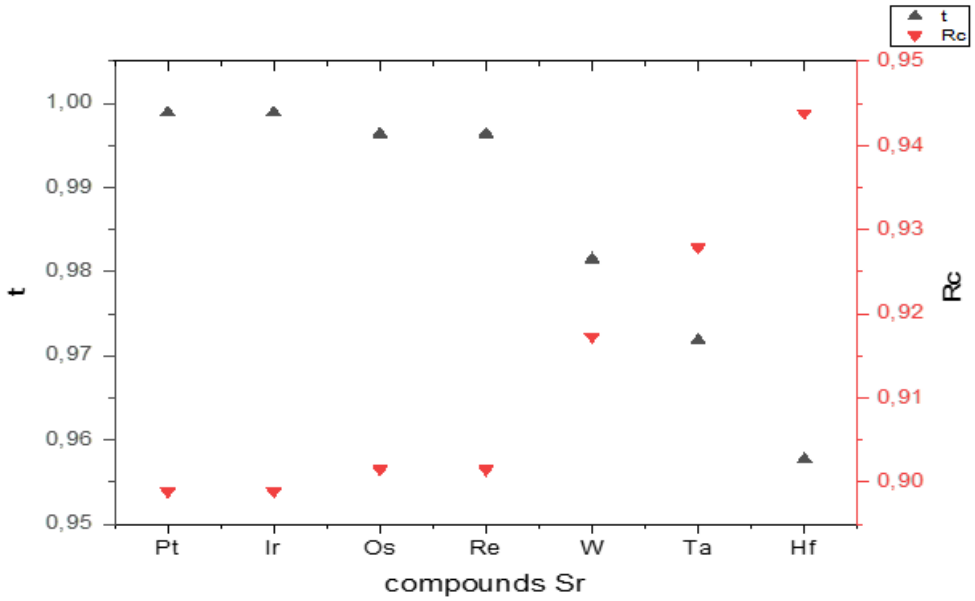

Figure 4.27: the variation of tolerance factor "t" and the critical radius "Rc" for the "Sr-Based perovskites of 5th raw of the periodic table".

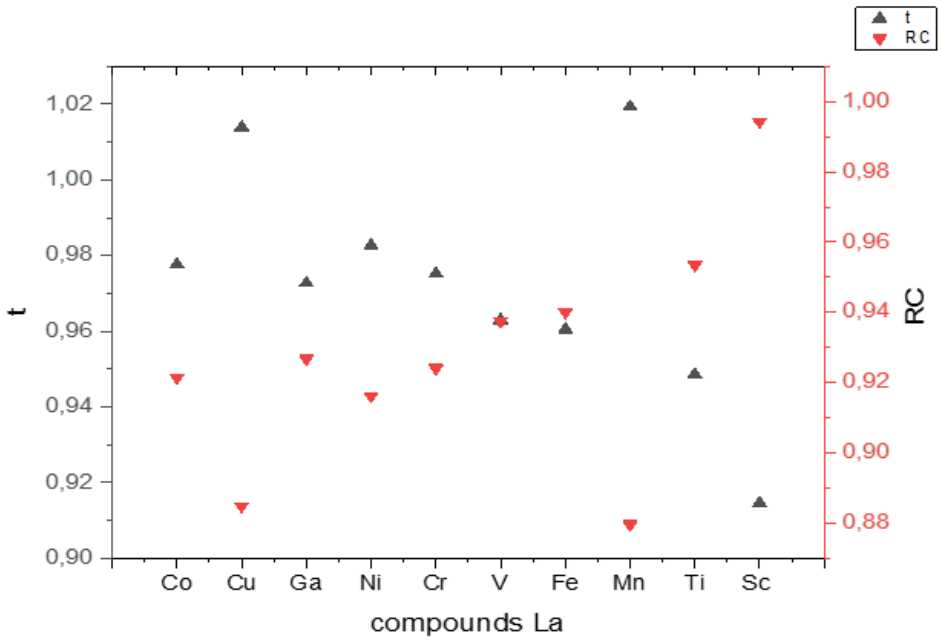

Figure 4.28: the variation of tolerance factor "t" and the critical radius "Rc" for the "La-Based perovskites of 3rd raw of the periodic table".

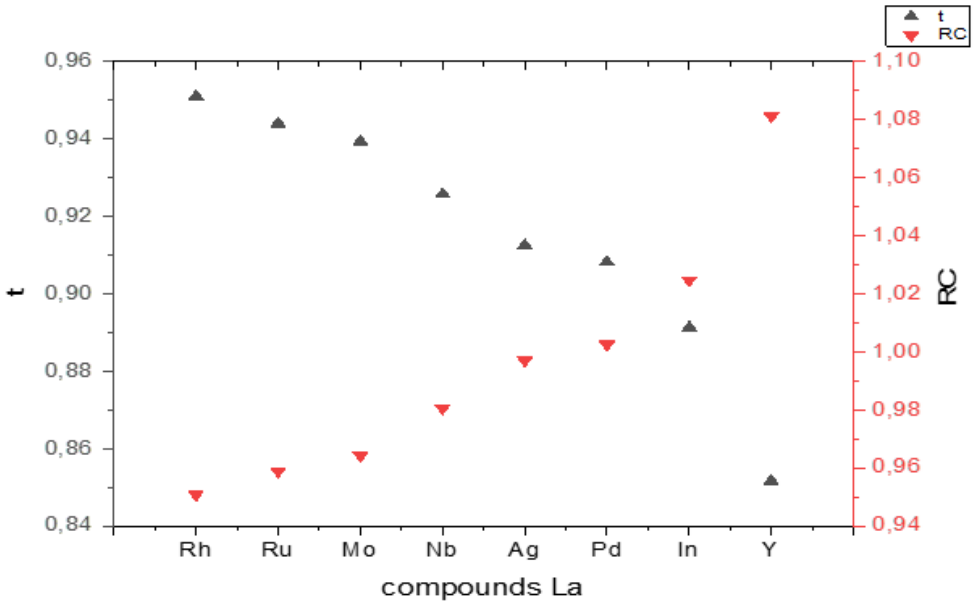

Figure 4.29: the variation of tolerance factor "t" and the critical radius "Rc" for the "La-Based perovskites of 4th raw of the periodic table".

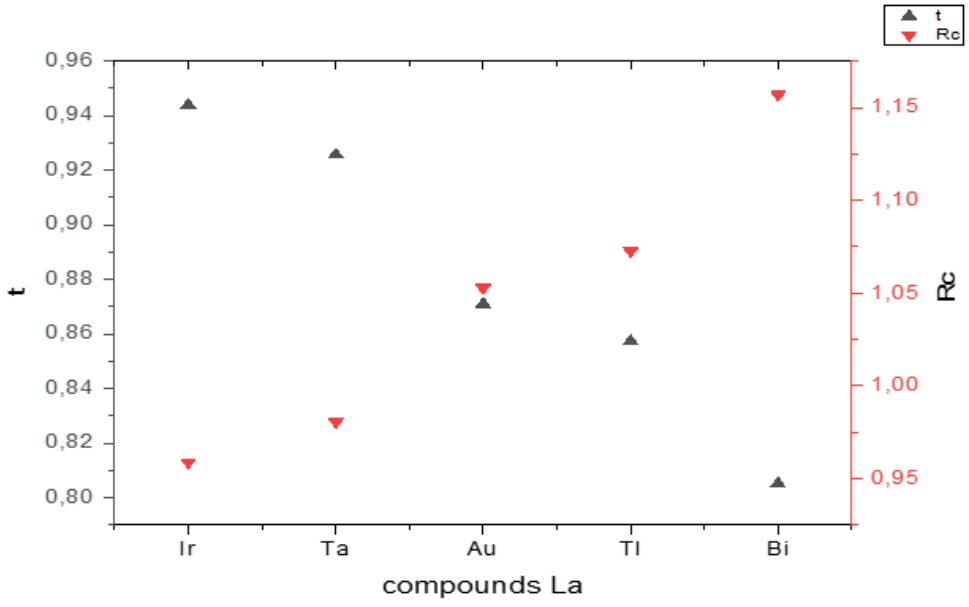

Figure 4.30: the variation of tolerance factor "t" and the critical radius "Rc" for the "La-Based perovskites of 5th raw of the periodic table".

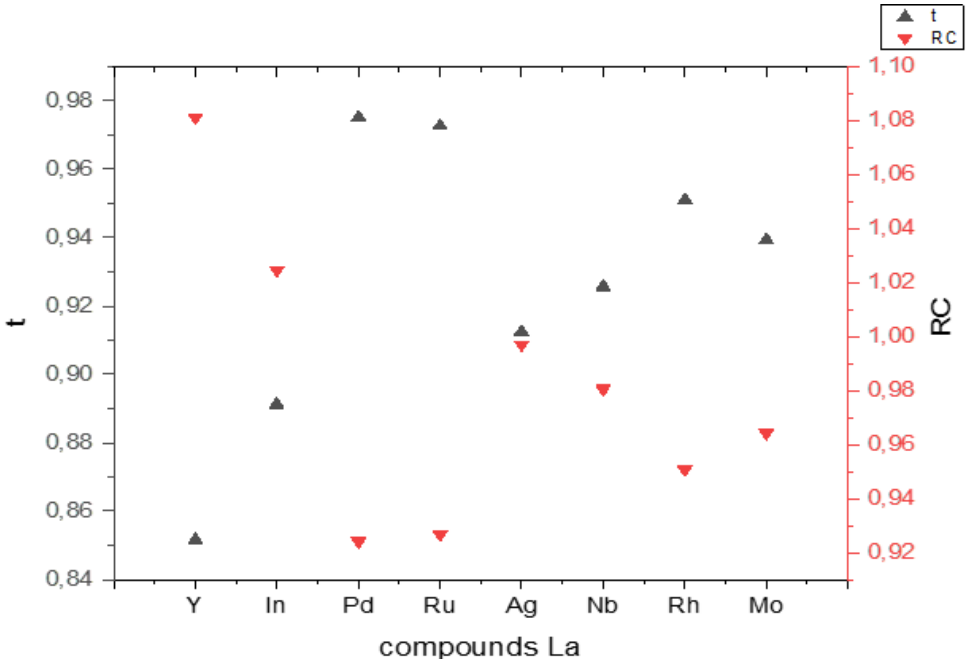

Figure 4.31: the variation of tolerance factor "t" and the critical radius "Rc" for the "La-Based perovskites of 4th raw of the periodic table".

4.4 Double Halide Perovskite

We selected a class of compounds of composition A_2BX_6, on which little structural research has been done and which have structures closely related to a class of compounds of composition ABX_3, which have been the subject of extensive research. In the present paper certain assumptions will be used. Our work is based on some rules derived from a simple ionic model, which has been shown to explain a great many structures of compounds ABX_3. The structures derived in the present paper will be compared with the structures of the ABX_3 halides. Also, semiempirical rules will be derived for making the selection of a structure for a particular compound possible. These rules will be checked against the vast number of experimental structural data on ABX_3 halides.

First, we will try to respond to this question: Is it possible to design a double halide perovskites A_2BX_6 from only the structural information of ABX_3 perovskites?

However, despite such difficulty in identifying a correct condition of formability, it would still be interesting to perform a more systematic investigation of the potential/-efficiency of the available dataset on double halide perovskites through an intuitive and accessible manner. Thus, one particularly important technique is the PCA regarding its efficiency for simplifying, through decorrelation, data sets typically found in the real-world or simulations. PCA is a classification method which projects the spatial data into

a set of principal components (PC) and maps the data on a dimensionally reduced space. The PC capturing the most information is associated with the eigenvalue corresponding with the largest eigenvalue of the covariance matrix of the original dataset. All PC's are orthogonal to each other, and thus each capture unique information. The advantage of PCA is that typically a few PC's are sufficient for describing a system, and a dataset of n-dimensions can be reduced to a few dimensions with minimal loss of information. The PC's do not necessarily have an obvious physical meaning, but rather are a combination of variables which explain the largest variation in the data. The reduction in dimensionality makes trends and correlations which are "hidden" in the data to become easily visualized and described in PC space. PCA decomposes the original data matrix into the scores and loadings matrices, where the scores values classify the samples and the loadings values classify the descriptors in terms of their separation of the samples. The correlations among the descriptors become obvious in a PCA analysis, and by defining the correlations in the data, we can then reduce the number of descriptors to a minimum to permit a more convenient data analysis.

In (table. 5.16) we have collected structural information on some ABX_3 and their related A_2BX_6 ($r_A, r_B^{+2}, r_B^{+4}, r_X, a^{+2}, a^{+4}, t^{+2}, t^{+4}, \mu^{+2}$ and μ^{+4}). The CN's of the ions in Table5.16 for ABX_3 structure are 12, 6 and 6 for A^+, B^{+2}, X^+, respectively. Whereas for A_2BX_6 structures are 12, 6, and 6 for A^+, B^{+4}, and X^+, respectively.

We display in (Fig. 4.33) the loadings plot of the PCA method, which it represents the variance among descriptors. When two vectors are close, forming a small angle, the two variables they represent are positively correlated. If they meet each other at $90°$, they are not likely to be correlated. When they diverge and form a large angle (close to $180°$), they are negative correlated. It's known also that properties near the origin are not important, whereas those far from the origin are the more dominant. The relative impact of each descriptor in a loading score is identified by measuring the absolute distance from the origin. The impact of the descriptors is increased as its distance from the origin is increased. We notice from (Fig. 4.33), that the lattice constants for A_2BX_6 "a^{+4}" are highly correlated to the lattice constants of ABX_3 "a^{+2}", and also the different t andμ behave in the same manner.

We have calculated the lattice parameter of A_2BX_6 as twice ($2 * a^{+2}$) of that of ABX_3, the results are compared with the lattice parameter (a^{+4}) reported in the ICSD database (Table. 5.17). We notice a quite interesting matching, since the error do not exceed 7%. We may then as a first approximation predict roughly the value of the lattice constant

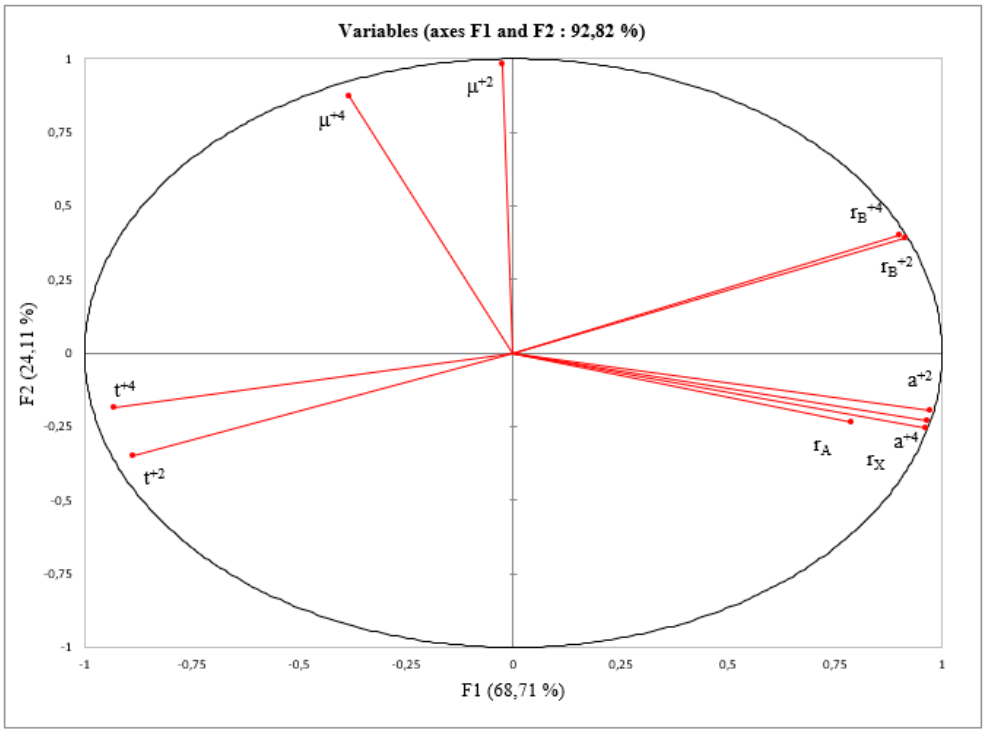

Figure 4.32: PCA loading (F1-F2) plot for a dataset of table5.16 corresponding for B^{+2} (r_B^{2+}) and B^{+4} (r_B^{+4}).

of any A_2BX_6 from the corresponding ABX_3 compounds. On the other hand, we have plotted on (Fig.4.34) the variation of the tolerance factor t with the octahedral factorμ for the ABX_3 (red dot) and A_2BX_6 (bleu dot). We notice clear shift towards larger "t" and smallest "μ " for the A_2BX_6 comparatively with the ABX_3. For example, if ABF_3 are within the range of cubic perovskites, the A_2BF_6 have a very high "t", which suggest that whether they crystallize in hexagonal structure or they are not perovskites. On the other hand, almost all the A_2BX_6 have μ <0,41. This difference is mainly due to the size of the B-cation radius, since the B-radius for ABX_3 corresponds to charge +2 and that for A_2BX_6 with a charge +4.

4.4.1 Determination of the lattice parameter

The initial data set used are presented in (Table5.18). Altogether, the total number of samples used for the model development consists of 78 cubic double halide perovskites, each with 13 predictor variables ($r_A, r_B, r_X, E_A, E_B, E_X, (r_A + r_X), (r_B + r_X)$, $(E_X + E_A), (E_X + E_B), t$,and a). In terms of the anion composition, the dataset consists of 35 chlorides, 16 bromides, 18 fluorides, and 9 iodides. The CN's of the ions in the (table. 5.18) for A_2BX_6 structures are 12, 6, and 6 for A, B, and X, respectively.

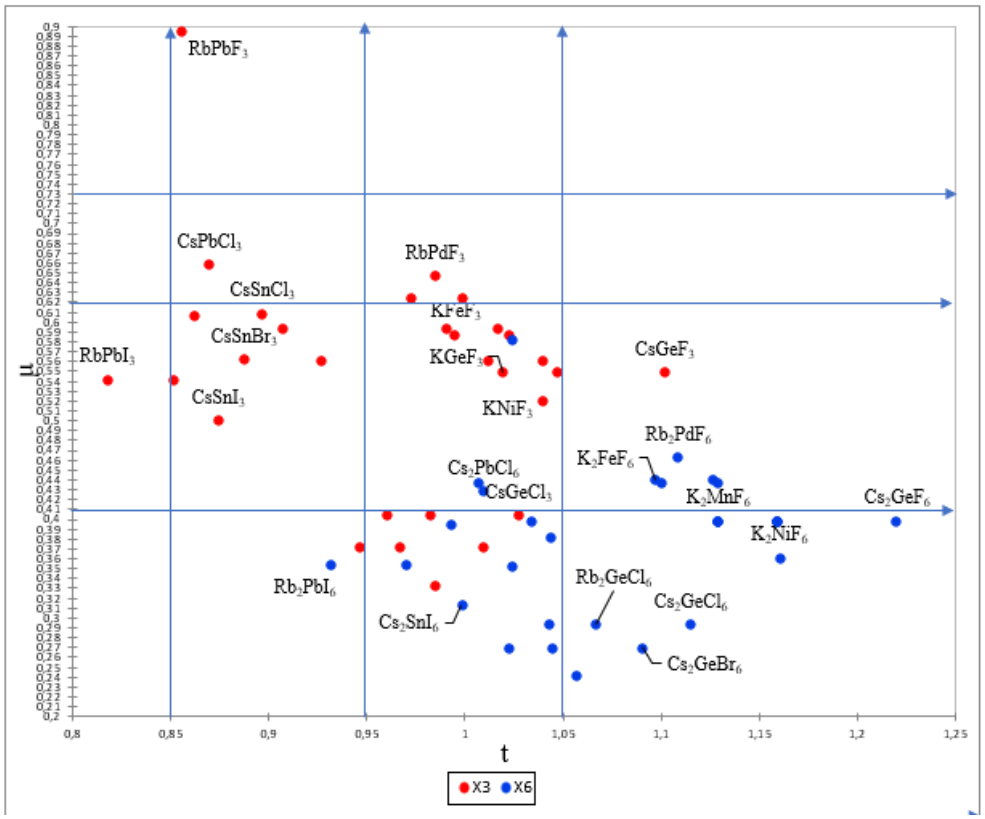

Figure 4.33: The variation of the tolerance factor versus the octahedral factor for the compounds of table5.16 .

The knowledge of lattice constants of unknown double halide perovskites is necessary for analyzing their structures and properties. Several empirical models were established that can predict lattice constant of perovskites from selected atomic properties of their constituent elements. Among them that developed by Brik and Kityk [108] and Sidey [109], which allows one to predict the lattice constant of double perovskites by using the known ionic radii and the electronegativities of the cation and anion.

We will use two sums of ionic radii $(r_A + r_X)$, $(r_B + r_X)$ and two differences of electronegativities $(E_X + E_A)$, $(E_X + E_B)$. The choice of these variables seems to be quite natural, since both A and B ions are surrounded by the X ions. The sum of ionic radii of two neighboring ions can be taken as an interionic separation. This is, of course, an approximation only, since it is based on a model representing both atoms as rigid incompressible spheres. The difference of electronegativities of two neighboring ions is a characteristic of degree of ionicity (covalency) of the chemical bond: the greater the difference, the more ionic the bond.

In this work, the relationships between the lattice parameter (a) and the radii of A-site,

B-site and X-site and the respective electronegativities are calculated by the using the partial least square method (PLS) for double halide perovskites [12–22].

Partial least squares regression (PLS regression) is a statistical method that bears some relation to principal components regression; instead of finding hyperplanes of minimum variance between the response and independent variables, it finds a linear regression model by projecting the predicted variables and the observable variables to a new space.

The prediction was performed on the basis of the datasets of (Table5.18), named as the test set. Using PLS, we connected the matrix X of predictor variables with the matrix Y of predicted (response) variables. The SIMPLS algorithm and leave-one-out method were used for cross validation in PLS. In other words, without any information on structural properties of the double halide perovskite in the test set (Table5.18), it was possible to predict these quantities using the prediction model for the training set (experimental and theoretical lattice constants available in the literature). The predicted model is:

$$a = +0,204 + 2,156(r_A + r_X) + 0,939(r_B + r_X) + 0,110(E_X + E_A) + 0.044(E_X + E_B) \tag{4.24}$$

The correlation coefficient between the literature reported values of "a" and the values got from the above equation is more than 98,43%

$$a = 0,51 + 2,134(r_A + r_X) + 0,802(r_B + r_X) \tag{4.25}$$

The correlation coefficient between the literature reported values of "a" and the values got from the above equation is more than 98,66%

Before we can apply equation4.25 to a set of unknown compounds, it was first tested on our training data set. (Fig.4.34) shows predicted against calculated values of "a", for the training set. The values predicted for the test set are in good agreement with the training set (tables5.19).

Once again (Fig.4.34) demonstrates the robustness of the analysis using the training dataset (Table5.18).

We compare, these results with the loadings plot of the PCA method (Fig.4.35). We notice from (Fig.4.35), that the lattice constant "a", "r_B", E_B (electronegativity of B) and "μ" are the less dominant parameters compared to the other descriptors. This is what we observe on equation 4.24, since the parameter associated with $(E_X + E_B)$ is "0,044"

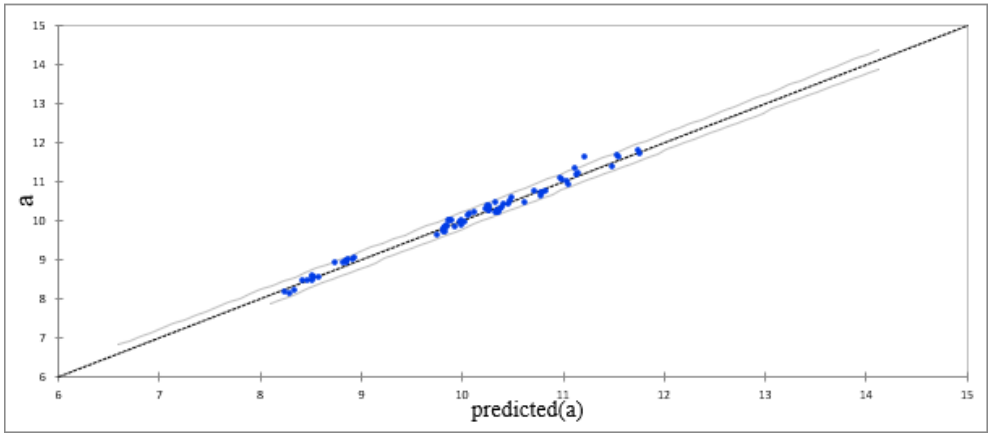

Figure 4.34: PLS results for the predicted lattice constants versus the measured one for the oxide perovskites.

which is small comparatively to the parameter associated to $(E_X + E_A)$ "0.110".

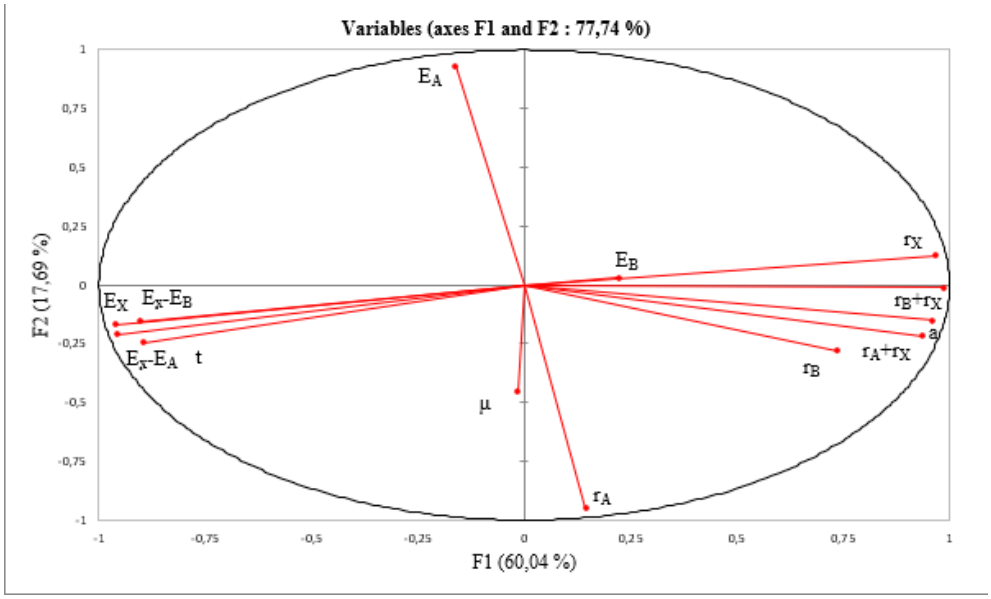

Figure 4.35: PCA loading (F1-F2) plot for a dataset of table5.18.

On the other hand, we observed that the electronegativities E_X, and E_A and the atomic radius r_X and r_A are on opposite direction, respectively, this means that if the atomic radius increases the electronegativity decreases. In contrast, it seems that E_B and r_B behaves in the same manner. On the other hand, "t" and "μ " meet each other at 90, then they are not correlated, whereas "t" is highly correlated to E_x and E_A and inversely correlated to r_X , r_B and "a".

We have developed a datamining approach for predicting the lattice parameter of the

double halide perovskite. However, we are not able to predict whether the formation of any combinations of these compounds is possible or not?

4.4.2 Formability of double halide perovskites

Importantly, the applicability of "t" and "μ" factors for A_2BX_6 double halide perovskites have never been extensively studied and so far, limited [110–112]. These studies of the geometrical factors are limited to $A_2B^{'}B^{"}X_6$. [110–112]. As a result, it limits their synthesis and study to a labor-consuming trial and error approach. Reducing the complexity of the choice and limiting the number of compounds potentially interesting for valuable applications are a reason to reexamine these geometrical conditions for the formability of double halide perovskites.

The initial data set used are presented in (Table5.18). Altogether, the total number of samples used for the model development consists of 119 cubic and non-cubic double halide perovskites, each with 8 predictor variables ($r_A, r_B, r_X, E_A, E_B, E_X, t, \mu$). In terms of the anion composition, the dataset consists of 43 chlorides, 18 bromides, 44 fluorides, and 14 iodides. The CN's of the ions in (Table5.18) for A_2BX_6 structures are 12, 6, and 6 for A, B, and X, respectively. The resulting scores plot of this analysis is shown in (Fig.4.36). The objective of the present analysis is to use the present knowledge about double perovskites to determine the formability of these compounds. PCA is used to assess the correlation between each of the descriptors input into the regression analyses and the stability of the compounds. The results of these analyses can then be compared with the predictive models to understand the physics and limitations of the models. The PCs do not necessarily have an obvious physical meaning, but rather are a combination of descriptors which explain the largest variation in the data. The advantage of PCA is that, since each PC uniquely captures the effect of a certain combination of relevant descriptors, typically a few PCs are sufficient for describing a system.

We notice that PC1(F1) captures 54,88% of the variance, whereas PC2(F2) captures 20,09%. Therefore, a dataset of n-dimensions (8 initial descriptors in this case) can be reduced to two dimensions (2 PCs) while capturing ~ 75% of the original information. The reduction in dimensionality makes trends and correlations, which are "hidden" in the data, become easily visualized and described in PC space as can be seen in (Fig.4.36). From this figure, it appears two important clustering, it corresponds to cubic perovskites (red dot) and non-cubic perovskites (bleu dot). Therefore, the values of PC1's clearly distinguish between the different structures of double halide perovskites. We observe also two different group, those corresponding to fluorides, and another corresponding to iodides,

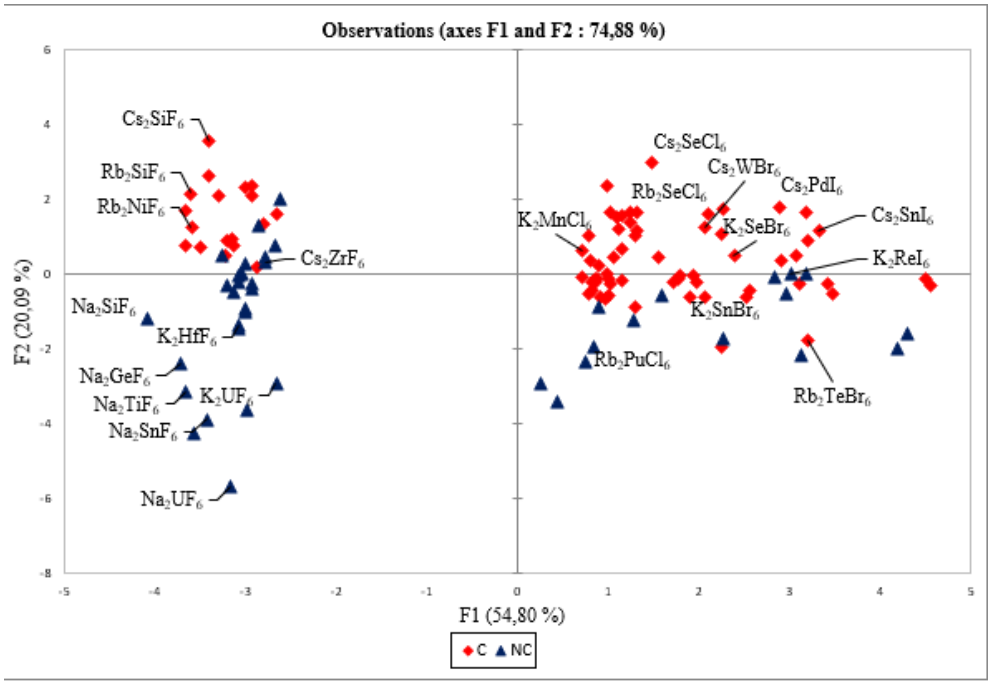

Figure 4.36: PCA score (F1-F2) plot for double halide perovskites from a dataset of table5.18.

chlorides and bromides. The PCA clearly separates between compounds with a high and low electronegativity of the anion.

We have plotted on (Fig.4.37) the variation the lattice parameter versus the tolerance factor for only the cubic double halides, we clearly distinguish four zones, according to the nature of X atom. Since those with the largest lattice parameters are the Iodide and those with the lowest "a" are the fluoride. We may conclude that as the electronegativity of the X atom decreases (or the value the ionic radii increases) the value of the lattice parameter of the double halide perovskites increases. On the other hand, for the same group of the double halide perovskites, as the value of ionic radii of the A-atom increases the lattice parameter increases. We notice also, that the largest tolerance factor for cubic double perovskite is Cs_2SiF_6, and the lowest one is Cs_2PoI_6. These trends are clearly observed on the PCA's score plot (Fig.4.36), as Cs_2SiF_6 has le lowest PC2 and Cs_2PoI_6 has the largest PC1. Therefore, from to PCA results we may have an insight on the formability all halide double perovskites according to their position on the score plot PC1-PC2.

In 1964, Brown considered the size of the A site cavity in the A_2BX_6 in double perovskite structure, and empirically predict the formation and distortion of the crystalline structure in vacancy-ordered double perovskites A_2BX_6 on the basis of the ratio of the

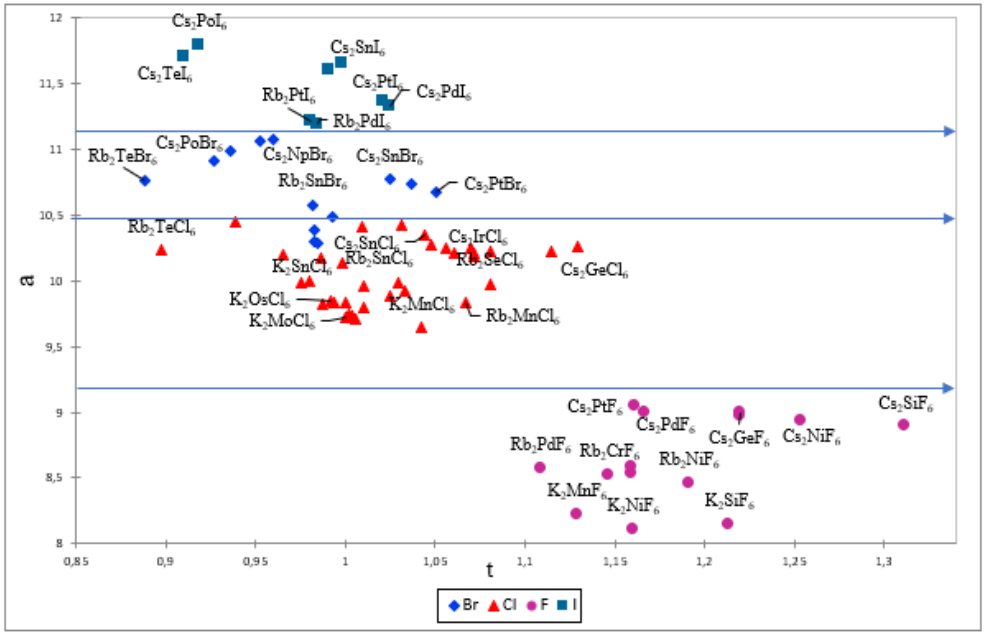

Figure 4.37: The variation of the tolerance factor versus the lattice parameter for the double halide perovskites of table5.18.

cavity size to the A site ionic radius [113]. This radius ratio "R" is defined as:

$$R = r_A/(D_{XX} + r_X) \tag{4.26}$$

Where D_{XX} is the nearest neighbor X-X bond length as calculated for the cubic phase.

Jong et al [114] demonstrate that the octahedral factor "μ " and radius ratio "R" decrease on going from X=Cl to X=I, implying that as the ionic radius of the halogen anion increases, the perovskite structure undergoes octahedral tilting and accordingly its symmetry is lowered from the cubic structure to a lower-symmetry structure at room temperature.

When 0.89 < R < 1, no octahedral tilting is expected at room temperature. Smaller A-site cations yield R < 0.89, and the octahedral framework will undergo cooperative tilting to optimize coordination to the A-site cation.

We have calculated the tolerance factors and the octahedral factor for the 78 cubic double halide perovskites and the 41 non perovskites compounds as shown on (Table5.18). We have plotted on (Fig.4.38) the variation of the tolerance factor versus the octahedral factor. As can be seen in (Fig.4.38), all 119 (cubic and non-cubic) compounds fall within the range $0,866 \leq t \leq 1,31$ and 0,276<μ <0,706. We notice no clear separation between

the cubic and non-cubic double for all halides as in the case of ABX_3. We observe a very high "t" for fluorides, presumably because of the greater ionicity of the fluorides, and almost all the cubic perovskites have "μ " below 0,41. This behavior highlights an important difference between the A_2BX_6 cubic double halide perovskites and the ABX_3 cubic perovskites. Since, in ABX_3, the corner sharing connectivity of the BX_3 framework fixes the size of the A site cavity for a given B-X bond length; it is this restriction that gives rise to Goldschmidt's tolerance factor equation. Whereas, in double halide perovskites, the fact that the BX_6 octahedra are not connected means that the separation between them, and thus the size of the A site cavity, can change independently of the size of the octahedra themselves.

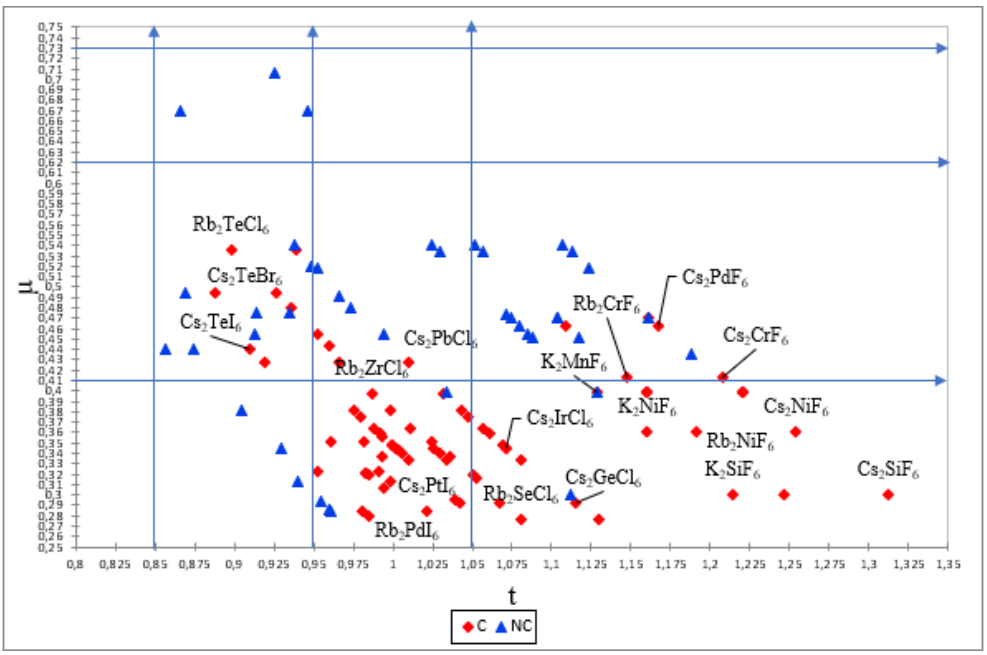

Figure 4.38: The variation of the tolerance factor versus the octahedral factor for the double halide perovskites of table5.18.

We know for oxides that the cubic perovskite structure could be maintained for 0,95 <t < 1,04. As "t" decreases from 1, the perovskite structure deforms towards structures with lower coordination for A. The transition from orthorhombic (0,76 < t < 0,88) to cubic (0,88 < t < 1,003) to hexagonal (1,05 < t < 1,3) is consistent with the increase in the tolerance factor t for each compound as the size of A increases, this very simple hard-sphere concepts is quantitatively much more successful for fluorides than oxides, presumably because of the greater ionicity of fluorides. The majority of the hexagonal perovskites contain large alkali or alkaline-earth metals on the A-site and transition metals on the B-site and could be explain by metal-metal bonding.

We conclude that the results of formability give false non-cubic perovskites, and more

false positives cubic perovskites (according to the data reported in the Inorganic Crystal Structure Database "ICSD" [115]). Therefore, we may attribute these anomalies to the non-reliability of the data reported in the ICSD database [115], because of the unavoidable human and measurement, those data require further preprocessing to make them more reliable and should include all the formability information (reflected by the different ICSD numbers for one compound in the ICSD). As it has also been observed by Xu et al [116] that for a given formula $M^1M^2X_3$ (M^1 and M^2 are cations), it is important to identify which one of M^1 and M^2 is A or B, in particular for some double halide perovskites. We should not forget that the fitting of the halogen into a scheme also accounts for all the halides is difficult. In perovskite, A and B have 12 and 6 coordination, respectively. However, in tilt perovskite, the coordination number of A can be largely reduced. We assume that the octahedral coordination of B is a critical sign for the perovskite phase.

We have assessed numerous other structures mapping schemes, including taking into account electronegativity as Brik and Kityk [108], yet we have found no better solution that is still based on geometry.

In order to take into account this difference Cheng et al [117] derive a set of formability rules by defining four limiting models, and by comparing the lattice parameters calculated with the experimental values from the Inorganic Crystal Structure Database (ICSD) they identify changes in the crystal chemistry that occur across the range of compositions that form A_2BX_6 structures. However, they have mentioned, that the tolerance factor is a necessary but not a sufficient condition for the formation of these systems. A first approach suggested by these authors is to include in the discussion the values of the octahedral factor μ =rB/rX. As we know the lowest limit of the octahedral factor for cubic perovskite formation is 0,414 and the highest value of cubic perovskites is 0,6785. The results of Cheng et al [117] demonstrate that A_2BX_6 compounds may have an octahedral factor far below 0.41.

The explanation for this difference in formability between ABX_3 and A_2BX_6 is probably that in the cubic A_2BX_6 structure, each anion coordinates to only one B site cation, i.e., is only part of one BX_6 octahedron. This allows the six anions of an octahedron to overlap with each other in order to coordinate a small B site cation without affecting the coordination of the neighboring B site. Whereas, in the ABX_3 perovskites, each anion forms bonds to two B site cations, so cannot move to coordinate a smaller B site without lengthening the bond to the other B site cation to which it coordinates. Thus, it appears that the reason for adherence to the rule of μ > 0,41 for ABX_3 perovskites is not that

the anions are forbidden from overlapping, but that they must each bond to two B site cations. The lifting of the latter requirement in the cubic A_2BX_6 compounds allows μ values considerably less than 0,41. Consequently, we may define for each different X-anion in double halide perovskites its proper conditions of formability. Thus, we have plotted in (Fig.4.42) the variation of "t" with "μ " for different X-anions.

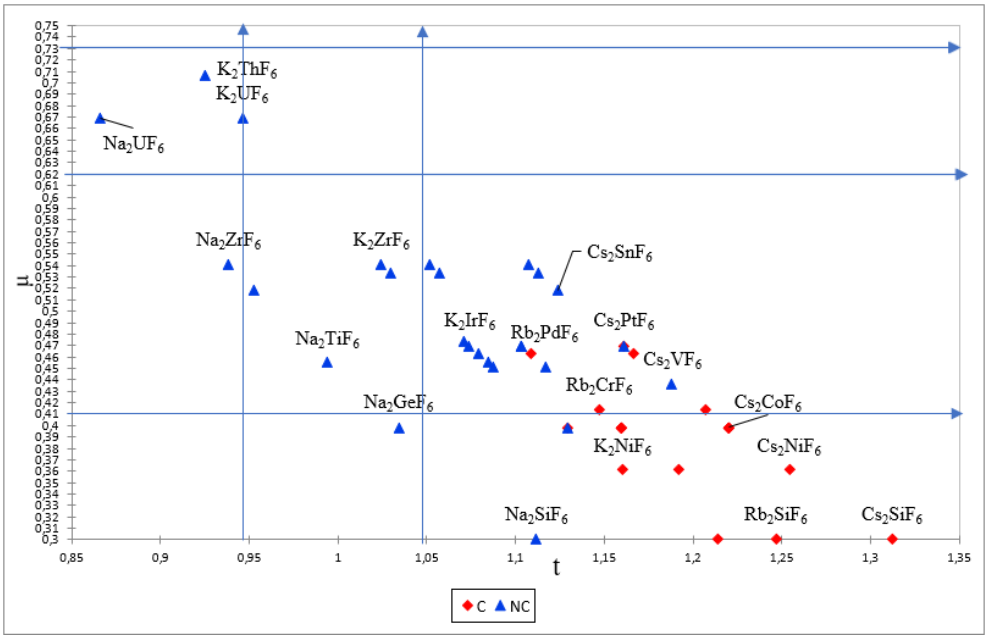

Figure 4.39: The variation of the tolerance factor versus the octahedral factor for the double fluoride perovskites of table 5.18.

Since for overall double halide perovskites the prediction of formability gives few false positives for heavier halides, and more false positives for fluorides. It seems that fitting the fluorides into a scheme that also accounts for all the other halides is difficult. We may therefore define for each group of halides a formability range as seen on (Fig.4.42). We propose then, that the limit of "μ " for the formability for all the double halide perovskites should be >0,25, whereas for the tolerance factor, for Fluorides 0,85<t<1,33, Chlorides 0,85<t<1,11, Bromides 0,85<t<1,05 and Iodides 0,85<t<1,04.

We conclude from the above analysis that having a tolerance factor and an octahedral factor within a specific range (calculated from traditional Shannon radii) may be a necessary condition for perovskite formation but it is not a sufficient condition, and the traditional approach that works reasonably effectively for oxide perovskite compounds cannot be used to explain the known structures of double halide perovskites.

A question then presents itself: is it possible to use the Shannon radii and the ge-

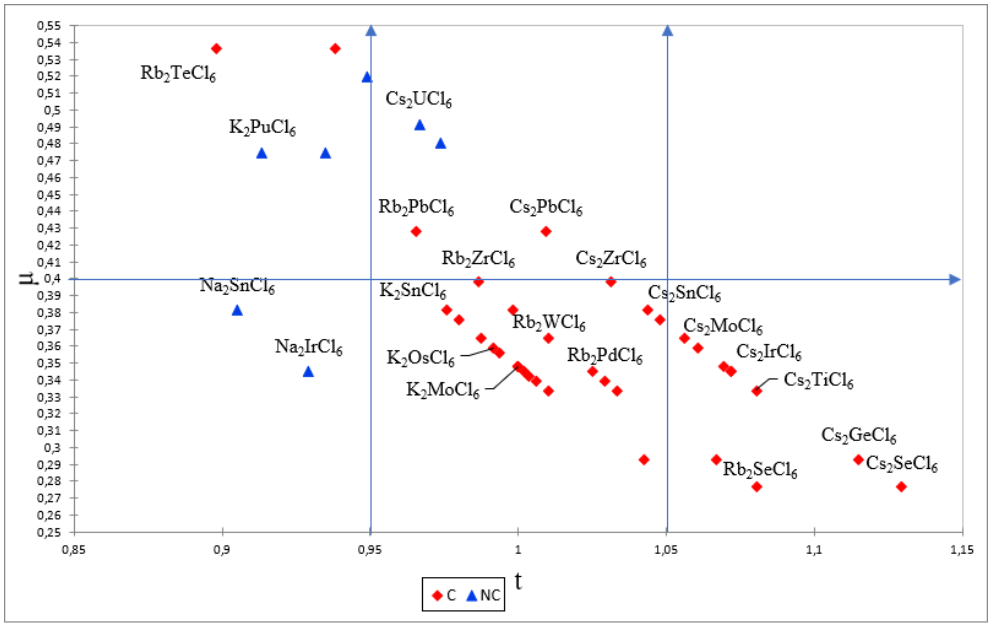

Figure 4.40: The variation of the tolerance factor versus the octahedral factor for the double chloride perovskites of table5.18.

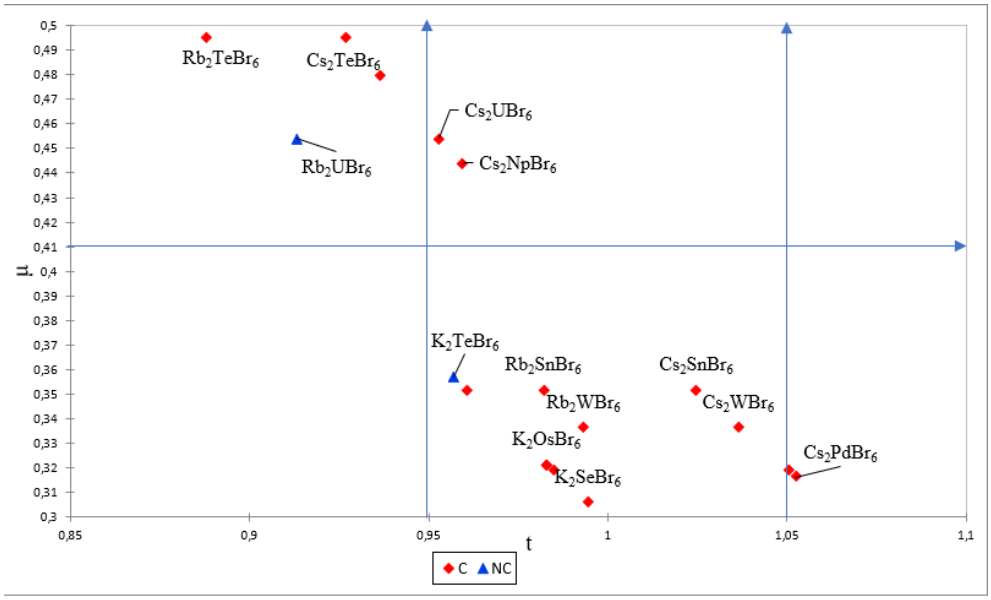

Figure 4.41: The variation of the tolerance factor versus the octahedral factor for the double bromide perovskites of table 5.18.

ometric methods to understand and predict double halide perovskite? Halogen anions have several important chemical differences compared with oxides for which the concept of Shannon radii and tolerance factors were originally developed. This means bonds between heavier halides and metals will tend to have greater covalency, which should increase down the halogen group, and the model of hard spheres will be less applicable.

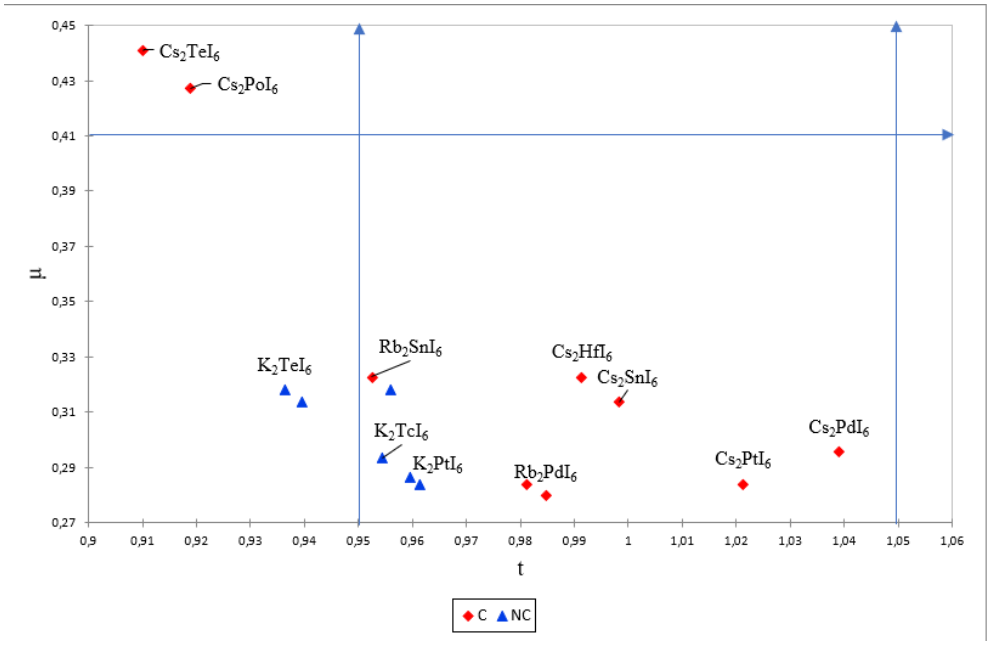

Figure 4.42: The variation of the tolerance factor versus the octahedral factor for the double iodide perovskites of table 5.18.

In order to overcome this difficulty, Travis el al [118] propose an alternative method. they introduced a revised set of ionic radii for cations that is anion dependent for heavier halides. Whereas, Ouyang [119] have extended the Shannon radii to unusual oxidation states and arbitrary coordination by using a data driven method. His newly complemented radii were found to be consistent with existing Shannon's data, which have enabled reliable input of radii for studying novel compounds. His results give a more accurate prediction of formability of halide perovskites. However, even the use of these improved Shannon radii for heavier halides, we are not able to decide on the formability of double halide perovskites.

We expanded this study by introducing a new modified model for the tolerance factor, as proposed by Bartel et al [120]. The improved tolerance factor (τ) proposed by Bartel et al [120] has the form:

$$\tau = \frac{r_X}{r_B} + n_A(n_A + \frac{\frac{r_A}{r_B}}{ln\frac{r_A}{r_B}}) \tag{4.27}$$

where n_A is the oxidation state of A.

Bartel's tolerance factor has proved its efficiency, since it distinguishes between oxide perovskites and non-perovskites with an accuracy of 92%, compared to only 74% accuracy for the Goldschmidt tolerance factor. Although ? was only trained on ABX_3 compounds, it is readily adaptable to double perovskites because it depends only on com-

position and not structure [116].

The accurate and probabilistic nature of τ as well as its applicability over a broad range of compounds creates a whole new physical insight into the stability and the prediction of new stable double perovskites. Also, there is a monotonic dependence of perovskite stability on τ (e.g., as τ decreases, the probability of being perovskite increases). Empirically, stable perovskites are expected when τ < 4,18. However, the stability of the perovskite structure does not increase or decrease monotonically with t and in contrast to the usual 2D descriptor (t, μ), τ incorporates μ as a 1D descriptor.

The results using τ are shown in (Fig.4.43) and (table5.18). We observe that τ has higher classification accuracy than t on existing structure data (a clear separation between cubic and non-cubic compounds). However, the physical meaning of "τ" is not as clear as that of "t", and thus it may be risky to extrapolate too far. Bartel et al [120] predicts that most of the considered perovskites with τ<4,18 is formable of perovskites compounds. However, even with this model, we cannot decide on the formability of A_2BX_6. As in the case of (Fig.4.36, 4.37, 4.38 and 4.42), we may then propose a different limit for "τ" for each group of halides. In our case for the formability of double halide perovskites according to assumptions made above for "t" and "μ ", we propose that ?τ - 5,35 <0 for their formability.

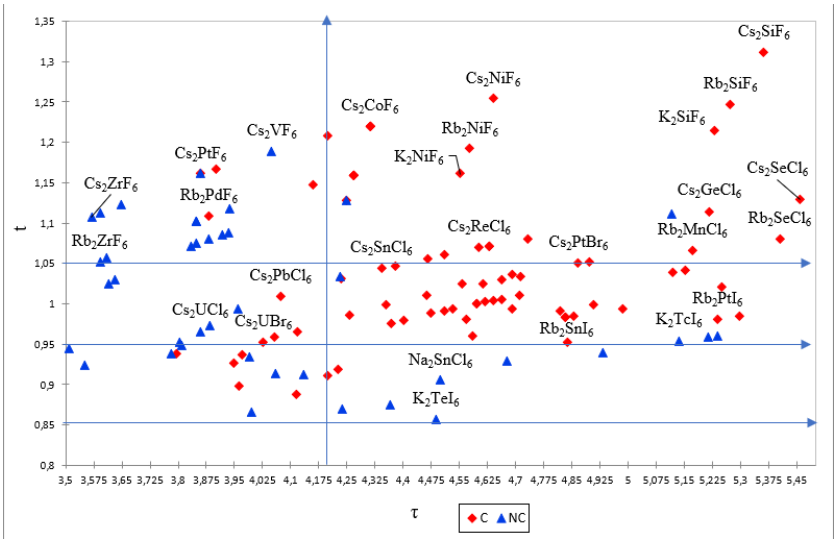

Figure 4.43: The variation of the tolerance factor "t" versus the modified tolerance factor "τ" for the double halide perovskites of table5.18.

We have also extended the approach used of Ouyang [119] for halide perovskites to double halide perovskites. Ouyang introduced [119] simultaneously criterion t &τ (t log-

ical AND τ). Thus, in our case the two conditions of 0.8 < t≤ 1.1 and τ - 5,35 < 0 jointly define a "green light" region for the formability of double halide perovskites. We display in (Table5.20)the results of t &τ.

4.4.3 Thermodynamic stability of oxide perovskites

A good stability descriptor should not only provide quantitative guidance in experiments to stabilize these structures but also their thermodynamics stability which a key parameter for searching new emerging stable double halide perovskites through massive calculations and several experimental syntheses. Sun et al. [112] identified an interesting correlation between the thermodynamic stability and the descriptor $(t+\mu)^{\eta}$ for oxide perovskites. where "η " is the atomic packing fraction (APF). Their results showed that APF is an important factor. Theη factor has never been considered in previous studies for the formability of perovskites, his calculated as:

$$\eta = (V_A + V_B + 3V_X)/a^3 \tag{4.28}$$

We extend this approach to our double halide perovskites. We have reported on (table5.21), the energy of formation ΔH calculated by Faizan et al [121] for several double halide perovskites. On the basis of (table{z21) data, we have applied a PLS regression method and predicted an empirical relation between ΔH and the different ionic radius of A_2BX_6. This equation is:

$$\Delta H = +10,19 + 3,25r_A + 21,88r_B + 10,29r_X \tag{4.29}$$

The correlation coefficient between the values of (table5.21) and the values obtained from the above equation is more than 98%.

Using equation4.29, we predict ΔH for our 119 double halide perovskites of (table5.18). The results are given in (table5.22). We display on (Fig.4.44) the variation of ΔH with $(t+\mu)^{\eta}$, we observe a clear separation between the cubic (red square) and non-cubic (bleu triangle) perovskites. It seems that non cubic perovskites have smaller ΔH than cubic one.

Based on the overall results of this work, we embark on completing our analysis of property prediction of 640 new double halide perovskites based on our predicted models. The results corresponding to their related "t", "μ ", "τ", "ΔH" and "$(t+\mu)^{\eta}$" are given

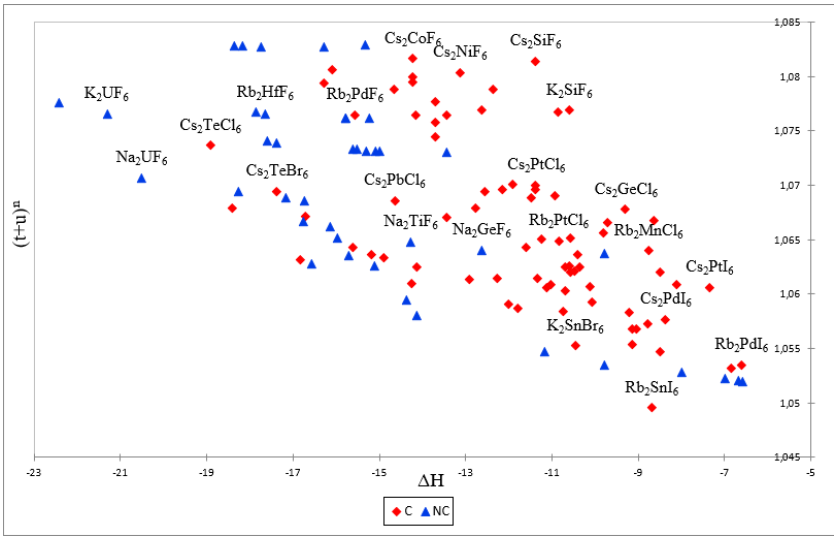

Figure 4.44: The variation of the energy of formation "ΔH" versus the $(t+\mu)^{\eta}$ factor for the double halide perovskites of table 5.18.

in (table5.23). According to the above proposed new formability range for each group of halides, we may therefore predict 487 compounds among the 640 predicted which will form a perovskite structure as seen in (Fig.4.47)and highlighted in bold in (table5.23). While this new database shows promise, the ultimate challenge which remain is to develop a robust validation test for some of these predictions, whether or not the design of any of these combinations could be designed experimentally.

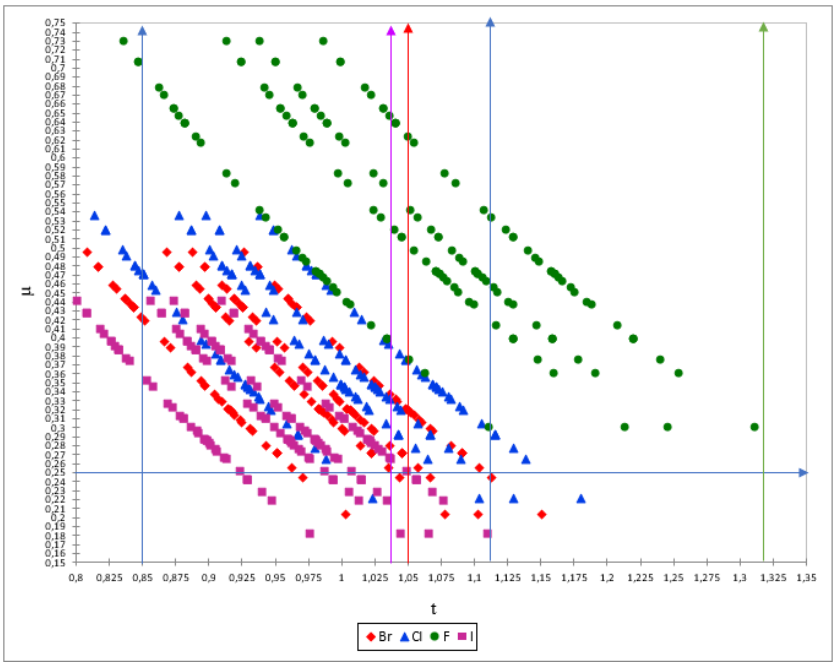

Figure 4.45: The variation of the tolerance factor versus the octahedral factor for the predicted double halide perovskites of (table5.23).

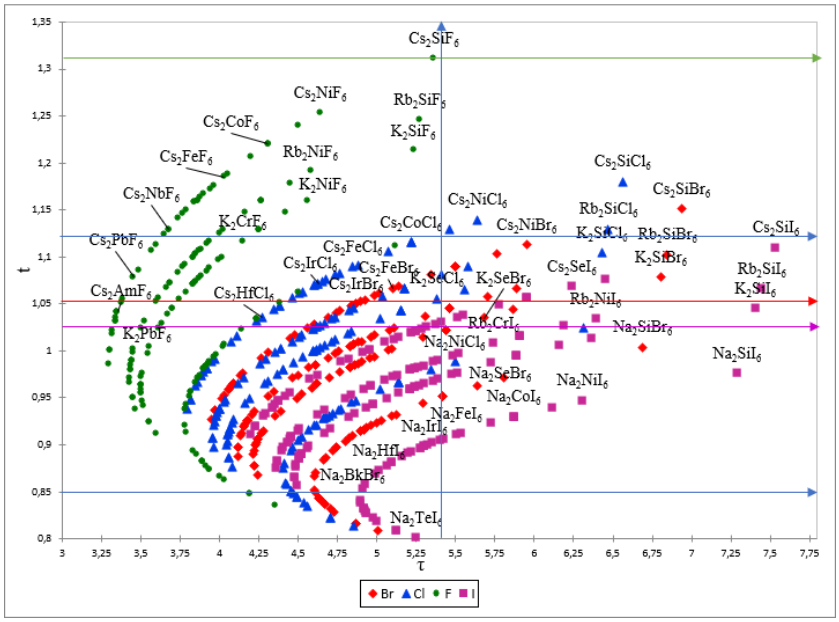

Figure 4.46: The variation of the tolerance factor "t" versus the modified tolerance factor "τ" for the predicted double halide perovskites of (table5.23).

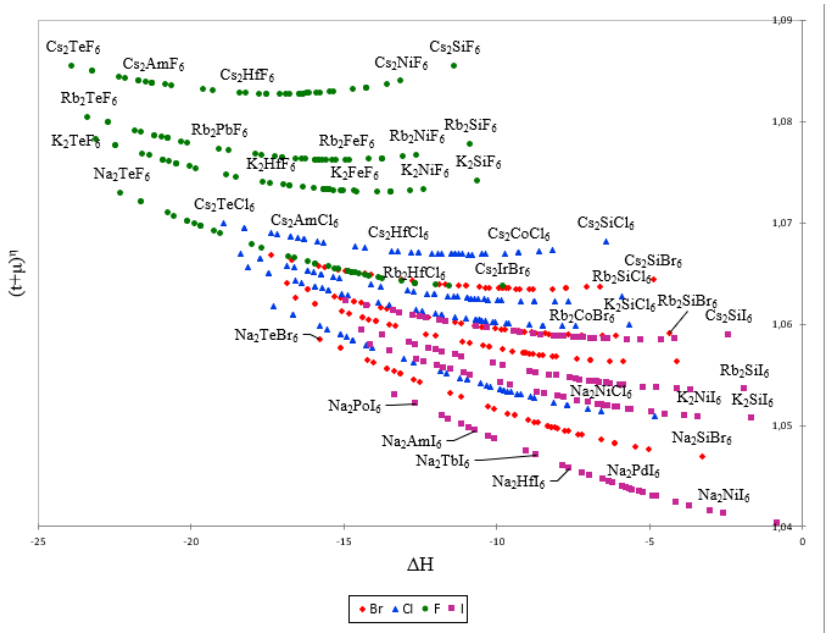

Figure 4.47: The variation of the energy of formation "ΔH" versus the $(t+\mu)^{\eta}$ factor for the predicted double halide perovskites of (table5.23).

4.5 mechanical properties of perovskites and inverse perovskites

4.5.1 introduction

Perovskites and inverse perovskites have a wide range of interesting physical and chemical properties including electro-optical effects, piezo-, ferro- and pyroelectricity, some of them possess also interesting, thermal properties, mechanical properties such as strength, stiffness, corrosion resistance, and high temperature corrosion superior to ordinary metals.

Thermal barrier coatings (TBC) are ceramic coatings deposited onto the surface of gas turbine blades used in the hottest section of gas turbine engines to protect the superalloy substrate from the hot-gas stream [122–128]. The upper layer is a ceramic topcoat with the prime function to provide heat insulation by its low thermal conductivity and it must withstand complex stress conditions [129–134].

Therefore, the selection of topcoat materials is constrained by some basic requirements: high temperature capability, low thermal conductivity, and superior fracture resistance (i.e. good damage tolerance) during thermal cycling under severe operating conditions. However, the current commercial TBC material YSZ (Y_2O_3 partially stabilized ZrO_2) has an application temperature limit of $1200°C$ and therefore cannot be used for the next generation of gas turbine engines with higher operating temperatures. Therefore, the perovskites or inverse perovskites could be considered as promising alternative for extremely high temperature TBC applications, and consequently the efficiency, of turbine engines? Unfortunately, it is known that their room temperature brittleness and poor fracture toughness severely restrict their use. Therefore, the question which remains, how to overcome this constraint and increase the ductility and high fracture toughness in these compounds? One solution could be through nanolayered superlattice coatings.

Several studies reveal that in order to produce nanolayered superlattice coatings [135–139] with appreciable hardness enhancement; the layer materials should be chosen in such a way that they exhibit a large difference in shear modulus (ΔG) [140]. When the superlattice period is below a certain threshold, which is a function of the layer materials, a large ΔG will allow the layer interfaces to act as effective barriers to dislocation propagation from the softer layers to the harder layers under mechanical loading. We will adopt this approach in order to predict new superlattice perovskite-based TBC materials.

In the present work, we primarily aim to understand the trend in the elastic and mechanical properties of some perovskites and inverse perovskites using datamining techniques. We have noticed through the literature an important number of data have been produced for perovskites or inverse perovskites. However, not only is the creation of data whether through calculation or experiment important, but a way to analyze the data in a comprehensive and robust manner is also necessary. Some of the challenges in searching through discrete data include the difficulty of analyzing large amounts of data, understanding the correlations among various properties, and using the correlations to better understand the underlying physics of the system. Utilizing a multivariate analysis, the data can be examined so that trends and correlations become apparent. A multiple selection criteria approach is proposed to screen the data rationality.

4.5.2 Results of mechanical properties

From a coating design perspective, knowledge discovery in databases can provide useful guidance for materials selection. In order to identify the trends or clustering in materials property data, we construct a database for 71 perovskites compounds (28 oxides, 7 chlorides, 8 bromides, 25 fluorides and 3 iodides) and 15 descriptors, including the ionic radius (r_A, r_B, r_X), lattice parameters (a),elastic constants (C_{ij}), bulk modulus (B), shear modulus (G), hardness (H),Cauchy pressure (C_p), the Pugh modulus ratio (B/G) and the fracture toughness(K_{ic}). (Table.5.24)contains the dataset used.

The Cauchy pressure is given by:

$$C_p = (C_{12} + C_{44}) \tag{4.30}$$

The Hardness is calculated according the model of Chen et al [141]

$$H = 2(\frac{G^3}{B^2})^{0.585} + 3 \tag{4.31}$$

Whereas, the facture toughness which measures the resistance of a material against crack propagation, is calculated according to the model of Niu et al [142]

$$K_{ic} = V_0^{1/6} G^2 (\frac{B}{G})^{1/2} \tag{4.32}$$

Where V_0 is the volume per atom (in m^3), B and G are in MPa.

PCA is used to assess the correlation between each of the descriptors input into the regression analyses and the stability of the compounds. The results of these analyses can then be compared with the predictive models to understand the physics and limitations of the models. The PCs do not necessarily have an obvious physical meaning, but rather are a combination of descriptors which explain the largest variation in the data. The advantage of PCA is that, since each PC uniquely captures the effect of a certain combination of relevant descriptors, typically a few PCs are sufficient for describing a system.

The first analysis done, was to examine if in our case the PCA captures the differences between the different perovskites? The resulting scores plot of this analysis is shown in (Fig.4.48). For this analysis (Fig. 4.48), the sign of each principal component has only relational meaning. We notice that PC1(F1) captures 55.02% of the variance, whereas PC2(F2) captures 18.15%. The two PCs together capture ~ 74% of the variance of the data in (Table. 5.24). Therefore, a dataset of n-dimensions (15 initial descriptors in this case) can be reduced to a few dimensions (2 PCs) while capturing ~ 74% of the original information. The reduction in dimensionality makes trends and correlations, which are hidden in the data, become easily visualized and described in PC space as can be seen in (Fig.4.48).

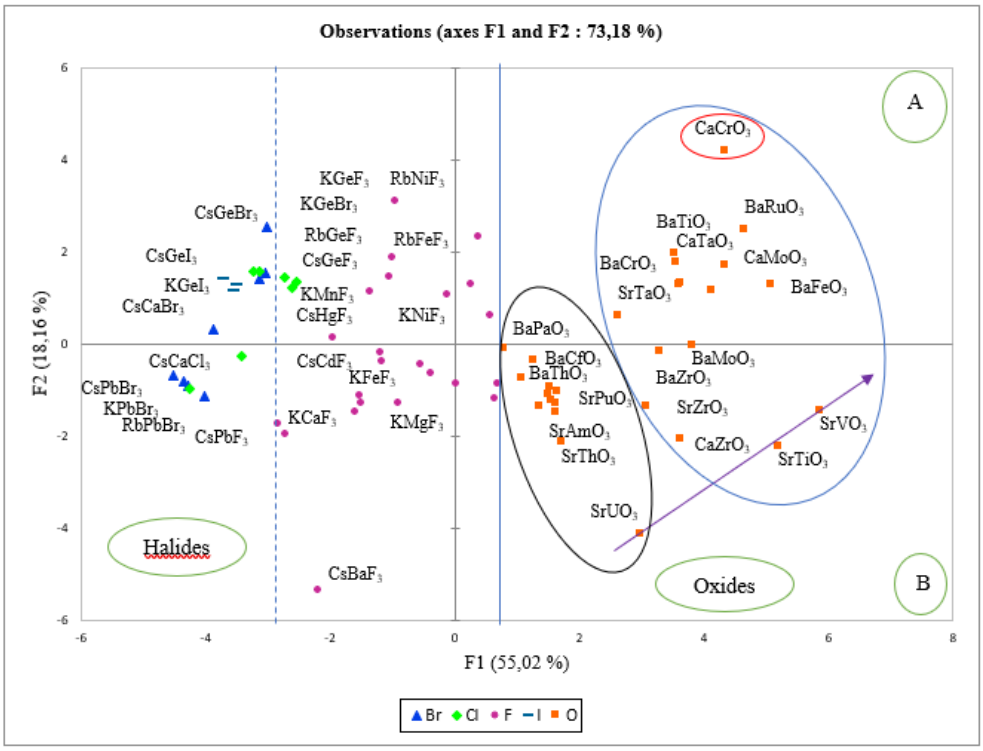

Figure 4.48: Principal component analysis score plot for perovskites.

From looking at this figure it appears two important clustering those belonging to oxide perovskites and those to halide perovskites. Furthermore, within the oxide region, we observe a clear separation between the lanthanides and the transition metals. We notice that as PC1 increases the shear modulus (G) and toughness fracture (K_{ic}) increases, on the other hand as PC2 increases the B/G, and H increase (See table.5.24). Therefore, a simple score plot could be a simple tool to identify the compounds with interesting mechanical and structural properties.

The loadings plot corresponds with the scores plot but represents the variance among descriptors. (Fig.4.49) shows the loadings plot corresponding with the samples shown in (Fig.4.48). The axes of the scores plot and loadings plot are the same so the information in the plots can be compared directly. The angles between the vectors tell us how characteristics correlate with one another. When two vectors are close, forming a small angle, the two variables they represent are positively correlated. If they meet each other at $90°$, they are not likely to be correlated. When they diverge and form a large angle (close to $180°$), they are negative correlated.

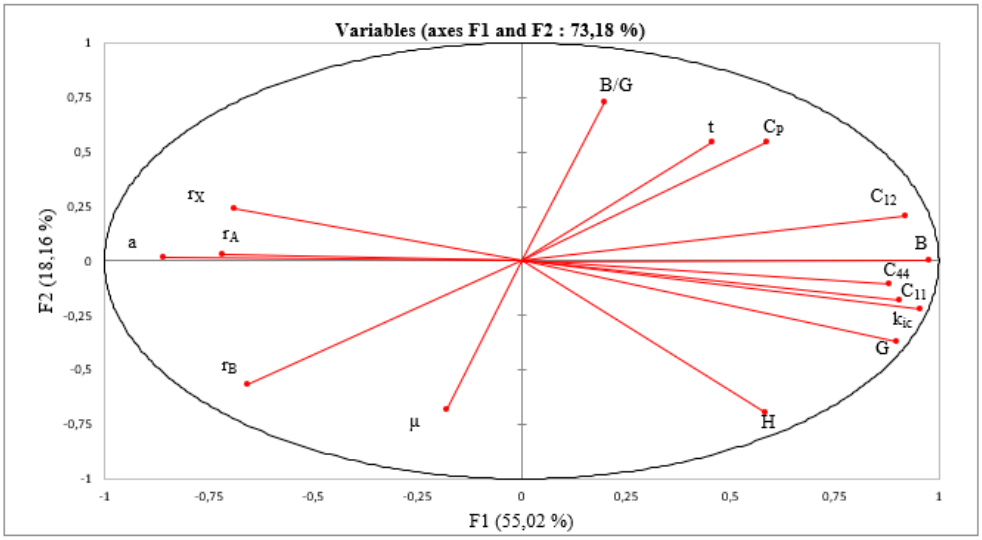

Figure 4.49: Principal component analysis PCA loading plot for perovskites.

The impact of the descriptors is increased as its distance from the origin is increased. We notice from (figure.4.49) two different clustering, those with negative PC1 (a, r_A, r_B, μ, and r_X) and those with a positive PC1 (t, $C_{12}, B, C_{44}, C_{11}, G, H, C_p, K_{ic}$). Globally, we observe that "a" is inversely correlated to all the mechanical properties. We clearly observe that "a" and "B" are inversely correlated, that means, as "a" increases "B" decreases. It seems that B/G is not correlated to H ($\sim 90°$). B/G is inversely correlated too to octahedral factor μ. Therefore, the fact that perovskites with a low "μ" should have a large

B/G and could be more ductile. Whereas, the tolerance factor "t" is correlated to "C_p", that means that the Cauchy pressure is highly sensitive to the crystalline structures of perovskites.

Since, the relative impact of each descriptor in a loading score is identified by measuring the absolute distance from the origin, we display below the different PCs equations as derived from the eigenvalue analysis:

$$PC1 = +0.717r_A + 0.657r_B + 0.688r_X + 0.857a + 0.458t \quad (4.33)$$
$$+0.178\mu + 0.905C_{11} + 0.922C_{12} + 0.882C_{44} + 0.977B + 0.901G + 0.198(B/G) + 0.590C_p + 0.585H + 0.957K_i$$

$$PC2 = +0.033r_A + 0.568r_B + 0.240r_X + 0.014a + 0.543t + 0.685\mu + 0.181C_{11} + 0.206C_{12}$$
$$+ 0.103C_{44} + 0.006B + 0.255G + 0.368(B/G) + 0.542C_p + 0.542H + 0.218K_{ic} \quad (4.34)$$

For PC1 the coefficients (C11, C12, C44, B, G and Kic)) are the more important descriptors ($\sim 0,9$), whereas for PC2 (μ, H, B/G) have the highest weighting ($\sim 0,7$). These results confirm the observations noticed on the score plot of (Fig.4.48).

Properties with similar PC values are highly correlated, while inverse PC values indicate inverse correlations. Globally, we observe that a, and the ionic radius are inversely correlated to almost all the mechanical properties. On the other hand, we notice that C_{11}, C_{44} and K_{ic} behave in the same manner (too close). We have also performed PCA calculation for 58 inverse perovskites. The resulting scores plot of this analysis is shown in (Fig.4.50), we notice that PC1(F1) captures 40.47% of the variance, whereas PC2(F2) captures 27.45%. The two PCs together capture ~ 68% of the variance of the data in (Table.5.25). We notice three regions, the region A corresponds to the group of column 2 of the periodic table (Ca, Sr, Ba), as PC1 decreases the ionic radius of X increases. Region B corresponds to column 3 (Sc), we observe also that as PC1 decreases the radius of ion A decreases (Tl, In, Ga, Al). Finally, region C corresponds to the other columns. On the other hand, we notice that as PC2's increases the G and H increase, whereas, as PC1's increases B/G and K_{ic} increase. These behaviors are completely different than those observed for perovskites.

(Fig.4.51) display the loading results for the inverse perovskites. We clearly observe that "a" and "B" are inversely correlated as in the oxide perovskites. It seems that B/G is inversely correlated to H ($\sim 180°$). Whereas, the tolerance factor "t" is correlated to "B".

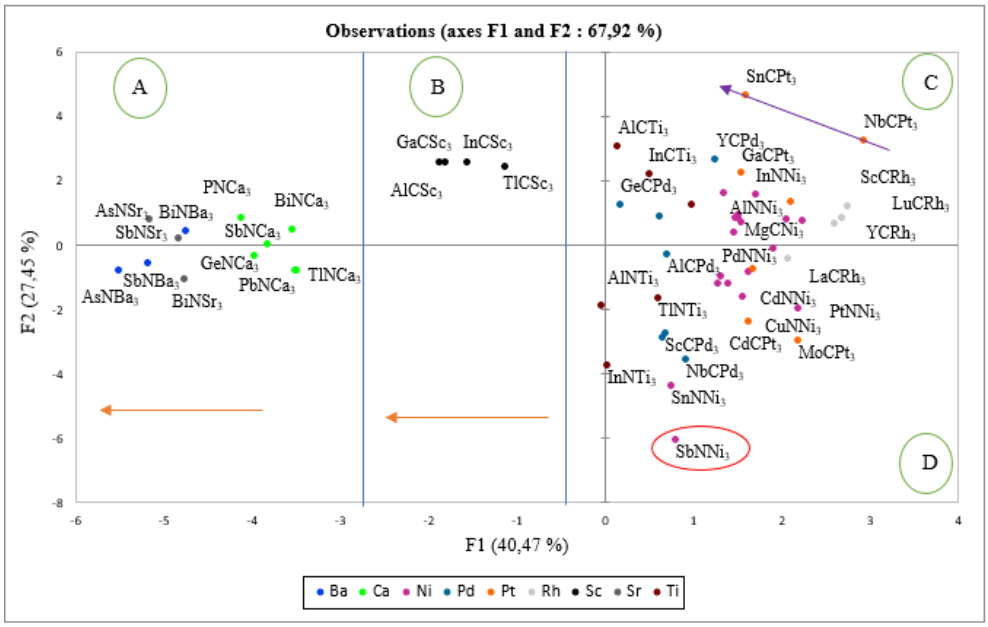

Figure 4.50: Principal component analysis score plot for inverse perovskites.

The PC's equations as derived from the eigenvalue analysis are:

$$\begin{aligned} PC1 \\ &= +0.963r_A + 0.213r_B + 0.414r_X + 0.899a + 0.460t \\ &\quad +0.148\mu + 0.824C_{11} + 0.840C_{12} + 0.362C_{44} + 0.977B + 0.476G + 0.281(B/G) + 0.591C_p \\ &\quad + 0.310H + 0.783K_{ic} \end{aligned} \tag{4.35}$$

$$\begin{aligned} PC2 = &+0.038r_A + 0.011r_B + 0.403r_X + 0.112a + 0.064t + 0.127\mu + 0.241C_{11} \\ &+ 0.358C_{12} + 0.762C_{44} + 0.101B + 0.864G \\ &+ 0.793(B/G) + 0.782C_p + 0.899H + 0.593K_{ic} \end{aligned} \tag{4.36}$$

For PC1 the coefficients for $(r_A, a, C_{11}, C_{12}, C_{44}, B)$ are the more important descriptors ($\sim 0,85$) for PC1, whereas for PC2 (C_{44}, G, H) have the highest weighting ($\sim 0,8$). These results confirm the observations noticed on the score plot of (Fig.4.50).

In this work we are mainly interested to the ability of perovskites and inverse perovskites to deform (ductility) or to fracture (brittleness). It is well known that among those compounds some have superior mechanical properties; but almost are brittle. It is known that ductility occurs as atoms slide past one another in a bulk solid through dislocations.

There are two independent engineering elastic moduli: the shear (G) and the bulk (B) modulus. These quantities can be connected to single crystal elastic constants using

different averaging techniques. The shear modulus encompasses is an indicator of the mechanical hardness H. Whereas, the bulk modulus represents a measure of the average bond strength of the atoms in the crystal, and it is proportional to the cohesive energy.

We present in (Fig.4.52 and Fig.4.53) the variation of B versus G in order to reveal their ductility trend, as indicated by the ductility arrow. $SrUO_3, SrTiO_3, SrVO_3$ for oxides perovskites and $NbCPt_3, SnCPt_3$ for inverse perovskites have a large B and G, we notice, that this behavior is also clearly seen on the PCA results (Fig.4.48, Fig.4.50, the arrow).

On the other hand, we display in (Fig.4.54and Fig.4.55) the Cauchy pressure C_P versus B/G, since the ductility trend of certain cubic materials is based on the degree of the angular character of chemical bonding. As a general observation, ductile materials have positive values of Cauchy pressure, which correspond to more isotropic metallic bonding. On the other hand, brittle materials exhibit negative values of Cauchy pressure, which result from more angular character of the bonding. Whereas, the ratio B/G is considered as a parameter of ductility versus brittleness performance of solids. Ductility is characterized by a high B/G ratio (>1.75), while low B/G is representative of brittleness. We observe that $CaCrO_3$ and $SbNNi_3$, respectively for oxide perovskites and inverse perovskites, have a large B/G and C_p. This is also clearly seen on the PCA results, since these compounds are isolated form all the other materials (Fig.4.48 and Fig.4.50).

We also display on (Fig.4.56 and Fig.4.57) the variation of hardness versus the toughness fracture. The compound which seems to present high hardness H and fracture toughness Kic (Fig.4.56 and Fig.4.57) is $SnPtC_3$ and $SrVO_3$ for inverse perovskites and perovskites, respectively. However, even that $CaCrO_3$ and $SbNNi_3$ have high bulk modulus (Fig.4.58 and Fig.4.59), they have a poor hardness and fracture toughness. Based on these results, we may conclude that from principal components analysis results, we may predict the mechanical properties of perovskites and inverse perovskites.

Based on these intrinsic properties of the compounds we introduce a new criterion B/G & C_p & H & K_{ic} & B (where & is logical AND) in order to predict the more interesting compound which could be used as thermal barrier coating (TBC). We propose, any compound which satisfy these five conditions jointly (Cp>0, B/G>1.75, H>2, Kic>2 and B>140) will define a minimal green light region for the potential TBC compounds. Thus, the perovskites and inverse perovskites which may be good candidates as TBC are displayed on (table.5.26). We notice that the inverse perovskites seem to be a more reliable

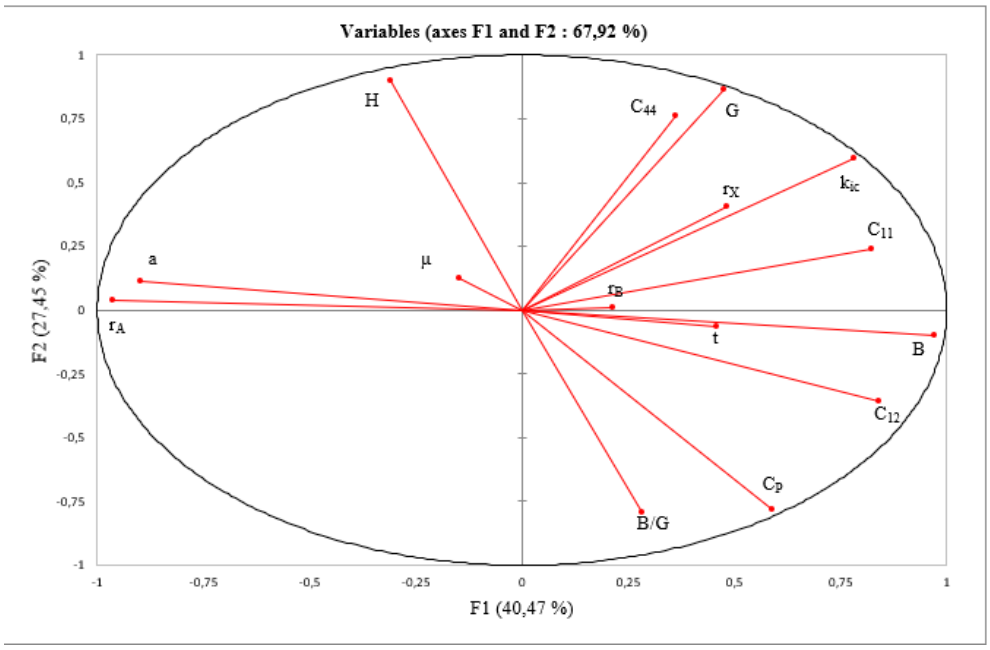

Figure 4.51: Principal component analysis PCA loading plot for inverse perovskites.

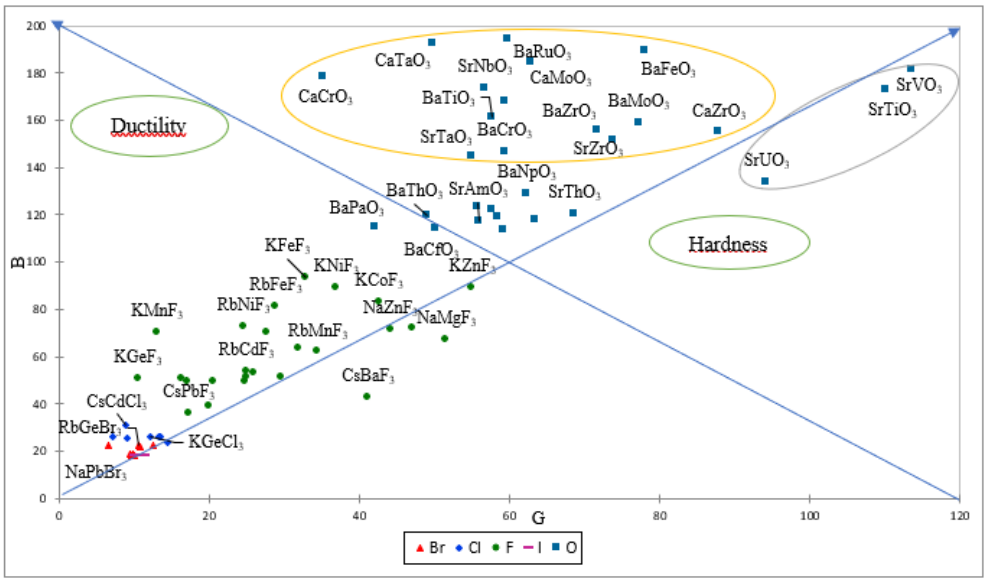

Figure 4.52: The variation of the bulk modulus versus the shear modulus for perovskites.

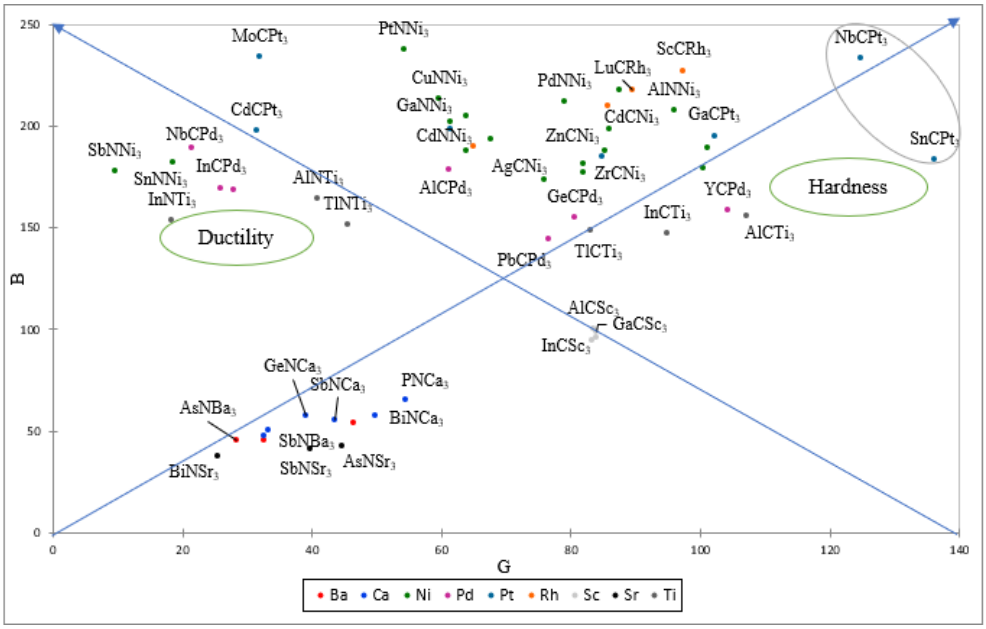

Figure 4.53: The variation of the bulk modulus versus the shear modulus for inverse perovskites.

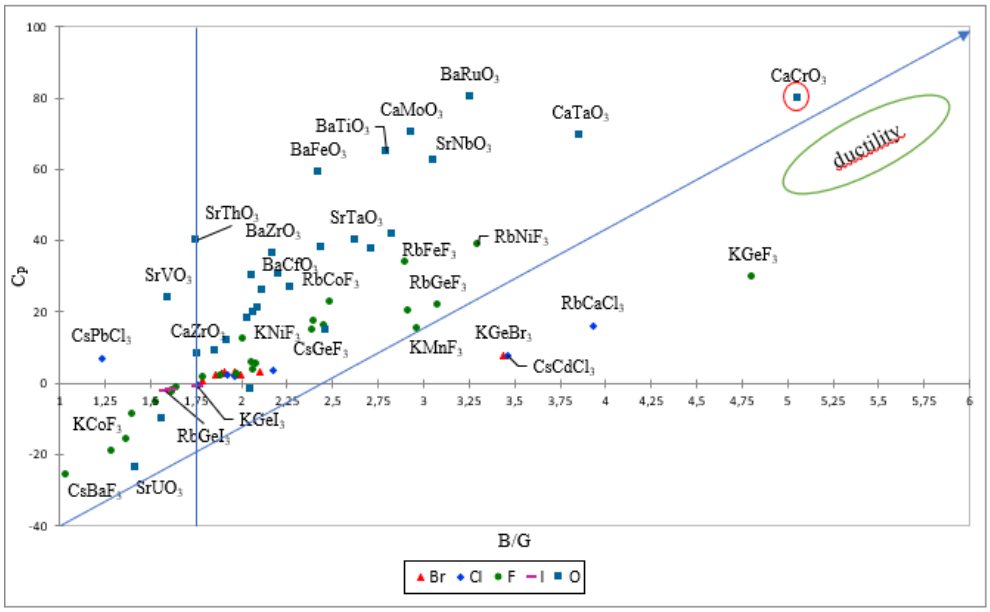

Figure 4.54: The variation of the Cauchy pressure versus the Pugh ratio for perovskites.

candidates than oxide perovskites.

The question, which remains, are we able to select from the results of the principal component analysis materials that can potentially meet the property requirements? One needs to concentrate on the region where the materials exhibit a combination of relatively high hardness and ductility. The high hardness and high fracture toughness correspond

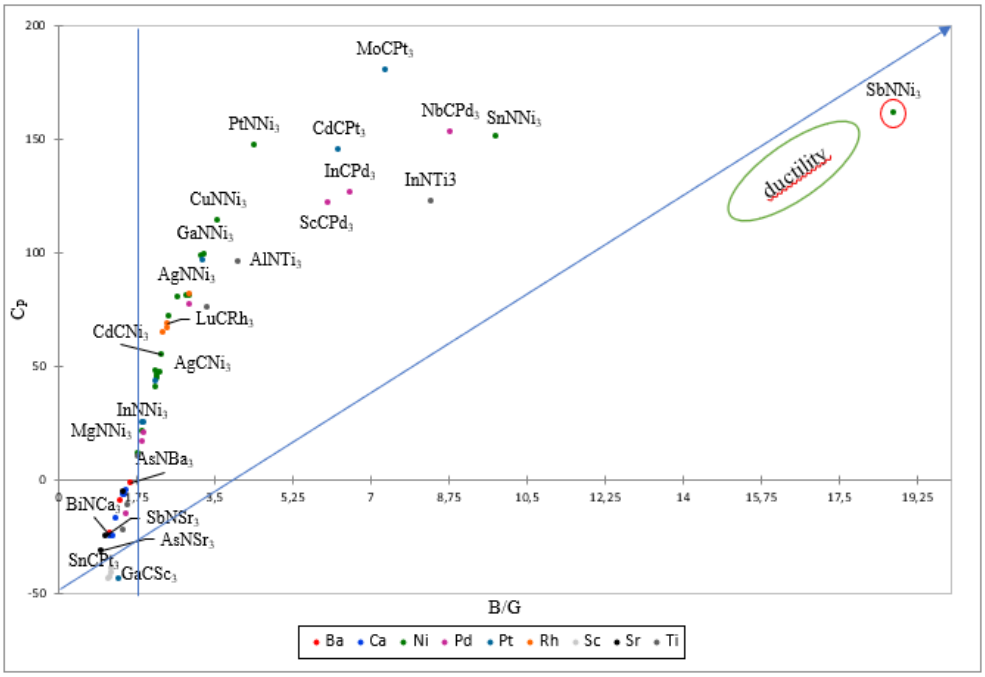

Figure 4.55: The variation of the Cauchy pressure versus the Pugh ratio for inverse perovskites.

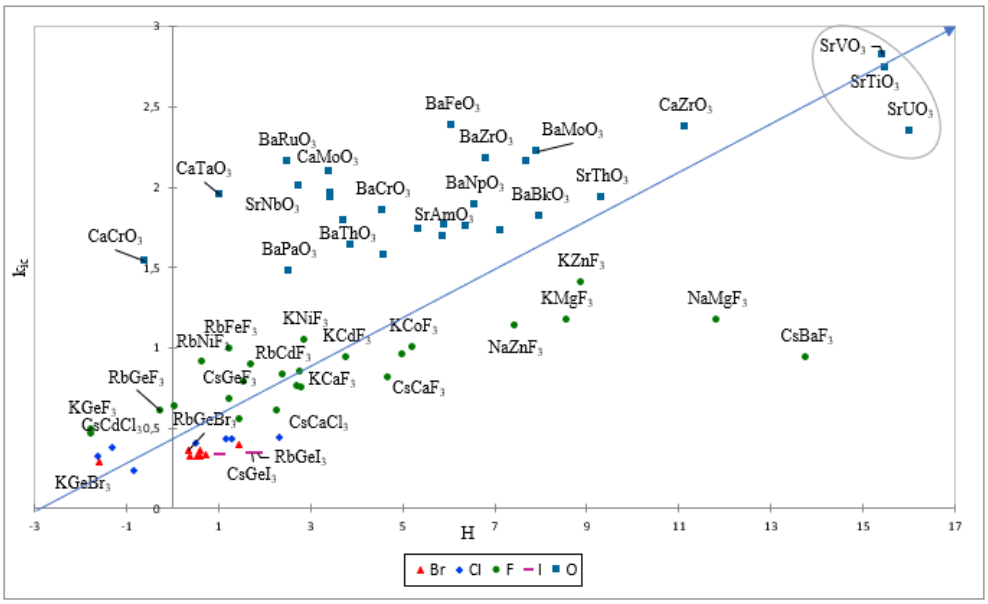

Figure 4.56: The variation of the Hardness versus the Fracture toughness for perovskites.

to the region A in the score plot, whereas, region B represents ductile compounds. The situation is inversed for inverse perovskites. Therefore, interesting materials could be at the frontier between these two regions.

In this work we have also been interested by the possibility to make artificial materi-

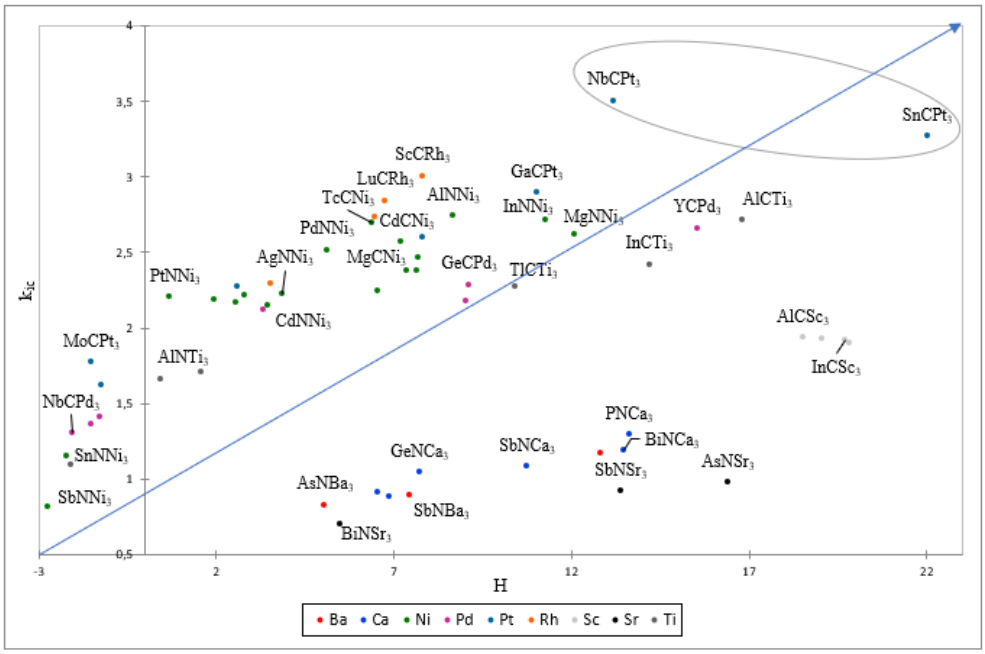

Figure 4.57: The variation of the Hardness versus the Fracture toughness for inverse perovskites.

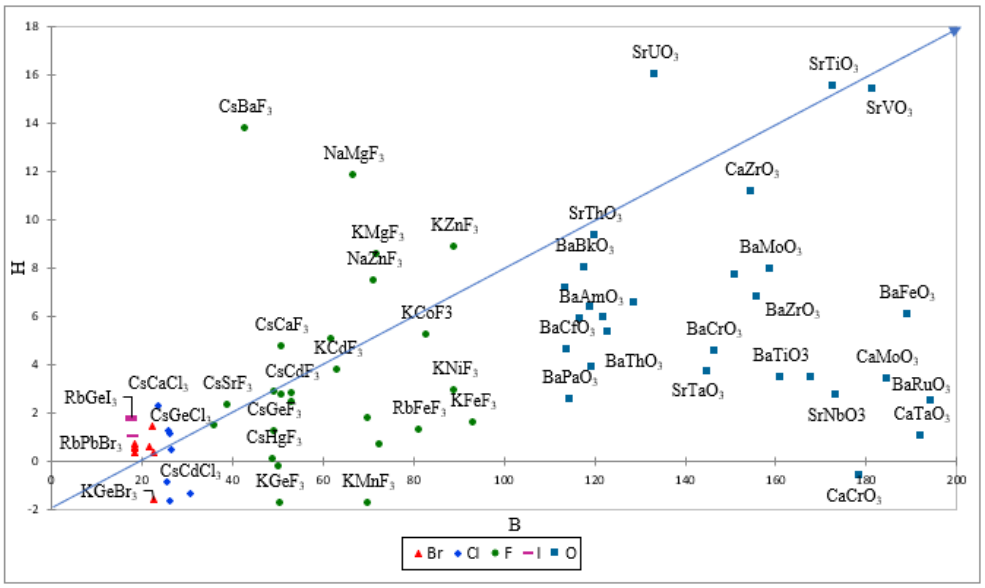

Figure 4.58: The variation of the Hardness versus the bulk modulus for perovskites

als with high hardness and toughness fracture through a thin coating approach. It consists of a method of obtaining high-hardness coatings in which a repeating layered structure of two materials with nanometer scale dimensions are deposited onto the surface. These structures are called "superlattices". As it has been studied by several authors [143–145], superlattices are characterized by the distance between each successive pair of layers d, which is known as the "bilayer repeat period". Xi Chu et al [146] have demonstrated

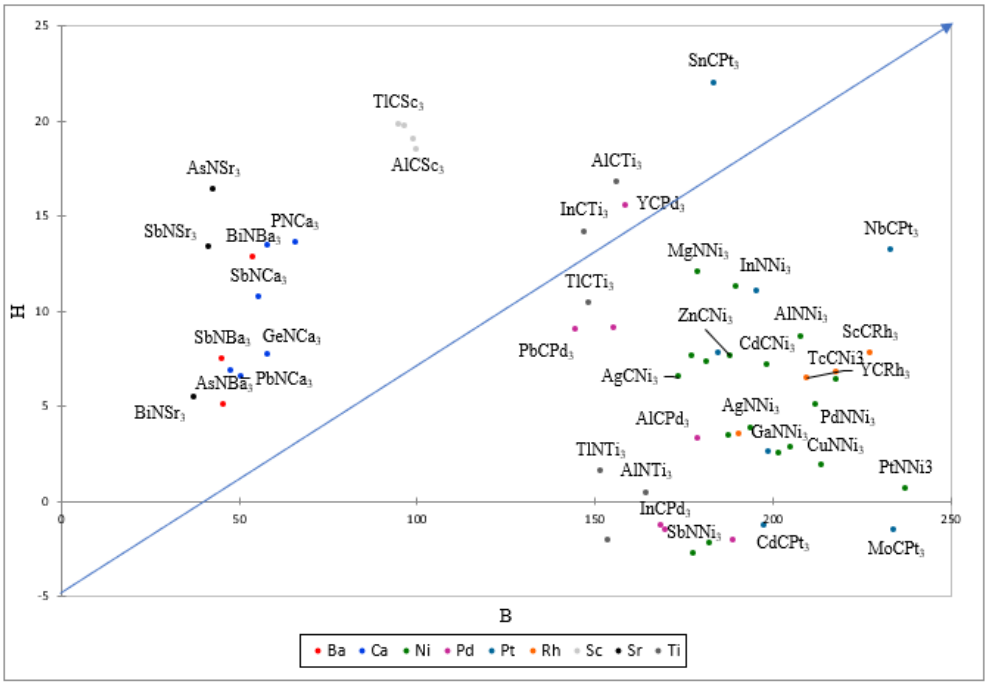

Figure 4.59: The variation of the Hardness versus the bulk modulus for inverse perovskites

that the hardening effect of the interfaces is reduced when the layers are narrow. They explained the decrease in hardness at large d is due to the dislocations moving within individual layers since they are not able to cross the interfaces.

In this work we have used the approach introduced by Koehler [147], who suggested for the first time in 1970 that a high-strength material could be obtained by fabricating a layered structure of two materials with the same crystal structure. Since, it is known that the interfaces between the layers could act as barriers to the motion of dislocations. Therefore, restricting the motion of dislocations will strengthen this type of material. So, if a dislocation moves into a layer with a higher shear modulus, the strain energy increases. Inducing a superlattice (A/B) a repulsive force that increases as dislocations in a layer B with a smaller modulus, G_B, approach the interfaces with the layer A with a larger modulus, G_A. According to Koehler's model, the critical stress required to move a dislocation across an abrupt interface is proportional to:

$$Q = (G_A + G_B)/(G_A + G_B) \tag{4.37}$$

Therefore, a superlattice in which the difference in modulus between the two layers ΔG is large will therefore have a large critical stress and so a large hardness enhancement.

Since perovskites or inverse perovskites-based superlattices remain almost unexplored,

we may ask this question. Do the perovskites or inverse perovskites offer a better material combination for superlattice (SL) coatings?

The information presented in (Figs.4.52 to Fig.4.57) are used to design superlattice hard coatings. As discussed, materials with a small Q should be considered for synthesizing superlattice coatings to achieve effective hardness enhancement. Applying this criterion to the calculated perovskites and inverse perovskites, we may anticipate from (Table.5.27), that superlattices $CaZrO_3/SrNbO_3$, $CaZrO_3/BaRuO_3$, $CaZrO_3/CaMoO_3$, $NbCPt_3/AlCPd_3$, $NbCPt_3/GaNNi_3$, $NbCPt_3/ZnNNi_3$ and $NbCPt_3/ScCPt_3$ have good potentials to offer enhanced hardness; in contrast, superlattices based on halides would show marginal hardness enhancement due to their small ΔG. These perovskites and inverse perovskites are all cubic structure according to the values of their tolerance and octahedral factors (table.5.27). However, we observe a large lattice mismatch for $CaZrO_3/CaMoO_3, NbCPt_3/GaNNi_3$ and $NbCPt_3/ZnNNi_3$, these may further enhance the hardness of these superlattices. These analyses are purely predictive and should be supported experimentally.

We can anticipate also from the PCA results, those potential materials for superlattice hard coatings. So, any combination of materials from region A as template and any materials from region B as substrate could give interesting superlattices e.g. ($CaCrO_3/SrVO_3$, $SnCPt_3/SbNNi_3$). We notice from the different calculations of ΔG and the position of each compound in the PCA score plots, that the distance between two materials from different clusters are correlated to ΔG. Since as this distance increases, ΔG increases.

Therefore, the logic presented here can be applied to any system with any number of samples and descriptors. Combining informatics with calculated data and physical properties will allow for the greatest understanding of structureproperty relationships. With that knowledge, materials can then be engineered to maximize the desired properties. The use of PCA here demonstrates how informatics can be used to screen information to determine what is necessary and useful, and then to use that knowledge in experimental, computational, and materials design.

BIBLIOGRAPHY

[1] https://explorermaterials.wordpress.com/basic-concepts/perovskite-structure/

[2] L.Q. Jiang, J.K. Guo, H.B. Liu, M. Zhu, X. Zhou, P. Wu, C.H. Li, *"Prediction oflattice constant in cubic perovskites"*, J. Phys. Chem. Solids. 67 (2006) 1531-1536.

[3] C. Ye, J. Yang, L. Yao, N. Chen,*" Regularities of formation and lattice distortion of perovskite-type compounds"*, Chinese Sci. Bull. 47 (2002) 458-460.

[4] R.L. Moreira, A. Dias,*" Comment on Prediction of lattice constant in cubic perovskites"* J. Phys. Chem. Solids. 68 (2007) 1617-1622.

[5] Goldschmidt, *"Die Gesetze der Krystallochemie"*. Naturwissenschaften 14, 477-485 (1926).

[6] Zachariasen, H. & Verteilungsgesetze, G. *"A Set of Empirical Crystal Radii for Ions with Inert Gas Configuration"* . DE GRUYTER 80, 137-153 (1931).

[7] Linus Pauling, *"the size of ions ans the structure of ionic crystals"* J. Am. Chem. Soc. 49, 765-790(1927).

[8] Ahrens, L,*"The use of ionization potentials Part 1 . Ionic radii of the elements"*. Geochim cosmochim acta 2, 155-169 (1952).

[9] Shannon, R. D. & Prewitt, C. T, *"Effective ionic radii in oxides and fluorides"*. Acta Crystallogr.Sect. B Struct. Crystallogr. Cryst. Chem. 25, 925-946 (1969).

[10] C.T. Prewitt, R. Shannon,*"effective ionic radii and crystal chemistry"*. J. Inorg. Nucl. Chem. 32,1427-1441(1970).

[11] Shannon, R. D, *"Revised Effective Ionic Radii and Systematic Studies of Interatomie Distances in Halides and Chaleogenides"*. Acta Crystallogr. A32, 751-767 (1976).

[12] Nowers, J. R., Broderick, S. R., Rajan, K. & Narasimhan, B.*"Combinatorial methods and informatics provide insight into physical properties and structure relationships during IPN formation"*. Macromol. Rapid Commun. 28, 972-976 (2007).

[13] Suh, C. & Rajan, K.*"Combinatorial design of semiconductor chemistry for bandgap engineering:Virtual combinatorial experimentation"*. Appl. Surf. Sci. 223, 148-158 (2004).

[14] Sieg, S. C.*"Principal component analysis of catalytic functions in the composition space of heterogeneous catalysts"*. QSAR Comb. Sci. 26, 528-535 (2007).

[15] Suh, C. & Rajan, K.*"Virtual screening and QSAR formulations for crystal chemistry"*. QSAR Comb. Sci. 24, 114-119 (2005).

[16] Zenasni, H., Aourag, H., Broderick, S. R. & Rajan, K.*"Electronic structure prediction via datamining the empirical pseudopotential method"*. Phys. Status Solidi Basic Res. 121, 115-121(2010).

[17] Aourag, H. & Guittom, A. *"Mining the bulk positron lifetime"*. Phys. Status Solidi Basic Res. 396,392-396 (2009).

[18] Aourag, H., Saidi, F., Broderick, S. & Rajan, K.*"Designing Superlattices Ultra Hard Coatings Datamining Approach"*. J. Comput. Theor. Nanosci. 6, 828-833 (2009).

[19] Broderick, S. R., Aourag, H. & Rajan, K.*"Data Mining Density of States Spectra for Crystal Structure Classification an Inverse Problem Approach"*. Stat. Anal. Data Min. 1, 353-360(2009).

[20] Broderick, S. R., Aourag, H. & Rajan, K.*"Data mining of Ti, Al semi-empirical parameters for developing reduced order models"*. Phys. B Phys. Condens. Matter 406, 2055-2060 (2011).

[21] Broderick, S. R., Aourag, H. & Rajan, K.*"Classification of Oxide Compounds through DataMining Density of States Spectra"*. J. Am. Ceram. Soc. 94, 2974-2980 (2011).

[22] Suh, C., Rajagopalan, A., Li, X. & Rajan, K.*"THE APPLICATION OF PRINCIPAL COMPONENT ANALYSIS TO MATERIALS SCIENCE DATA"*. J. data Sci. 1, 19-26 (2002).

[23] L.M. Feng, L.Q. Jiang, M. Zhu, H.B. Liu, X. Zhou, C.H.Ã. Li, *"Formability of ABO_3 cubic perovskites"*, J. Phys. Chem. Solids. 69 (2008) 967-974.

[24] C. Li, K.C.K. Soh, P. Wu, *"Formability of ABO_3 perovskites"*, J. Alloys Compd. 372(2004) 40-48.

[25] R.D. Shannon, *"Synthesis of some new perovskites containing indium and thallium"*,Inorg. Chem. 6 (1967) 1474-1478.

[26] K.Y. Tsui, N. Onishi, R.F. Berger,*"Tolerance Factors Revisited: Geometrically Designing the Ideal Environment for Perovskite Dopants"*, J. Phys. Chem. C. 120(2016) 23293-23298.

[27] X. Liu, R. Hong, C. Tian,*"Tolerance factor and the stability discussion of ABO_3-type ilmenite"*, J. Mater. Sci. Mater. Electron. 20 (2009) 323-327.

[28] W. Li, E. Ionescu, R. Riedel, A. Gurlo,*"Can we predict the formability of perovskite oxynitrides from tolerance and octahedral factors?"*, J. Mater. Chem. A. 1 (2013)12239.

[29] C.J. Bartel, C. Sutton, B.R. Goldsmith, R. Ouyang, C.B. Musgrave, L.M.Ghiringhelli, M. Scheffler,*"New tolerance factor to predict the stability of perovskite oxides and halides"*, Sci. Adv. 5 (2019) 2-4.

[30] R. Ubic,*"Revised Method for the Prediction of Lattice Constants in Cubic and Pseudocubic Perovskites"*, J. Am. Ceram. Soc. 90 (2007) 3326-3330.

[31] W. Travis, E.N.K. Glover, H. Bronstein, D.O. Scanlon, R.G. Palgrave,*"On the application of the tolerance factor to inorganic and hybrid halide perovskites: a revised system"*, Chem. Sci. 7 (2016) 4548-4556.

[32] C.E. Hu, Z.Y. Zeng, C.Y. Kong, Y.T. Cui, L. Zhang,*"Equation of state and elastic properties of $ACrO_3$(A=Pb, Ca, Sr and Ba) perovskites under high pressure"*, Phys. B Condens. Matter. (2012).

[33] Somia, S. Mehmood, Z. Ali, I. Khan, F. Khan, I. Ahmad,*"First-Principles Study of Perovskite Molybdates $AMoO_3$ (A = Ca, Sr, Ba)"*, J. Electron. Mater. 48 (2019)1730-1739.

[34] N. Iles, A. Kellou, K. Driss Khodja, B. Amrani, F. Lemoigno, D. Bourbie, H.Aourag,*"Atomistic study of structural, elastic, electronic and thermal properties of perovskites $Ba(Ti, Zr, Nb)O_3$"*, Comput. Mater. Sci. 39 (2007) 896-902.

[35] S.A. Khandy, D.C. Gupta,*"Structural, elastic and magneto-electronic properties of half-metallic $BaNpO_3$"* perovskite, Mater. Chem. Phys. 198 (2017) 380-385.

[36] S.A. Khandy, D.C. Gupta,*"Understanding Ferromagnetic Phase Stability, Electronic and Transport Properties of $BaPaO_3$ and $BaNpO_3$ from Ab-Initio Calculations"*, J.Electron. Mater. 46 (2017) 5531-5539.

[37] Z. Ali, I. Ahmad, A.H. Reshak,*"GGA+U studies of the cubic perovskites $BaMO_3$(M=Pr, Th and U)"*, Phys. B Condens. Matter. 410 (2013) 217-221.

[38] S.A. Dar, V. Srivastava, U.K. Sakalle, G. Pagare,*"Insight into Structural, Electronic,Magnetic, Mechanical, and Thermodynamic Properties of Actinide Perovskite$BaPuO_3$"*, J. Supercond. Nov. Magn. 31 (2018) 3201-3208.

[39] D.M. Han, X.J. Liu, S.H. Lv, H.P. Li, J. Meng,*"Elastic properties of cubic perovskite $BaRuO_3$ from first-principles calculations"*, Phys. B Condens. Matter. 405(2010) 3117-3119.

[40] M.B. Saddique, M. Rashid, A. Afzal, S.M. Ramay, F. Aziz, A. Mahmood,*"Ground state opto-electronic and thermoelectric response of cubic $XSnO_3$ (X = Ba, Sr)compounds"*, Curr. Appl. Phys. 17 (2017) 1079-1086.

[41] Z. Ali, I. Khan, I. Ahmad, M.S. Khan, S.J. Asadabadi,*"Theoretical studies of the paramagnetic perovskites $MTaO_3$ (M = Ca, Sr and Ba)"*, Mater. Chem. Phys. 162(2015) 308-315.

[42] C. Ma, L. Ye, Z. Yang,*"Electronic structures of perovskite $BaTbO_3$ studied by the LSDA + U method"*, J. Phys. Condens. Matter. 17 (2005) 7963-7969.

[43] Y.B. Cherif, A. Labdelli, A. Boukortt, H. Abbassa, D. Aimouch, R. Hayn,*"Modified Becke Johnson (mBJ) exchange potential investigation of the optoelectronic properties of $XThO_3$(X = Sa, Sr and Ba)"*, Int. J. Comput. Mater. Sci. Eng. 08 (2019)1850029.

[44] G. Mustafa, N. ul Aarifeen, A. Afaq, M. Asif,*"Electronic and magnetic properties of$BaUO_3$ by modified Becke Johnson (mBJ) functional"*, Mod. Phys. Lett. B. 32(2018) 1850164.

[45] D. Cherrad, D. Maouche, M. Reffas, A. Benamrani,*"Structural, elastic, electronic and optical properties of the cubic perovskites $CaXO_3$ (X=Hf and Sn)"*, Solid State Commun. 150 (2010) 350-355.

[46] X. Wu, Y. Dong, S. Qin, M. Abbas, Z. Wu,*"First-principles study of the pressureinduced phase transition in $CaTiO_3$"*, Solid State Commun. 136 (2005) 416-420.

[47] Z.F. Hou,*"Ab initio calculations of elastic modulus and electronic structures of cubic $CaZrO_3$"*, Phys. B Condens. Matter. 403 (2008) 2624-2628.

[48] Z. Ali, I. Ahmad, B. Amin, M. Maqbool, G. Murtaza, I. Khan, M.J. Akhtar, F.Ghaffor,*"Theoretical studies of structural and magnetic properties of cubic perovskites $PrCoO_3$ and $NdCoO_3$"*, Phys. B Condens. Matter. 406 (2011) 3800-3804.

[49] M. Rezaiguia, W. Benstaali, A. Abbad, S. Bentata, B. Bouhafs,*"GGA + U Study of Electronic and Magnetic Properties of $Pr(Fe/Cr)O_3$ Cubic Perovskites"*, J.Supercond. Nov. Magn. 30 (2017) 2581-2590.

[50] B. Bouadjemi, S. Bentata, A. Abbad, W. Benstaali, B. Bouhafs,*"Half-metallic ferromagnetism in $PrMnO_3$ perovskite from first principles calculations"*, Solid State Commun. 168 (2013) 6-10.

[51] B. Sabir, G. Murtaza, Q. Mahmood, R. Ahmad, K.C. Bhamu,*"First principles investigations of electronics, magnetic, and thermoelectric properties of rare earth based $PrYO_3$ (Y=Cr, V) perovskites"*, Curr. Appl. Phys. 17 (2017) 1539-1546.

[52] I.R. Shein, V.L. Kozhevnikov, A.L. Ivanovskii,*"First-principles calculations of the elastic and electronic properties of the cubic perovskites $SrMO_3$ (M=Ti, V, Zr andNb) in comparison with $SrSnO_3$"*, Solid State Sci. 10 (2008) 217-225.

[53] S.A. Dar, V. Srivastava, U.K. Sakalle, A. Rashid, G. Pagare,*"First-principles investigation on electronic structure, magnetic, mechanical and thermodynamic properties of $SrPuO_3$ perovskite oxide"*, Mater. Res. Express. 5 (2018) 026106.

[54] Y. Benaissa Cherif, M. Rouaighia, A. Zaoui, A. Boukortt,*"Optoelectronic, Elastic and Thermal Properties of Cubic Perovskite-Type $SrThO_3$"*, Acta Phys. Pol. A. 131(2017) 406-414.

[55] B. Sahli, H. Bouafia, B. Abidri, A. Abdellaoui, S. Hiadsi, A. Akriche, N.Benkhettou, D. Rached,*"First-principles prediction of structural, elastic, electronic and thermodynamic properties of the cubic $SrUO_3$ -Perovskite"*, J. Alloys Compd.635 (2015) 163-172.

[56] Q. Sun, W.J. Yin,*"Thermodynamic Stability Trend of Cubic Perovskites"*, J. Am.Chem. Soc. 139 (2017) 14905-14908.

[57] Elements, rayons atomiques et rayons periodiques. http://www.crystalmaker.com/support/tutorials/atomic-radii/.

[58] J.C. Slater,*"Atomic radii in crystals"*, J. Chem. Phys. 41 (1964) 3199-3204.

[59] J.C. Slater,*"Quantum Theory of Molecules & Solids"*, vol. 2, 1965.

[60] E. Clementi, D.L. Raimondi,*"Atomic screening constants from SCF functions"*, J. Chem. Phys. 38 (1963) 2686-2689.

[61] V.V. Bannikov, I.R. Shein, A.L. Ivanovski,*"Band structure , elastic and magnetic properties , and stability of antiperovskites $MCNi_3$ (M= Y, Ag) according to FPLAPW-GGA calculations"*, Phys. Solid State 49 (2007) 1704-1714.

[62] I.R. Shein, V.V. Bannikov, A.L. Ivanovskii,*"Structural, elastic and electronic properties of superconducting anti-perovskites $MgCNi_3, ZnCNi_3$ and $CdCNi_3$ from first principles"*, Physica C 468 (2008) 1-6.

[63] I.R. Shein, A.L. Ivanovskii,*"Electronic and elastic properties of non-oxide anti- perovskites from first principles superconducting $CdCNi_3$ in comparison with magnetic $InCNi_3$"*, Phys. Rev. B 77 (2008) 1-8, 104101.

[64] I.R. Shein, A.L. Ivanovskii,*"Structural electronic and magnetic properties of $CaCNi_3, SrCNi_3, ANDBaCNi_3$ antiperovskites in comparison to superconducting $MgCNi_3$"*, J. Struct. Chem. 51 (2010) 176-178.

[65] D. Cherrad, D. Maouche, L. Louail, M. Maamache,*"Ab initio comparative study of the structural, elastic and electronic properties of $SnAMn_3$ (A = N, C) antiperovskite cubic compounds"*, Solid State Commun. 150 (2010) 782-787.

[66] N. Ennassiri, N. Tahiri, O. El Bounagui, H. Ez-Zahraouy, A. Benyoussef, *"Magnetic, magnetocaloric and transport properties in $AlCMn_3$ antiperovskite compound"*, J. Alloys Compd. 741 (2018) 1196-1202.

[67] J.H. Shim, S.K. Kwon, B.I. Min,*"Electronic structure of metallic antiperovskite compound"*, Phys. Rev. B - Condens. Matter Mater. Phys. 66 (2002) 1-4.

[68] D.V. Suetin, V.V. Bannikov, I.R. Shein, A.L. Ivanovskii,*"Electronic and elastic properties basic solid state physics of perovskite-like W_3NiC, W_3NiN and Co_3WC from first-principles calculations"*, Phys. Status Solidi 1651 (2009) 1646-1651.

[69] Y. Medkour, A. Roumili, M. Boudissa, D. Maouche,*"Structural, elastic and electronic properties of $ACTi_3$ (A = Al, in and Tl) antiperovskite"*, Solid State Commun. 149 (2009) 919-922.

[70] Y. Ouyang, M. Tang, J. Fang, P. Xiang, Y. Du,*"The elastic constants for Fe_3AlX (X = B , C and N) with anti-perovskite structure"*, Phys. Scr. 80 (2009), 055603.

[71] A. Bouhemadou, *"Elastic properties of mono and polycrystalline $RCRh_3$ (R=Sc,Y,La and Lu) under pressure effect"*, Solid State Commun. 149 (2009) 1658-1662.

[72] D.V. Suetin, I.R. Shein, A.L. Ivanovskii,*"Structural , elastic , electronic and magnetic properties of perovskite-like Co_3WC, Rh_3WC and Ir_3WC from first principles calculations"*, Solid State Sci. 12 (2010) 814-817.

[73] Y. Medkour, A. Roumili, D. Maouche, M. Reffas, A. Saoudi,*"First principles study of structural, elastic and electronic properties of ACY_3 (A = Al , in and Tl)"*, Comput. Mater. Sci. 47 (2010) 973-976.

[74] A.H. Reshak, F. Semari, *"FP-LAPW-lo study of the elastic , electronic and optical properties for the cubic antiperovskite $ANSr_3$ (A = as , Sb and Bi) under pressure effect"*, Phys. B Phys. Condens. Matter 405 (2010) 1894-1900.

[75] K. Amara, M. Zemouli, M. Elkeurti, A. Belfedal, F. Saadaoui,*"First-principles study of $XNMg_3$ (X = P,as ,Sb and Bi) antiperovskite compounds"*, J. Alloys Compd. 576 (2013) 398-403.

[76] M. Hichour, D. Rached, M. Rabah,*"Structural and elastic properties of antiperovskites $XNBa_3$ (X = as , Sb) under pressure effect"*, Phys. B Phys. Condens. Matter 404 (2009) 4034-4038

[77] D. Rached, M. Hichour, M. Rabah, S. Benalia,*"Prediction study of the structural , elastic , electronic and optical properties of the $BiNBa_3$"*, Solid State Commun. 149 (2009) 2002-2006.

[78] P.Y. Ming Chern, D.A. Vennos, F.J. DiSalvo,*"Synthesis, structure, and properties of anti-perovskite nitrides A-f"*, J. Solid State Chem. 96 (1992) 415-425.

[79] K. Haddadi, A. Bouhemadou, L. Louail,*"Ab initio investigation of the structural, elastic and electronic properties of the anti-perovskite $TlNCa_3$"*, Solid State Commun. 150 (2010) 932-937.

[80] M.G. Moreno-Armenta, W.L. Perez, N. Takeuchi,*"First-principles calculations of the structural and electronic properties of Cu_3MN compounds with M = Ni, Cu, Zn, Pd, Ag, and Cd"*, Solid State Sci. 9 (2007) 166-172.

[81] M. Sieberer, S. Khmelevskyi, P. Mohn,*"Magnetic instability within the series TCu_3N (T=Pd, Rh, and Ru) a first-principles study"*, Phys. Rev. B - Condens. Matter Mater. Phys. 74 (2006) 4-7.

[82] V.V. Bannikov, I.R. Shein, A.L. Ivanovskii, *"Elastic properties of antiperovskite-type Ni-rich nitrides $MNNi_3$ (M = Zn , Cd , Mg , Al , Ga , in , Sn , Sb , Pd , Cu ,Ag and Pt) as predicted from first-principles calculations"*, Phys. B Phys.Condens. Matter 405 (2010) 4615-4619.

[83] E.F. Bertaut, D. Fruchart, J.P. Bouchaud, R. Fruchart, *"Diffraction neutronique de Mn_3GaN"*, Solid State Commun. 6 (1968) 251-256.

[84] L. Hua, L. Wang, L.F. Chen,*"First-principles investigation of Ge doping effects on the structural, electronic and magnetic properties in antiperovskite Mn_3CuN"*, J. Phys. Condens. Matter 22 (2010).

[85] Y. Medkour, A. Roumili, D. Maouche, M. Maamache,*"First-principles study of the structural, electronic, and magnetic properties of $InCCo_3$ and $InNCo_3$"*, Solid State Commun. 151 (2011) 1916-1919.

[86] C.A. Kuhnen, A.V. Dos Santos,*"Electronic and magnetic properties of $AlFe_3$ and $AlFe_3N$ nitride"*, J. Alloys Compd. 384 (2004) 80-87.

[87] Z. Wu, J. Meng,*"Elastic and electronic properties of $CoFe_3N, RhFe_3N,$ and $IrFe_3N$ from first principles"*, Appl. Phys. Lett. 90 (2007) 241901.

[88] A. Muller Houben, P. Von Appen, J. Lueken, H.*"Synthesis, Crystal structure, and magnetic properties of the semihard itinerant ferromagnet $RhFe_3N$"*, Angew. Chem. Int. Ed. 44 (2005) 7212-7215.

[89] E. Zhao,*"First-principles investigation on the elastic, magnetic and electronic properties of MFe_3N (M = Fe,Ru,Os)"*, Chem. Phys. Lett. 449 (2007) 96-100.

[90] C. Li, K.C.K. Soh, P. Wu,*"Formability of ABO_3 perovskites"*, J. Alloys Compd. 372 (2004) 40-48.

[91] A. SAMMELLS, R. COOK, J. WHITE, J. OSBORNE, R. MACDUFF,*"Rational selection of advanced solid electrolytes for intermediate temperature fuel cells"*, Solid State Ionics. 52 (1992) 111-123.

[92] J. KILNER, R. BROOK, *"A study of oxygen ion conductivity in doped nonstoichiometric oxides"*, Solid State Ionics. 6 (1982) 237-252.

[93] Y.A. Mastrikov, R. Merkle, E.A. Kotomin, M.M. Kuklja, J. Maier,*"Formation and migration of oxygen vacancies in $La_{1+x}Sr_xCo_{1+y}Fe_yO_{3+\sigma}$ perovskites insight from ab initio calculations and comparison with $Ba_{1+x}Sr_xCo_{1+y}Fe_yO_{3+\sigma}$"*, Phys. Chem. Chem. Phys. 15 (2013) 911-918.

[94] J. Richter, P. Holtappels, T. Graule, T. Nakamura, L.J. Gauckler,*"Materials design for perovskite SOFC cathodes"*, Monatshefte Fur Chemie - Chem. Mon. 140 (2009) 985-999.

[95] M. MOGENSEN, D. LYBYE, N. BONANOS, P. HENDRIKSEN, F. POULSEN,*"Factors controlling the oxide ion conductivity of fluorite and perovskite structured oxides"*, Solid State Ionics. 174 (2004) 279-286.

[96] M. Pavone, A.M. Ritzmann, E.A. Carter,*"Quantum-mechanics-based design principles for solid oxide fuel cell cathode materials"*, Energy Environ. Sci. 4 (2011) 4933.

[97] R. Merkle, Y.A. Mastrikov, E.A. Kotomin, M.M. Kuklja, J. Maier,*"First Principles Calculations of Oxygen Vacancy Formation and Migration in* $Ba_{1+x}Sr_xCo_{1+y}Fe_yO_{3+\sigma}$ *Perovskites"*, J. Electrochem. Soc. 159 (2011) B219-B226.

[98] E.D. Wachsman,*"Development of a Lower Temperature SOFC"*, ECS Trans. 25(2019) 783-788.

[99] L. Malavasi, C.A.J. Fisher, M.S. Islam,*"Oxide-ion and proton conducting electrolyte materials for clean energy applications: structural and mechanistic features"*, Chem. Soc. Rev. 39 (2010) 4370.

[100] H. Hayashi,*"Structural consideration on the ionic conductivity of perovskite-type oxides"*, Solid State Ionics. 122 (1999) 1-15.

[101] T. Shimizu,*"EFFECT OF ELECTRONIC STRUCTURE AND TOLERANCE FACTOR ON CO OXIDATION ACTIVITY OF PEROVSKITE OXIDES"*, Chem.Lett. 9 (1980) 1-4.

[102] A. Mitsui,*"Evaluation of the activation energy for proton conduction in perovskite-type oxides"*, Solid State Ionics. 22 (1987) 213-217.

[103] H. Kwon, J. Park, B.-K. Kim, J.W. Han,*"Effect of B-Cation Doping on Oxygen Vacancy Formation and Migration in* $LaBO_3$*,A Density Functional Theory Study"*, J. Korean Ceram. Soc. 52 (2015) 331-337.

[104] T.T. Mayeshiba, D.D. Morgan,*"Factors controlling oxygen migration barriers in perovskites"*, Solid State Ionics. 296 (2016) 71-77.

[105] J. RICHTER, P. HOLTAPPELS, U. VOGT, T. GRAULE, L. GAUCKLER,*"Conduction behavior of* $Pr_{1+x}Sr_xMn_{1+y}In_yO_{3+\sigma}$ *perovskites"*, Solid State Ionics. 177(2006) 3105-3108.

[106] M. Islam,*"Computer modelling of defects and transport in perovskite oxides"*, Solid State Ionics.155(2002) 75-85.

[107] R. COOK, A. SAMMELLS,*"On the systematic selection of perovskite solid electrolytes for intermediate temperature fuel cells"*, Solid State Ionics. 45 (1991) 311-321.

[108] M.G. Brik, I.V. Kityk, J. Phys. Chem. Solids., 2011, 72, 1256-1260.

[109] V. Sidey, J. Phys. Chem. Solids., 2019, 126, 310-313.

[110] Y. Cai, W. Xie, Y.T. Teng, P.C. Harikesh, B. Ghosh, P. Huck, K.A. Persson, N. Mathews, S.G. Mhaisalkar, M. Sherburne, M. Asta, Chem. Mater., 2019, 31, 5392-5401.

[111] Y. Cai, W. Xie, H. Ding, Y. Chen, K. Thirumal, L.H. Wong, N. Mathews, S.G. Mhaisalkar, M. Sherburne, M. Asta, Chem. Mater., 2017, 29, 7740-7749.

[112] Q. Sun, W.J. Yin, J. Am. Chem. Soc., 2017, 139, 14905-14908.

[113] I.D. Brown, Can. J. Chem., 1964, 42, 2758-2767.

[114] U.G. Jong, C.J. Yu, Y.H. Kye, RSC Adv., 2020, 10, 201-209.

[115] "ICSD - Details on Search Result," https://icsd.fizkarlsruhe.de/display/details.xhtml,

[116] Q. Xu, Z. Li, M. Liu, W.-J. Yin, J. Phys. Chem. Lett., 2018, 9, 6948-6954.

[117] W. Rahim, A. Cheng, C. Lyu, T. Shi, Z. Wang, D.O. Scanlon, R.G. Palgrave, Chem. Mater., 2020.

[118] W. Travis, E.N.K. Glover, H. Bronstein, D.O. Scanlon, R.G. Palgrave, Chem. Sci., 2016, 7, 4548-4556.

[119] R. Ouyang, Chem. Mater., 2020, 32, 595-604.

[120] C.J. Bartel, C. Sutton, B.R. Goldsmith, R. Ouyang, C.B. Musgrave, L.M. Ghiringhelli, M. Scheffler, Sci. Adv., 2019, 5, eaav0693.

[121] M. Faizan, K.C. Bhamu, S.H. Khan, G. Murtaza, X. He, 2020. http://arxiv.org/abs/2002.07543.

[122] N.P. Padture,*" Advanced structural ceramics in aerospace propulsion"*, Nat. Mater. 15 (2016) 804809.

[123] D.R. Clarke, M. Oechsner, N.P. Padture,*"Thermal-barrier coatings for more efficient gas-turbine engines"*, MRS Bull. 37 (2012) 891898.

[124] R. Van, M.O. Jarligo, T. Steinke, D.E. Mack, D. Stver, *"Overview on advanced thermal barrier coatings"*, Surf. Coatings Technol. 205 (2010)938942.

[125] J.H. Perepezko,*"The Hotter the Engine, the Better"*, Science. 326 (2009) 10681069.

[126] M. Gupta, N. Curry, P. Nyl N. Markocsan, R. Van, *"Design of next generation thermal barrier coatings Experiments and modelling"*, Surf.Coatings Technol. 220 (2013) 2026.

[127] R. Vassen, X. Cao, F. Tietz, D. Basu, D. Stver,*"Zirconates as New Materials for Thermal Barrier Coatings"*, J. Am. Ceram. Soc. 83 (2004)20232028.

[128] A. Du, C. Wan, Z. Qu, W. Pan,*"Thermal Conductivity of Monazite-Type $REPO_4$ (RE=La, Ce, Nd, Sm, Eu, Gd)"*, J. Am. Ceram. Soc. 92 (2009)26872692.

[129] Y. Luo, J. Wang, J. Wang, J. Li, Z. Hu,*"Theoretical Predictions on Elastic Stiffness and Intrinsic Thermal Conductivities of Yttrium Silicates"*, J. Am.Ceram. Soc. 97 (2014) 945951.

[130] B. Liu, J.Y. Wang, Y.C. Zhou, T. Liao, F.Z. Li,*"Theoretical elastic stiffness, structure stability and thermal conductivity of $La_2Zr_2O_7$ pyrochlore"*, Acta Mater. 55 (2007) 29492957.

[131] B. Liu, J.Y. Wang, F.Z. Li, Y.C. Zhou,*"Theoretical elastic stiffness,structural stability and thermal conductivity of $La_2T_2O_7$ (T=Ge, Ti, Sn, Zr,Hf) pyrochlore"*, Acta Mater. 58 (2010) 43694377.

[132] D.R. Clarke,*"Materials selection guidelines for low thermal conductivity thermal barrier coatings"*, Surf. Coatings Technol. 163164 (2003) 6774.

[133] J. Feng, B. Xiao, R. Zhou, W. Pan,*"Anisotropy in elasticity and thermal conductivity of monazite-type $REPO_4$ (RE=La, Ce, Nd, Sm, Eu and Gd) from first-principles calculations"*, Acta Mater. 61 (2013) 73647383.

[134] Y. Liu, B. Liu, H. Xiang, Y. Zhou, H. Nian, H. Chen, G. Yang, Y. Gao,*"Theoretical investigation of anisotropic mechanical and thermal propertiesof ABO_3 (A =Sr, Ba; B =Ti, Zr, Hf) perovskites"*, J. Am. Ceram. Soc. 101(2018) 35273540.

[135] Y. Liu, V.R. Cooper, B. Wang, H. Xiang, Q. Li, Y. Gao, J. Yang, Y. Zhou,B. Liu,*"Discovery of ABO_3 perovskites as thermal barrier coatings through high-throughput first principles calculations"*, Mater. Res. Lett. 7 (2019)145151.

[136] N. Ejaz, L. Ali, A. Ahmad, M. Mansoor, M.M. Asim, A. Rauf, K.Mehmood,*"Thermo-Physical Properties Measurement of Advanced TBC Materials with Pyrochlore and Perovskite Structures"*, Key Eng. Mater. 778(2018)

[137] W. Ma, M.O. Jarligo, D.E. Mack, D. Pitzer, J. Malzbender, R. Van, D.Stver,*"New Generation Perovskite Thermal Barrier Coating Materials"*, J.Therm. Spray Technol. 17 (2008) 831837.

[138] A. Dck, N. Gamer, W. Gesatzke, M. Griepentrog, W. terle, M. Sahre,I. Urban,*"Ti/TiN multilayer coatings: deposition technique,characterization and mechanical properties"*, Surf. Coatings Technol. 142144 (2001) 579584.

[139] C. Wang, K. Shi, C. Gross, J.M. Pureza, M. de Mesquita Lacerda, Y.W.Chung,*"Toughness enhancement of nanostructured hard coatings: Design strategies and toughness measurement techniques"*, Surf. Coatings Technol. 257 (2014) 206212.

[140] L.R. Zhao, K. Chen, Q. Yang, J.R. Rodgers, S.H. Chiou,*"Materials informatics for the design of novel coatings"*, Surf. Coatings Technol. 200(2005) 15951599.

[141] X.Q. Chen, H. Niu, D. Li, Y. Li,*"Modeling hardness of polycrystalline materials and bulk metallic glasses"*, Intermetallics. 19 (2011) 12751281.

[142] H. Niu, S. Niu, A.R. Oganov,*"Simple and accurate model of fracture toughness of solids"*, J. Appl. Phys. 125 (2019) 065105.

[143] H. Aourag,*"Prediction of Superlattices Ultra Hard Aluminum Rare-Earth Intermetallic Compounds"*, J. Comput. Theor. Nanosci. 11 (2014) 589595.

[144] J. Buchinger, N. Koutn. Chen, Z. Zhang, P.H. Mayrhofer, D. Holec,M. Bartosik,*"Toughness enhancement in TiN/WN superlattice thin films"*,Acta Mater. 172 (2019) 1829.

[145] N. Koutn. Brenner, D. Holec, P.H. Mayrhofer,*"High-throughput firstprinciples search for ceramic superlattices with improved ductility and fracture resistance"*, Acta Mater. 206 (2021) 116615.

[146] X. Chu, S.A. Barnett,*"Model of superlattice yield stress and hardness enhancements"*, J. Appl. Phys. 77 (1995) 44034411.

[147] J.S. Koehler,*"Attempt to Design a Strong Solid"*, Phys. Rev. B. 2 (1970)547551.

CHAPTER 5

ANNEXES TABLES

5.1 oxide perovskite

compounds	a_0(Å)	r_A(Å)	r_B(Å)	E_A	E_B	Z_A	Z_B	t	μ	τ
BaCrO3	3.95 [1]	1.61	0.55	0.89	1.66	56	24	1.101	0.407	3.180
BaMoO3	4.01 [2]	1.61	0.65	0.89	2.16	56	42	1.046	0.481	2.808
BaNbO3	4.1287 [3]	1.61	0.68	0.89	1.6	56	41	1.031	0.503	2.732
BaNpO3	4.437 [4]	1.61	0.87	0.89	1.36	56	93	0.942	0.644	2.558
BaPaO3	4.51 [5]	1.61	0.9	0.89	1.5	56	91	0.930	0.666	2.576
BaPrO3	4.363 [6]	1.61	0.85	0.89	1.13	56	59	0.951	0.629	2.554
BaPuO3	4.421 [7]	1.61	0.86	0.89	1.28	56	94	0.947	0.637	2.555
BaRuO3	4.0059 [8]	1.61	0.62	0.89	2.2	56	44	1.062	0.459	2.899
BaSnO3	4.13 [9]	1.61	0.69	0.89	1.96	56	50	1.025	0.511	2.710
BaTaO3	4.057 [10]	1.61	0.68	0.89	1.5	56	73	1.031	0.503	2.732
BaTbO3	4.278 [11]	1.61	0.76	0.89	1.22	56	65	0.991	0.562	2.598
BaThO3	4.555 [12]	1.61	0.94	0.89	1.3	56	90	0.913	0.696	2.619
BaTiO3	4.022 [3]	1.61	0.605	0.89	1.54	56	22	1.070	0.448	2.950
BaUO3	4.38 [13]	1.61	0.89	0.89	1.38	56	92	0.934	0.659	2.569
BaZrO3	4.2269 [3]	1.61	0.72	0.89	1.33	56	40	1.011	0.533	2.654
CaCrO3	3.777 [1]	1.34	0.55	1	1.66	20	24	1.001	0.407	3.190
CaSnO3	3.964 [14]	1.34	0.69	1	1.96	20	50	0.932	0.511	2.882
CaTaO3	3.975 [10]	1.34	0.68	1	1.5	20	73	0.937	0.503	2.890
CaTiO3	3.9 [15]	1.34	0.605	1	1.54	20	22	0.972	0.448	3.017
CaZrO3	4.138 [16]	1.34	0.72	1	1.33	20	40	0.918	0.533	2.871
PrCoO3	3.73 [17]	1.3	0.61	1.13	1.88	59	27	0.956	0.451	2.030

PrCrO3	3.819 [18]	1.3	0.55	1.13	1.66	59	24	0.986	0.407	2.202
PrFeO3	3.777 [18]	1.3	0.645	1.13	1.83	59	26	0.939	0.477	1.969
PrMnO3	3.88 [19]	1.3	0.645	1.13	1.55	59	25	0.939	0.477	1.969
PrVO3	3.87 [20]	1.3	0.64	1.13	1.63	59	23	0.941	0.474	1.976
SrCrO3	3.844 [1]	1.44	0.55	0.95	1.66	38	24	1.038	0.407	3.175
SrNbO3	4.073 [21]	1.44	0.68	0.95	1.6	38	41	0.971	0.503	2.808
SrPuO3	4.378 [22]	1.44	0.86	0.95	1.28	38	94	0.892	0.637	2.818
SrTaO3	4.007 [10]	1.44	0.68	0.95	1.5	38	73	0.971	0.503	2.808
SrThO3	4.53 [23]	1.44	0.94	0.95	1.3	38	90	0.861	0.696	3.028
SrTiO3	3.945 [21]	1.44	0.605	0.95	1.54	38	22	1.009	0.448	2.976
SrUO3	4.37 [24]	1.44	0.89	0.95	1.38	38	92	0.880	0.659	2.879
SrVO3	3.866 [21]	1.44	0.64	0.95	1.63	38	23	0.991	0.474	2.884
SrZrO3	4.179 [21]	1.44	0.72	0.95	1.33	38	40	0.953	0.533	2.760

Table 5.1: The training dataset used in the PCA calculations.

compounds	a_0(Å)	predicted a	Δa
BaCrO3	3.957	3.902	0.055
BaMoO3	4.010	4.069	-0.059
BaNbO3	4.128	4.119	0.009
BaNpO3	4.437	4.438	-0.001
BaPaO3	4.510	4.488	0.022
BaPrO3	4.364	4.404	-0.041
BaPuO3	4.421	4.421	0.000
BaRuO3	4.006	4.019	-0.013
BaSnO3	4.130	4.136	-0.006
BaTaO3	4.057	4.119	-0.062
BaTbO3	4.278	4.253	0.025
BaThO3	4.555	4.555	0.000
BaTiO3	4.023	3.994	0.029
BaUO3	4.380	4.471	-0.091
BaZrO3	4.227	4.186	0.040
CaCrO3	3.777	3.762	0.015
CaSnO3	3.965	3.996	-0.032
CaTaO3	3.975	3.979	-0.004
CaTiO3	3.900	3.854	0.046
CaZrO3	4.138	4.046	0.092

PrCoO3	3.730	3.841	-0.111
PrCrO3	3.820	3.741	0.079
PrFeO3	3.777	3.900	-0.123
PrMnO3	3.880	3.900	-0.020
PrVO3	3.870	3.892	-0.022
SrCrO3	3.844	3.813	0.031
SrNbO3	4.073	4.031	0.042
SrPuO3	4.378	4.333	0.045
SrTaO3	4.007	4.031	-0.024
SrThO3	4.530	4.467	0.063
SrTiO3	3.946	3.906	0.040
SrUO3	4.376	4.383	-0.007
SrVO3	3.866	3.964	-0.098
SrZrO3	4.179	4.098	0.081

Table 5.2: The predicted lattice parameters with our PLS model with those measured or calculated one.

compounds	a_0(Å)	r_A(Å)	r_B(Å)	t	μ	τ	structure
ErPmO3	4,320	1,06	0,97	0,735	0,719	10,708	Non perovskite
DyNdO3	4,352	1,08	0,983	0,737	0,728	10,048	Non perovskite
YNdO3	4,352	1,08	0,983	0,737	0,728	10,048	Non perovskite
HoHgO3	4,435	1,12	1,02	0,737	0,756	10,064	Non perovskite
ErSmO3	4,300	1,06	0,958	0,738	0,710	9,345	Non perovskite
EuAcO3	4,659	1,23	1,12	0,739	0,830	9,928	Non perovskite
DyPmO3	4,330	1,08	0,97	0,741	0,719	8,757	Non perovskite
YPmO3	4,330	1,08	0,97	0,741	0,719	8,757	Non perovskite
ErAgO3	4,286	1,06	0,95	0,741	0,704	8,605	Non perovskite
ErCdO3	4,286	1,06	0,95	0,741	0,704	8,605	Non perovskite
SmAcO3	4,665	1,24	1,12	0,741	0,830	9,083	Non perovskite
ErEuO3	4,281	1,06	0,947	0,742	0,701	8,355	Non perovskite
ErThO3	4,270	1,06	0,94	0,744	0,696	7,822	Non perovskite
DySmO3	4,310	1,08	0,958	0,744	0,710	7,814	Non perovskite
YSmO3	4,310	1,08	0,958	0,744	0,710	7,814	Non perovskite
ErGdO3	4,266	1,06	0,938	0,745	0,695	7,681	Non perovskite
GdNdO3	4,368	1,11	0,983	0,746	0,728	7,667	Non perovskite
DyAgO3	4,297	1,08	0,95	0,747	0,704	7,285	Non perovskite
DyCdO3	4,297	1,08	0,95	0,747	0,704	7,285	Non perovskite

YAgO3	4,297	1,08	0,95	0,747	0,704	7,285	Non perovskite
YCdO3	4,297	1,08	0,95	0,747	0,704	7,285	Non perovskite
DyEuO3	4,292	1,08	0,947	0,748	0,701	7,104	Non perovskite
YEuO3	4,292	1,08	0,947	0,748	0,701	7,104	Non perovskite
HoNdO3	4,373	1,12	0,983	0,749	0,728	7,106	Non perovskite
GdPmO3	4,346	1,11	0,97	0,750	0,719	6,880	orthorombic
DyThO3	4,280	1,08	0,94	0,750	0,696	6,712	Orthorombic
YThO3	4,280	1,08	0,94	0,750	0,696	6,712	Orthorombic
DyGdO3	4,277	1,08	0,938	0,751	0,695	6,607	Orthorombic
YGdO3	4,277	1,08	0,938	0,751	0,695	6,607	Orthorombic
HoPmO3	4,351	1,12	0,97	0,753	0,719	6,422	Orthorombic
ErDyO3	4,223	1,06	0,912	0,753	0,676	6,209	Orthorombic
GdSmO3	4,326	1,11	0,958	0,754	0,710	6,277	Orthorombic
GdAgO3	4,312	1,11	0,95	0,756	0,704	5,928	Orthorombic
GdCdO3	4,312	1,11	0,95	0,756	0,704	5,928	Orthorombic
HoSmO3	4,331	1,12	0,958	0,757	0,710	5,892	Orthorombic
ErHoO3	4,204	1,06	0,901	0,757	0,667	5,737	Orthorombic
GdEuO3	4,307	1,11	0,947	0,757	0,701	5,806	Orthorombic
ErPaO3	4,203	1,06	0,9	0,757	0,667	5,698	Orthorombic
ErYO3	4,203	1,06	0,9	0,757	0,667	5,698	Orthorombic
PrAcO3	4,696	1,3	1,12	0,759	0,830	5,994	Orthorombic
HoAgO3	4,317	1,12	0,95	0,759	0,704	5,583	Orthorombic
HoCdO3	4,317	1,12	0,95	0,759	0,704	5,583	Orthorombic
GdThO3	4,296	1,11	0,94	0,760	0,696	5,540	Orthorombic
YDyO3	4,233	1,08	0,912	0,760	0,676	5,484	Orthorombic
HoEuO3	4,312	1,12	0,947	0,760	0,701	5,474	Orthorombic
ErUO3	4,186	1,06	0,89	0,761	0,659	5,330	Orthorombic
CdAcO3	4,701	1,31	1,12	0,761	0,830	6,670	Orthorombic
HoThO3	4,301	1,12	0,94	0,763	0,696	5,237	Orthorombic
DyHoO3	4,215	1,08	0,901	0,763	0,667	5,113	Orthorombic
YHoO3	4,215	1,08	0,901	0,763	0,667	5,113	Orthorombic
HoGdO3	4,297	1,12	0,938	0,763	0,695	5,172	Orthorombic
DyPaO3	4,213	1,08	0,9	0,764	0,667	5,082	Orthorombic
DyYO3	4,213	1,08	0,9	0,764	0,667	5,082	Orthorombic
YPaO3	4,213	1,08	0,9	0,764	0,667	5,082	Orthorombic
ErTmO3	4,169	1,06	0,88	0,764	0,652	5,007	Orthorombic
EuLaO3	4,512	1,23	1,032	0,766	0,764	5,099	Orthorombic

DyErO3	4,196	1,08	0,89	0,767	0,659	4,788	Orthorombic
DyUO3	4,196	1,08	0,89	0,767	0,659	4,788	Orthorombic
YErO3	4,196	1,08	0,89	0,767	0,659	4,788	Orthorombic
YUO3	4,196	1,08	0,89	0,767	0,659	4,788	Orthorombic
ErCeO3	4,152	1,06	0,87	0,768	0,644	4,720	Orthorombic
ErNpO3	4,152	1,06	0,87	0,768	0,644	4,720	Orthorombic
ErYbO3	4,149	1,06	0,868	0,768	0,643	4,666	Orthorombic
YTlO3	4,188	1,08	0,885	0,769	0,656	4,654	Orthorombic
SmLaO3	4,517	1,24	1,032	0,769	0,764	4,852	orthorombic
GdDyO3	4,249	1,11	0,912	0,769	0,676	4,675	Orthorombic
EuHgO3	4,492	1,23	1,02	0,770	0,756	4,765	Orthorombic
CaAcO3	4,716	1,34	1,12	0,770	0,830	5,877	Orthorombic
CeAcO3	4,716	1,34	1,12	0,770	0,830	4,877	Orthorombic
DyTmO3	4,179	1,08	0,88	0,771	0,652	4,527	Orthorombic
YTmO3	4,179	1,08	0,88	0,771	0,652	4,527	Orthorombic
ErLuO3	4,137	1,06	0,861	0,771	0,638	4,489	Orthorombic
ErPuO3	4,136	1,06	0,86	0,771	0,637	4,465	Orthorombic
HoDyO3	4,254	1,12	0,912	0,772	0,676	4,458	Orthorombic
SmHgO3	4,497	1,24	1,02	0,773	0,756	4,548	Orthorombic
GdHoO3	4,230	1,11	0,901	0,773	0,667	4,404	Orthorombic
GdPaO3	4,229	1,11	0,9	0,773	0,667	4,381	Orthorombic
GdYO3	4,229	1,11	0,9	0,773	0,667	4,381	Orthorombic
DyCeO3	4,163	1,08	0,87	0,774	0,644	4,293	Orthorombic
DyNpO3	4,163	1,08	0,87	0,774	0,644	4,293	Orthorombic
YCeO3	4,163	1,08	0,87	0,774	0,644	4,293	Orthorombic
YNpO3	4,163	1,08	0,87	0,774	0,644	4,293	Orthorombic
ErAuO3	4,119	1,06	0,85	0,775	0,630	4,236	Orthorombic
ErPrO3	4,119	1,06	0,85	0,775	0,630	4,236	Orthorombic
DyYbO3	4,159	1,08	0,868	0,775	0,643	4,249	Orthorombic
YYbO3	4,159	1,08	0,868	0,775	0,643	4,249	Orthorombic
LaAcO3	4,727	1,36	1,12	0,776	0,830	4,460	Orthorombic
HoPaO3	4,234	1,12	0,9	0,776	0,667	4,190	Orthorombic
HoYO3	4,234	1,12	0,9	0,776	0,667	4,190	Orthorombic
GdErO3	4,212	1,11	0,89	0,777	0,659	4,163	Orthorombic
GdUO3	4,212	1,11	0,89	0,777	0,659	4,163	Orthorombic
DyLuO3	4,148	1,08	0,861	0,777	0,638	4,103	Orthorombic
YLuO3	4,148	1,08	0,861	0,777	0,638	4,103	Orthorombic

DyPuO3	4,146	1,08	0,86	0,777	0,637	4,083	Orthorombic
YPuO3	4,146	1,08	0,86	0,777	0,637	4,083	Orthorombic
HoErO3	4,217	1,12	0,89	0,780	0,659	3,992	Orthorombic
HoUO3	4,217	1,12	0,89	0,780	0,659	3,992	Orthorombic
GdTmO3	4,195	1,11	0,88	0,780	0,652	3,966	Orthorombic
DyAuO3	4,129	1,08	0,85	0,781	0,630	3,894	Orthorombic
DyPrO3	4,129	1,08	0,85	0,781	0,630	3,894	Orthorombic
YAuO3	4,129	1,08	0,85	0,781	0,630	3,894	Orthorombic
YPrO3	4,129	1,08	0,85	0,781	0,630	3,894	Orthorombic
BiAcO3	4,737	1,38	1,12	0,782	0,830	4,108	Orthorombic
EuNdO3	4,430	1,23	0,983	0,782	0,728	3,955	Orthorombic
HoTmO3	4,200	1,12	0,88	0,783	0,652	3,812	Orthorombic
GdCeO3	4,178	1,11	0,87	0,784	0,644	3,789	Orthorombic
GdNpO3	4,178	1,11	0,87	0,784	0,644	3,789	orthorombic
GdYbO3	4,175	1,11	0,868	0,784	0,643	3,755	Orthorombic
NaAcO3	4,742	1,39	1,12	0,784	0,830	5,952	Orthorombic
SmNdO3	4,435	1,24	0,983	0,785	0,728	3,805	Orthorombic
EuPmO3	4,408	1,23	0,97	0,786	0,719	3,731	Orthorombic
PrLaO3	4,548	1,3	1,032	0,787	0,764	3,765	Orthorombic
HoCeO3	4,183	1,12	0,87	0,787	0,644	3,648	Orthorombic
HoNpO3	4,183	1,12	0,87	0,787	0,644	3,648	Orthorombic
GdLuO3	4,163	1,11	0,861	0,787	0,638	3,643	Orthorombic
GdPuO3	4,162	1,11	0,86	0,787	0,637	3,628	Orthorombic
HoYbO3	4,180	1,12	0,868	0,787	0,643	3,618	Orthorombic
SmPmO3	4,413	1,24	0,97	0,789	0,719	3,597	Orthorombic
CdLaO3	4,553	1,31	1,032	0,790	0,764	4,630	Orthorombic
HoLuO3	4,168	1,12	0,861	0,790	0,638	3,514	orthorombic
HoPuO3	4,167	1,12	0,86	0,790	0,637	3,500	Orthorombic
EuSmO3	4,388	1,23	0,958	0,790	0,710	3,546	Orthorombic
PrHgO3	4,528	1,3	1,02	0,791	0,756	3,578	Orthorombic
GdAuO3	4,145	1,11	0,85	0,791	0,630	3,481	Orthorombic
GdPrO3	4,145	1,11	0,85	0,791	0,630	3,481	Orthorombic
EuAgO3	4,375	1,23	0,95	0,793	0,704	3,433	Orthorombic
EuCdO3	4,375	1,23	0,95	0,793	0,704	3,433	Orthorombic
CdHgO3	4,533	1,31	1,02	0,794	0,756	4,456	Orthorombic
HoAuO3	4,150	1,12	0,85	0,794	0,630	3,365	Orthorombic
HoPrO3	4,150	1,12	0,85	0,794	0,630	3,365	Orthorombic

SmAgO3	4,380	1,24	0,95	0,796	0,704	3,321	Orthorombic
SmCdO3	4,380	1,24	0,95	0,796	0,704	3,321	Orthorombic
EuThO3	4,358	1,23	0,94	0,797	0,696	3,303	Orthorombic
SmEuO3	4,375	1,24	0,947	0,797	0,701	3,283	Orthorombic
EuGdO3	4,354	1,23	0,938	0,797	0,695	3,278	Orthorombic
CaLaO3	4,569	1,34	1,032	0,799	0,764	4,280	Orthorombic
CeLaO3	4,569	1,34	1,032	0,799	0,764	3,280	Orthorombic
SrAcO3	4,768	1,44	1,12	0,799	0,830	4,321	Orthorombic
YInO3	4,045	1,08	0,8	0,799	0,593	3,186	Orthorombic
SmThO3	4,363	1,24	0,94	0,800	0,696	3,199	Orthorombic
SmGdO3	4,360	1,24	0,938	0,800	0,695	3,175	Orthorombic
CaHgO3	4,549	1,34	1,02	0,803	0,756	4,138	Orthorombic
CeHgO3	4,549	1,34	1,02	0,803	0,756	3,138	Orthorombic
PrNdO3	4,466	1,3	0,983	0,803	0,728	3,105	Orthorombic
CdNdO3	4,471	1,31	0,983	0,806	0,728	4,014	Orthorombic
EuDyO3	4,311	1,23	0,912	0,807	0,676	2,989	Orthorombic
ErTbO3	3,968	1,06	0,76	0,808	0,563	2,968	Orthorombic
PrPmO3	4,444	1,3	0,97	0,808	0,719	2,969	Orthorombic
LaHgO3	4,559	1,36	1,02	0,809	0,756	2,958	Orthorombic
SmDyO3	4,316	1,24	0,912	0,810	0,676	2,906	Orthorombic
BiLaO3	4,590	1,38	1,032	0,810	0,764	2,910	Orthorombic
EuHoO3	4,292	1,23	0,901	0,810	0,667	2,884	Orthorombic
CdPmO3	4,450	1,31	0,97	0,811	0,719	3,886	Orthorombic
EuPaO3	4,291	1,23	0,9	0,811	0,667	2,875	Orthorombic
EuYO3	4,291	1,23	0,9	0,811	0,667	2,875	Orthorombic
PrSmO3	4,424	1,3	0,958	0,812	0,710	2,854	Orthorombic
PbAcO3	4,794	1,49	1,12	0,813	0,830	3,866	Orthorombic
NaLaO3	4,595	1,39	1,032	0,813	0,764	4,831	Orthorombic
ErScO3	3,943	1,06	0,745	0,813	0,552	2,847	Orthorombic
SmHoO3	4,298	1,24	0,901	0,814	0,667	2,808	Orthorombic
SmPaO3	4,296	1,24	0,9	0,814	0,667	2,799	Orthorombic
SmYO3	4,296	1,24	0,9	0,814	0,667	2,799	Orthorombic
DyTbO3	3,978	1,08	0,76	0,814	0,563	2,820	Orthorombic
YTbO3	3,978	1,08	0,76	0,814	0,563	2,820	Orthorombic
EuErO3	4,274	1,23	0,89	0,814	0,659	2,788	Orthorombic
EuUO3	4,274	1,23	0,89	0,814	0,659	2,788	Orthorombic
BiHgO3	4,570	1,38	1,02	0,815	0,756	2,799	Orthorombic

PrAgO3	4,411	1,3	0,95	0,815	0,704	2,784	Orthorombic
PrCdO3	4,411	1,3	0,95	0,815	0,704	2,784	Orthorombic
CdSmO3	4,429	1,31	0,958	0,815	0,710	3,779	Orthorombic
CaNdO3	4,487	1,34	0,983	0,815	0,728	3,773	Orthorombic
CeNdO3	4,487	1,34	0,983	0,815	0,728	2,773	Orthorombic
ErZnO3	3,935	1,06	0,74	0,815	0,548	2,810	Orthorombic
PrEuO3	4,406	1,3	0,947	0,816	0,701	2,758	Orthorombic
NaHgO3	4,575	1,39	1,02	0,817	0,756	4,727	Orthorombic
SmErO3	4,279	1,24	0,89	0,818	0,659	2,718	Orthorombic
SmUO3	4,279	1,24	0,89	0,818	0,659	2,718	orthorombic
CdAgO3	4,416	1,31	0,95	0,818	0,704	3,713	Orthorombic
EuTmO3	4,257	1,23	0,88	0,818	0,652	2,708	Orthorombic
YZrO3	3,962	1,08	0,75	0,818	0,556	2,749	Orthorombic
PrThO3	4,394	1,3	0,94	0,818	0,696	2,701	orthorombic
CdEuO3	4,411	1,31	0,947	0,819	0,701	3,689	Orthorombic
PrGdO3	4,391	1,3	0,938	0,819	0,695	2,686	Orthorombic
ErCuO3	3,918	1,06	0,73	0,819	0,541	2,742	Orthorombic
SmTlO3	4,271	1,24	0,885	0,819	0,656	2,680	Orthorombic
CaPmO3	4,465	1,34	0,97	0,820	0,719	3,667	Orthorombic
CePmO3	4,465	1,34	0,97	0,820	0,719	2,667	Orthorombic
DyScO3	3,953	1,08	0,745	0,820	0,552	2,716	Orthorombic
YScO3	3,953	1,08	0,745	0,820	0,552	2,716	Orthorombic
SmTmO3	4,262	1,24	0,88	0,821	0,652	2,643	Orthorombic
CdThO3	4,399	1,31	0,94	0,821	0,696	3,635	Orthorombic
LaNdO3	4,497	1,36	0,983	0,821	0,728	2,635	Orthorombic
EuCeO3	4,241	1,23	0,87	0,822	0,644	2,635	Orthorombic
EuNpO3	4,241	1,23	0,87	0,822	0,644	2,635	Orthorombic
CdGdO3	4,396	1,31	0,938	0,822	0,695	3,620	Orthorombic
DyZnO3	3,945	1,08	0,74	0,822	0,548	2,685	Orthorombic
YZnO3	3,945	1,08	0,74	0,822	0,548	2,685	Orthorombic
EuYbO3	4,237	1,23	0,868	0,823	0,643	2,621	Orthorombic
ErZrO3	3,901	1,06	0,72	0,823	0,533	2,681	Orthorombic
CaSmO3	4,445	1,34	0,958	0,824	0,710	3,577	Orthorombic
CeSmO3	4,445	1,34	0,958	0,824	0,710	2,577	Orthorombic
GdTbO3	3,994	1,11	0,76	0,824	0,563	2,632	Orthorombic
SmCeO3	4,246	1,24	0,87	0,825	0,644	2,574	Orthorombic
SmNpO3	4,246	1,24	0,87	0,825	0,644	2,574	Orthorombic

EuLuO3	4,225	1,23	0,861	0,825	0,638	2,573	Orthorombic
EuPuO3	4,224	1,23	0,86	0,825	0,637	2,567	Orthorombic
SmYbO3	4,242	1,24	0,868	0,826	0,643	2,561	Orthorombic
LaPmO3	4,476	1,36	0,97	0,826	0,719	2,541	Orthorombic
DyCuO3	3,928	1,08	0,73	0,826	0,541	2,627	Orthorombic
YCuO3	3,928	1,08	0,73	0,826	0,541	2,627	Orthorombic
CaAgO3	4,432	1,34	0,95	0,827	0,704	3,522	Orthorombic
CaCdO3	4,432	1,34	0,95	0,827	0,704	3,522	Orthorombic
CeAgO3	4,432	1,34	0,95	0,827	0,704	2,522	Orthorombic
CeCdO3	4,432	1,34	0,95	0,827	0,704	2,522	Orthorombic
ErHfO3	3,884	1,06	0,71	0,827	0,526	2,627	Orthorombic
BiNdO3	4,508	1,38	0,983	0,827	0,728	2,512	Orthorombic
HoTbO3	3,999	1,12	0,76	0,828	0,563	2,577	Orthorombic
CaEuO3	4,427	1,34	0,947	0,828	0,701	3,502	Orthorombic
CeEuO3	4,427	1,34	0,947	0,828	0,701	2,502	Orthorombic
SrLaO3	4,621	1,44	1,032	0,828	0,764	3,497	Orthorombic
SmLuO3	4,231	1,24	0,861	0,828	0,638	2,516	Orthorombic
PrDyO3	4,347	1,3	0,912	0,828	0,676	2,501	Orthorombic
SmPuO3	4,229	1,24	0,86	0,829	0,637	2,510	Orthorombic
EuAuO3	4,207	1,23	0,85	0,829	0,630	2,504	Orthorombic
EuPrO3	4,207	1,23	0,85	0,829	0,630	2,504	Orthorombic
DyZrO3	3,911	1,08	0,72	0,830	0,533	2,574	Orthorombic
LaSmO3	4,455	1,36	0,958	0,830	0,710	2,461	Orthorombic
GdScO3	3,969	1,11	0,745	0,830	0,552	2,549	Orthorombic
NaNdO3	4,513	1,39	0,983	0,830	0,728	4,455	Orthorombic
CaThO3	4,415	1,34	0,94	0,831	0,696	3,457	Orthorombic
CeThO3	4,415	1,34	0,94	0,831	0,696	2,457	Orthorombic
CaGdO3	4,412	1,34	0,938	0,831	0,695	3,444	Orthorombic
CeGdO3	4,412	1,34	0,938	0,831	0,695	2,444	Orthorombic
CdDyO3	4,352	1,31	0,912	0,832	0,676	3,447	Orthorombic
BiPmO3	4,486	1,38	0,97	0,832	0,719	2,427	Orthorombic
GdZnO3	3,961	1,11	0,74	0,832	0,548	2,524	orthorombic
SrHgO3	4,601	1,44	1,02	0,832	0,756	3,417	orthorombic
PrHoO3	4,329	1,3	0,901	0,832	0,667	2,434	Orthorombic
SmAuO3	4,212	1,24	0,85	0,832	0,630	2,451	Orthorombic
SmPrO3	4,212	1,24	0,85	0,832	0,630	2,451	Orthorombic
PrPaO3	4,327	1,3	0,9	0,833	0,667	2,428	Orthorombic

PrYO3	4,327	1,3	0,9	0,833	0,667	2,428	Orthorombic
LaAgO3	4,442	1,36	0,95	0,833	0,704	2,411	Orthorombic
LaCdO3	4,442	1,36	0,95	0,833	0,704	2,411	orthorombic
HoScO3	3,974	1,12	0,745	0,834	0,552	2,499	Orthorombic
DyHfO3	3,895	1,08	0,71	0,834	0,526	2,528	Orthorombic
YHfO3	3,895	1,08	0,71	0,834	0,526	2,528	Orthorombic
LaEuO3	4,437	1,36	0,947	0,834	0,701	2,393	orthorombic
NaPmO3	4,491	1,39	0,97	0,835	0,719	4,375	Orthorombic
CdHoO3	4,334	1,31	0,901	0,836	0,667	3,383	Orthorombic
HoZnO3	3,966	1,12	0,74	0,836	0,548	2,476	Orthorombic
CdPaO3	4,332	1,31	0,9	0,836	0,667	3,377	orthorombic
CdYO3	4,332	1,31	0,9	0,836	0,667	3,377	Orthorombic
GdCuO3	3,944	1,11	0,73	0,836	0,541	2,478	orthorombic
BiSmO3	4,466	1,38	0,958	0,836	0,710	2,356	Orthorombic
PrErO3	4,310	1,3	0,89	0,837	0,659	2,372	Orthorombic
PrUO3	4,310	1,3	0,89	0,837	0,659	2,372	Orthorombic
LaThO3	4,425	1,36	0,94	0,837	0,696	2,353	Orthorombic
LaGdO3	4,422	1,36	0,938	0,838	0,695	2,342	Orthorombic
BiAgO3	4,452	1,38	0,95	0,839	0,704	2,312	Orthorombic
BiCdO3	4,452	1,38	0,95	0,839	0,704	2,312	Orthorombic
NaSmO3	4,471	1,39	0,958	0,839	0,710	4,307	Orthorombic
ErNbO3	3,834	1,06	0,68	0,839	0,504	2,497	Orthorombic
ErTaO3	3,834	1,06	0,68	0,839	0,504	2,497	Orthorombic
CdErO3	4,316	1,31	0,89	0,840	0,659	3,325	Orthorombic
CdUO3	4,316	1,31	0,89	0,840	0,659	3,325	Orthorombic
HoCuO3	3,949	1,12	0,73	0,840	0,541	2,434	Orthorombic
PrTmO3	4,294	1,3	0,88	0,840	0,652	2,320	Orthorombic
GdZrO3	3,927	1,11	0,72	0,840	0,533	2,437	Orthorombic
BiEuO3	4,447	1,38	0,947	0,840	0,701	2,296	Orthorombic
CaDyO3	4,368	1,34	0,912	0,841	0,676	3,299	Orthorombic
CeDyO3	4,368	1,34	0,912	0,841	0,676	2,299	Orthorombic
NaAgO3	4,458	1,39	0,95	0,842	0,704	4,265	Orthorombic
NaCdO3	4,458	1,39	0,95	0,842	0,704	4,265	Orthorombic
BiThO3	4,436	1,38	0,94	0,843	0,696	2,260	Orthorombic
PbLaO3	4,647	1,49	1,032	0,843	0,764	3,239	Orthorombic
CdTmO3	4,299	1,31	0,88	0,843	0,652	3,276	Orthorombic
NaEuO3	4,453	1,39	0,947	0,843	0,701	4,250	Orthorombic

BiGdO3	4,432	1,38	0,938	0,844	0,695	2,250	Orthorombic
HoZrO3	3,932	1,12	0,72	0,844	0,533	2,396	Orthorombic
PrCeO3	4,277	1,3	0,87	0,844	0,644	2,272	Orthorombic
PrNpO3	4,277	1,3	0,87	0,844	0,644	2,272	orthorombic
GdHfO3	3,910	1,11	0,71	0,844	0,526	2,400	Orthorombic
PrYbO3	4,274	1,3	0,868	0,845	0,643	2,263	orthorombic
CaHoO3	4,350	1,34	0,901	0,845	0,667	3,245	Orthorombic
CeHoO3	4,350	1,34	0,901	0,845	0,667	2,245	Orthorombic
CaPaO3	4,348	1,34	0,9	0,845	0,667	3,241	Orthorombic
CaYO3	4,348	1,34	0,9	0,845	0,667	3,241	orthorombic
CePaO3	4,348	1,34	0,9	0,845	0,667	2,241	Orthorombic
CeYO3	4,348	1,34	0,9	0,845	0,667	2,241	Orthorombic
SrNdO3	4,539	1,44	0,983	0,846	0,728	3,210	Orthorombic
NaThO3	4,441	1,39	0,94	0,846	0,696	4,216	Orthorombic
DyNbO3	3,844	1,08	0,68	0,846	0,504	2,418	Orthorombic
DyTaO3	3,844	1,08	0,68	0,846	0,504	2,418	Orthorombic
YNbO3	3,844	1,08	0,68	0,846	0,504	2,418	Orthorombic
YTaO3	3,844	1,08	0,68	0,846	0,504	2,418	Orthorombic
NaGdO3	4,437	1,39	0,938	0,847	0,695	4,207	Orthorombic
LaDyO3	4,378	1,36	0,912	0,847	0,676	2,212	Orthorombic
CdCeO3	4,282	1,31	0,87	0,847	0,644	3,231	Orthorombic
CdNpO3	4,282	1,31	0,87	0,847	0,644	3,231	Orthorombic
PbHgO3	4,627	1,49	1,02	0,847	0,756	3,178	Orthorombic
BaAcO3	4,857	1,61	1,12	0,847	0,830	3,166	Orthorombic
PrLuO3	4,262	1,3	0,861	0,848	0,638	2,232	Orthorombic
ErWO3	3,801	1,06	0,66	0,848	0,489	2,435	Orthorombic
HoHfO3	3,915	1,12	0,71	0,848	0,526	2,362	Orthorombic
PrPuO3	4,260	1,3	0,86	0,848	0,637	2,228	Orthorombic
CdYbO3	4,279	1,31	0,868	0,848	0,643	3,222	Orthorombic
CaErO3	4,331	1,34	0,89	0,849	0,659	3,196	Orthorombic
CaUO3	4,331	1,34	0,89	0,849	0,659	3,196	Orthorombic
CeErO3	4,331	1,34	0,89	0,849	0,659	2,196	Orthorombic
CeUO3	4,331	1,34	0,89	0,849	0,659	2,196	Orthorombic
SrPmO3	4,517	1,44	0,97	0,850	0,719	3,149	Orthorombic
CdLuO3	4,267	1,31	0,861	0,851	0,638	3,193	Orthorombic
CdPuO3	4,265	1,31	0,86	0,851	0,637	3,189	Orthorombic
LaHoO3	4,360	1,36	0,901	0,851	0,667	2,164	Orthorombic

LaPaO3	4,358	1,36	0,9	0,852	0,667	2,160	Orthorombic
LaYO3	4,358	1,36	0,9	0,852	0,667	2,160	Orthorombic
PrAuO3	4,243	1,3	0,85	0,852	0,630	2,188	Orthorombic
SmInO3	4,128	1,24	0,8	0,852	0,593	2,224	Orthorombic
ErMoO3	3,784	1,06	0,65	0,852	0,481	2,411	Orthorombic
CaTmO3	4,314	1,34	0,88	0,853	0,652	3,155	Orthorombic
CeTmO3	4,314	1,34	0,88	0,853	0,652	2,155	Orthorombic
BiDyO3	4,389	1,38	0,912	0,853	0,676	2,133	Orthorombic
ErTcO3	3,775	1,06	0,645	0,854	0,478	2,401	Orthorombic
SrSmO3	4,497	1,44	0,958	0,855	0,710	3,097	Orthorombic
DyWO3	3,811	1,08	0,66	0,855	0,489	2,368	Orthorombic
YWO3	3,811	1,08	0,66	0,855	0,489	2,368	Orthorombic
CdAuO3	4,249	1,31	0,85	0,855	0,630	3,151	Orthorombic
CdPrO3	4,249	1,31	0,85	0,855	0,630	3,151	Orthorombic
LaErO3	4,342	1,36	0,89	0,855	0,659	2,121	Orthorombic
LaUO3	4,342	1,36	0,89	0,855	0,659	2,121	Orthorombic
KAcO3	4,872	1,64	1,12	0,856	0,830	4,045	Orthorombic
ErVO3	3,767	1,06	0,64	0,856	0,474	2,392	Orthorombic
NaDyO3	4,394	1,39	0,912	0,857	0,676	4,097	Orthorombic
CaCeO3	4,298	1,34	0,87	0,857	0,644	3,118	Orthorombic
CaNpO3	4,298	1,34	0,87	0,857	0,644	3,118	Orthorombic
CeNpO3	4,298	1,34	0,87	0,857	0,644	2,118	Orthorombic
GdNbO3	3,860	1,11	0,68	0,857	0,504	2,316	Orthorombic
GdTaO3	3,860	1,11	0,68	0,857	0,504	2,316	Orthorombic
LaTlO3	4,333	1,36	0,885	0,857	0,656	2,102	Orthorombic
BiHoO3	4,370	1,38	0,901	0,858	0,667	2,091	Orthorombic
CaYbO3	4,294	1,34	0,868	0,858	0,643	3,110	Orthorombic
CeYbO3	4,294	1,34	0,868	0,858	0,643	2,110	Orthorombic
SrAgO3	4,484	1,44	0,95	0,858	0,704	3,065	Orthorombic
SrCdO3	4,484	1,44	0,95	0,858	0,704	3,065	Orthorombic
BiPaO3	4,369	1,38	0,9	0,858	0,667	2,087	Orthorombic
BiYO3	4,369	1,38	0,9	0,858	0,667	2,087	Orthorombic
SrEuO3	4,479	1,44	0,947	0,859	0,701	3,054	Orthorombic
DyMoO3	3,794	1,08	0,65	0,859	0,481	2,349	Orthorombic
YMoO3	3,794	1,08	0,65	0,859	0,481	2,349	Orthorombic
LaTmO3	4,325	1,36	0,88	0,859	0,652	2,084	Orthorombic
CaLuO3	4,283	1,34	0,861	0,860	0,638	3,086	Orthorombic

CeLuO3	4,283	1,34	0,861	0,860	0,638	2,086	Orthorombic
HoNbO3	3,865	1,12	0,68	0,860	0,504	2,286	Orthorombic
HoTaO3	3,865	1,12	0,68	0,860	0,504	2,286	Orthorombic
ErOsO3	3,750	1,06	0,63	0,861	0,467	2,377	Orthorombic
ErReO3	3,750	1,06	0,63	0,861	0,467	2,377	orthorombic
CaPuO3	4,281	1,34	0,86	0,861	0,637	3,083	Orthorombic
CePuO3	4,281	1,34	0,86	0,861	0,637	2,083	Orthorombic
NaHoO3	4,376	1,39	0,901	0,861	0,667	4,057	Orthorombic
PbNdO3	4,565	1,49	0,983	0,861	0,728	3,018	Orthorombic
NaPaO3	4,374	1,39	0,9	0,861	0,667	4,053	Orthorombic
NaYO3	4,374	1,39	0,9	0,861	0,667	4,053	Orthorombic
DyTcO3	3,786	1,08	0,645	0,861	0,478	2,341	Orthorombic
YTcO3	3,786	1,08	0,645	0,861	0,478	2,341	Orthorombic
SrThO3	4,530	1,44	0,94	0,861	0,696	3,028	Orthorombic
BiErO3	4,352	1,38	0,89	0,862	0,659	2,052	Orthorombic
BiUO3	4,352	1,38	0,89	0,862	0,659	2,052	Orthorombic
SrGdO3	4,463	1,44	0,938	0,862	0,695	3,021	Orthorombic
ErIrO3	3,742	1,06	0,625	0,863	0,463	2,370	Orthorombic
ErPtO3	3,742	1,06	0,625	0,863	0,463	2,370	Orthorombic
LaCeO3	4,308	1,36	0,87	0,863	0,644	2,051	Orthorombic
LaNpO3	4,308	1,36	0,87	0,863	0,644	2,051	Orthorombic
DyVO3	3,777	1,08	0,64	0,863	0,474	2,334	Orthorombic
YVO3	3,777	1,08	0,64	0,863	0,474	2,334	Orthorombic
LaYbO3	4,305	1,36	0,868	0,864	0,643	2,045	Orthorombic
CaAuO3	4,264	1,34	0,85	0,865	0,630	3,052	Orthorombic
CaPrO3	4,264	1,34	0,85	0,865	0,630	3,052	Orthorombic
CeAuO3	4,264	1,34	0,85	0,865	0,630	2,052	Orthorombic
CePrO3	4,264	1,34	0,85	0,865	0,630	2,052	Orthorombic
EuTbO3	4,056	1,23	0,76	0,865	0,563	2,138	Orthorombic
NaErO3	4,357	1,39	0,89	0,865	0,659	4,020	Orthorombic
NaUO3	4,357	1,39	0,89	0,865	0,659	4,020	orthorombic
ErGaO3	3,734	1,06	0,62	0,865	0,459	2,365	Orthorombic
ErRuO3	3,734	1,06	0,62	0,865	0,459	2,365	Orthorombic
GdWO3	3,827	1,11	0,66	0,865	0,489	2,280	Orthorombic
PbPmO3	4,543	1,49	0,97	0,866	0,719	2,970	Orthorombic
BiTmO3	4,335	1,38	0,88	0,866	0,652	2,020	Orthorombic
LaLuO3	4,293	1,36	0,861	0,867	0,638	2,023	Orthorombic

LaPuO3	4,291	1,36	0,86	0,867	0,637	2,020	Orthorombic
ErPdO3	3,725	1,06	0,615	0,867	0,456	2,361	Orthorombic
DyOsO3	3,761	1,08	0,63	0,868	0,467	2,323	Orthorombic
DyReO3	3,761	1,08	0,63	0,868	0,467	2,323	Orthorombic
YOsO3	3,761	1,08	0,63	0,868	0,467	2,323	Orthorombic
YReO3	3,761	1,08	0,63	0,868	0,467	2,323	Orthorombic
SmTbO3	4,061	1,24	0,76	0,868	0,563	2,109	Orthorombic
NaTmO3	4,340	1,39	0,88	0,869	0,652	3,989	Orthorombic
HoWO3	3,832	1,12	0,66	0,869	0,489	2,254	Orthorombic
ErCoO3	3,717	1,06	0,61	0,869	0,452	2,358	Orthorombic
BiCeO3	4,318	1,38	0,87	0,870	0,644	1,990	Orthorombic
BiNpO3	4,318	1,38	0,87	0,870	0,644	1,990	Orthorombic
GdMoO3	3,810	1,11	0,65	0,870	0,481	2,268	orthorombic
DyIrO3	3,752	1,08	0,625	0,870	0,463	2,319	Orthorombic
DyPtO3	3,752	1,08	0,625	0,870	0,463	2,319	Orthorombic
YIrO3	3,752	1,08	0,625	0,870	0,463	2,319	Orthorombic
YPtO3	3,752	1,08	0,625	0,870	0,463	2,319	Orthorombic
PbSmO3	4,523	1,49	0,958	0,870	0,710	2,931	Orthorombic
BiYbO3	4,315	1,38	0,868	0,870	0,643	1,984	Orthorombic
EuScO3	4,031	1,23	0,745	0,871	0,552	2,105	Orthorombic
LaAuO3	4,275	1,36	0,85	0,871	0,630	1,992	Orthorombic
LaPrO3	4,275	1,36	0,85	0,871	0,630	1,992	Orthorombic
ErTiO3	3,708	1,06	0,605	0,872	0,448	2,356	Orthorombic
GdTcO3	3,801	1,11	0,645	0,872	0,478	2,263	Orthorombic
SrDyO3	4,420	1,44	0,912	0,872	0,676	2,937	Orthorombic
DyGaO3	3,744	1,08	0,62	0,872	0,459	2,316	Orthorombic
DyRuO3	3,744	1,08	0,62	0,872	0,459	2,316	Orthorombic
YGaO3	3,744	1,08	0,62	0,872	0,459	2,316	Orthorombic
YRuO3	3,744	1,08	0,62	0,872	0,459	2,316	Orthorombic
NaCeO3	4,324	1,39	0,87	0,873	0,644	3,961	Orthorombic
NaNpO3	4,324	1,39	0,87	0,873	0,644	3,961	Orthorombic
EuZnO3	4,023	1,23	0,74	0,873	0,548	2,096	Orthorombic
BiLuO3	4,303	1,38	0,861	0,873	0,638	1,966	Orthorombic
PbAgO3	4,509	1,49	0,95	0,873	0,704	2,906	Orthorombic
PbCdO3	4,509	1,49	0,95	0,873	0,704	2,906	Orthorombic
HoMoO3	3,815	1,12	0,65	0,873	0,481	2,244	Orthorombic
BiPuO3	4,302	1,38	0,86	0,873	0,637	1,963	Orthorombic

NaYbO3	4,320	1,39	0,868	0,874	0,643	3,956	Orthorombic
ErRhO3	3,700	1,06	0,6	0,874	0,444	2,354	Orthorombic
GdVO3	3,793	1,11	0,64	0,874	0,474	2,259	Orthorombic
SmScO3	4,036	1,24	0,745	0,874	0,552	2,079	orthorombic
PbEuO3	4,504	1,49	0,947	0,874	0,701	2,897	Orthorombic
DyPdO3	3,736	1,08	0,615	0,874	0,456	2,314	Orthorombic
YPdO3	3,736	1,08	0,615	0,874	0,456	2,314	Orthorombic
HoTcO3	3,807	1,12	0,645	0,875	0,478	2,240	Orthorombic
SmZnO3	4,028	1,24	0,74	0,876	0,548	2,070	Orthorombic
NaLuO3	4,309	1,39	0,861	0,876	0,638	3,939	Orthorombic
SrHoO3	4,401	1,44	0,901	0,876	0,667	2,907	Orthorombic
DyCoO3	3,727	1,08	0,61	0,877	0,452	2,312	Orthorombic
YCoO3	3,727	1,08	0,61	0,877	0,452	2,312	Orthorombic
NaPuO3	4,307	1,39	0,86	0,877	0,637	3,936	Orthorombic
SrPaO3	4,400	1,44	0,9	0,877	0,667	2,904	Orthorombic
SrYO3	4,400	1,44	0,9	0,877	0,667	2,904	Orthorombic
PbThO3	4,493	1,49	0,94	0,877	0,696	2,877	Orthorombic
EuCuO3	4,006	1,23	0,73	0,877	0,541	2,079	Orthorombic
BiAuO3	4,285	1,38	0,85	0,877	0,630	1,938	Orthorombic
BiPrO3	4,285	1,38	0,85	0,877	0,630	1,938	Orthorombic
HoVO3	3,798	1,12	0,64	0,878	0,474	2,237	Orthorombic
PbGdO3	4,489	1,49	0,938	0,878	0,695	2,872	Orthorombic
GdOsO3	3,776	1,11	0,63	0,879	0,467	2,254	Orthorombic
GdReO3	3,776	1,11	0,63	0,879	0,467	2,254	Orthorombic
BaLaO3	4,709	1,61	1,032	0,879	0,764	2,816	Orthorombic
DyTiO3	3,719	1,08	0,605	0,879	0,448	2,312	Orthorombic
YTiO3	3,719	1,08	0,605	0,879	0,448	2,312	orthorombic
SmCuO3	4,011	1,24	0,73	0,880	0,541	2,055	Orthorombic
NaAuO3	4,290	1,39	0,85	0,881	0,630	3,913	Orthorombic
NaPrO3	4,290	1,39	0,85	0,881	0,630	3,913	Orthorombic
ErFeO3	3,675	1,06	0,585	0,881	0,433	2,356	Orthorombic
SrErO3	4,383	1,44	0,89	0,881	0,659	2,879	Orthorombic
SrUO3	4,376	1,44	0,89	0,881	0,659	2,879	Orthorombic
GdIrO3	3,768	1,11	0,625	0,881	0,463	2,252	Orthorombic
GdPtO3	3,768	1,11	0,625	0,881	0,463	2,252	Orthorombic
DyRhO3	3,710	1,08	0,6	0,881	0,444	2,312	Orthorombic
YRhO3	3,710	1,08	0,6	0,881	0,444	2,312	Orthorombic

EuZrO3	3,989	1,23	0,72	0,881	0,533	2,065	Orthorombic
HoOsO3	3,781	1,12	0,63	0,882	0,467	2,233	Orthorombic
HoReO3	3,781	1,12	0,63	0,882	0,467	2,233	Orthorombic
GdRuO3	3,760	1,11	0,62	0,883	0,459	2,251	Orthorombic
BaHgO3	4,689	1,61	1,02	0,883	0,756	2,782	Orthorombic
HoIrO3	3,773	1,12	0,625	0,884	0,463	2,232	orthorombic
HoPtO3	3,773	1,12	0,625	0,884	0,463	2,232	Orthorombic
SrTmO3	4,366	1,44	0,88	0,885	0,652	2,857	Orthorombic
SmZrO3	3,994	1,24	0,72	0,885	0,533	2,043	Orthorombic
GdPdO3	3,751	1,11	0,615	0,885	0,456	2,252	Orthorombic
EuHfO3	3,973	1,23	0,71	0,886	0,526	2,054	Orthorombic
HoRuO3	3,765	1,12	0,62	0,887	0,459	2,232	Orthorombic
GdCoO3	3,743	1,11	0,61	0,887	0,452	2,253	Orthorombic
KLaO3	4,725	1,64	1,032	0,888	0,764	3,739	Orthorombic
PbDyO3	4,446	1,49	0,912	0,888	0,676	2,808	Orthorombic
DyFeO3	3,685	1,08	0,585	0,888	0,433	2,319	Orthorombic
YFeO3	3,685	1,08	0,585	0,888	0,433	2,319	Orthorombic
PrTbO3	4,093	1,3	0,76	0,888	0,563	1,963	Orthorombic
SrCeO3	4,350	1,44	0,87	0,889	0,644	2,836	orthorombic
SrNpO3	4,350	1,44	0,87	0,889	0,644	2,836	orthorombic
HoPdO3	3,756	1,12	0,615	0,889	0,456	2,233	Orthorombic
SmHfO3	3,978	1,24	0,71	0,889	0,526	2,034	Orthorombic
SrYbO3	4,346	1,44	0,868	0,889	0,643	2,833	Orthorombic
GdTiO3	3,734	1,11	0,605	0,890	0,448	2,255	Orthorombic
HoCoO3	3,748	1,12	0,61	0,891	0,452	2,235	Orthorombic
LaInO3	4,191	1,36	0,8	0,891	0,593	1,891	orthorombic
CdTbO3	4,098	1,31	0,76	0,891	0,563	2,942	Orthorombic
GdRhO3	3,726	1,11	0,6	0,892	0,444	2,257	orthorombic
KHgO3	4,705	1,64	1,02	0,892	0,756	3,709	Orthorombic
PbHoO3	4,427	1,49	0,901	0,892	0,667	2,786	Orthorombic
SrLuO3	4,334	1,44	0,861	0,892	0,638	2,820	Orthorombic
PbPaO3	4,426	1,49	0,9	0,893	0,667	2,784	Orthorombic
PbYO3	4,426	1,49	0,9	0,893	0,667	2,784	Orthorombic
SrPuO3	4,378	1,44	0,86	0,893	0,637	2,818	Orthorombic
HoTiO3	3,740	1,12	0,605	0,893	0,448	2,237	Orthorombic
PrScO3	4,067	1,3	0,745	0,894	0,552	1,946	Orthorombic
HoRhO3	3,731	1,12	0,6	0,896	0,444	2,241	orthorombic

PbErO3	4,409	1,49	0,89	0,897	0,659	2,766	Orthorombic
PbUO3	4,409	1,49	0,89	0,897	0,659	2,766	orthorombic
PrZnO3	4,059	1,3	0,74	0,897	0,548	1,942	Orthorombic
SrAuO3	4,316	1,44	0,85	0,897	0,630	2,802	Orthorombic
SrPrO3	4,316	1,44	0,85	0,897	0,630	2,802	Orthorombic
ErCrO3	3,616	1,06	0,55	0,897	0,407	2,392	Orthorombic
BaNdO3	4,627	1,61	0,983	0,897	0,728	2,693	orthorombic
CdScO3	4,073	1,31	0,745	0,898	0,552	2,928	Orthorombic
EuNbO3	3,922	1,23	0,68	0,899	0,504	2,037	orthorombic
EuTaO3	3,922	1,23	0,68	0,899	0,504	2,037	Orthorombic
GdFeO3	3,701	1,11	0,585	0,899	0,433	2,270	Orthorombic
CdZnO3	4,064	1,31	0,74	0,900	0,548	2,924	Orthorombic
PbTmO3	4,392	1,49	0,88	0,901	0,652	2,749	Orthorombic
PrCuO3	4,042	1,3	0,73	0,901	0,541	1,935	Orthorombic
CaTbO3	4,113	1,34	0,76	0,901	0,563	2,885	Orthorombic
CeTbO3	4,113	1,34	0,76	0,901	0,563	1,885	Orthorombic
BaPmO3	4,605	1,61	0,97	0,902	0,719	2,667	Orthorombic
SmNbO3	3,927	1,24	0,68	0,902	0,504	2,021	Orthorombic
SmTaO3	3,927	1,24	0,68	0,902	0,504	2,021	Orthorombic
HoFeO3	3,706	1,12	0,585	0,903	0,433	2,256	orthorombic
ErAlO3	3,591	1,06	0,535	0,904	0,396	2,421	orthorombic
CdCuO3	4,048	1,31	0,73	0,904	0,541	2,918	Orthorombic
DyCrO3	3,627	1,08	0,55	0,904	0,407	2,365	Orthorombic
YCrO3	3,627	1,08	0,55	0,904	0,407	2,365	Orthorombic
PbCeO3	4,375	1,49	0,87	0,905	0,644	2,735	orthorombic
PbNpO3	4,375	1,49	0,87	0,905	0,644	2,735	Orthorombic
PrZrO3	4,026	1,3	0,72	0,905	0,533	1,931	Orthorombic
PbYbO3	4,372	1,49	0,868	0,905	0,643	2,732	Orthorombic
KNdO3	4,643	1,64	0,983	0,906	0,728	3,633	orthorombic
ErMnO3	3,583	1,06	0,53	0,906	0,393	2,433	orthorombic
BaSmO3	4,585	1,61	0,958	0,907	0,710	2,646	Orthorombic
EuWO3	3,889	1,23	0,66	0,908	0,489	2,039	orthorombic
CaScO3	4,088	1,34	0,745	0,908	0,552	2,876	Orthorombic
CeScO3	4,088	1,34	0,745	0,908	0,552	1,876	orthorombic
LaTbO3	4,124	1,36	0,76	0,908	0,563	1,851	Orthorombic
PbLuO3	4,360	1,49	0,861	0,908	0,638	2,723	Orthorombic
CdZrO3	4,031	1,31	0,72	0,909	0,533	2,915	Orthorombic

PbPuO3	4,359	1,49	0,86	0,909	0,637	2,722	orthorombic
PrHfO3	4,009	1,3	0,71	0,910	0,526	1,929	orthorombic
BaAgO3	4,572	1,61	0,95	0,910	0,704	2,634	Orthorombic
BaCdO3	4,572	1,61	0,95	0,910	0,704	2,634	Orthorombic
CaZnO3	4,080	1,34	0,74	0,910	0,548	2,874	Orthorombic
CeZnO3	4,080	1,34	0,74	0,910	0,548	1,874	Orthorombic
SmWO3	3,894	1,24	0,66	0,911	0,489	2,025	Orthorombic
BaEuO3	4,567	1,61	0,947	0,911	0,701	2,629	Orthorombic
KPmO3	4,621	1,64	0,97	0,911	0,719	3,611	Orthorombic
DyAlO3	3,602	1,08	0,535	0,912	0,396	2,397	Orthorombic
YAlO3	3,602	1,08	0,535	0,912	0,396	2,397	Orthorombic
EuMoO3	3,872	1,23	0,65	0,912	0,481	2,044	Orthorombic
PbAuO3	4,342	1,49	0,85	0,913	0,630	2,711	Orthorombic
PbPrO3	4,342	1,49	0,85	0,913	0,630	2,711	Orthorombic
CdHfO3	4,014	1,31	0,71	0,913	0,526	2,914	Orthorombic
DyMnO3	3,593	1,08	0,53	0,914	0,393	2,410	Orthorombic
YMnO3	3,593	1,08	0,53	0,914	0,393	2,410	orthorombic
BaThO3	4,555	1,61	0,94	0,914	0,696	2,619	Orthorombic
EuTcO3	3,864	1,23	0,645	0,914	0,478	2,047	Orthorombic
CaCuO3	4,063	1,34	0,73	0,914	0,541	2,872	Orthorombic
CeCuO3	4,063	1,34	0,73	0,914	0,541	1,872	Orthorombic
LaScO3	4,099	1,36	0,745	0,915	0,552	1,845	orthorombic
BaGdO3	4,552	1,61	0,938	0,915	0,695	2,616	Orthorombic
BiTbO3	4,134	1,38	0,76	0,915	0,563	1,820	orthorombic
GdCrO3	3,642	1,11	0,55	0,916	0,407	2,329	Orthorombic
SmMoO3	3,877	1,24	0,65	0,916	0,481	2,030	Orthorombic
KSmO3	4,601	1,64	0,958	0,916	0,710	3,594	Orthorombic
EuVO3	3,855	1,23	0,64	0,917	0,474	2,051	orthorombic
LaZnO3	4,090	1,36	0,74	0,917	0,548	1,844	Orthorombic
SmTcO3	3,869	1,24	0,645	0,918	0,478	2,034	Orthorombic
NaTbO3	4,139	1,39	0,76	0,918	0,563	3,806	Orthorombic
CaZrO3	4,138	1,34	0,72	0,919	0,533	2,871	Orthorombic
CeZrO3	4,046	1,34	0,72	0,919	0,533	1,871	Orthorombic
HoCrO3	3,647	1,12	0,55	0,919	0,407	2,318	Orthorombic
KAgO3	4,587	1,64	0,95	0,919	0,704	3,583	orthorombic
KCdO3	4,587	1,64	0,95	0,919	0,704	3,583	orthorombic
SmVO3	3,860	1,24	0,64	0,920	0,474	2,039	orthorombic

KEuO3	4,582	1,64	0,947	0,920	0,701	3,579	Orthorombic
LaCuO3	4,073	1,36	0,73	0,921	0,541	1,844	Orthorombic
EuOsO3	3,839	1,23	0,63	0,921	0,467	2,061	orthorombic
EuReO3	3,839	1,23	0,63	0,921	0,467	2,061	Orthorombic
BiScO3	4,109	1,38	0,745	0,921	0,552	1,817	orthorombic
PrNbO3	3,959	1,3	0,68	0,923	0,504	1,935	Orthorombic
PrTaO3	3,959	1,3	0,68	0,923	0,504	1,935	orthorombic
KThO3	4,571	1,64	0,94	0,923	0,696	3,571	Orthorombic
CaHfO3	4,030	1,34	0,71	0,923	0,526	2,873	Orthorombic
CeHfO3	4,030	1,34	0,71	0,923	0,526	1,873	Orthorombic
BiZnO3	4,101	1,38	0,74	0,924	0,548	1,817	orthorombic
EuIrO3	3,830	1,23	0,625	0,924	0,463	2,067	Orthorombic
EuPtO3	3,830	1,23	0,625	0,924	0,463	2,067	Orthorombic
KGdO3	4,567	1,64	0,938	0,924	0,695	3,569	Orthorombic
NaScO3	4,114	1,39	0,745	0,925	0,552	3,804	Orthorombic
SmOsO3	3,844	1,24	0,63	0,925	0,467	2,050	Orthorombic
SmReO3	3,844	1,24	0,63	0,925	0,467	2,050	Orthorombic
GdMnO3	3,609	1,11	0,53	0,925	0,393	2,380	orthorombic
BaDyO3	4,508	1,61	0,912	0,925	0,676	2,586	Orthorombic
LaZrO3	4,057	1,36	0,72	0,926	0,533	1,845	Orthorombic
EuRuO3	3,822	1,23	0,62	0,926	0,459	2,073	Orthorombic
CdNbO3	3,964	1,31	0,68	0,927	0,504	2,923	Orthorombic
CdTaO3	3,964	1,31	0,68	0,927	0,504	2,923	Orthorombic
NaZnO3	4,106	1,39	0,74	0,927	0,548	3,804	orthorombic
SmIrO3	3,835	1,24	0,625	0,927	0,463	2,056	orthorombic
SmPtO3	3,835	1,24	0,625	0,927	0,463	2,056	orthorombic
BiCuO3	4,084	1,38	0,73	0,928	0,541	1,818	Orthorombic
EuPdO3	3,813	1,23	0,615	0,928	0,456	2,081	orthorombic
HoMnO3	3,614	1,12	0,53	0,929	0,393	2,372	Orthorombic
SmGaO3	3,827	1,24	0,62	0,930	0,459	2,063	Orthorombic
SmRuO3	3,827	1,24	0,62	0,930	0,459	2,063	orthorombic
BaHoO3	4,490	1,61	0,901	0,930	0,667	2,577	orthorombic
LaHfO3	4,040	1,36	0,71	0,930	0,526	1,848	Orthorombic
BaPaO3	4,510	1,61	0,9	0,930	0,667	2,576	orthorombic
BaYO3	4,488	1,61	0,9	0,930	0,667	2,576	Orthorombic
EuCoO3	3,805	1,23	0,61	0,931	0,452	2,088	Orthorombic
ErNiO3	3,499	1,06	0,48	0,931	0,356	2,600	Orthorombic

NaCuO3	4,089	1,39	0,73	0,931	0,541	3,806	orthorombic
SmPdO3	3,819	1,24	0,615	0,932	0,456	2,070	orthorombic
PrWO3	3,925	1,3	0,66	0,932	0,489	1,951	orthorombic
CaSnO3	3,965	1,34	0,69	0,932	0,511	2,882	orthorombic
BiZrO3	4,067	1,38	0,72	0,933	0,533	1,821	Orthorombic
EuTiO3	3,797	1,23	0,605	0,933	0,448	2,097	Orthorombic
BaErO3	4,471	1,61	0,89	0,934	0,659	2,569	Orthorombic
BaUO3	4,380	1,61	0,89	0,934	0,659	2,569	Orthorombic
SmCoO3	3,810	1,24	0,61	0,934	0,452	2,079	Orthorombic
KDyO3	4,524	1,64	0,912	0,935	0,676	3,545	Orthorombic
SrTbO3	4,165	1,44	0,76	0,935	0,563	2,741	Orthorombic
EuRhO3	3,788	1,23	0,6	0,936	0,444	2,106	orthorombic
CdWO3	3,930	1,31	0,66	0,936	0,489	2,941	Orthorombic
NaZrO3	4,072	1,39	0,72	0,936	0,533	3,810	Orthorombic
SmTiO3	3,802	1,24	0,605	0,937	0,448	2,087	Orthorombic
PrMoO3	3,908	1,3	0,65	0,937	0,481	1,962	Orthorombic
CaNbO3	3,979	1,34	0,68	0,937	0,504	2,890	orthorombic
CaTaO3	3,975	1,34	0,68	0,937	0,504	2,890	Orthorombic
CeNbO3	3,979	1,34	0,68	0,937	0,504	1,890	Orthorombic
CeTaO3	3,979	1,34	0,68	0,937	0,504	1,890	Orthorombic
BiHfO3	4,050	1,38	0,71	0,937	0,526	1,826	Orthorombic
BaTmO3	4,454	1,61	0,88	0,939	0,652	2,563	Orthorombic
DyNiO3	3,509	1,08	0,48	0,939	0,356	2,587	Orthorombic
YNiO3	3,509	1,08	0,48	0,939	0,356	2,587	Orthorombic
SmRhO3	3,793	1,24	0,6	0,939	0,444	2,097	Orthorombic
KHoO3	4,505	1,64	0,901	0,939	0,667	3,537	Orthorombic
PrFeO3	3,777	1,3	0,645	0,939	0,478	1,969	Orthorombic
PrMnO3	3,880	1,3	0,645	0,939	0,478	1,969	Orthorombic
PrTcO3	3,900	1,3	0,645	0,939	0,478	1,969	Orthorombic
KPaO3	4,504	1,64	0,9	0,940	0,667	3,537	Cubic
KYO3	4,504	1,64	0,9	0,940	0,667	3,537	Cubic
CdMoO3	3,914	1,31	0,65	0,940	0,481	2,953	Cubic
NaHfO3	4,056	1,39	0,71	0,941	0,526	3,816	Cubic
PrVO3	3,870	1,3	0,64	0,942	0,474	1,976	Cubic
SrScO3	4,140	1,44	0,745	0,942	0,552	2,745	Cubic
BaCeO3	4,438	1,61	0,87	0,943	0,644	2,558	Cubic
BaNpO3	4,437	1,61	0,87	0,943	0,644	2,558	Cubic

CdTcO3	3,905	1,31	0,645	0,943	0,478	2,960	Cubic
EuFeO3	3,763	1,23	0,585	0,943	0,433	2,137	Cubic
BaYbO3	4,434	1,61	0,868	0,944	0,643	2,558	Cubic
KErO3	4,487	1,64	0,89	0,944	0,659	3,532	Cubic
KUO3	4,487	1,64	0,89	0,944	0,659	3,532	Cubic
SrZnO3	4,132	1,44	0,74	0,944	0,548	2,747	Cubic
LaNbO3	3,990	1,36	0,68	0,944	0,504	1,871	Cubic
LaTaO3	3,990	1,36	0,68	0,944	0,504	1,871	Cubic
CdVO3	3,897	1,31	0,64	0,945	0,474	2,967	Cubic
CaWO3	3,946	1,34	0,66	0,946	0,489	2,912	Cubic
CeWO3	3,946	1,34	0,66	0,946	0,489	1,912	Cubic
PrOsO3	3,875	1,3	0,63	0,946	0,467	1,991	Cubic
PrReO3	3,875	1,3	0,63	0,946	0,467	1,991	Cubic
SmFeO3	3,768	1,24	0,585	0,946	0,433	2,129	Cubic
BaLuO3	4,423	1,61	0,861	0,947	0,638	2,556	Cubic
BaPuO3	4,421	1,61	0,86	0,947	0,637	2,555	Cubic
KTmO3	4,470	1,64	0,88	0,948	0,652	3,528	Cubic
SrCuO3	4,115	1,44	0,73	0,948	0,541	2,753	Cubic
PrIrO3	3,866	1,3	0,625	0,949	0,463	2,000	Cubic
PrPtO3	3,866	1,3	0,625	0,949	0,463	2,000	Cubic
CdOsO3	3,880	1,31	0,63	0,950	0,467	2,983	Cubic
CdReO3	3,880	1,31	0,63	0,950	0,467	2,983	Cubic
GdNiO3	3,525	1,11	0,48	0,951	0,356	2,571	Cubic
BiNbO3	4,000	1,38	0,68	0,951	0,504	1,853	Cubic
BiTaO3	4,000	1,38	0,68	0,951	0,504	1,853	Cubic
CaMoO3	3,929	1,34	0,65	0,951	0,481	2,927	Cubic
CeMoO3	3,929	1,34	0,65	0,951	0,481	1,927	Cubic
PrGaO3	3,858	1,3	0,62	0,951	0,459	2,009	Cubic
PrRuO3	3,858	1,3	0,62	0,951	0,459	2,009	Cubic
BaAuO3	4,404	1,61	0,85	0,951	0,630	2,554	Cubic
BaPrO3	4,364	1,61	0,85	0,951	0,630	2,554	Cubic
PbTbO3	4,191	1,49	0,76	0,952	0,563	2,689	Cubic
CdIrO3	3,872	1,31	0,625	0,952	0,463	2,992	Cubic
CdPtO3	3,872	1,31	0,625	0,952	0,463	2,992	Cubic
KCeO3	4,453	1,64	0,87	0,952	0,644	3,525	Cubic
KNpO3	4,453	1,64	0,87	0,952	0,644	3,525	Cubic
SrZrO3	4,179	1,44	0,72	0,953	0,533	2,760	Cubic

KYbO3	4,450	1,64	0,868	0,953	0,643	3,525	Cubic
LaWO3	3,956	1,36	0,66	0,953	0,489	1,896	Cubic
CaTcO3	3,921	1,34	0,645	0,953	0,478	2,934	Cubic
CeTcO3	3,921	1,34	0,645	0,953	0,478	1,934	Cubic
PrPdO3	3,850	1,3	0,615	0,954	0,456	2,019	Cubic
HoNiO3	3,530	1,12	0,48	0,954	0,356	2,566	Cubic
NaNbO3	4,005	1,39	0,68	0,954	0,504	3,844	Cubic
NaTaO3	4,005	1,39	0,68	0,954	0,504	3,844	Cubic
CdRuO3	3,863	1,31	0,62	0,955	0,459	3,002	Cubic
CaVO3	3,912	1,34	0,64	0,956	0,474	2,943	Cubic
CeVO3	3,912	1,34	0,64	0,956	0,474	1,943	Cubic
PrCoO3	3,730	1,3	0,61	0,956	0,452	2,030	Cubic
KLuO3	4,438	1,64	0,861	0,956	0,638	3,524	Cubic
KPuO3	4,437	1,64	0,86	0,957	0,637	3,524	Cubic
CdPdO3	3,855	1,31	0,615	0,957	0,456	3,012	Cubic
SrHfO3	4,082	1,44	0,71	0,958	0,526	2,770	Cubic
LaMoO3	3,939	1,36	0,65	0,958	0,481	1,911	Cubic
PrTiO3	3,833	1,3	0,605	0,958	0,448	2,041	Cubic
PbScO3	4,166	1,49	0,745	0,959	0,552	2,697	Cubic
CdCoO3	3,847	1,31	0,61	0,960	0,452	3,023	Cubic
EuCrO3	3,705	1,23	0,55	0,960	0,407	2,233	Cubic
BiWO3	3,967	1,38	0,66	0,960	0,489	1,880	Cubic
LaTcO3	3,931	1,36	0,645	0,961	0,478	1,920	Cubic
CaOsO3	3,896	1,34	0,63	0,961	0,467	2,961	Cubic
CaReO3	3,896	1,34	0,63	0,961	0,467	2,961	Cubic
CeOsO3	3,896	1,34	0,63	0,961	0,467	1,961	Cubic
CeReO3	3,896	1,34	0,63	0,961	0,467	1,961	Cubic
PbZnO3	4,158	1,49	0,74	0,961	0,548	2,701	Cubic
PrRhO3	3,825	1,3	0,6	0,961	0,444	2,052	Cubic
KAuO3	4,420	1,64	0,85	0,961	0,630	3,524	Cubic
KPrO3	4,420	1,64	0,85	0,961	0,630	3,524	Cubic
CdTiO3	3,838	1,31	0,605	0,962	0,448	3,034	Cubic
LaVO3	3,923	1,36	0,64	0,963	0,474	1,929	Cubic
CaIrO3	3,887	1,34	0,625	0,963	0,463	2,971	Cubic
CaPtO3	3,887	1,34	0,625	0,963	0,463	2,971	Cubic
CeIrO3	3,887	1,34	0,625	0,963	0,463	1,971	Cubic
CePtO3	3,887	1,34	0,625	0,963	0,463	1,971	Cubic

SmCrO3	3,710	1,24	0,55	0,964	0,407	2,228	Cubic
NaWO3	3,972	1,39	0,66	0,964	0,489	3,873	Cubic
CdRhO3	3,830	1,31	0,6	0,965	0,444	3,046	Cubic
BiMoO3	3,950	1,38	0,65	0,965	0,481	1,897	Cubic
PbCuO3	4,141	1,49	0,73	0,965	0,541	2,710	Cubic
CaRuO3	3,879	1,34	0,62	0,966	0,459	2,982	Cubic
CeRuO3	3,879	1,34	0,62	0,966	0,459	1,982	Cubic
BiTcO3	3,941	1,38	0,645	0,968	0,478	1,906	Cubic
LaOsO3	3,906	1,36	0,63	0,968	0,467	1,948	Cubic
LaReO3	3,906	1,36	0,63	0,968	0,467	1,948	Cubic
CaPdO3	3,870	1,34	0,615	0,968	0,456	2,993	Cubic
CePdO3	3,870	1,34	0,615	0,968	0,456	1,993	Cubic
NaMoO3	3,955	1,39	0,65	0,969	0,481	3,890	Cubic
BiVO3	3,933	1,38	0,64	0,970	0,474	1,916	Cubic
PbZrO3	4,124	1,49	0,72	0,970	0,533	2,720	Cubic
LaIrO3	3,898	1,36	0,625	0,970	0,463	1,959	Cubic
LaPtO3	3,898	1,36	0,625	0,970	0,463	1,959	Cubic
EuMnO3	3,671	1,23	0,53	0,970	0,393	2,304	Cubic
CaCoO3	3,862	1,34	0,61	0,970	0,452	3,004	Cubic
CeCoO3	3,862	1,34	0,61	0,970	0,452	2,004	Cubic
NaTcO3	3,947	1,39	0,645	0,971	0,478	3,900	Cubic
SmAlO3	3,685	1,24	0,535	0,972	0,396	2,281	Cubic
SrNbO3	4,073	1,44	0,68	0,972	0,504	2,808	Cubic
SrTaO3	4,007	1,44	0,68	0,972	0,504	2,808	Cubic
CdFeO3	3,805	1,31	0,585	0,972	0,433	3,085	Cubic
LaGaO3	3,889	1,36	0,62	0,973	0,459	1,970	Cubic
LaRuO3	3,889	1,36	0,62	0,973	0,459	1,970	Cubic
CaTiO3	3,900	1,34	0,605	0,973	0,448	3,017	Cubic
CeTiO3	3,854	1,34	0,605	0,973	0,448	2,017	Cubic
NaVO3	3,938	1,39	0,64	0,974	0,474	3,910	Cubic
SmMnO3	3,676	1,24	0,53	0,974	0,393	2,300	Cubic
PbHfO3	4,107	1,49	0,71	0,975	0,526	2,732	Cubic
BiOsO3	3,916	1,38	0,63	0,975	0,467	1,936	Cubic
BiReO3	3,916	1,38	0,63	0,975	0,467	1,936	Cubic
LaPdO3	3,881	1,36	0,615	0,975	0,456	1,982	Cubic
CaRhO3	3,845	1,34	0,6	0,975	0,444	3,030	Cubic
CeRhO3	3,845	1,34	0,6	0,975	0,444	2,030	Cubic

BiIrO3	3,908	1,38	0,625	0,977	0,463	1,948	Cubic
BiPtO3	3,908	1,38	0,625	0,977	0,463	1,948	Cubic
LaCoO3	3,872	1,36	0,61	0,978	0,452	1,994	Cubic
NaOsO3	3,922	1,39	0,63	0,979	0,467	3,931	Cubic
NaReO3	3,922	1,39	0,63	0,979	0,467	3,931	Cubic
BiRuO3	3,900	1,38	0,62	0,980	0,459	1,959	Cubic
LaTiO3	3,864	1,36	0,605	0,980	0,448	2,007	Cubic
NaIrO3	3,913	1,39	0,625	0,981	0,463	3,942	Cubic
NaPtO3	3,913	1,39	0,625	0,981	0,463	3,942	Cubic
SrWO3	3,998	1,44	0,66	0,982	0,489	2,842	Cubic
BiPdO3	3,891	1,38	0,615	0,982	0,456	1,971	Cubic
LaRhO3	3,856	1,36	0,6	0,983	0,444	2,020	Cubic
CaFeO3	3,820	1,34	0,585	0,983	0,433	3,071	Cubic
CeFeO3	3,820	1,34	0,585	0,983	0,433	2,071	Cubic
NaRuO3	3,905	1,39	0,62	0,983	0,459	3,954	Cubic
BiCoO3	3,883	1,38	0,61	0,985	0,452	1,984	Cubic
NaPdO3	3,896	1,39	0,615	0,986	0,456	3,967	Cubic
PrCrO3	3,820	1,3	0,55	0,986	0,407	2,202	Cubic
SrMoO3	3,981	1,44	0,65	0,986	0,481	2,862	Cubic
BiTiO3	3,874	1,38	0,605	0,987	0,448	1,998	Cubic
NaCoO3	3,888	1,39	0,61	0,989	0,452	3,980	Cubic
SrTcO3	3,973	1,44	0,645	0,989	0,478	2,873	Cubic
PbNbO3	4,057	1,49	0,68	0,989	0,504	2,779	Cubic
PbTaO3	4,057	1,49	0,68	0,989	0,504	2,779	Cubic
BiRhO3	3,866	1,38	0,6	0,990	0,444	2,011	Cubic
CdCrO3	3,746	1,31	0,55	0,990	0,407	3,199	Cubic
LaFeO3	3,831	1,36	0,585	0,990	0,433	2,063	Cubic
NaTiO3	3,880	1,39	0,605	0,991	0,448	3,993	Cubic
SrVO3	3,866	1,44	0,64	0,991	0,474	2,884	Cubic
BaTbO3	4,278	1,61	0,76	0,992	0,563	2,598	Cubic
NaRhO3	3,871	1,39	0,6	0,994	0,444	4,008	Cubic
SrOsO3	3,948	1,44	0,63	0,996	0,467	2,908	Cubic
SrReO3	3,948	1,44	0,63	0,996	0,467	2,908	Cubic
EuNiO3	3,587	1,23	0,48	0,997	0,356	2,536	Cubic
BiFeO3	3,841	1,38	0,585	0,998	0,433	2,056	Cubic
SrIrO3	3,939	1,44	0,625	0,999	0,463	2,920	Cubic
SrPtO3	3,939	1,44	0,625	0,999	0,463	2,920	Cubic

BaScO3	4,228	1,61	0,745	0,999	0,552	2,616	Cubic
PbWO3	4,024	1,49	0,66	0,999	0,489	2,818	Cubic
CdMnO3	3,713	1,31	0,53	1,000	0,393	3,279	Cubic
SmNiO3	3,592	1,24	0,48	1,001	0,356	2,534	Cubic
CaCrO3	3,777	1,34	0,55	1,001	0,407	3,190	Cubic
CeCrO3	3,762	1,34	0,55	1,001	0,407	2,190	Cubic
NaFeO3	3,846	1,39	0,585	1,001	0,433	4,053	Cubic
SrRuO3	3,931	1,44	0,62	1,001	0,459	2,934	Cubic
BaZnO3	4,220	1,61	0,74	1,001	0,548	2,623	Cubic
KTbO3	4,269	1,64	0,76	1,002	0,563	3,582	Cubic
SrPdO3	3,922	1,44	0,615	1,004	0,456	2,947	Cubic
PbMoO3	4,007	1,49	0,65	1,004	0,481	2,840	Cubic
BaCuO3	4,203	1,61	0,73	1,006	0,541	2,638	Cubic
SrCoO3	3,914	1,44	0,61	1,007	0,452	2,961	Cubic
PbTcO3	3,999	1,49	0,645	1,007	0,478	2,852	Cubic
LaCrO3	3,772	1,36	0,55	1,009	0,407	2,186	Cubic
SrTiO3	3,946	1,44	0,605	1,009	0,448	2,976	Cubic
PbVO3	3,990	1,49	0,64	1,009	0,474	2,864	Cubic
KScO3	4,244	1,64	0,745	1,009	0,552	3,602	Cubic
BaZrO3	4,227	1,61	0,72	1,011	0,533	2,654	Cubic
KZnO3	4,236	1,64	0,74	1,012	0,548	3,609	Cubic
SrRhO3	3,897	1,44	0,6	1,012	0,444	2,991	Cubic
CaMnO3	3,728	1,34	0,53	1,012	0,393	3,273	Cubic
CeMnO3	3,728	1,34	0,53	1,012	0,393	2,273	Cubic
PbOsO3	3,973	1,49	0,63	1,014	0,467	2,890	Cubic
PbReO3	3,973	1,49	0,63	1,014	0,467	2,890	Cubic
BiCrO3	3,782	1,38	0,55	1,016	0,407	2,182	Cubic
BaHfO3	4,170	1,61	0,71	1,016	0,526	2,671	Cubic
KCuO3	4,219	1,64	0,73	1,016	0,541	3,625	Cubic
LaAlO3	3,747	1,36	0,535	1,017	0,396	2,248	Cubic
PbIrO3	3,965	1,49	0,625	1,017	0,463	2,904	Cubic
PbPtO3	3,965	1,49	0,625	1,017	0,463	2,904	Cubic
LaMnO3	3,738	1,36	0,53	1,019	0,393	2,270	Cubic
PbRuO3	3,957	1,49	0,62	1,019	0,459	2,918	Cubic
SrFeO3	3,872	1,44	0,585	1,020	0,433	3,040	Cubic
NaCrO3	3,788	1,39	0,55	1,020	0,407	4,180	Cubic
KZrO3	4,202	1,64	0,72	1,021	0,533	3,642	Cubic

PbPdO3	3,948	1,49	0,615	1,022	0,456	2,933	Cubic
PrNiO3	3,624	1,3	0,48	1,024	0,356	2,531	Cubic
PbCoO3	3,940	1,49	0,61	1,025	0,452	2,948	Cubic
BaSnO3	4,136	1,61	0,69	1,026	0,511	2,710	Cubic
BaSnO3	4,130	1,61	0,69	1,026	0,511	2,710	Cubic
KHfO3	4,185	1,64	0,71	1,026	0,526	3,660	Cubic
BiMnO3	3,749	1,38	0,53	1,027	0,393	2,268	Cubic
PbTiO3	3,932	1,49	0,605	1,027	0,448	2,964	Cubic
CdNiO3	3,629	1,31	0,48	1,028	0,356	3,531	Cubic
PbRhO3	3,923	1,49	0,6	1,030	0,444	2,980	Cubic
NaMnO3	3,754	1,39	0,53	1,031	0,393	4,267	Cubic
BaNbO3	4,129	1,61	0,68	1,031	0,504	2,732	Cubic
BaTaO3	4,057	1,61	0,68	1,031	0,504	2,732	Cubic
PbFeO3	3,898	1,49	0,585	1,038	0,433	3,032	Cubic
SrCrO3	3,844	1,44	0,55	1,038	0,407	3,175	Cubic
CeNiO3	3,644	1,34	0,48	1,039	0,356	2,532	Cubic
BaWO3	4,086	1,61	0,66	1,041	0,489	2,781	Hexagonal
KNbO3	4,135	1,64	0,68	1,042	0,504	3,725	Hexagonal
KTaO3	4,135	1,64	0,68	1,042	0,504	3,725	Hexagonal
BaMoO3	4,010	1,61	0,65	1,047	0,481	2,808	Hexagonal
LaNiO3	3,655	1,36	0,48	1,047	0,356	2,533	Hexagonal
BaTcO3	4,061	1,61	0,645	1,049	0,478	2,822	Hexagonal
SrMnO3	3,780	1,44	0,53	1,049	0,393	3,265	Hexagonal
BaVO3	4,052	1,61	0,64	1,052	0,474	2,836	Hexagonal
KWO3	4,102	1,64	0,66	1,052	0,489	3,775	Hexagonal
PbCrO3	3,839	1,49	0,55	1,057	0,407	3,173	Hexagonal
BaOsO3	4,036	1,61	0,63	1,057	0,467	2,867	Hexagonal
BaReO3	4,036	1,61	0,63	1,057	0,467	2,867	Hexagonal
KMoO3	4,085	1,64	0,65	1,057	0,481	3,803	Hexagonal
NaNiO3	3,670	1,39	0,48	1,059	0,356	4,536	Hexagonal
BaIrO3	4,027	1,61	0,625	1,060	0,463	2,882	Hexagonal
BaPtO3	4,027	1,61	0,625	1,060	0,463	2,882	Hexagonal
KTcO3	4,076	1,64	0,645	1,060	0,478	3,818	Hexagonal
KVO3	4,068	1,64	0,64	1,062	0,474	3,833	Hexagonal
BaRuO3	4,006	1,61	0,62	1,062	0,459	2,899	Hexagonal
BaPdO3	4,011	1,61	0,615	1,065	0,456	2,915	Hexagonal
KOsO3	4,051	1,64	0,63	1,068	0,467	3,864	Hexagonal

KReO3	4,051	1,64	0,63	1,068	0,467	3,864	Hexagonal
BaCoO3	4,002	1,61	0,61	1,068	0,452	2,933	Hexagonal
PbMnO3	3,806	1,49	0,53	1,068	0,393	3,267	Hexagonal
KIrO3	4,043	1,64	0,625	1,071	0,463	3,880	Hexagonal
KPtO3	4,043	1,64	0,625	1,071	0,463	3,880	Hexagonal
BaTiO3	4,023	1,61	0,605	1,071	0,448	2,950	Hexagonal
KRuO3	4,035	1,64	0,62	1,073	0,459	3,897	Hexagonal
BaRhO3	3,985	1,61	0,6	1,073	0,444	2,969	Hexagonal
KPdO3	4,026	1,64	0,615	1,076	0,456	3,914	Hexagonal
SrNiO3	3,696	1,44	0,48	1,078	0,356	3,543	Hexagonal
KCoO3	4,018	1,64	0,61	1,079	0,452	3,932	Hexagonal
KTiO3	4,009	1,64	0,605	1,081	0,448	3,950	Hexagonal
BaFeO3	3,960	1,61	0,585	1,082	0,433	3,026	Hexagonal
KRhO3	4,001	1,64	0,6	1,084	0,444	3,968	Hexagonal
KFeO3	3,976	1,64	0,585	1,093	0,433	4,027	Hexagonal
PbNiO3	3,722	1,49	0,48	1,097	0,356	3,553	Hexagonal
BaCrO3	3,957	1,61	0,55	1,102	0,407	3,180	Hexagonal
KCrO3	3,917	1,64	0,55	1,113	0,407	4,184	Hexagonal
BaMnO3	3,868	1,61	0,53	1,113	0,393	3,281	Hexagonal
KMnO3	3,884	1,64	0,53	1,125	0,393	4,287	Hexagonal
KNiO3	3,800	1,64	0,48	1,155	0,356	4,593	Hexagonal

Table 5.3: The predicted lattice parameters of new synthesized or hypothetical oxide perovskites not included in our training data set.

compounds	ΔH_C	predicted ΔH_C	$\Delta H_C + predicted\Delta H_C$
BaHfO3	216.740	226.701	-9.961
BaTiO3	235.580	304.018	-68.438
BaZrO3	195.540	183.764	11.776
CaHfO3	-93.320	-1.485	-91.835
CaTiO3	51.720	27.297	24.423
CaZrO3	-139.100	-66.558	-72.542
SrHfO3	118.600	75.613	42.987
SrTiO3	213.700	120.508	93.192
SrZrO3	81.600	11.201	70.399

Table 5.4: The calculated and predicted decomposition energies.

compounds	a_0(Å)	r_A(Å)	r_B(Å)	$(t+\mu)^\eta$	ΔH_C predicted
ErPmO3	4.320	1.06	0.97	1.202	-216.173681
ErSmO3	4.300	1.06	0.958	1.202	-215.455749
ErAgO3	4.286	1.06	0.95	1.203	-214.941392
ErCdO3	4.286	1.06	0.95	1.203	-214.941392
ErEuO3	4.281	1.06	0.947	1.203	-214.741041
ErThO3	4.270	1.06	0.94	1.203	-214.257547
ErGdO3	4.266	1.06	0.938	1.203	-214.11526
ErDyO3	4.223	1.06	0.912	1.203	-212.094218
ErHoO3	4.204	1.06	0.901	1.204	-211.140969
ErPaO3	4.203	1.06	0.9	1.204	-211.051342
ErYO3	4.203	1.06	0.9	1.204	-211.051342
ErUO3	4.186	1.06	0.89	1.204	-210.127447
DyNdO3	4.352	1.08	0.983	1.204	-209.436088
YNdO3	4.352	1.08	0.983	1.204	-209.436088
ErTmO3	4.169	1.06	0.88	1.204	-209.152579
DyPmO3	4.330	1.08	0.97	1.205	-208.579294
YPmO3	4.330	1.08	0.97	1.205	-208.579294
ErCeO3	4.152	1.06	0.87	1.205	-208.125626
ErNpO3	4.152	1.06	0.87	1.205	-208.125626
ErYbO3	4.149	1.06	0.868	1.205	-207.913883
DySmO3	4.310	1.08	0.958	1.205	-207.7189
YSmO3	4.310	1.08	0.958	1.205	-207.7189
ErLuO3	4.137	1.06	0.861	1.205	-207.155866
DyAgO3	4.297	1.08	0.95	1.205	-207.107527
DyCdO3	4.297	1.08	0.95	1.205	-207.107527
YAgO3	4.297	1.08	0.95	1.205	-207.107527
YCdO3	4.297	1.08	0.95	1.205	-207.107527
ErPuO3	4.136	1.06	0.86	1.205	-207.045413
DyEuO3	4.292	1.08	0.947	1.205	-206.870364
YEuO3	4.292	1.08	0.947	1.205	-206.870364
DyThO3	4.280	1.08	0.94	1.205	-206.30005
YThO3	4.280	1.08	0.94	1.205	-206.30005
DyGdO3	4.277	1.08	0.938	1.205	-206.132716
YGdO3	4.277	1.08	0.938	1.205	-206.132716
ErAuO3	4.119	1.06	0.85	1.205	-205.910701
ErPrO3	4.119	1.06	0.85	1.205	-205.910701

YDyO3	4.233	1.08	0.912	1.206	-203.775961
DyHoO3	4.215	1.08	0.901	1.207	-202.674819
YHoO3	4.215	1.08	0.901	1.207	-202.674819
DyPaO3	4.213	1.08	0.9	1.207	-202.571568
DyYO3	4.213	1.08	0.9	1.207	-202.571568
YPaO3	4.213	1.08	0.9	1.207	-202.571568
DyErO3	4.196	1.08	0.89	1.207	-201.509755
DyUO3	4.196	1.08	0.89	1.207	-201.509755
YErO3	4.196	1.08	0.89	1.207	-201.509755
YUO3	4.196	1.08	0.89	1.207	-201.509755
YTlO3	4.188	1.08	0.885	1.207	-200.958641
DyTmO3	4.179	1.08	0.88	1.207	-200.393858
YTmO3	4.179	1.08	0.88	1.207	-200.393858
DyCeO3	4.163	1.08	0.87	1.208	-199.222672
DyNpO3	4.163	1.08	0.87	1.208	-199.222672
YCeO3	4.163	1.08	0.87	1.208	-199.222672
YNpO3	4.163	1.08	0.87	1.208	-199.222672
DyYbO3	4.159	1.08	0.868	1.208	-198.981689
YYbO3	4.159	1.08	0.868	1.208	-198.981689
DyLuO3	4.148	1.08	0.861	1.208	-198.120284
YLuO3	4.148	1.08	0.861	1.208	-198.120284
DyPuO3	4.146	1.08	0.86	1.208	-197.994927
YPuO3	4.146	1.08	0.86	1.208	-197.994927
GdNdO3	4.368	1.11	0.983	1.208	-197.992601
HoHgO3	4.435	1.12	1.02	1.208	-196.941432
GdPmO3	4.346	1.11	0.97	1.208	-196.909539
DyAuO3	4.129	1.08	0.85	1.208	-196.709288
DyPrO3	4.129	1.08	0.85	1.208	-196.709288
YAuO3	4.129	1.08	0.85	1.208	-196.709288
YPrO3	4.129	1.08	0.85	1.208	-196.709288
GdSmO3	4.326	1.11	0.958	1.209	-195.834731
GdAgO3	4.312	1.11	0.95	1.209	-195.077362
GdCdO3	4.312	1.11	0.95	1.209	-195.077362
GdEuO3	4.307	1.11	0.947	1.209	-194.784807
HoNdO3	4.373	1.12	0.983	1.209	-194.101037
GdThO3	4.296	1.11	0.94	1.209	-194.083853
ErTbO3	3.968	1.06	0.76	1.210	-193.005218

HoPmO3	4.351	1.12	0.97	1.210	-192.942272
HoSmO3	4.331	1.12	0.958	1.210	-191.795736
GdDyO3	4.249	1.11	0.912	1.210	-191.017035
HoAgO3	4.317	1.12	0.95	1.210	-190.98953
HoCdO3	4.317	1.12	0.95	1.210	-190.98953
HoEuO3	4.312	1.12	0.947	1.210	-190.678447
ErScO3	3.943	1.06	0.745	1.211	-190.33099
HoThO3	4.301	1.12	0.94	1.211	-189.933798
HoGdO3	4.297	1.12	0.938	1.211	-189.716173
GdHoO3	4.230	1.11	0.901	1.211	-189.693449
GdPaO3	4.229	1.11	0.9	1.211	-189.569707
GdYO3	4.229	1.11	0.9	1.211	-189.569707
ErZnO3	3.935	1.06	0.74	1.211	-189.402661
YInO3	4.045	1.08	0.8	1.211	-189.360811
GdErO3	4.212	1.11	0.89	1.211	-188.300479
GdUO3	4.212	1.11	0.89	1.211	-188.300479
ErCuO3	3.918	1.06	0.73	1.211	-187.488859
GdTmO3	4.195	1.11	0.88	1.212	-186.972508
HoDyO3	4.254	1.12	0.912	1.212	-186.685479
GdCeO3	4.178	1.11	0.87	1.212	-185.584451
GdNpO3	4.178	1.11	0.87	1.212	-185.584451
ErZrO3	3.901	1.06	0.72	1.212	-185.496805
GdYbO3	4.175	1.11	0.868	1.212	-185.299506
HoPaO3	4.234	1.12	0.9	1.212	-185.156921
HoYO3	4.234	1.12	0.9	1.212	-185.156921
GdLuO3	4.163	1.11	0.861	1.213	-184.282662
GdPuO3	4.162	1.11	0.86	1.213	-184.134898
HoErO3	4.217	1.12	0.89	1.213	-183.818346
HoUO3	4.217	1.12	0.89	1.213	-183.818346
ErHfO3	3.884	1.06	0.71	1.213	-183.423905
GdAuO3	4.145	1.11	0.85	1.213	-182.622369
GdPrO3	4.145	1.11	0.85	1.213	-182.622369
HoTmO3	4.200	1.12	0.88	1.213	-182.419476
DyTbO3	3.978	1.08	0.76	1.213	-182.275017
YTbO3	3.978	1.08	0.76	1.213	-182.275017
HoCeO3	4.183	1.12	0.87	1.214	-180.958923
HoNpO3	4.183	1.12	0.87	1.214	-180.958923

HoYbO3	4.180	1.12	0.868	1.214	-180.659283
YZrO3	3.962	1.08	0.75	1.214	-180.319505
HoLuO3	4.168	1.12	0.861	1.214	-179.590482
HoPuO3	4.167	1.12	0.86	1.214	-179.435229
DyScO3	3.953	1.08	0.745	1.214	-179.312593
YScO3	3.953	1.08	0.745	1.214	-179.312593
DyZnO3	3.945	1.08	0.74	1.214	-178.285838
YZnO3	3.945	1.08	0.74	1.214	-178.285838
HoAuO3	4.150	1.12	0.85	1.215	-177.846865
HoPrO3	4.150	1.12	0.85	1.215	-177.846865
ErNbO3	3.834	1.06	0.68	1.215	-176.692051
ErTaO3	3.834	1.06	0.68	1.215	-176.692051
DyCuO3	3.928	1.08	0.73	1.215	-176.17154
YCuO3	3.928	1.08	0.73	1.215	-176.17154
DyZrO3	3.911	1.08	0.72	1.216	-173.974003
ErWO3	3.801	1.06	0.66	1.217	-171.745707
DyHfO3	3.895	1.08	0.71	1.217	-171.690483
YHfO3	3.895	1.08	0.71	1.217	-171.690483
ErMoO3	3.784	1.06	0.65	1.217	-169.124868
ErTcO3	3.775	1.06	0.645	1.218	-167.775922
ErVO3	3.767	1.06	0.64	1.218	-166.400647
GdTbO3	3.994	1.11	0.76	1.219	-165.890871
DyNbO3	3.844	1.08	0.68	1.219	-164.294338
DyTaO3	3.844	1.08	0.68	1.219	-164.294338
YNbO3	3.844	1.08	0.68	1.219	-164.294338
YTaO3	3.844	1.08	0.68	1.219	-164.294338
EuAcO3	4.659	1.23	1.12	1.219	-163.596763
ErOsO3	3.750	1.06	0.63	1.219	-163.569092
ErReO3	3.750	1.06	0.63	1.219	-163.569092
GdScO3	3.969	1.11	0.745	1.220	-162.495552
ErIrO3	3.742	1.06	0.625	1.220	-162.11177
ErPtO3	3.742	1.06	0.625	1.220	-162.11177
GdZnO3	3.961	1.11	0.74	1.220	-161.320965
ErGaO3	3.734	1.06	0.62	1.220	-160.626035
ErRuO3	3.734	1.06	0.62	1.220	-160.626035
HoTbO3	3.999	1.12	0.76	1.220	-160.347815
SmAcO3	4.665	1.24	1.12	1.221	-159.896287

ErPdO3	3.725	1.06	0.615	1.221	-159.11133
GdCuO3	3.944	1.11	0.73	1.221	-158.905539
DyWO3	3.811	1.08	0.66	1.221	-158.876406
YWO3	3.811	1.08	0.66	1.221	-158.876406
ErCoO3	3.717	1.06	0.61	1.221	-157.567083
HoScO3	3.974	1.12	0.745	1.222	-156.807901
GdZrO3	3.927	1.11	0.72	1.222	-156.399405
DyMoO3	3.794	1.08	0.65	1.222	-156.010611
YMoO3	3.794	1.08	0.65	1.222	-156.010611
ErTiO3	3.708	1.06	0.605	1.222	-155.992709
HoZnO3	3.966	1.12	0.74	1.222	-155.583937
EuLaO3	4.512	1.23	1.032	1.222	-155.118832
DyTcO3	3.786	1.08	0.645	1.222	-154.536815
YTcO3	3.786	1.08	0.645	1.222	-154.536815
ErRhO3	3.700	1.06	0.6	1.222	-154.387605
GdHfO3	3.910	1.11	0.71	1.223	-153.799588
EuHgO3	4.492	1.23	1.02	1.223	-153.630091
HoCuO3	3.949	1.12	0.73	1.223	-153.067936
DyVO3	3.777	1.08	0.64	1.223	-153.035073
YVO3	3.777	1.08	0.64	1.223	-153.035073
SmLaO3	4.517	1.24	1.032	1.223	-150.978082
HoZrO3	3.932	1.12	0.72	1.224	-150.458737
DyOsO3	3.761	1.08	0.63	1.224	-149.945637
DyReO3	3.761	1.08	0.63	1.224	-149.945637
YOsO3	3.761	1.08	0.63	1.224	-149.945637
YReO3	3.761	1.08	0.63	1.224	-149.945637
SmHgO3	4.497	1.24	1.02	1.224	-149.423393
ErFeO3	3.675	1.06	0.585	1.224	-149.381647
EuNdO3	4.430	1.23	0.983	1.224	-148.496253
DyIrO3	3.752	1.08	0.625	1.224	-148.356849
DyPtO3	3.752	1.08	0.625	1.224	-148.356849
YIrO3	3.752	1.08	0.625	1.224	-148.356849
YPtO3	3.752	1.08	0.625	1.224	-148.356849
HoHfO3	3.915	1.12	0.71	1.224	-147.753288
DyGaO3	3.744	1.08	0.62	1.225	-146.737929
DyRuO3	3.744	1.08	0.62	1.225	-146.737929
YGaO3	3.744	1.08	0.62	1.225	-146.737929

YRuO3	3.744	1.08	0.62	1.225	-146.737929
EuPmO3	4.408	1.23	0.97	1.225	-146.489865
GdNbO3	3.860	1.11	0.68	1.225	-145.405946
GdTaO3	3.860	1.11	0.68	1.225	-145.405946
DyPdO3	3.736	1.08	0.615	1.225	-145.088291
YPdO3	3.736	1.08	0.615	1.225	-145.088291
EuSmO3	4.388	1.23	0.958	1.226	-144.540447
SmNdO3	4.435	1.24	0.983	1.226	-144.076081
DyCoO3	3.727	1.08	0.61	1.226	-143.407339
YCoO3	3.727	1.08	0.61	1.226	-143.407339
EuAgO3	4.375	1.23	0.95	1.226	-143.187729
EuCdO3	4.375	1.23	0.95	1.226	-143.187729
SmPmO3	4.413	1.24	0.97	1.226	-141.990838
DyTiO3	3.719	1.08	0.605	1.226	-141.694457
YTiO3	3.719	1.08	0.605	1.226	-141.694457
EuThO3	4.358	1.23	0.94	1.227	-141.435826
EuGdO3	4.354	1.23	0.938	1.227	-141.077195
DyRhO3	3.710	1.08	0.6	1.227	-139.949013
YRhO3	3.710	1.08	0.6	1.227	-139.949013
GdWO3	3.827	1.11	0.66	1.227	-139.279949
HoNbO3	3.865	1.12	0.68	1.227	-139.026542
HoTaO3	3.865	1.12	0.68	1.227	-139.026542
SmAgO3	4.380	1.24	0.95	1.227	-138.563213
SmCdO3	4.380	1.24	0.95	1.227	-138.563213
SmEuO3	4.375	1.24	0.947	1.228	-138.02554
SmThO3	4.363	1.24	0.94	1.228	-136.746589
PrAcO3	4.696	1.3	1.12	1.228	-136.717398
ErCrO3	3.616	1.06	0.55	1.228	-136.501826
SmGdO3	4.360	1.24	0.938	1.228	-136.374851
EuDyO3	4.311	1.23	0.912	1.228	-136.157725
GdMoO3	3.810	1.11	0.65	1.228	-136.046385
DyFeO3	3.685	1.08	0.585	1.229	-134.510759
YFeO3	3.685	1.08	0.585	1.229	-134.510759
GdTcO3	3.801	1.11	0.645	1.229	-134.385144
EuHoO3	4.292	1.23	0.901	1.229	-133.928328
EuPaO3	4.291	1.23	0.9	1.229	-133.721162
EuYO3	4.291	1.23	0.9	1.229	-133.721162

GdVO3	3.793	1.11	0.64	1.229	-132.693535
CdAcO3	4.701	1.31	1.12	1.229	-132.685853
HoWO3	3.832	1.12	0.66	1.229	-132.664111
EuErO3	4.274	1.23	0.89	1.230	-131.607598
EuUO3	4.274	1.23	0.89	1.230	-131.607598
SmDyO3	4.316	1.24	0.912	1.230	-131.27986
ErAlO3	3.591	1.06	0.535	1.230	-130.419474
EuTmO3	4.257	1.23	0.88	1.230	-129.416565
HoMoO3	3.815	1.12	0.65	1.231	-129.307748
GdOsO3	3.776	1.11	0.63	1.231	-129.216941
GdReO3	3.776	1.11	0.63	1.231	-129.216941
SmHoO3	4.298	1.24	0.901	1.231	-128.973228
SmPaO3	4.296	1.24	0.9	1.231	-128.75895
SmYO3	4.296	1.24	0.9	1.231	-128.75895
ErMnO3	3.583	1.06	0.53	1.231	-128.311037
HoTcO3	3.807	1.12	0.645	1.231	-127.58392
GdIrO3	3.768	1.11	0.625	1.231	-127.430785
GdPtO3	3.768	1.11	0.625	1.231	-127.430785
EuCeO3	4.241	1.23	0.87	1.231	-127.146168
EuNpO3	4.241	1.23	0.87	1.231	-127.146168
EuYbO3	4.237	1.23	0.868	1.231	-126.682393
SmErO3	4.279	1.24	0.89	1.231	-126.57341
SmUO3	4.279	1.24	0.89	1.231	-126.57341
HoVO3	3.798	1.12	0.64	1.232	-125.828915
GdRuO3	3.760	1.11	0.62	1.232	-125.611916
SmTlO3	4.271	1.24	0.885	1.232	-125.451116
PrLaO3	4.548	1.3	1.032	1.232	-125.10761
EuLuO3	4.225	1.23	0.861	1.232	-125.033321
EuPuO3	4.224	1.23	0.86	1.232	-124.794429
SmTmO3	4.262	1.24	0.88	1.232	-124.30882
GdPdO3	3.751	1.11	0.615	1.232	-123.759711
PrHgO3	4.528	1.3	1.02	1.233	-123.149959
EuAuO3	4.207	1.23	0.85	1.233	-122.359278
EuPrO3	4.207	1.23	0.85	1.233	-122.359278
HoOsO3	3.781	1.12	0.63	1.233	-122.223053
HoReO3	3.781	1.12	0.63	1.233	-122.223053
SmCeO3	4.246	1.24	0.87	1.233	-121.96324

SmNpO3	4.246	1.24	0.87	1.233	-121.96324
GdCoO3	3.743	1.11	0.61	1.233	-121.873528
SmYbO3	4.242	1.24	0.868	1.233	-121.484228
CdLaO3	4.553	1.31	1.032	1.233	-120.618292
DyCrO3	3.627	1.08	0.55	1.233	-120.552453
YCrO3	3.627	1.08	0.55	1.233	-120.552453
HoIrO3	3.773	1.12	0.625	1.233	-120.370998
HoPtO3	3.773	1.12	0.625	1.233	-120.370998
CeAcO3	4.716	1.34	1.12	1.233	-120.290265
CaAcO3	4.716	1.34	1.12	1.233	-120.290265
GdTiO3	3.734	1.11	0.605	1.234	-119.95271
SmLuO3	4.231	1.24	0.861	1.234	-119.781296
SmPuO3	4.229	1.24	0.86	1.234	-119.53464
CdHgO3	4.533	1.31	1.02	1.234	-118.59214
HoRuO3	3.765	1.12	0.62	1.234	-118.48537
GdRhO3	3.726	1.11	0.6	1.234	-117.996583
SmAuO3	4.212	1.24	0.85	1.235	-117.020904
SmPrO3	4.212	1.24	0.85	1.235	-117.020904
HoPdO3	3.756	1.12	0.615	1.235	-116.565529
PrNdO3	4.466	1.3	0.983	1.235	-116.49863
HoCoO3	3.748	1.12	0.61	1.235	-114.610823
DyAlO3	3.602	1.08	0.535	1.236	-113.975821
YAlO3	3.602	1.08	0.535	1.236	-113.975821
PrPmO3	4.444	1.3	0.97	1.236	-113.931831
HoTiO3	3.740	1.12	0.605	1.236	-112.62058
GdFeO3	3.701	1.11	0.585	1.236	-111.909347
LaAcO3	4.727	1.36	1.12	1.236	-111.769604
CdNdO3	4.471	1.31	0.983	1.236	-111.719188
DyMnO3	3.593	1.08	0.53	1.236	-111.698086
YMnO3	3.593	1.08	0.53	1.236	-111.698086
PrSmO3	4.424	1.3	0.958	1.236	-111.451789
HoRhO3	3.731	1.12	0.6	1.237	-110.59411
PrAgO3	4.411	1.3	0.95	1.237	-109.73799
PrCdO3	4.411	1.3	0.95	1.237	-109.73799
PrEuO3	4.406	1.3	0.947	1.237	-109.08264
CdPmO3	4.450	1.31	0.97	1.237	-109.070566
PrThO3	4.394	1.3	0.94	1.238	-107.52625

PrGdO3	4.391	1.3	0.938	1.238	-107.074498
CeLaO3	4.569	1.34	1.032	1.238	-106.831829
CaLaO3	4.569	1.34	1.032	1.238	-106.831829
CdSmO3	4.429	1.31	0.958	1.238	-106.51306
ErNiO3	3.499	1.06	0.48	1.239	-104.758
CdAgO3	4.416	1.31	0.95	1.239	-104.746554
CeHgO3	4.549	1.34	1.02	1.239	-104.597594
CaHgO3	4.549	1.34	1.02	1.239	-104.597594
HoFeO3	3.706	1.12	0.585	1.239	-104.29019
CdEuO3	4.411	1.31	0.947	1.239	-104.071215
SmInO3	4.128	1.24	0.8	1.239	-103.094051
BiAcO3	4.737	1.38	1.12	1.239	-103.037657
CdThO3	4.399	1.31	0.94	1.239	-102.467698
CdGdO3	4.396	1.31	0.938	1.239	-102.002357
PrDyO3	4.347	1.3	0.912	1.240	-100.908184
NaAcO3	4.742	1.39	1.12	1.241	-98.5909103
PrHoO3	4.329	1.3	0.901	1.241	-98.1302201
PrPaO3	4.327	1.3	0.9	1.241	-97.8725406
PrYO3	4.327	1.3	0.9	1.241	-97.8725406
CeNdO3	4.487	1.34	0.983	1.241	-97.051515
CaNdO3	4.487	1.34	0.983	1.241	-97.051515
GdCrO3	3.642	1.11	0.55	1.241	-96.3319414
EuTbO3	4.056	1.23	0.76	1.241	-96.2976073
CdDyO3	4.352	1.31	0.912	1.242	-95.6540969
PrErO3	4.310	1.3	0.89	1.242	-95.2478143
PrUO3	4.310	1.3	0.89	1.242	-95.2478143
LaHgO3	4.559	1.36	1.02	1.242	-94.9931295
CePmO3	4.465	1.34	0.97	1.242	-94.1544048
CaPmO3	4.465	1.34	0.97	1.242	-94.1544048
CdHoO3	4.334	1.31	0.901	1.242	-92.7960991
PrTmO3	4.294	1.3	0.88	1.243	-92.5344329
CdPaO3	4.332	1.31	0.9	1.243	-92.5310503
CdYO3	4.332	1.31	0.9	1.243	-92.5310503
CeSmO3	4.445	1.34	0.958	1.243	-91.3616637
CaSmO3	4.445	1.34	0.958	1.243	-91.3616637
EuScO3	4.031	1.23	0.745	1.243	-91.1459114
SmTbO3	4.061	1.24	0.76	1.243	-90.1652452

CdErO3	4.316	1.31	0.89	1.243	-89.8317554
CdUO3	4.316	1.31	0.89	1.243	-89.8317554
PrCeO3	4.277	1.3	0.87	1.243	-89.7301724
PrNpO3	4.277	1.3	0.87	1.243	-89.7301724
CeAgO3	4.432	1.34	0.95	1.244	-89.4351093
CeCdO3	4.432	1.34	0.95	1.244	-89.4351093
CaAgO3	4.432	1.34	0.95	1.244	-89.4351093
CaCdO3	4.432	1.34	0.95	1.244	-89.4351093
EuZnO3	4.023	1.23	0.74	1.244	-89.3716268
PrYbO3	4.274	1.3	0.868	1.244	-89.1582123
CeEuO3	4.427	1.34	0.947	1.244	-88.6990729
CaEuO3	4.427	1.34	0.947	1.244	-88.6990729
HoCrO3	3.647	1.12	0.55	1.244	-88.1721885
BiLaO3	4.590	1.38	1.032	1.244	-87.6803399
PrLuO3	4.262	1.3	0.861	1.244	-87.1267204
CdTmO3	4.299	1.31	0.88	1.244	-87.0421813
LaNdO3	4.497	1.36	0.983	1.244	-86.99096
CeThO3	4.415	1.34	0.94	1.244	-86.9524602
CaThO3	4.415	1.34	0.94	1.244	-86.9524602
PrPuO3	4.260	1.3	0.86	1.244	-86.8327123
GdMnO3	3.609	1.11	0.53	1.245	-86.4813103
CeGdO3	4.412	1.34	0.938	1.245	-86.4458525
CaGdO3	4.412	1.34	0.938	1.245	-86.4458525
DyNiO3	3.509	1.08	0.48	1.245	-86.3172055
YNiO3	3.509	1.08	0.48	1.245	-86.3172055
EuCuO3	4.006	1.23	0.73	1.245	-85.7347915
BiHgO3	4.570	1.38	1.02	1.245	-85.1621261
SmScO3	4.036	1.24	0.745	1.245	-84.8641987
CdCeO3	4.282	1.31	0.87	1.245	-84.1600557
CdNpO3	4.282	1.31	0.87	1.245	-84.1600557
LaPmO3	4.476	1.36	0.97	1.245	-83.9255049
PrAuO3	4.243	1.3	0.85	1.245	-83.8396313
CdYbO3	4.279	1.31	0.868	1.245	-83.5723176
SmZnO3	4.028	1.24	0.74	1.246	-83.0389263
NaLaO3	4.595	1.39	1.032	1.246	-82.7503373
EuZrO3	3.989	1.23	0.72	1.246	-81.9771412
CdLuO3	4.267	1.31	0.861	1.246	-81.4850544

CdPuO3	4.265	1.31	0.86	1.246	-81.1830086
LaSmO3	4.455	1.36	0.958	1.246	-80.9734083
NaHgO3	4.575	1.39	1.02	1.247	-80.1598682
CeDyO3	4.368	1.34	0.912	1.247	-79.5451757
CaDyO3	4.368	1.34	0.912	1.247	-79.5451757
SmCuO3	4.011	1.24	0.73	1.247	-79.2982528
LaAgO3	4.442	1.36	0.95	1.247	-78.9384379
LaCdO3	4.442	1.36	0.95	1.247	-78.9384379
LaEuO3	4.437	1.36	0.947	1.247	-78.1612861
CdAuO3	4.249	1.31	0.85	1.247	-78.1085674
CdPrO3	4.249	1.31	0.85	1.247	-78.1085674
EuHfO3	3.973	1.23	0.71	1.247	-78.0947676
HoMnO3	3.614	1.12	0.53	1.247	-77.9889025
BiNdO3	4.508	1.38	0.983	1.248	-76.6975693
CeHoO3	4.350	1.34	0.901	1.248	-76.4442001
CaHoO3	4.350	1.34	0.901	1.248	-76.4442001
LaThO3	4.425	1.36	0.94	1.248	-76.3177466
CePaO3	4.348	1.34	0.9	1.248	-76.1567791
CeYO3	4.348	1.34	0.9	1.248	-76.1567791
CaPaO3	4.348	1.34	0.9	1.248	-76.1567791
CaYO3	4.348	1.34	0.9	1.248	-76.1567791
LaGdO3	4.422	1.36	0.938	1.248	-75.7831878
SrAcO3	4.768	1.44	1.12	1.248	-75.5247548
SmZrO3	3.994	1.24	0.72	1.248	-75.4342165
BiPmO3	4.486	1.38	0.97	1.249	-73.4614615
CeErO3	4.331	1.34	0.89	1.249	-73.231111
CeUO3	4.331	1.34	0.89	1.249	-73.231111
CaErO3	4.331	1.34	0.89	1.249	-73.231111
CaUO3	4.331	1.34	0.89	1.249	-73.231111
NaNdO3	4.513	1.39	0.983	1.249	-71.461642
SmHfO3	3.978	1.24	0.71	1.249	-71.4428297
BiSmO3	4.466	1.38	0.958	1.250	-70.3478325
CeTmO3	4.314	1.34	0.88	1.250	-70.2102423
CaTmO3	4.314	1.34	0.88	1.250	-70.2102423
LaDyO3	4.378	1.36	0.912	1.250	-68.5083633
SrThO3	4.530	1.44	0.94	1.251	-68.2636788
BiAgO3	4.452	1.38	0.95	1.251	-68.2029694

BiCdO3	4.452	1.38	0.95	1.251	-68.2029694
NaPmO3	4.491	1.39	0.97	1.251	-68.1392997
BiEuO3	4.447	1.38	0.947	1.251	-67.3841431
CeNpO3	4.298	1.34	0.87	1.251	-67.0917553
CaCeO3	4.298	1.34	0.87	1.251	-67.0917553
CaNpO3	4.298	1.34	0.87	1.251	-67.0917553
CaZrO3	4.138	1.34	0.72	1.251	-66.5579929
CeYbO3	4.294	1.34	0.868	1.251	-66.4561237
CaYbO3	4.294	1.34	0.868	1.251	-66.4561237
EuNbO3	3.922	1.23	0.68	1.251	-65.6573761
EuTaO3	3.922	1.23	0.68	1.251	-65.6573761
BiThO3	4.436	1.38	0.94	1.251	-65.4423604
LaHoO3	4.360	1.36	0.901	1.251	-65.2428358
NaSmO3	4.471	1.39	0.958	1.252	-64.9440478
LaPaO3	4.358	1.36	0.9	1.252	-64.9402642
LaYO3	4.358	1.36	0.9	1.252	-64.9402642
BiGdO3	4.432	1.38	0.938	1.252	-64.8794712
CeLuO3	4.283	1.34	0.861	1.252	-64.1995723
CaLuO3	4.283	1.34	0.861	1.252	-64.1995723
CePuO3	4.281	1.34	0.86	1.252	-63.8731294
CaPuO3	4.281	1.34	0.86	1.252	-63.8731294
NaAgO3	4.458	1.39	0.95	1.252	-62.7436568
NaCdO3	4.458	1.39	0.95	1.252	-62.7436568
NaEuO3	4.453	1.39	0.947	1.253	-61.903773
LaErO3	4.342	1.36	0.89	1.253	-61.861298
LaUO3	4.342	1.36	0.89	1.253	-61.861298
CeAuO3	4.264	1.34	0.85	1.253	-60.5517366
CePrO3	4.264	1.34	0.85	1.253	-60.5517366
CaAuO3	4.264	1.34	0.85	1.253	-60.5517366
CaPrO3	4.264	1.34	0.85	1.253	-60.5517366
LaTlO3	4.333	1.36	0.885	1.253	-60.2850226
NaThO3	4.441	1.39	0.94	1.253	-59.9123502
NaGdO3	4.437	1.39	0.938	1.253	-59.3351465
LaTmO3	4.325	1.36	0.88	1.254	-58.683806
SmNbO3	3.927	1.24	0.68	1.254	-58.6617937
SmTaO3	3.927	1.24	0.68	1.254	-58.6617937
GdNiO3	3.525	1.11	0.48	1.254	-58.3558112

BiDyO3	4.389	1.38	0.912	1.254	-57.2254434
SrLaO3	4.621	1.44	1.032	1.254	-57.2120822
EuWO3	3.889	1.23	0.66	1.254	-56.6616871
LaCeO3	4.308	1.36	0.87	1.255	-55.4052721
LaNpO3	4.308	1.36	0.87	1.255	-55.4052721
LaYbO3	4.305	1.36	0.868	1.255	-54.7372115
SrHgO3	4.601	1.44	1.02	1.255	-54.252072
BiHoO3	4.370	1.38	0.901	1.255	-53.7931516
BiPaO3	4.369	1.38	0.9	1.255	-53.475226
BiYO3	4.369	1.38	0.9	1.255	-53.475226
LaLuO3	4.293	1.36	0.861	1.256	-52.3660356
PrTbO3	4.093	1.3	0.76	1.256	-52.1428378
LaPuO3	4.291	1.36	0.86	1.256	-52.0230739
EuMoO3	3.872	1.23	0.65	1.256	-51.937782
NaDyO3	4.394	1.39	0.912	1.256	-51.4895246
PbAcO3	4.794	1.49	1.12	1.256	-51.0143776
BiErO3	4.352	1.38	0.89	1.256	-50.2409066
BiUO3	4.352	1.38	0.89	1.256	-50.2409066
EuTcO3	3.864	1.23	0.645	1.257	-49.5169801
SmWO3	3.894	1.24	0.66	1.257	-49.4222763
HoNiO3	3.530	1.12	0.48	1.257	-48.9468666
LaAuO3	4.275	1.36	0.85	1.257	-48.5344782
LaPrO3	4.275	1.36	0.85	1.257	-48.5344782
NaHoO3	4.376	1.39	0.901	1.257	-47.9729781
NaPaO3	4.374	1.39	0.9	1.257	-47.6472953
NaYO3	4.374	1.39	0.9	1.257	-47.6472953
EuVO3	3.855	1.23	0.64	1.257	-47.0560131
BiTmO3	4.335	1.38	0.88	1.257	-46.9046971
PrScO3	4.067	1.3	0.745	1.258	-45.9314694
CdTbO3	4.098	1.31	0.76	1.258	-45.5903684
SmMoO3	3.877	1.24	0.65	1.258	-44.5717513
SrNdO3	4.539	1.44	0.983	1.258	-44.3589043
NaErO3	4.357	1.39	0.89	1.258	-44.3344887
NaUO3	4.357	1.39	0.89	1.258	-44.3344887
PrZnO3	4.059	1.3	0.74	1.259	-43.795432
BiCeO3	4.318	1.38	0.87	1.259	-43.4639815
BiNpO3	4.318	1.38	0.87	1.259	-43.4639815

BiYbO3	4.315	1.38	0.868	1.259	-42.7630598
SmTcO3	3.869	1.24	0.645	1.259	-42.0864188
EuOsO3	3.839	1.23	0.63	1.259	-42.0106855
EuReO3	3.839	1.23	0.63	1.259	-42.0106855
NaTmO3	4.340	1.39	0.88	1.259	-40.9180941
SrPmO3	4.517	1.44	0.97	1.260	-40.595625
BiLuO3	4.303	1.38	0.861	1.260	-40.2757345
BiPuO3	4.302	1.38	0.86	1.260	-39.9160344
SmVO3	3.860	1.24	0.64	1.260	-39.56009
EuIrO3	3.830	1.23	0.625	1.260	-39.4248317
EuPtO3	3.830	1.23	0.625	1.260	-39.4248317
PrCuO3	4.042	1.3	0.73	1.260	-39.4219004
CdScO3	4.073	1.31	0.745	1.260	-39.224589
NaCeO3	4.324	1.39	0.87	1.261	-37.395445
NaNpO3	4.324	1.39	0.87	1.261	-37.395445
CdZnO3	4.064	1.31	0.74	1.261	-37.0358413
SrSmO3	4.497	1.44	0.958	1.261	-36.9830386
EuRuO3	3.822	1.23	0.62	1.261	-36.7958255
NaYbO3	4.320	1.39	0.868	1.261	-36.6779222
BiAuO3	4.285	1.38	0.85	1.261	-36.258016
BiPrO3	4.285	1.38	0.85	1.261	-36.258016
PrZrO3	4.026	1.3	0.72	1.261	-34.9095081
SrAgO3	4.484	1.44	0.95	1.262	-34.4987487
SrCdO3	4.484	1.44	0.95	1.262	-34.4987487
SmOsO3	3.844	1.24	0.63	1.262	-34.381491
SmReO3	3.844	1.24	0.63	1.262	-34.381491
NaLuO3	4.309	1.39	0.861	1.262	-34.1319201
EuPdO3	3.813	1.23	0.615	1.262	-34.1228743
NaPuO3	4.307	1.39	0.86	1.262	-33.7637641
SrEuO3	4.479	1.44	0.947	1.262	-33.5512064
CdCuO3	4.048	1.31	0.73	1.262	-32.5549709
SmIrO3	3.835	1.24	0.625	1.262	-31.7277
SmPtO3	3.835	1.24	0.625	1.262	-31.7277
EuCoO3	3.805	1.23	0.61	1.263	-31.405166
SrGdO3	4.463	1.44	0.938	1.263	-30.6556135
SrPuO3	4.378	1.44	0.86	1.263	-30.5731394
PrHfO3	4.009	1.3	0.71	1.263	-30.2537804

PbLaO3	4.647	1.49	1.032	1.263	-30.128085
NaAuO3	4.290	1.39	0.85	1.263	-30.0201577
NaPrO3	4.290	1.39	0.85	1.263	-30.0201577
LaInO3	4.191	1.36	0.8	1.263	-29.3914176
SmGaO3	3.827	1.24	0.62	1.263	-29.0298702
SmRuO3	3.827	1.24	0.62	1.263	-29.0298702
EuTiO3	3.797	1.23	0.605	1.263	-28.6418691
CdZrO3	4.031	1.31	0.72	1.264	-27.9326155
PbHgO3	4.627	1.49	1.02	1.264	-26.7834625
SmPdO3	3.819	1.24	0.615	1.264	-26.2871943
EuRhO3	3.788	1.23	0.6	1.264	-25.8321313
CeTbO3	4.113	1.34	0.76	1.264	-25.5407699
CaTbO3	4.113	1.34	0.76	1.264	-25.5407699
SmCoO3	3.810	1.24	0.61	1.265	-23.4988457
CdHfO3	4.014	1.31	0.71	1.265	-23.1642175
SrDyO3	4.420	1.44	0.912	1.266	-21.8305451
SmTiO3	3.802	1.24	0.605	1.266	-20.6639775
CeScO3	4.088	1.34	0.745	1.267	-18.7064559
CaScO3	4.088	1.34	0.745	1.267	-18.7064559
SrHoO3	4.401	1.44	0.901	1.267	-17.8833137
SmRhO3	3.793	1.24	0.6	1.267	-17.7817225
SrPaO3	4.400	1.44	0.9	1.267	-17.5179792
SrYO3	4.400	1.44	0.9	1.267	-17.5179792
EuFeO3	3.763	1.23	0.585	1.267	-17.1154365
CeZnO3	4.080	1.34	0.74	1.267	-16.3577708
CaZnO3	4.080	1.34	0.74	1.267	-16.3577708
PbNdO3	4.565	1.49	0.983	1.268	-15.646795
PrNbO3	3.959	1.3	0.68	1.268	-15.3786744
PrTaO3	3.959	1.3	0.68	1.268	-15.3786744
SrErO3	4.383	1.44	0.89	1.268	-13.8039872
LaTbO3	4.124	1.36	0.76	1.269	-11.8360646
CeCuO3	4.063	1.34	0.73	1.269	-11.5512101
CaCuO3	4.063	1.34	0.73	1.269	-11.5512101
PbPmO3	4.543	1.49	0.97	1.269	-11.4247252
SrTmO3	4.366	1.44	0.88	1.270	-9.97774375
SrUO3	4.376	1.44	0.89	1.270	-9.35469339
SmFeO3	3.768	1.24	0.585	1.270	-8.84164137

CdNbO3	3.964	1.31	0.68	1.270	-7.93398247
CdTaO3	3.964	1.31	0.68	1.270	-7.93398247
PbSmO3	4.523	1.49	0.958	1.270	-7.37793692
CeZrO3	4.046	1.34	0.72	1.271	-6.59520709
SrCeO3	4.350	1.44	0.87	1.271	-6.03632528
SrNpO3	4.350	1.44	0.87	1.271	-6.03632528
SrYbO3	4.346	1.44	0.868	1.271	-5.23395494
LaScO3	4.099	1.36	0.745	1.271	-4.6846307
PrWO3	3.925	1.3	0.66	1.271	-4.65342796
PbAgO3	4.509	1.49	0.95	1.271	-4.5982901
PbCdO3	4.509	1.49	0.95	1.271	-4.5982901
PbEuO3	4.504	1.49	0.947	1.272	-3.53874766
SrLuO3	4.334	1.44	0.861	1.272	-2.38806126
LaZnO3	4.090	1.36	0.74	1.272	-2.22769692
CeHfO3	4.030	1.34	0.71	1.272	-1.48495235
CaHfO3	4.030	1.34	0.71	1.272	-1.48495235
PbThO3	4.493	1.49	0.94	1.273	-1.02952745
PbGdO3	4.489	1.49	0.938	1.273	-0.30301343
PrMoO3	3.908	1.3	0.65	1.273	0.96861759
BiTbO3	4.134	1.38	0.76	1.274	2.15001828
SrAuO3	4.316	1.44	0.85	1.274	2.20433545
SrPrO3	4.316	1.44	0.85	1.274	2.20433545
LaCuO3	4.073	1.36	0.73	1.274	2.79929392
CdWO3	3.930	1.31	0.66	1.274	3.04321431
PrTcO3	3.900	1.3	0.645	1.274	3.84714541
EuCrO3	3.705	1.23	0.55	1.274	5.02258868
PrCrO3	3.820	1.3	0.55	1.275	6.63033723
LaZrO3	4.057	1.36	0.72	1.275	7.98110877
CdMoO3	3.914	1.31	0.65	1.276	8.79609285
NaTbO3	4.139	1.39	0.76	1.276	9.25145678
PbDyO3	4.446	1.49	0.912	1.276	9.54087355
BiScO3	4.109	1.38	0.745	1.276	9.62270635
SrZrO3	4.179	1.44	0.72	1.277	11.2011758
CdTcO3	3.905	1.31	0.645	1.277	11.7412979
BiZnO3	4.101	1.38	0.74	1.277	12.1892985
PrOsO3	3.875	1.3	0.63	1.277	12.7623737
PrReO3	3.875	1.3	0.63	1.277	12.7623737

LaHfO3	4.040	1.36	0.71	1.277	13.322728
SmCrO3	3.710	1.24	0.55	1.277	13.8538032
PbHoO3	4.427	1.49	0.901	1.277	13.9360608
BaAcO3	4.857	1.61	1.12	1.277	14.1718297
PbPaO3	4.426	1.49	0.9	1.278	14.3426359
PbYO3	4.426	1.49	0.9	1.278	14.3426359
CdVO3	3.897	1.31	0.64	1.278	14.7334219
CeNbO3	3.979	1.34	0.68	1.278	14.8227681
CeTaO3	3.979	1.34	0.68	1.278	14.8227681
CaNbO3	3.979	1.34	0.68	1.278	14.8227681
PrIrO3	3.866	1.3	0.625	1.278	15.830116
PrPtO3	3.866	1.3	0.625	1.278	15.830116
NaScO3	4.114	1.39	0.745	1.278	16.8864093
BiCuO3	4.084	1.38	0.73	1.279	17.4395882
CaTaO3	3.975	1.34	0.68	1.279	17.9784999
PbErO3	4.409	1.49	0.89	1.279	18.4738783
PbUO3	4.409	1.49	0.89	1.279	18.4738783
PrMnO3	3.880	1.3	0.645	1.279	18.5173456
EuMnO3	3.671	1.23	0.53	1.279	18.910872
PrGaO3	3.858	1.3	0.62	1.279	18.9472999
PrRuO3	3.858	1.3	0.62	1.279	18.9472999
NaZnO3	4.106	1.39	0.74	1.279	19.5083891
CdOsO3	3.880	1.31	0.63	1.280	20.8617667
CdReO3	3.880	1.31	0.63	1.280	20.8617667
PrPdO3	3.850	1.3	0.615	1.280	22.1148215
PbTmO3	4.392	1.49	0.88	1.280	22.7263629
PrVO3	3.870	1.3	0.64	1.280	22.7466092
BiZrO3	4.067	1.38	0.72	1.280	22.8501514
CdIrO3	3.872	1.31	0.625	1.281	23.9997065
CdPtO3	3.872	1.31	0.625	1.281	23.9997065
SmAlO3	3.685	1.24	0.535	1.281	24.4355294
NaCuO3	4.089	1.39	0.73	1.281	24.8714647
CeWO3	3.946	1.34	0.66	1.282	26.5643886
CaWO3	3.946	1.34	0.66	1.282	26.5643886
PbCeO3	4.375	1.49	0.87	1.282	27.1032805
PbNpO3	4.375	1.49	0.87	1.282	27.1032805
CdRuO3	3.863	1.31	0.62	1.282	27.1880047

CaTiO3	3.900	1.34	0.605	1.282	27.297262
PbYbO3	4.372	1.49	0.868	1.282	27.9938858
SmMnO3	3.676	1.24	0.53	1.282	28.0852107
BiHfO3	4.050	1.38	0.71	1.282	28.4261418
PrTiO3	3.833	1.3	0.605	1.282	28.6045686
LaNbO3	3.990	1.36	0.68	1.283	30.3596632
LaTaO3	3.990	1.36	0.68	1.283	30.3596632
NaZrO3	4.072	1.39	0.72	1.283	30.3975657
CdPdO3	3.855	1.31	0.615	1.283	30.4275722
PbLuO3	4.360	1.49	0.861	1.283	31.151638
PbPuO3	4.359	1.49	0.86	1.283	31.6079513
PrRhO3	3.825	1.3	0.6	1.283	31.9286948
KAcO3	4.872	1.64	1.12	1.283	31.9670578
CaSnO3	3.965	1.34	0.69	1.283	32.1150185
CeMoO3	3.929	1.34	0.65	1.284	32.7142175
CaMoO3	3.929	1.34	0.65	1.284	32.7142175
CdCoO3	3.847	1.31	0.61	1.284	33.7193419
CeTcO3	3.921	1.34	0.645	1.285	35.861723
CaTcO3	3.921	1.34	0.645	1.285	35.861723
NaHfO3	4.056	1.39	0.71	1.285	36.0919336
PbAuO3	4.342	1.49	0.85	1.285	36.2438303
PbPrO3	4.342	1.49	0.85	1.285	36.2438303
CdTiO3	3.838	1.31	0.605	1.285	37.0642688
CeVO3	3.912	1.34	0.64	1.286	39.0587535
CaVO3	3.912	1.34	0.64	1.286	39.0587535
CdRhO3	3.830	1.31	0.6	1.286	40.4633303
BaLaO3	4.709	1.61	1.032	1.287	41.7192902
LaWO3	3.956	1.36	0.66	1.287	42.6186217
CeOsO3	3.896	1.34	0.63	1.288	45.6049012
CeReO3	3.896	1.34	0.63	1.288	45.6049012
CaOsO3	3.896	1.34	0.63	1.288	45.6049012
CaReO3	3.896	1.34	0.63	1.288	45.6049012
SrTbO3	4.165	1.44	0.76	1.288	45.8888596
BaHgO3	4.689	1.61	1.02	1.288	46.0592059
BiNbO3	4.000	1.38	0.68	1.288	46.2017625
BiTaO3	4.000	1.38	0.68	1.288	46.2017625
CeIrO3	3.887	1.34	0.625	1.289	48.9558255

CePtO3	3.887	1.34	0.625	1.289	48.9558255
CaIrO3	3.887	1.34	0.625	1.289	48.9558255
CaPtO3	3.887	1.34	0.625	1.289	48.9558255
LaMoO3	3.939	1.36	0.65	1.289	49.0370953
CdFeO3	3.805	1.31	0.585	1.290	50.9954535
LaTcO3	3.931	1.36	0.645	1.290	52.3215129
CeRuO3	3.879	1.34	0.62	1.290	52.3598902
CaRuO3	3.879	1.34	0.62	1.290	52.3598902
NaNbO3	4.005	1.39	0.68	1.291	54.2406523
NaTaO3	4.005	1.39	0.68	1.291	54.2406523
SrScO3	4.140	1.44	0.745	1.291	54.3529055
LaVO3	3.923	1.36	0.64	1.291	55.6572197
CePdO3	3.870	1.34	0.615	1.291	55.8180528
CaPdO3	3.870	1.34	0.615	1.291	55.8180528
SrZnO3	4.132	1.44	0.74	1.292	57.2578867
EuNiO3	3.587	1.23	0.48	1.292	58.1647087
BiWO3	3.967	1.38	0.66	1.292	58.9847789
CeCoO3	3.862	1.34	0.61	1.292	59.3312931
CaCoO3	3.862	1.34	0.61	1.292	59.3312931
BaNdO3	4.627	1.61	0.983	1.293	60.4134631
KLaO3	4.725	1.64	1.032	1.293	61.3010615
LaOsO3	3.906	1.36	0.63	1.293	62.4861296
LaReO3	3.906	1.36	0.63	1.293	62.4861296
CeTiO3	3.854	1.34	0.605	1.293	62.9006142
SrCuO3	4.115	1.44	0.73	1.294	63.1972358
SrNbO3	4.073	1.44	0.68	1.294	63.5938633
BiMoO3	3.950	1.38	0.65	1.294	65.675389
BaPmO3	4.605	1.61	0.97	1.294	65.822549
KHgO3	4.705	1.64	1.02	1.294	65.9079293
LaIrO3	3.898	1.36	0.625	1.294	65.9812
LaPtO3	3.898	1.36	0.625	1.294	65.9812
CeRhO3	3.845	1.34	0.6	1.295	66.5270428
CaRhO3	3.845	1.34	0.6	1.295	66.5270428
NaWO3	3.972	1.39	0.66	1.295	67.2883633
SmNiO3	3.592	1.24	0.48	1.295	68.2851444
BiTcO3	3.941	1.38	0.645	1.295	69.098499
LaGaO3	3.889	1.36	0.62	1.296	69.5312949

LaRuO3	3.889	1.36	0.62	1.296	69.5312949
BaSmO3	4.585	1.61	0.958	1.296	70.992682
BiVO3	3.933	1.38	0.64	1.297	72.5746862
LaPdO3	3.881	1.36	0.615	1.297	73.1374033
NaMoO3	3.955	1.39	0.65	1.297	74.1164272
BaAgO3	4.572	1.61	0.95	1.297	74.5364325
BaCdO3	4.572	1.61	0.95	1.297	74.5364325
SrHfO3	4.082	1.44	0.71	1.298	75.6128743
BaEuO3	4.567	1.61	0.947	1.298	75.8857194
LaCoO3	3.872	1.36	0.61	1.298	76.8005371
NaTcO3	3.947	1.39	0.645	1.298	77.6095899
CdCrO3	3.746	1.31	0.55	1.298	77.6639393
CeFeO3	3.820	1.34	0.585	1.298	77.7596089
CaFeO3	3.820	1.34	0.585	1.298	77.7596089
BaThO3	4.555	1.61	0.94	1.299	78.9432607
BiOsO3	3.916	1.38	0.63	1.299	79.6900398
BiReO3	3.916	1.38	0.63	1.299	79.6900398
BaGdO3	4.552	1.61	0.938	1.299	80.0013803
LaTiO3	3.864	1.36	0.605	1.299	80.5217322
KNdO3	4.643	1.64	0.983	1.299	81.125206
NaVO3	3.938	1.39	0.64	1.299	81.1567333
BaPaO3	4.510	1.61	0.9	1.300	83.1130767
BiIrO3	3.908	1.38	0.625	1.300	83.3311344
BiPtO3	3.908	1.38	0.625	1.300	83.3311344
LaRhO3	3.856	1.36	0.6	1.300	84.3020486
PbTbO3	4.191	1.49	0.76	1.301	84.5164944
KPmO3	4.621	1.64	0.97	1.301	86.852678
BiRuO3	3.900	1.38	0.62	1.301	87.0291635
NaOsO3	3.922	1.39	0.63	1.302	88.41677
NaReO3	3.922	1.39	0.63	1.302	88.41677
BiPdO3	3.891	1.38	0.615	1.303	90.785148
NaIrO3	3.913	1.39	0.625	1.303	92.1316222
NaPtO3	3.913	1.39	0.625	1.303	92.1316222
KSmO3	4.601	1.64	0.958	1.303	92.3241219
BaDyO3	4.508	1.61	0.912	1.303	92.4807393
CaCrO3	3.777	1.34	0.55	1.303	93.1437548
PbScO3	4.166	1.49	0.745	1.304	93.8424849

CdMnO3	3.713	1.31	0.53	1.304	94.3413645
BiCoO3	3.883	1.38	0.61	1.304	94.6001325
NaRuO3	3.905	1.39	0.62	1.304	95.9043742
LaFeO3	3.831	1.36	0.585	1.304	96.0087056
KAgO3	4.587	1.64	0.95	1.304	96.072827
KCdO3	4.587	1.64	0.95	1.304	96.072827
PbZnO3	4.158	1.49	0.74	1.305	97.0416804
KEuO3	4.582	1.64	0.947	1.305	97.4998322
BaHoO3	4.490	1.61	0.901	1.305	98.0346307
BiTiO3	3.874	1.38	0.605	1.305	98.4751861
BaYO3	4.488	1.61	0.9	1.305	98.5478789
NaPdO3	3.896	1.39	0.615	1.305	99.736063
PrFeO3	3.777	1.3	0.645	1.306	100.084814
KThO3	4.571	1.64	0.94	1.306	100.875239
KGdO3	4.567	1.64	0.938	1.306	101.851518
BiRhO3	3.866	1.38	0.6	1.306	102.411403
PbCuO3	4.141	1.49	0.73	1.307	103.580137
NaCoO3	3.888	1.39	0.61	1.307	103.62775
BaErO3	4.471	1.61	0.89	1.307	103.758368
CeCrO3	3.762	1.34	0.55	1.308	106.176353
NaTiO3	3.880	1.39	0.605	1.308	107.580521
BaTmO3	4.454	1.61	0.88	1.309	109.113328
SrWO3	3.998	1.44	0.66	1.309	110.068108
PbZrO3	4.124	1.49	0.72	1.309	110.310294
NaRhO3	3.871	1.39	0.6	1.309	111.595487
BiFeO3	3.841	1.38	0.585	1.310	114.598363
BaCeO3	4.438	1.61	0.87	1.310	114.616645
KDyO3	4.524	1.64	0.912	1.310	115.037809
SrTaO3	4.007	1.44	0.68	1.311	115.049059
BaNpO3	4.437	1.61	0.87	1.311	115.161911
BaYbO3	4.434	1.61	0.868	1.311	115.735463
PrCoO3	3.730	1.3	0.61	1.311	115.836416
PbHfO3	4.107	1.49	0.71	1.311	117.238317
SrMoO3	3.981	1.44	0.65	1.311	117.598522
BaLuO3	4.423	1.61	0.861	1.312	119.699809
BaPuO3	4.421	1.61	0.86	1.312	120.267828
SrTiO3	3.946	1.44	0.605	1.312	120.508373

KHoO3	4.505	1.64	0.901	1.312	120.902517
KPaO3	4.504	1.64	0.9	1.313	121.44438
KYO3	4.504	1.64	0.9	1.313	121.44438
SrTcO3	3.973	1.44	0.645	1.313	121.44964
CeMnO3	3.728	1.34	0.53	1.313	123.930334
CaMnO3	3.728	1.34	0.53	1.313	123.930334
NaFeO3	3.846	1.39	0.585	1.313	124.025066
LaCrO3	3.772	1.36	0.55	1.314	125.608854
BaAuO3	4.404	1.61	0.85	1.314	126.08466
KErO3	4.487	1.64	0.89	1.314	126.944377
KUO3	4.487	1.64	0.89	1.314	126.944377
PrNiO3	3.624	1.3	0.48	1.316	130.61269
KTmO3	4.470	1.64	0.88	1.316	132.595082
SrOsO3	3.948	1.44	0.63	1.316	133.358723
SrReO3	3.948	1.44	0.63	1.316	133.358723
SrIrO3	3.939	1.44	0.625	1.318	137.450484
SrPtO3	3.939	1.44	0.625	1.318	137.450484
KCeO3	4.453	1.64	0.87	1.318	138.400567
KNpO3	4.453	1.64	0.87	1.318	138.400567
PbNbO3	4.057	1.49	0.68	1.318	139.275336
PbTaO3	4.057	1.49	0.68	1.318	139.275336
LaAlO3	3.747	1.36	0.535	1.318	139.357051
KYbO3	4.450	1.64	0.868	1.319	139.580608
CdNiO3	3.629	1.31	0.48	1.319	141.287723
SrRuO3	3.931	1.44	0.62	1.319	141.605083
KLuO3	4.438	1.64	0.861	1.320	143.761336
LaMnO3	3.738	1.36	0.53	1.320	144.09165
KPuO3	4.437	1.64	0.86	1.320	144.365066
BiCrO3	3.782	1.38	0.55	1.320	145.397516
SrPdO3	3.922	1.44	0.615	1.321	145.823641
SrCoO3	3.914	1.44	0.61	1.322	150.107305
KAuO3	4.420	1.64	0.85	1.322	150.492976
KPrO3	4.420	1.64	0.85	1.322	150.492976
PbWO3	4.024	1.49	0.66	1.324	155.081785
NaCrO3	3.788	1.39	0.55	1.324	155.429917
BaPrO3	4.364	1.61	0.85	1.324	157.059679
SrRhO3	3.897	1.44	0.6	1.325	158.874667

PbMoO3	4.007	1.49	0.65	1.326	163.342524
BiMnO3	3.749	1.38	0.53	1.327	164.618814
BaTbO3	4.278	1.61	0.76	1.327	166.207135
PbTcO3	3.999	1.49	0.645	1.328	167.56587
PbVO3	3.990	1.49	0.64	1.329	171.852633
BaUO3	4.380	1.61	0.89	1.329	172.520782
SrFeO3	3.872	1.44	0.585	1.329	172.544222
CeNiO3	3.644	1.34	0.48	1.330	173.847161
NaMnO3	3.754	1.39	0.53	1.330	175.024313
SrCrO3	3.844	1.44	0.55	1.331	178.781031
PbOsO3	3.973	1.49	0.63	1.332	180.620854
PbReO3	3.973	1.49	0.63	1.332	180.620854
BaZrO3	4.227	1.61	0.72	1.333	183.764096
PbIrO3	3.965	1.49	0.625	1.333	185.104596
PbPtO3	3.965	1.49	0.625	1.333	185.104596
PbRuO3	3.957	1.49	0.62	1.335	189.656326
PbPdO3	3.948	1.49	0.615	1.336	194.277253
LaNiO3	3.655	1.36	0.48	1.337	196.019888
BaScO3	4.228	1.61	0.745	1.338	197.779751
PbCoO3	3.940	1.49	0.61	1.338	198.968613
BaZnO3	4.220	1.61	0.74	1.339	201.740032
PbTiO3	3.932	1.49	0.605	1.340	203.73167
PbRhO3	3.923	1.49	0.6	1.341	208.567717
BaCuO3	4.203	1.61	0.73	1.342	209.828346
SrVO3	3.866	1.44	0.64	1.342	211.7889
KTbO3	4.269	1.64	0.76	1.343	213.816715
PbFeO3	3.898	1.49	0.585	1.346	223.527191
KScO3	4.244	1.64	0.745	1.347	225.97077
BaHfO3	4.170	1.61	0.71	1.347	226.701215
SrMnO3	3.780	1.44	0.53	1.348	228.546938
NaNiO3	3.670	1.39	0.48	1.348	230.021093
KZnO3	4.236	1.64	0.74	1.348	230.135351
KCuO3	4.219	1.64	0.73	1.351	238.639722
BaSnO3	4.136	1.61	0.69	1.353	244.553344
BaNbO3	4.129	1.61	0.68	1.353	245.437215
KZrO3	4.202	1.64	0.72	1.354	247.383921
BaSnO3	4.130	1.61	0.69	1.355	250.21497

KHfO3	4.185	1.64	0.71	1.357	256.375684
PbCrO3	3.839	1.49	0.55	1.358	261.249626
BaWO3	4.086	1.61	0.66	1.362	273.313308
PbMnO3	3.806	1.49	0.53	1.366	284.736883
KNbO3	4.135	1.64	0.68	1.366	284.918799
KTaO3	4.135	1.64	0.68	1.366	284.918799
BaTcO3	4.061	1.61	0.645	1.367	288.651762
SrNiO3	3.696	1.44	0.48	1.367	288.811228
BaVO3	4.052	1.61	0.64	1.369	293.91477
BaTiO3	4.023	1.61	0.605	1.372	304.017949
BaOsO3	4.036	1.61	0.63	1.373	304.673941
BaReO3	4.036	1.61	0.63	1.373	304.673941
KWO3	4.102	1.64	0.66	1.373	305.342907
BaIrO3	4.027	1.61	0.625	1.374	310.172832
BaPtO3	4.027	1.61	0.625	1.374	310.172832
BaTaO3	4.057	1.61	0.68	1.375	313.47184
KMoO3	4.085	1.64	0.65	1.376	316.002298
BaPdO3	4.011	1.61	0.615	1.378	321.416269
KTcO3	4.076	1.64	0.645	1.378	321.44832
KVO3	4.068	1.64	0.64	1.380	326.973679
BaCoO3	4.002	1.61	0.61	1.380	327.163731
BaRuO3	4.006	1.61	0.62	1.380	328.895005
KOsO3	4.051	1.64	0.63	1.384	338.267951
KReO3	4.051	1.64	0.63	1.384	338.267951
BaRhO3	3.985	1.61	0.6	1.384	338.917677
BaMoO3	4.010	1.61	0.65	1.385	342.337085
BaCrO3	3.957	1.61	0.55	1.385	343.403419
KIrO3	4.043	1.64	0.625	1.385	344.039712
KPtO3	4.043	1.64	0.625	1.385	344.039712
KRuO3	4.035	1.64	0.62	1.387	349.896508
PbNiO3	3.722	1.49	0.48	1.388	350.486969
KPdO3	4.026	1.64	0.615	1.389	355.839843
BaFeO3	3.960	1.61	0.585	1.390	357.219804
KCoO3	4.018	1.64	0.61	1.391	361.871256
KTiO3	4.009	1.64	0.605	1.393	367.992322
KRhO3	4.001	1.64	0.6	1.395	374.204649
KFeO3	3.976	1.64	0.585	1.402	393.405845

BaMnO3	3.868	1.61	0.53	1.414	431.933331
KCrO3	3.917	1.64	0.55	1.417	441.728799
KMnO3	3.884	1.64	0.53	1.427	471.75431
KNiO3	3.800	1.64	0.48	1.455	555.592268

Table 5.5: The predicted decomposition energies for the 892 perovskites..

5.2 inverse perovskite

compounds	a_0(Å)	r_A(Å)	r_B(Å)	r_X(Å)	E_A	E_B	E_X	t	Z_A	Z_B	Z_X
ZrCNi3	3.915 [28]	1.55	0.7	1.35	1.33	2.55	1.91	1.000	40	6	28
CdCNi3	3.867 [29]	1.55	0.7	1.35	1.69	2.55	1.91	1.000	48	6	28
AgCNi3	3.825 [28]	1.6	0.7	1.35	1.93	2.55	1.91	1.017	47	6	28
TcCNi3	3.825 [28]	1.35	0.7	1.35	1.9	2.55	1.91	0.931	43	6	28
ZnCNi3	3.793 [28]	1.35	0.7	1.35	1.65	2.55	1.91	0.931	30	6	28
AlCNi3	3.77 [30]	1.25	0.7	1.35	1.61	2.55	1.91	0.896	13	6	28
GaCNi3	3.79 [31]	1.3	0.7	1.35	1.81	2.55	1.91	0.914	31	6	28
InCNi3	3.88 [32]	1.55	0.7	1.35	1.78	2.55	1.91	1.000	49	6	28
CaCNi3	3.956 [33]	1.8	0.7	1.35	1	2.55	1.91	1.086	20	6	28
SrCNi3	4.053 [33]	2	0.7	1.35	0.95	2.55	1.91	1.155	38	6	28
BaCNi3	4.143 [33]	2.15	0.7	1.35	0.89	2.55	1.91	1.207	56	6	28
YCNi3	3.975 [28]	1.85	0.7	1.35	1.22	2.55	1.91	1.103	39	6	28
NbCNi3	3.863 [28]	1.45	0.7	1.35	1.6	2.55	1.91	0.965	41	6	28
MoCNi3	3.84 [28]	1.45	0.7	1.35	2.16	2.55	1.91	0.965	42	6	28
RuCNi3	3.8 [28]	1.3	0.7	1.35	2.2	2.55	1.91	0.914	44	6	28
PdCNi3	3.813 [28]	1.4	0.7	1.35	2.2	2.55	1.91	0.948	46	6	28
RhCNi3	3.8 [28]	1.35	0.7	1.35	2.28	2.55	1.91	0.931	45	6	28
MgCNi3	3.834 [28]	1.5	0.7	1.35	1.31	2.55	1.91	0.983	12	6	28
SnCMn3	3.866 [34]	1.45	0.7	1.4	1.96	2.55	1.55	0.959	50	6	25
AlCMn3	3.78 [35]	1.25	0.7	1.4	1.61	2.55	1.55	0.892	13	6	25
GaCMn3	3.89 [36]	1.3	0.7	1.4	1.81	2.55	1.55	0.909	31	6	25
NiCW3	4.092 [37]	1.35	0.7	1.35	1.91	2.55	2.36	0.931	28	6	74
AlCTi3	4.159 [38]	1.25	0.7	1.4	1.61	2.55	1.54	0.892	13	6	22
InCTi3	4.235 [38]	1.55	0.7	1.4	1.78	2.55	1.54	0.993	49	6	22
TlCTi3	4.247 [38]	1.9	0.7	1.4	1.62	2.55	1.54	1.111	81	6	22
WCCo3	3.8075 [37]	1.35	0.7	1.35	2.36	2.55	1.88	0.931	74	6	27
AlCFe3	3.78 [39]	1.25	0.7	1.4	1.61	2.55	1.83	0.892	13	6	26

ScCRh3	4.082 [40]	1.6	0.7	1.35	1.36	2.55	2.28	1.017	21	6	45
LuCRh3	4.147 [40]	1.75	0.7	1.35	1.27	2.55	2.28	1.069	71	6	45
YCRh3	4.160 [40]	1.85	0.7	1.35	1.22	2.55	2.28	1.103	39	6	45
LaCRh3	4.262 [40]	1.95	0.7	1.35	1.1	2.55	2.28	1.138	57	6	45
WCRh3	4.06 [41]	1.35	0.7	1.35	2.36	2.55	2.28	0.931	74	6	45
WCIr3	4.095 [41]	1.35	0.7	1.35	2.36	2.55	2.2	0.931	74	6	77
AlCY3	4.858 [42]	1.25	0.7	1.85	1.61	2.55	1.22	0.859	13	6	39
InCY3	4.9 [42]	1.55	0.7	1.85	1.78	2.55	1.22	0.942	49	6	39
TlCY3	4.897 [42]	1.9	0.7	1.85	1.62	2.55	1.22	1.039	81	6	39
AsNSr3	5.118 [43]	1.15	0.65	2	2.18	3.04	0.95	0.840	33	7	38
SbNSr3	5.123 [43]	1.45	0.65	2	2.05	3.04	0.95	0.920	51	7	38
BiNSr3	5.269 [43]	1.6	0.65	2	2.02	3.04	0.95	0.960	83	7	38
SbNMg3	4.340 [44]	1.45	0.65	1.5	2.05	3.04	1.31	0.970	51	7	12
AsNMg3	4.207 [44]	1.15	0.65	1.5	2.18	3.04	1.31	0.871	33	7	12
AsNBa3	5.306 [45]	1.15	0.65	2.15	2.18	3.04	0.89	0.833	33	7	56
SbNBa3	5.404 [45]	1.45	0.65	2.15	2.05	3.04	0.89	0.909	51	7	56
BiNBa3	5.42 [45]	1.6	0.65	2.15	2.02	3.04	0.89	0.947	83	7	56
SbNCa3	4.854 [46]	1.45	0.65	1.8	2.05	3.04	1	0.937	51	7	20
SnNCa3	4.946 [46]	1.45	0.65	1.8	1.96	3.04	1	0.937	50	7	20
PbNCa3	4.955 [46]	1.8	0.65	1.8	2.33	3.04	1	1.039	82	7	20
TlNCa3	4.949 [47]	1.9	0.65	1.8	1.62	3.04	1	1.067	81	7	20
GeNCa3	4.757 [46]	1.25	0.65	1.8	2.01	3.04	1	0.880	32	7	20
AsNCa3	4.77 [46]	1.15	0.65	1.8	2.18	3.04	1	0.851	33	7	20
BiNCa3	4.88 [46]	1.6	0.65	1.8	2.02	3.04	1	0.981	83	7	20
PNCa3	4.73 [46]	1	0.65	1.8	2.19	3.04	1	0.808	15	7	20
PdNCu3	3.89 [48]	1.4	0.65	1.35	2.2	3.04	1.9	0.972	46	7	29
RhNCu3	3.872 [49]	1.35	0.65	1.35	2.28	3.04	1.9	0.954	45	7	29
RuNCu3	3.885 [49]	1.3	0.65	1.35	2.2	3.04	1.9	0.936	44	7	29
NiNCu3	3.83 [48]	1.35	0.65	1.35	1.91	3.04	1.9	0.954	28	7	29
ZnNCu3	3.94 [48]	1.35	0.65	1.35	1.65	3.04	1.9	0.954	30	7	29
AgNCu3	3.96 [48]	1.6	0.65	1.35	1.93	3.04	1.9	1.042	47	7	29
CdNCu3	4.03 [48]	1.55	0.65	1.35	1.69	3.04	1.9	1.025	48	7	29
MgNNi3	3.815 [50]	1.5	0.65	1.35	1.31	3.04	1.91	1.007	12	7	28
ZnNNi3	3.77 [50]	1.35	0.65	1.35	1.65	3.04	1.91	0.954	30	7	28
CdNNi3	3.861 [50]	1.55	0.65	1.35	1.69	3.04	1.91	1.025	48	7	28
AlNNi3	3.777 [50]	1.25	0.65	1.35	1.61	3.04	1.91	0.919	13	7	28
GaNNi3	3.788 [50]	1.3	0.65	1.35	1.81	3.04	1.91	0.936	31	7	28

InNNi3	3.881 [50]	1.55	0.65	1.35	1.78	3.04	1.91	1.025	49	7	28
SnNNi3	3.91 [50]	1.45	0.65	1.35	1.96	3.04	1.91	0.989	50	7	28
PdNNi3	3.803 [50]	1.4	0.65	1.35	2.2	3.04	1.91	0.972	46	7	28
PtNNi3	3.809 [50]	1.35	0.65	1.35	2.28	3.04	1.91	0.954	78	7	28
CuNNi3	3.745 [50]	1.35	0.65	1.35	1.9	3.04	1.91	0.954	29	7	28
AgNNi3	3.832 [50]	1.6	0.65	1.35	1.93	3.04	1.91	1.042	47	7	28
SbNNi3	3.942 [50]	1.45	0.65	1.35	2.05	3.04	1.91	0.989	51	7	28
SnNMn3	3.859 [34]	1.45	0.65	1.4	1.96	3.04	1.55	0.983	50	7	25
GaNMn3	3.898 [51]	1.3	0.65	1.4	1.81	3.04	1.55	0.931	31	7	25
CuNMn3	3.903 [52]	1.35	0.65	1.4	1.9	3.04	1.55	0.948	29	7	25
InNCo3	3.870 [53]	1.55	0.65	1.35	1.78	3.04	1.88	1.025	49	7	27
AlNFe3	3.798 [54]	1.25	0.65	1.4	1.61	3.04	1.83	0.914	13	7	26
CoNFe3	3.755 [55]	1.35	0.65	1.4	1.88	3.04	1.83	0.948	27	7	26
RhNFe3	3.829 [56]	1.35	0.65	1.4	2.28	3.04	1.83	0.948	45	7	26
IrNFe3	3.808 [55]	1.35	0.65	1.4	2.2	3.04	1.83	0.948	77	7	26
RuNFe3	3.792 [57]	1.3	0.65	1.4	2.2	3.04	1.83	0.931	44	7	26
OsNFe3	3.778 [57]	1.3	0.65	1.4	2.2	3.04	1.83	0.931	76	7	26
NiNW3	4.063 [37]	1.35	0.65	1.35	1.91	3.04	2.36	0.954	28	7	74
BaRuO3	4.005 [8]	2.15	1.3	0.6	0.89	2.2	3.44	1.023	56	44	8
BaTiO3	4.022 [3]	2.15	1.55	0.6	0.89	1.33	3.44	0.904	56	40	8
BaNbO3	4.128 [3]	2.15	1.45	0.6	0.89	1.6	3.44	0.948	56	41	8
BaTaO3	4.057 [10]	2.15	1.45	0.6	0.89	1.5	3.44	0.948	56	73	8
BaSnO3	4.13 [9]	2.15	1.45	0.6	0.89	1.96	3.44	0.948	56	50	8
BaFeO3	3.85 [58]	2.15	1.4	0.6	0.89	1.83	3.44	0.972	56	26	8
BaMoO3	4.01 [2]	2.15	1.45	0.6	0.89	2.16	3.44	0.948	56	42	8
BaCrO3	3.95 [1]	2.15	1.4	0.6	0.89	1.66	3.44	0.972	56	24	8
BaPrO3	4.36 [6]	2.15	1.85	0.6	0.89	1.13	3.44	0.793	56	59	8
BaTbO3	4.27 [11]	2.15	1.75	0.6	0.89	1.22	3.44	0.827	56	85	8
SrZrO3	4.17 [21]	2	1.55	0.6	0.95	1.33	3.44	0.855	38	40	8
SrTiO3	3.94 [21]	2	1.4	0.6	0.95	1.54	3.44	0.919	38	22	8
SrVO3	3.866 [21]	2	1.35	0.6	0.95	1.63	3.44	0.942	38	23	8
SrNbO3	4.073 [21]	2	1.45	0.6	0.95	1.6	3.44	0.896	38	41	8
SrTaO3	4.007 [10]	2	1.45	0.6	0.95	1.5	3.44	0.896	38	73	8
SrFeO3	3.74 [58]	2	1.4	0.6	0.95	1.83	3.44	0.919	38	26	8
SrCrO3	3.84 [1]	2	1.4	0.6	0.95	1.66	3.44	0.919	38	24	8
CaTaO3	3.975 [10]	1.8	1.45	0.6	1	1.5	3.44	0.827	20	73	8
CaTiO3	3.89 [15]	1.8	1.4	0.6	1	1.54	3.44	0.848	20	22	8

CaSnO3	3.964 [14]	1.8	1.45	0.6	1	1.96	3.44	0.827	20	50	8
CaZrO3	4.138 [16]	1.8	1.55	0.6	1	1.33	3.44	0.789	20	40	8
CaCrO3	3.777 [1]	1.8	1.4	0.6	1	1.66	3.44	0.848	20	24	8
BiScO3	4.048 [59]	1.6	1.6	0.6	2.02	1.36	3.44	0.707	83	21	8
BiAlO3	3.81 [60]	1.6	1.25	0.6	2.02	1.61	3.44	0.840	83	13	8
BiGaO3	3.89 [61]	1.6	1.3	0.6	2.02	1.81	3.44	0.818	83	31	8
PbTiO3	3.96 [62]	1.8	1.4	0.6	2.33	1.54	3.44	0.848	82	22	8
PbTaO3	4.09 [63]	1.8	1.45	0.6	2.33	1.5	3.44	0.827	82	73	8
BaPaO3	4.51 [5]	2.15	1.8	0.6	0.89	1.5	3.44	0.810	56	91	8
BaAmO3	4.416 [64]	2.15	1.75	0.6	0.89	1.3	3.44	0.827	56	95	8
BaNpO3	4.437 [4]	2.15	1.75	0.6	0.89	1.36	3.44	0.827	56	93	8
BaPuO3	4.421 [7]	2.15	1.75	0.6	0.89	1.28	3.44	0.827	56	94	8
BaUO3	4.38 [13]	2.15	1.75	0.6	0.89	1.38	3.44	0.827	56	92	8
BaThO3	4.55 [12]	2.15	1.8	0.6	0.89	1.3	3.44	0.810	56	90	8
SrPuO3	4.37 [22]	2	1.75	0.6	0.95	1.28	3.44	0.782	38	94	8
SrUO3	4.37 [24]	2	1.75	0.6	0.95	1.38	3.44	0.782	38	92	8
SrThO3	4.53 [23]	2	1.8	0.6	0.95	1.3	3.44	0.766	38	90	8
BiInO3	4.072 [61]	1.6	1.55	0.6	2.02	1.78	3.44	0.723	83	49	8
PrCoO3	3.73 [17]	1.85	1.35	0.6	1.13	1.88	3.44	0.888	59	27	8
PrFeO3	3.777 [18]	1.85	1.4	0.6	1.13	1.83	3.44	0.866	59	26	8
PrCrO3	3.819 [18]	1.85	1.4	0.6	1.13	1.66	3.44	0.866	59	24	8
PrMnO3	3.88 [19]	1.85	1.4	0.6	1.13	1.55	3.44	0.866	59	25	8
PrVO3	3.87 [20]	1.85	1.35	0.6	1.13	1.63	3.44	0.888	59	23	8

Table 5.6: The training dataset used in the PCA calculations

compounds	a_0(Å)	(other)	predicted a	Δa
ZrCNi3	3.915	-	3.935	-0.020
CdCNi3	3.867	3.871 [65]	3.935	-0.068
AgCNi3	3.825	-	3.954	-0.129
TcCNi3	3.825	-	3.860	-0.035
ZnCNi3	3.793	3.66 [66]	3.860	-0.067
AlCNi3	3.77	3.587 [67]	3.823	-0.047
GaCNi3	3.79	3.604 [68]	3.842	-0.051
InCNi3	3.88	-	3.935	-0.046
CaCNi3	3.956	-	4.028	-0.072
SrCNi3	4.053	-	4.103	-0.050

BaCNi3	4.143	-	4.158	-0.015
YCNi3	3.975	-	4.047	-0.072
NbCNi3	3.863	-	3.898	-0.035
MoCNi3	3.840	-	3.898	-0.058
RuCNi3	3.800	-	3.842	-0.042
PdCNi3	3.813	-	3.879	-0.066
RhCNi3	3.800	-	3.860	-0.060
MgCNi3	3.834	3.81 [66]	3.916	-0.082
SnCMn3	3.866	3.989 [69]	3.999	-0.133
AlCMn3	3.780	-	3.924	-0.144
GaCMn3	3.890	-	3.943	-0.053
NiCW3	4.092	-	3.860	0.232
AlCTi3	4.159	-	3.924	0.235
InCTi3	4.235	-	4.036	0.199
TlCTi3	4.247	-	4.166	0.081
WCCo3	3.8075	-	3.860	-0.053
AlCFe3	3.780	3.752 [70]	3.924	-0.144
ScCRh3	4.082	4.10 [70]	3.954	0.128
LuCRh3	4.147	-	4.009	0.138
YCRh3	4.160	4.19 [71]	4.047	0.114
LaCRh3	4.262	-	4.084	0.178
WCRh3	4.060	-	3.860	0.200
WCIr3	4.095	-	3.860	0.235
AlCY3	4.858	4.878 [72]	4.833	0.025
InCY3	4.900	-	4.945	-0.045
TlCY3	4.897	4.889 [72]	5.075	-0.178
AsNSr3	5.118	5.084 [73]	5.070	0.048
SbNSr3	5.123	5.172 [73]	5.182	-0.059
BiNSr3	5.269	5.204 [73]	5.238	0.031
SbNMg3	4.340	4.382 [74]	4.172	0.168
AsNMg3	4.207	4.244 [75]	4.060	0.147
AsNBa3	5.306	5.529 [76]	5.373	-0.067
SbNBa3	5.404	5.622 [76]	5.485	-0.081
BiNBa3	5.42	5.48 [77]	5.541	-0.121
SbNCa3	4.854	4.831 [78]	4.778	0.076
SnNCa3	4.946	4.862 [79]	4.778	0.168
PbNCa3	4.955	4.919 [80]	4.908	0.047

TlNCa3	4.949	-	4.946	0.003
GeNCa3	4.757	4.787 [79]	4.704	0.054
AsNCa3	4.770	4.737 [78]	4.666	0.104
BiNCa3	4.888	4.864 [78]	4.834	0.054
PNCa3	4.73	4.703 [78]	4.610	0.120
PdNCu3	3.890	-	3.851	0.009
RhNCu3	3.872	-	3.832	0.040
RuNCu3	3.885	-	3.813	0.072
NiNCu3	3.830	-	3.832	-0.002
ZnNCu3	3.940	-	3.832	0.108
AgNCu3	3.960	-	3.925	0.035
CdNCu3	4.030	-	3.907	0.123
MgNNi3	3.815	3.82 [80]	3.888	-0.073
ZnNNi3	3.770	3.774 [81]	3.832	-0.062
CdNNi3	3.861	3.868 [80]	3.907	-0.046
AlNNi3	3.777	3.78 [80]	3.795	-0.018
GaNNi3	3.788	3.79 [80]	3.813	-0.025
InNNi3	3.881	3.854 [82]	3.907	-0.026
SnNNi3	3.910	3.927 [83]	3.869	0.041
PdNNi3	3.803	3.809 [84]	3.851	-0.048
PtNNi3	3.809	3.821 [84]	3.832	-0.023
CuNNi3	3.745	3.749 [85]	3.832	-0.087
AgNNi3	3.832	3.846 [84]	3.925	-0.093
SbNNi3	3.942	-	3.869	0.073
SnNMn3	3.859	-	3.970	-0.111
GaNMn3	3.898	-	3.914	-0.016
CuNMn3	3.903	-	3.933	-0.030
InNCo3	3.870	3.844 [82]	3.907	-0.036
AlNFe3	3.798	-	3.896	-0.097
CoNFe3	3.755	3.8851 [86]	3.933	-0.178
RhNFe3	3.829	3.826 [87]	3.933	-0.104
IrNFe3	3.808	3.85 [86]	3.933	-0.128
RuNFe3	3.792	4.052 [88]	3.914	-0.119
OsNFe3	3.778	4.038 [88]	3.914	-0.136
NiNW3	4.063	-	3.832	0.231
BaRuO3	4.005	-	3.853	0.153
BaTiO3	4.022	3.96 [62]	3.975	0.048

BaZrO3	4.226	4.192 [89]	4.156	0.070
BaNbO3	4.128	4.085 [90]	4.035	0.093
BaTaO3	4.057	-	4.035	0.022
BaSnO3	4.130	4.142 [91]	4.035	0.095
BaFeO3	3.850	3.971 [92]	3.975	-0.125
BaMoO3	4.010	4.039 [93]	4.035	-0.025
BaCrO3	3.957	-	3.975	-0.018
BaPrO3	4.364	4.35 [94]	4.520	-0.157
BaTbO3	4.278	4.285 [94]	4.399	-0.121
SrZrO3	4.179	4.157 [95]	4.129	0.050
SrTiO3	3.945	3.94 [96]	3.947	-0.002
SrVO3	3.866	3.84 [97]	3.887	-0.021
SrNbO3	4.073	4.024 [98]	4.008	0.065
SrTaO3	4.007	-	4.008	-0.001
SrFeO3	3.74	3.868 [99]	3.947	-0.207
SrCrO3	3.844	3.811 [100]	3.947	-0.103
CaTaO3	3.975	3.88 [101]	3.972	0.003
CaTiO3	3.89	-	3.911	-0.011
CaSnO3	3.964	-	3.972	-0.007
CaZrO3	4.138	-	4.093	0.045
CaCrO3	3.777	-	3.911	-0.134
BiScO3	4.048	-	4.117	-0.068
BiAlO3	3.810	3.659 [102]	3.693	0.117
BiGaO3	3.899	3.905 [102]	3.754	0.145
PbTiO3	3.960	3.97 [103]	3.911	0.049
PbTaO3	4.090	-	3.972	0.118
BaPaO3	4.510	-	4.460	0.050
BaAmO3	4.417	-	4.399	0.018
BaNpO3	4.437	-	4.399	0.038
BaPuO3	4.421	4.39 [104]	4.399	0.022
BaUO3	4.380	-	4.399	-0.019
BaThO3	4.555	-	4.460	0.096
SrPuO3	4.378	-	4.372	0.006
SrUO3	4.376	-	4.372	0.004
SrThO3	4.53	4.542 [105]	4.432	0.098
BiInO3	4.072	-	4.057	0.015
PrCoO3	3.730	3.78 [106]	3.860	-0.130

PrFeO3	3.777	3.887 [106]	3.920	-0.143
PrCrO3	3.820	3.852 [106]	3.920	-0.100
PrMnO3	3.880	3.82 [106]	3.920	-0.040
PrVO3	3.870	3.89 [106]	3.860	0.010

Table 5.7: The predicted lattice parameters with our PLS model with those measured or calculated one

compounds	a_0(Å)	t	predicted a	Δa
VCRu3	3.957 [107]	0.936	3.759	0.197
NbCRu3	4.014 [107]	0.972	3.796	0.217
TaCRu3	4.05 [107]	0.972	3.796	0.253
ScCRu3	-	1.025	3.852	-
TiCRu3	-	0.954	3.778	-
CrCRu3	-	0.954	3.778	-
MnCRu3	-	0.954	3.778	-
FeCRu3	-	0.954	3.778	-
CoCRu3	-	0.936	3.759	-
NiCRu3	-	0.936	3.759	-
CuCRu3	-	0.936	3.759	-
ZnCRu3	-	0.936	3.759	-
ZrCRu3	-	1.007	3.833	-
MoCRu3	-	0.972	3.796	-
TcCRu3	-	0.936	3.759	-
RhCRu3	-	0.936	3.759	-
PdCRu3	-	0.954	3.778	-
AgCRu3	-	1.025	3.852	-
CdCRu3	-	1.007	3.833	-
HfCRu3	-	1.007	3.833	-
WCRu3	-	0.936	3.759	-
ReCRu3	-	0.936	3.759	-
OsCRu3	-	0.919	3.740	-
IrCRu3	-	0.936	3.759	-
PtCRu3	-	0.936	3.759	-
AuCRu3	-	0.936	3.759	-
HgCRu3	-	0.989	3.815	-
ScCNi3	-	1.017	3.953	-
TiCNi3	-	0.948	3.879	-

VCNi3	-	0.931	3.860	-
CrCNi3	-	0.948	3.879	-
MnCNi3	-	0.948	3.879	-
FeCNi3	-	0.948	3.879	-
CoCNi3	-	0.931	3.860	-
CuCNi3	-	0.931	3.860	-
NbCNi3	-	0.965	3.897	-
MoCNi3	-	0.965	3.897	-
RuCNi3	-	0.914	3.841	-
RhCNi3	-	0.931	3.860	-
PdCNi3	-	0.948	3.879	-
HfCNi3	-	1.000	3.934	-
TaCNi3	-	0.965	3.897	-
WCNi3	-	0.931	3.860	-
ReCNi3	-	0.931	3.860	-
OsCNi3	-	0.914	3.841	-
IrCNi3	-	0.931	3.860	-
PtCNi3	-	0.931	3.860	-
AuCNi3	-	0.931	3.860	-
HgCNi3	-	0.983	3.916	-
GaCTi3	4.158 [108]	0.909	3.942	0.216
SnCTi3	4.247 [108]	0.959	3.998	0.245
PbCTi3	-	1.077	4.129	-
BiCTi3	-	1.010	4.054	-
AlCSc3	4.51 [109]	0.876	4.328	0.182
GaCSc3	4.48 [109]	0.891	4.346	0.134
InCSc3	4.56 [109]	0.968	4.439	0.121
TlCSc3	4.56 [109]	1.076	4.570	-0.01
SnCSc3	-	0.937	4.402	-
PbCSc3	-	1.045	4.532	-
BiCSc3	-	0.983	4.458	-
TiCRh3	-	0.948	3.879	-
VCRh3	-	0.931	3.860	-
CrCRh3	-	0.948	3.879	-
MnCRh3	-	0.948	3.879	-
FeCRh3	-	0.948	3.879	-
CoCRh3	-	0.931	3.860	-

NiCRh3	-	0.931	3.860	-
CuCRh3	-	0.931	3.860	-
ZnCRh3	-	0.931	3.860	-
ZrCRh3	-	1.000	3.934	-
NbCRh3	-	0.965	3.897	-
MoCRh3	-	0.965	3.897	-
TcCRh3	-	0.931	3.860	-
RuCRh3	-	0.914	3.841	-
PdCRh3	-	0.948	3.879	-
AgCRh3	-	1.017	3.953	-
CdCRh3	-	1.000	3.934	-
HfCRh3	-	1.000	3.934	-
TaCRh3	-	0.965	3.897	-
WCRh3	-	0.931	3.860	-
ReCRh3	-	0.931	3.860	-
OsCRh3	-	0.914	3.841	-
IrCRh3	-	0.931	3.860	-
PtCRh3	-	0.931	3.860	-
AuCRh3	-	0.931	3.860	-
HgCRh3	-	0.983	3.916	-
CeCRh3	-	1.103	4.046	-
PrCRh3	-	1.103	4.046	-
NdCRh3	-	1.103	4.046	-
PmCRh3	-	1.103	4.046	-
SmCRh3	-	1.103	4.046	-
EuCRh3	-	1.103	4.046	-
GdCRh3	-	1.086	4.028	-
TbCRh3	-	1.069	4.009	-
DyCRh3	-	1.069	4.009	-
HoCRh3	-	1.069	4.009	-
ErCRh3	-	1.069	4.009	-
TmCRh3	-	1.069	4.009	-
YbCRh3	-	1.069	4.009	-
AlCPd3	4.132 [110]	0.892	3.924	0.216
InCPd3	4.206 [110]	0.993	4.035	0.171
GeCPd3	4.183 [110]	0.892	3.924	0.259
PbCPd3	4.293 [110]	1.077	4.129	0.164

SiCPd3	-	0.841	3.868	-
GaCPd3	-	0.909	3.942	-
AsCPd3	-	0.858	3.886	-
SnCPd3	-	0.959	3.998	-
SbCPd3	-	0.959	3.998	-
TeCPd3	-	0.942	3.980	-
BiCPd3	-	1.010	4.054	-
ScCPd3	4.207 [110]	1.010	4.054	0.153
YCPd3	4.292 [110]	1.094	4.147	0.145
NbCPd3	4.189 [110]	0.959	3.998	0.191
ZrCPd3	-	0.993	4.035	-
MoCPd3	-	0.959	3.998	-
TcCPd3	-	0.925	3.961	-
RhCPd3	-	0.925	3.961	-
AgCPd3	-	1.010	4.054	-
CdCPd3	-	0.993	4.035	-
HfCPd3	-	0.993	4.035	-
TaCPd3	-	0.959	3.998	-
WCPd3	-	0.925	3.961	-
ReCPd3	-	0.925	3.961	-
OsCPd3	-	0.909	3.942	-
IrCPd3	-	0.925	3.961	-
PtCPd3	-	0.925	3.961	-
AuCPd3	-	0.925	3.961	-
HgCPd3	-	0.976	4.017	-
CuCTi3	4.146 [108]	0.925	3.961	0.185
ZnCTi3	4.165 [108]	0.925	3.961	0.204
CdCTi3	4.236 [108]	0.993	4.035	0.201
ScCTi3	-	1.010	4.054	-
VCTi3	-	0.925	3.961	-
CrCTi3	-	0.942	3.980	-
MnCTi3	-	0.942	3.980	-
FeCTi3	-	0.942	3.980	-
CoCTi3	-	0.925	3.961	-
NiCTi3	-	0.925	3.961	-
ZrCTi3	-	0.993	4.035	-
NbCTi3	-	0.959	3.998	-

MoCTi3	-	0.959	3.998	-
TcCTi3	-	0.925	3.961	-
RuCTi3	-	0.909	3.942	-
RhCTi3	-	0.925	3.961	-
PdCTi3	-	0.942	3.980	-
AgCTi3	-	1.010	4.054	-
HfCTi3	-	0.993	4.035	-
TaCTi3	-	0.959	3.998	-
WCTi3	-	0.925	3.961	-
ReCTi3	-	0.925	3.961	-
OsCTi3	-	0.909	3.942	-
IrCTi3	-	0.925	3.961	-
PtCTi3	-	0.925	3.961	-
AuCTi3	-	0.925	3.961	-
HgCTi3	-	0.976	4.017	-
CdCPt3	4.231 [110]	1.000	3.934	0.297
ScCPt3	4.242 [110]	1.017	3.953	0.289
YCPt3	4.322 [110]	1.103	4.046	0.276
NbCPt3	4.222 [110]	0.965	3.897	0.325
MoCPt3	4.187 [110]	0.965	3.897	0.29
TiCPt3	-	0.948	3.879	-
VCPt3	-	0.931	3.860	-
CrCPt3	-	0.948	3.879	-
MnCPt3	-	0.948	3.879	-
FeCPt3	-	0.948	3.879	-
CoCPt3	-	0.931	3.860	-
NiCPt3	-	0.931	3.860	-
CuCPt3	-	0.931	3.860	-
ZnCPt3	-	0.931	3.860	-
ZrCPt3	-	1.000	3.934	-
TcCPt3	-	0.931	3.860	-
RuCPt3	-	0.914	3.841	-
RhCPt3	-	0.931	3.860	-
PdCPt3	-	0.948	3.-879	-
AgCPt3	-	1.017	3.953	-
HfCPt3	-	1.000	3.934	-
TaCPt3	-	0.965	3.897	-

WCPt3	-	0.931	3.860	-
ReCPt3	-	0.931	3.860	-
OsCPt3	-	0.914	3.841	-
IrCPt3	-	0.931	3.860	-
AuCPt3	-	0.931	3.860	-
ScNNi3	-	1.042	3.925	-
TiNNi3	-	0.972	3.850	-
VNNi3	-	0.954	3.832	-
CrNNi3	-	0.972	3.850	-
MnNNi3	-	0.972	3.850	-
FeNNi3	-	0.972	3.850	-
CoNNi3	-	0.954	3.832	-
ZrNNi3	-	1.025	3.906	-
NbNNi3	-	0.989	3.869	-
MoNNi3	-	0.989	3.869	-
TcNNi3	-	0.954	3.832	-
RuNNi3	-	0.936	3.813	-
RhNNi3	-	0.954	3.832	-
HfNNi3	-	1.025	3.906	-
TaNNi3	-	0.989	3.869	-
WNNi3	-	0.954	3.832	-
ReNNi3	-	0.954	3.832	-
OsNNi3	-	0.936	3.813	-
IrNNi3	-	0.954	3.832	-
AuNNi3	-	0.954	3.832	-
HgNNi3	-	1.007	3.887	-
AlNCa3	-	0.880	4.703	-
GaNCa3	-	0.894	4.722	-
InNCa3	-	0.966	4.815	-
SnNCa3	-	0.937	4.778	-
SiNCa3	-	0.836	4.647	-
AsNCa3	-	0.851	4.666	-
TeNCa3	-	0.923	4.759	-
SiNBa3	-	0.820	5.354	-
GeNBa3	-	0.858	5.410	-
TeNBa3	-	0.896	5.466	-
SnNBa3	-	0.909	5.484	-

InNBa3	-	0.934	5.522	-
TlNBa3	-	1.022	5.652	-
GaNBa3	-	0.871	5.428	-
AlNBa3	-	0.858	5.410	-
AlNSr3	-	0.867	5.107	-
SiNSr3	-	0.827	5.051	-
GaNSr3	-	0.880	5.126	-
GeNSr3	-	0.867	5.107	-
InNSr3	-	0.947	5.219	-
SnNSr3	-	0.920	5.181	-
TeNSr3	-	0.907	5.163	-
TlNSr3	-	1.040	5.349	-
PbNSr3	-	1.013	5.312	-
InNTi3	4.195 [111]	1.017	4.007	0.188
AlNTi3	4.11 [111]	0.914	3.895	0.216
TlNTi3	4.204 [111]	1.138	4.137	0.067
GaNTi3	4.105 [108]	0.931	3.914	0.191
SnNTi3	4.2 [108]	0.983	3.970	0.23
BiNTi3	-	1.034	4.026	-
CuNTi3	4.061 [108]	0.948	3.932	0.129
CdNTi3	4.179 [108]	1.017	4.007	0.172
ZnNTi3	4.087 [108]	0.948	3.932	0.155
ScNTi3	-	1.034	4.026	-
VNTi3	-	0.948	3.932	-
CrNTi3	-	0.965	3.951	-
MnNTi3	-	0.965	3.951	-
FeNTi3	-	0.965	3.951	-
CoNTi3	-	0.948	3.932	-
NiNTi3	-	0.948	3.932	-
ZrNTi3	-	1.017	4.007	-
NbNTi3	-	0.983	3.970	-
MoNTi3	-	0.983	3.970	-
TcNTi3	-	0.948	3.932	-
RuNTi3	-	0.931	3.914	-
RhNTi3	-	0.948	3.932	-
PdNTi3	-	0.965	3.951	-
AgNTi3	-	1.034	4.026	-

HfNTi3	-	1.017	4.007	-
TaNTi3	-	0.983	3.970	-
WNTi3	-	0.948	3.932	-
ReNTi3	-	0.948	3.932	-
OsNTi3	-	0.931	3.914	-
IrNTi3	-	0.948	3.932	-
PtNTi3	-	0.948	3.932	-
AuNTi3	-	0.948	3.932	-
HgNTi3	-	1.000	3.988	-
TlNNi3	-	1.149	4.036	-
PbNNi3	-	1.113	3.999	-
BiNNi3	-	1.042	3.925	-
BaAcO3	-	0.762	4.641	-
BaPaO3	-	0.810	4.459	-
BaUO3	-	0.827	4.399	-
BaCfO3	-	0.827	4.399	-
BaHfO3	4.28 [112]	0.904	4.156	0.13
BaTiO3	-	0.972	3.974	-
BaVO3	-	0.997	3.913	-
BaMnO3	-	0.972	3.974	-
BaCoO3	-	0.997	3.913	-
BaNiO3	-	0.997	3.913	-
BaCuO3	-	0.997	3.913	-
BaZnO3	-	0.997	3.913	-
BaNbO3	-	0.948	4.035	-
BaTcO3	-	0.997	3.913	-
BaRhO3	-	0.997	3.913	-
BaPdO3	-	0.972	3.974	-
BaWO3	-	0.997	3.913	-
BaReO3	-	0.997	3.913	-
BaOsO3	-	1.023	3.853	-
BaIrO3	-	0.997	3.913	-
BaPtO3	-	0.997	3.913	-
BaAuO3	-	0.997	3.913	-
BaHgO3	-	0.925	4.095	-
BiTlO3	-	0.622	4.481	-
BiSnO3	-	0.758	3.935	-

BiPbO3	-	0.648	4.359	-
BiTiO3	-	0.777	3.874	-
BiVO3	-	0.797	3.814	-
BiCrO3	-	0.777	3.874	-
BiMnO3	-	0.777	3.874	-
BiFeO3	-	0.777	3.874	-
BiCoO3	-	0.797	3.814	-
BiNiO3	-	0.797	3.814	-
BiCuO3	-	0.797	3.814	-
BiZnO3	-	0.797	3.814	-
BiYO3	-	0.634	4.420	-
BiZrO3	-	0.723	4.056	-
BiNbO3	-	0.758	3.935	-
BiMoO3	-	0.758	3.935	-
BiTcO3	-	0.797	3.814	-
BiRuO3	-	0.818	3.753	-
BiRhO3	-	0.797	3.814	-
BiPdO3	-	0.777	3.874	-
BiAgO3	-	0.707	4.117	-
BiCdO3	-	0.723	4.056	-
BiHfO3	-	0.723	4.056	-
BiTaO3	-	0.758	3.935	-
BiWO3	-	0.797	3.814	-
BiReO3	-	0.797	3.814	-
BiOsO3	-	0.818	3.753	-
BiIrO3	-	0.797	3.814	-
BiPtO3	-	0.797	3.814	-
BiAuO3	-	0.797	3.814	-
BiHgO3	-	0.740	3.996	-
CaMoO3	3.87 [2]	0.827	3.971	-0.096
CaTiO3	-	0.848	3.911	-
CaVO3	-	0.870	3.850	-
CaMnO3	-	0.848	3.911	-
CaFeO3	-	0.848	3.911	-
CaCoO3	-	0.870	3.850	-
CaZnO3	-	0.870	3.850	-
CaNbO3	-	0.827	3.971	-

SrAcO3	-	0.720	4.614	-
SrPaO3	-	0.766	4.432	-
SrNpO3	-	0.782	4.371	-
SrCmO3	-	0.782	4.371	-
SrBkO3	-	0.766	4.432	-
SrCfO3	-	0.766	4.432	-
SrHfO3	4.057 [113]	0.855	4.129	-0.072
SrScO3	-	0.835	4.189	-
SrTiO3	3.926 [114]	0.919	3.947	-0.021
SrVO3	-	0.942	3.886	-
SrMnO3	-	0.919	3.947	-
SrNiO3	-	0.942	3.886	-
SrCuO3	-	0.942	3.886	-
SrZnO3	-	0.942	3.886	-
SrYO3	-	0.750	4.493	-
SrNbO3	-	0.896	4.008	-
SrTcO3	-	0.942	3.886	-
SrRuO3	-	0.967	3.826	-
SrRhO3	-	0.942	3.886	-
SrPdO3	-	0.919	3.947	-
SrAgO3	-	0.835	4.189	-
SrCdO3	-	0.855	4.129	-
SrWO3	-	0.942	3.886	-
SrReO3	-	0.942	3.886	-
SrOsO3	-	0.967	3.826	-
SrIrO3	-	0.942	3.886	-
SrPtO3	-	0.942	3.886	-
SrAuO3	-	0.942	3.886	-
SrHgO3	-	0.875	4.068	-
PrTiO3	-	0.866	3.920	-
PrNiO3	-	0.888	3.859	-
PrCuO3	-	0.888	3.859	-
PrZnO3	-	0.888	3.859	-
PrZrO3	-	0.805	4.102	-
PrNbO3	-	0.845	3.980	-
PrMoO3	-	0.845	3.980	-
PrTcO3	-	0.888	3.859	-

PrRuO3	-	0.911	3.798	-
PrRhO3	-	0.888	3.859	-
PrPdO3	-	0.866	3.920	-
PrAgO3	-	0.787	4.162	-
PrCdO3	-	0.805	4.102	-
PrHfO3	-	0.805	4.102	-
PrTaO3	-	0.845	3.980	-
PrWO3	-	0.888	3.859	-
PrReO3	-	0.888	3.859	-
PrOsO3	-	0.911	3.798	-
PrIrO3	-	0.888	3.859	-
PrPtO3	-	0.888	3.859	-
PrAuO3	-	0.888	3.859	-
PrHgO3	-	0.824	4.041	-

Table 5.8: The predicted lattice parameters of new synthesized or hypothetical perovskites and inverse perovskites not included in our training data set.

5.3 the Ionic Conductivity in Oxide Perovskites

compounds	a_0(Å)	r_A(Å)	r_B(Å)	E_A	E_B	t	R_C(Å)	V_U	μ	V_L	V_S
BaCrO3	3,957	1,61	0,55	0,89	1,66	1,101	0,826	3,957	0,407	24,511	6,192
BaMoO3	4,01	1,61	0,65	0,89	2,16	1,046	0,817	4,099	0,481	24,823	6,055
BaNbO3	4,1287	1,61	0,68	0,89	1,6	1,031	0,868	4,141	0,503	24,947	6,023
BaNpO3	4,437	1,61	0,87	0,89	1,36	0,942	0,963	4,410	0,644	26,119	5,921
BaPaO3	4,51	1,61	0,9	0,89	1,5	0,930	0,991	4,453	0,666	26,371	5,922
BaPrO3	4,3637	1,61	0,85	0,89	1,13	0,951	0,931	4,382	0,629	25,961	5,924
BaPuO3	4,421	1,61	0,86	0,89	1,28	0,947	0,958	4,396	0,637	26,039	5,922
BaRuO3	4,005	1,61	0,62	0,89	2,2	1,062	0,826	4,056	0,459	24,713	6,091
BaSnO3	4,13	1,61	0,69	0,89	1,96	1,025	0,865	4,155	0,511	24,992	6,013
BaTaO3	4,057	1,61	0,68	0,89	1,5	1,031	0,830	4,141	0,503	24,947	6,023
BaTbO3	4,278	1,61	0,76	0,89	1,22	0,991	0,917	4,254	0,562	25,355	5,959
BaThO3	4,555	1,61	0,94	0,89	1,3	0,913	1,002	4,509	0,696	26,740	5,929
BaTiO3	4,022	1,61	0,605	0,89	1,54	1,070	0,840	4,035	0,448	24,664	6,111
BaUO3	4,38	1,61	0,89	0,89	1,38	0,934	0,926	4,438	0,659	26,285	5,921
BaZrO3	4,226	1,61	0,72	0,89	1,33	1,011	0,905	4,198	0,533	25,137	5,987
CaCrO3	3,777	1,34	0,55	1	1,66	1,001	0,905	3,775	0,407	17,295	4,580
CaSnO3	3,964	1,34	0,69	1	1,96	0,932	0,955	3,960	0,511	17,789	4,491
CaTaO3	3,975	1,34	0,68	1	1,5	0,937	0,964	3,947	0,503	17,743	4,495

CaTiO3	3,9	1,34	0,605	1	1,54	0,972	0,950	3,848	0,448	17,453	4,535
CaZrO3	4,138	1,34	0,72	1	1,33	0,918	1,036	3,999	0,533	17,937	4,484
PrCoO3	3,73	1,3	0,61	1,13	1,88	0,956	0,886	3,823	0,451	16,625	4,347
PrCrO3	3,819	1,3	0,55	1,13	1,66	0,986	0,954	3,745	0,407	16,449	4,391
PrFeO3	3,777	1,3	0,645	1,13	1,83	0,939	0,899	3,869	0,477	16,752	4,329
PrMnO3	3,88	1,3	0,645	1,13	1,55	0,939	0,952	3,869	0,477	16,752	4,329
PrVO3	3,87	1,3	0,64	1,13	1,63	0,941	0,949	3,862	0,474	16,733	4,331
SrCrO3	3,844	1,44	0,55	0,95	1,66	1,038	0,875	3,847	0,407	19,651	5,107
SrNbO3	4,073	1,44	0,68	0,95	1,6	0,971	0,949	4,026	0,503	20,094	4,994
SrPuO3	4,378	1,44	0,86	0,95	1,28	0,892	1,049	4,267	0,637	21,197	4,966
SrTaO3	4,007	1,44	0,68	0,95	1,5	0,971	0,915	4,023	0,503	20,094	4,994
SrThO3	4,53	1,44	0,94	0,95	1,3	0,861	1,104	4,376	0,696	21,903	5,005
SrTiO3	3,945	1,44	0,605	0,95	1,54	1,009	0,909	3,921	0,448	19,807	5,050
SrUO3	4,376	1,44	0,89	0,95	1,38	0,880	1,038	4,308	0,659	21,445	4,977
SrVO3	3,8662	1,44	0,64	0,95	1,63	0,991	0,855	3,969	0,474	19,930	5,020
SrZrO3	4,1794	1,44	0,72	0,95	1,33	0,953	0,991	4,077	0,533	20,286	4,974

Table 5.9: The training dataset used in the PCA calculations including 13 predictor variables.

compounds	a_0(Å)	t	R_C(Å)	V_U	η	μ	$(t+\mu)^\eta$	V_L	V_S
BaAuO3	4.404	0.951	0.952	4.382	0.596	0.629	1.314	25.961	5.924
BaCoO3	4.002	1.067	0.827	4.042	0.769	0.451	1.379	24.680	6.104
BaCuO3	4.203	1.006	0.889	4.212	0.673	0.540	1.341	25.189	5.979
BaFeO3	3.960	1.081	0.815	4.007	0.792	0.433	1.389	24.603	6.139
BaHfO3	4.169	1.016	0.878	4.184	0.687	0.525	1.347	25.087	5.995
BaIrO3	4.027	1.059	0.835	4.064	0.756	0.462	1.374	24.731	6.085
BaMoO3	4.01	1.046	0.817	4.099	0.768	0.481	1.384	24.823	6.055
BaNbO3	4.128	1.031	0.868	4.141	0.706	0.503	1.353	24.947	6.023
BaOsO3	4.035	1.057	0.837	4.071	0.751	0.466	1.372	24.748	6.079
BaPdO3	4.010	1.065	0.830	4.049	0.764	0.455	1.378	24.696	6.098
BaPrO3	4.363	0.951	0.931	4.382	0.613	0.629	1.324	25.961	5.924
BaPtO3	4.027	1.059	0.835	4.064	0.756	0.462	1.374	24.731	6.085
BaRhO3	3.985	1.073	0.822	4.028	0.778	0.444	1.383	24.648	6.118
BaRuO3	4.005	1.062	0.826	4.056	0.768	0.459	1.380	24.713	6.091
BaScO3	4.228	0.999	0.897	4.233	0.662	0.551	1.337	25.270	5.968
BaSnO3	4.13	1.025	0.865	4.155	0.706	0.511	1.354	24.992	6.013
BaTaO3	4.057	1.031	0.830	4.141	0.744	0.503	1.375	24.947	6.023
BaTbO3	4.278	0.991	0.917	4.254	0.641	0.562	1.327	25.355	5.959
BaTiO3	4.022	1.070	0.840	4.035	0.757	0.448	1.372	24.664	6.111

BaWO3	4.085	1.041	0.853	4.113	0.726	0.488	1.362	24.863	6.044
BaZnO3	4.219	1.001	0.894	4.226	0.666	0.548	1.338	25.242	5.972
BaZrO3	4.226	1.011	0.905	4.198	0.661	0.533	1.332	25.137	5.987
BiCoO3	3.882	0.984	0.913	3.885	0.732	0.451	1.303	18.368	4.728
BiFeO3	3.840	0.997	0.900	3.851	0.754	0.433	1.310	18.290	4.748
BiIrO3	3.907	0.977	0.921	3.905	0.719	0.462	1.300	18.420	4.717
BiMoO3	3.949	0.965	0.935	3.938	0.698	0.481	1.294	18.515	4.701
BiNbO3	4.000	0.950	0.951	3.978	0.675	0.503	1.287	18.641	4.685
BiOsO3	3.916	0.974	0.924	3.911	0.715	0.466	1.298	18.438	4.713
BiPdO3	3.891	0.982	0.916	3.891	0.727	0.455	1.302	18.385	4.724
BiPtO3	3.907	0.977	0.921	3.905	0.719	0.462	1.300	18.420	4.717
BiRhO3	3.866	0.989	0.908	3.871	0.740	0.444	1.306	18.336	4.735
BiRuO3	3.899	0.979	0.919	3.898	0.723	0.459	1.301	18.403	4.720
BiTaO3	4.000	0.950	0.951	3.978	0.675	0.503	1.287	18.641	4.685
BiTiO3	3.874	0.987	0.911	3.878	0.736	0.448	1.305	18.352	4.731
BiWO3	3.966	0.960	0.940	3.951	0.690	0.488	1.292	18.555	4.695
CaCoO3	3.862	0.970	0.929	3.854	0.727	0.451	1.292	17.469	4.531
CaFeO3	3.820	0.983	0.915	3.821	0.749	0.433	1.292	17.390	4.550
CaIrO3	3.887	0.963	0.937	3.874	0.715	0.462	1.288	17.521	4.522
CaMoO3	3.929	0.951	0.950	3.907	0.694	0.481	1.283	17.616	4.508
CaOsO3	3.895	0.960	0.939	3.881	0.710	0.466	1.287	17.539	4.519
CaPdO3	3.870	0.967	0.931	3.861	0.723	0.455	1.291	17.486	4.528
CaPtO3	3.887	0.963	0.937	3.874	0.715	0.462	1.288	17.521	4.522
CaRhO3	3.845	0.975	0.923	3.841	0.736	0.444	1.294	17.436	4.538
CaRuO3	3.878	0.965	0.934	3.868	0.719	0.459	1.289	17.504	4.525
CaTiO3	3.9	0.972	0.950	3.842	0.706	0.448	1.281	17.453	4.535
CdCoO3	3.846	0.959	0.940	3.831	0.725	0.451	1.283	16.831	4.392
CdFeO3	3.804	0.972	0.927	3.798	0.747	0.433	1.289	16.752	4.409
CdIrO3	3.871	0.952	0.948	3.851	0.712	0.462	1.280	16.883	4.384
CdNiO3	3.628	1.027	0.872	3.661	0.853	0.355	1.319	16.514	4.509
CdPdO3	3.854	0.957	0.943	3.838	0.720	0.455	1.282	16.848	4.389
CdPtO3	3.871	0.952	0.948	3.851	0.712	0.462	1.280	16.883	4.384
CdRhO3	3.829	0.964	0.935	3.818	0.733	0.444	1.286	16.798	4.399
CdRuO3	3.863	0.954	0.946	3.844	0.716	0.459	1.281	16.865	4.386
CdTiO3	3.838	0.962	0.938	3.825	0.729	0.448	1.284	16.814	4.395
CeCoO3	3.862	0.970	0.929	3.854	0.727	0.451	1.292	17.469	4.531
CeFeO3	3.820	0.983	0.915	3.821	0.749	0.433	1.298	17.390	4.550
CeIrO3	3.887	0.963	0.937	3.874	0.715	0.462	1.288	17.521	4.522
CeMoO3	3.929	0.951	0.950	3.907	0.694	0.481	1.283	17.616	4.508
CeNiO3	3.644	1.039	0.861	3.683	0.856	0.355	1.329	17.153	4.657

CeOsO3	3.895	0.960	0.939	3.881	0.710	0.466	1.287	17.539	4.519
CePdO3	3.870	0.967	0.931	3.861	0.723	0.455	1.291	17.486	4.528
CePtO3	3.887	0.963	0.937	3.874	0.715	0.462	1.288	17.521	4.522
CeRhO3	3.845	0.975	0.923	3.841	0.736	0.444	1.294	17.436	4.538
CeRuO3	3.878	0.965	0.934	3.868	0.719	0.459	1.289	17.504	4.525
CeTiO3	3.853	0.972	0.926	3.848	0.732	0.448	1.293	17.453	4.535
LaCoO3	3.872	0.977	0.921	3.870	0.729	0.451	1.297	17.912	4.628
LaFeO3	3.830	0.990	0.908	3.836	0.752	0.433	1.304	17.833	4.647
LaIrO3	3.897	0.970	0.929	3.889	0.717	0.462	1.294	17.964	4.618
LaMoO3	3.939	0.958	0.942	3.923	0.696	0.481	1.288	18.058	4.603
LaNiO3	3.654	1.047	0.854	3.697	0.858	0.355	1.337	17.597	4.759
LaOsO3	3.905	0.967	0.932	3.896	0.712	0.466	1.293	17.982	4.614
LaPdO3	3.880	0.975	0.924	3.876	0.725	0.455	1.296	17.929	4.624
LaPtO3	3.897	0.970	0.929	3.889	0.717	0.462	1.294	17.964	4.618
LaRhO3	3.855	0.982	0.916	3.856	0.738	0.444	1.300	17.879	4.635
LaRuO3	3.889	0.972	0.926	3.883	0.721	0.459	1.295	17.946	4.621
LaTiO3	3.864	0.980	0.918	3.863	0.734	0.448	1.299	17.895	4.632
LaWO3	3.956	0.953	0.948	3.936	0.688	0.488	1.286	18.099	4.598
PbCoO3	3.939	1.024	0.872	3.963	0.747	0.451	1.337	21.136	5.332
PbCuO3	4.140	0.965	0.935	4.128	0.653	0.540	1.306	21.650	5.243
PbFeO3	3.898	1.037	0.859	3.929	0.769	0.433	1.346	21.058	5.359
PbHfO3	4.107	0.974	0.924	4.101	0.667	0.525	1.311	21.547	5.254
PbIrO3	3.965	1.016	0.880	3.984	0.734	0.462	1.333	21.187	5.317
PbMoO3	4.006	1.004	0.893	4.018	0.713	0.481	1.326	21.281	5.295
PbNbO3	4.057	0.989	0.908	4.059	0.689	0.503	1.318	21.406	5.272
PbNiO3	3.722	1.097	0.806	3.785	0.876	0.355	1.387	20.828	5.502
PbOsO3	3.973	1.014	0.882	3.991	0.730	0.466	1.331	21.205	5.313
PbPdO3	3.948	1.021	0.874	3.970	0.742	0.455	1.336	21.153	5.327
PbPtO3	3.965	1.016	0.880	3.984	0.734	0.462	1.333	21.187	5.317
PbRhO3	3.923	1.029	0.867	3.949	0.756	0.444	1.341	21.104	5.342
PbRuO3	3.956	1.019	0.877	3.977	0.738	0.459	1.334	21.170	5.322
PbScO3	4.166	0.958	0.943	4.149	0.642	0.551	1.303	21.732	5.237
PbTaO3	4.057	0.989	0.908	4.059	0.689	0.503	1.318	21.406	5.272
PbTbO3	4.191	0.951	0.951	4.169	0.632	0.562	1.300	21.818	5.232
PbTiO3	3.931	1.027	0.869	3.956	0.751	0.448	1.339	21.120	5.337
PbWO3	4.023	0.999	0.898	4.032	0.705	0.488	1.323	21.321	5.287
PbZnO3	4.157	0.960	0.940	4.142	0.646	0.548	1.304	21.704	5.239
PbZrO3	4.124	0.970	0.929	4.114	0.660	0.533	1.308	21.597	5.248
PrCoO3	3.73	0.956	0.886	3.823	0.791	0.451	1.310	16.625	4.347
PrNiO3	3.623	1.023	0.876	3.654	0.852	0.355	1.315	16.307	4.462

PrPdO3	3.849	0.953	0.947	3.830	0.719	0.455	1.280	16.642	4.345
PrRhO3	3.824	0.960	0.939	3.810	0.732	0.444	1.283	16.592	4.351
PrRuO3	3.858	0.951	0.949	3.836	0.715	0.459	1.279	16.659	4.342
PrTiO3	3.832	0.958	0.941	3.817	0.728	0.448	1.282	16.608	4.351
SrCoO3	3.913	1.006	0.891	3.928	0.739	0.451	1.321	19.823	5.045
SrFeO3	3.872	1.019	0.878	3.894	0.762	0.433	1.329	19.745	5.069
SrHfO3	4.081	0.957	0.943	4.064	0.660	0.525	1.297	20.236	4.978
SrIrO3	3.939	0.998	0.898	3.949	0.726	0.462	1.317	19.875	5.032
SrMoO3	3.981	0.986	0.912	3.982	0.706	0.481	1.311	19.968	5.013
SrNbO3	4.073	0.971	0.949	4.023	0.661	0.503	1.293	20.094	4.994
SrNiO3	3.696	1.078	0.824	3.752	0.868	0.355	1.367	19.512	5.200
SrOsO3	3.947	0.996	0.901	3.955	0.722	0.466	1.316	19.893	5.028
SrPdO3	3.922	1.003	0.893	3.935	0.735	0.455	1.320	19.840	5.041
SrPtO3	3.939	0.998	0.898	3.949	0.726	0.462	1.317	19.875	5.032
SrRhO3	3.897	1.011	0.885	3.915	0.748	0.444	1.324	19.791	5.055
SrRuO3	3.930	1.001	0.896	3.942	0.731	0.459	1.319	19.857	5.037
SrTaO3	4.007	0.971	0.915	4.023	0.695	0.503	1.310	20.094	4.994
SrTiO3	3.945	1.009	0.909	3.921	0.721	0.448	1.312	19.807	5.050
SrWO3	3.997	0.981	0.917	3.996	0.698	0.488	1.308	20.009	5.006
SrZrO3	4.179	0.953	0.991	4.077	0.615	0.533	1.276	20.286	4.974

Table 5.10: The predicted potential oxide perovskites ionic conductors.

compounds	a_0(Å)	r_A(Å)	r_B(Å)	t	R_C(Å)	μ	V_S	O_M(eV) [25]	O_B(eV) [25]
BaTiO3	4.022	1.61	0.605	1.070	0.840	0.448	6.111	0.67	-0.09
BaZrO3	4.226	1.61	0.72	1.011	0.905	0.533	5.987	0.69	0.08
DyAlO3	3.601	1.08	0.535	0.911	0.990	0.396	3.575	0.55	0.04
DyGaO3	3.743	1.08	0.62	0.872	1.037	0.459	3.544	0.44	-0.65
ErAlO3	3.591	1.06	0.535	0.904	0.998	0.396	3.517	0.59	0.11
ErCoO3	3.716	1.06	0.61	0.869	1.040	0.451	3.491	1.22	1.08
ErGaO3	3.733	1.06	0.62	0.865	1.045	0.459	3.489	0.47	-0.62
LaAlO3	3.746	1.36	0.535	1.016	0.882	0.396	4.694	0.64	-0.06
LaCoO3	3.872	1.36	0.61	0.977	0.921	0.451	4.628	0.7	1.66
LaCrO3	3.771	1.36	0.55	1.008	0.890	0.407	4.679	0.97	3.92
LaFeO3	3.830	1.36	0.585	0.990	0.908	0.433	4.647	0.83	2.67
LaGaO3	3.889	1.36	0.62	0.972	0.926	0.459	4.621	0.35	-0.71
LaInO3	4.190	1.36	0.8	0.891	1.024	0.592	4.573	0.39	-0.6
LaMnO3	3.738	1.36	0.53	1.019	0.879	0.392	4.700	0.75	3.46
LaNiO3	3.654	1.36	0.48	1.047	0.854	0.355	4.759	0.81	0.94
LaPdO3	3.880	1.36	0.615	0.975	0.924	0.455	4.624	1.04	1.08

LaRuO3	3.889	1.36	0.62	0.972	0.926	0.459	4.621	1.43	2.99
LaScO3	4.098	1.36	0.745	0.914	0.994	0.551	4.572	0.46	0.1
LaTiO3	3.864	1.36	0.605	0.980	0.918	0.448	4.632	1.6	5.09
LaTlO3	4.333	1.36	0.885	0.857	1.072	0.655	4.604	0.21	-0.71
LaVO3	3.922	1.36	0.64	0.962	0.937	0.474	4.608	1.36	4.52
LaYO3	4.358	1.36	0.9	0.851	1.081	0.666	4.613	0.32	0.15
PrCoO3	3.73	1.3	0.61	0.956	0.886	0.451	4.347	0.68	1.71
PrCrO3	3.819	1.3	0.55	0.986	0.954	0.407	4.391	1.05	4.23
PrFeO3	3.777	1.3	0.645	0.939	0.899	0.477	4.329	0.8	2.73
PrGaO3	3.858	1.3	0.62	0.951	0.949	0.459	4.342	0.35	-0.48
PrMnO3	3.88	1.3	0.645	0.939	0.952	0.477	4.329	0.75	3.63
PrNiO3	3.623	1.3	0.48	1.023	0.876	0.355	4.462	0.85	1.17
PrScO3	4.067	1.3	0.745	0.894	1.018	0.551	4.308	0.49	0.17
PrTiO3	3.832	1.3	0.605	0.958	0.941	0.448	4.351	1.62	5.11
PrVO3	3.87	1.3	0.64	0.941	0.949	0.474	4.331	1.46	4.57
SmAlO3	3.684	1.24	0.535	0.971	0.927	0.396	4.143	0.55	-0.13
SmCuO3	4.011	1.24	0.73	0.880	1.034	0.540	4.068	0.66	0.23
SmGaO3	3.826	1.24	0.62	0.929	0.973	0.459	4.089	0.36	-0.56
SrTiO3	3.945	1.44	0.605	1.009	0.909	0.448	5.050	0.46	0.05
YCoO3	3.727	1.08	0.61	0.876	1.031	0.451	3.546	1.17	1.78
YCrO3	3.626	1.08	0.55	0.904	0.998	0.407	3.568	1.22	4.16
YFeO3	3.685	1.08	0.585	0.887	1.017	0.433	3.553	1.29	2.62
YGaO3	3.743	1.08	0.62	0.872	1.037	0.459	3.544	0.43	-0.68
YMnO3	3.593	1.08	0.53	0.913	0.987	0.392	3.578	0.93	3.74
YNiO3	3.509	1.08	0.48	0.938	0.960	0.355	3.611	1.11	1.49
YScO3	3.953	1.08	0.745	0.820	1.109	0.551	3.557	0.42	0.2
YTiO3	3.718	1.08	0.605	0.878	1.029	0.448	3.548	1.56	5.02
YVO3	3.777	1.08	0.64	0.863	1.048	0.474	3.542	1.43	4.7

Table 5.11: The oxygen migration barrier and the oxygen vacancy formation energy taken from the work of Mayeshebi et al.

compounds	a_0(Å)	r_A(Å)	r_B(Å)	t	R_C(Å)	V_U	μ	V_L	V_S	O_M(eV)	O_B(eV)
LaInO3	4.190	1.36	0.8	0.891	1.024	4.122	0.592	18.853	4.573	0.39	-0.6
LaPdO3	3.880	1.36	0.615	0.975	0.924	3.876	0.455	17.929	4.624	1.04	1.08
LaRuO3	3.889	1.36	0.62	0.972	0.926	3.883	0.459	17.946	4.621	1.43	2.99
LaYO3	4.358	1.36	0.9	0.851	1.081	4.254	0.666	19.629	4.613	0.32	0.15
LaNbO3	4.056	1.36	0.72	0.925	0.980	4.015	0.533	18.378	4.576	3.330	12.859
LaMoO3	4.006	1.36	0.69	0.939	0.964	3.976	0.511	18.231	4.585	3.820	14.985
LaRhO3	3.964	1.36	0.665	0.950	0.950	3.942	0.492	18.120	4.595	3.715	14.300
LaAgO3	4.106	1.36	0.75	0.912	0.997	4.055	0.555	18.542	4.571	2.433	8.788

Table 5.12: The predicted oxygen migration barrier and the oxygen vacancy formation energy for some La-based oxide perovskites.

compounds	r_A(Å)	r_B(Å)	r_C(Å)	t	μ	E_m(eV) [26]	E_a(eV) [27]
LaGaO3	1.36	0.62	1.35	0.972	0.459	0.73	-
LaMnO3	1.36	0.53	1.35	1.019	0.392	0.86	-
LaCoO3	1.36	0.61	1.35	0.977	0.451	0.61	-
LaYO3	1.36	0.9	1.35	0.851	0.666	1.22	-
PrMnO3	1.3	0.53	1.35	0.996	0.392	-	0.253
PrInO3	1.3	0.8	1.35	0.871	0.592	-	0.512
SrMnO3	1.44	0.53	1.35	1.049	0.392	-	0.346

Table 5.13: The activation energies taken from the work of Richter et al and the migration energies taken from the work of Islam for some oxide perovskites.

compounds	r_A(Å)	r_B(Å)	t	μ	E_m(eV)	a_0(Å)	R_C(Å)	V_S	V_U	V_L
LaBiO3	1.36	1.03	0.805	0.762	1.339	4.575	1.156	4.738	4.427	20.979
LaYO3	1.36	0.9	0.851	0.666	1.22	4.358	1.081	4.613	4.254	19.629
LaTlO3	1.36	0.885	0.857	0.655	1.147	4.333	1.072	4.604	4.234	19.499
LaAuO3	1.36	0.85	0.871	0.629	1.100	4.274	1.052	4.587	4.188	19.214
LaInO3	1.36	0.8	0.891	0.592	1.034	4.190	1.024	4.573	4.122	18.853
LaPdO3	1.36	0.76	0.908	0.562	0.981	4.123	1.002	4.571	4.068	18.600
LaAgO3	1.36	0.75	0.912	0.555	0.967	4.106	0.997	4.571	4.055	18.542
LaScO3	1.36	0.745	0.914	0.551	0.961	4.098	0.994	4.572	4.049	18.514
LaNbO3	1.36	0.72	0.925	0.533	0.928	4.056	0.980	4.576	4.015	18.378
LaTaO3	1.36	0.72	0.925	0.533	0.928	4.056	0.980	4.576	4.015	18.378
LaMoO3	1.36	0.69	0.939	0.511	0.888	4.006	0.964	4.585	3.976	18.231
LaRuO3	1.36	0.68	0.943	0.503	0.874	3.989	0.958	4.588	3.962	18.185
LaIrO3	1.36	0.68	0.943	0.503	0.874	3.989	0.958	4.588	3.962	18.185
LaTiO3	1.36	0.67	0.948	0.496	0.861	3.972	0.953	4.593	3.949	18.141
LaMnO3	1.36	0.53	1.019	0.392	0.86	3.738	0.879	4.700	3.763	17.691
LaRhO3	1.36	0.665	0.950	0.492	0.855	3.964	0.950	4.595	3.942	18.120
LaFeO3	1.36	0.645	0.960	0.477	0.828	3.931	0.940	4.605	3.916	18.039
LaVO3	1.36	0.64	0.962	0.474	0.821	3.922	0.937	4.608	3.909	18.019
LaCrO3	1.36	0.615	0.975	0.455	0.788	3.880	0.924	4.624	3.876	17.929
LaNiO3	1.36	0.6	0.982	0.444	0.768	3.855	0.916	4.635	3.856	17.879
LaGaO3	1.36	0.62	0.972	0.459	0.73	3.889	0.926	4.621	3.883	17.946
LaCuO3	1.36	0.54	1.013	0.4	0.689	3.755	0.884	4.689	3.777	17.714
LaCoO3	1.36	0.61	0.977	0.451	0.62	3.872	0.921	4.628	3.870	17.912

Table 5.14: The predicted migration energies for La-based oxide perovskites.

compounds	r_A(Å)	r_B(Å)	t	μ	E_a(eV)	R_C(Å)	V_S	a_0(Å)	V_U	V_L
PrBiO3	1.3	1.03	0.787	0.762	0.732	1.182	4.507	4.544	4.370	19.702
PrTlO3	1.3	0.885	0.838	0.655	0.593	1.097	4.356	4.301	4.181	18.218
PrAuO3	1.3	0.85	0.851	0.629	0.559	1.077	4.335	4.243	4.136	17.933
SrZrO3	1.44	0.72	0.953	0.533	0.528	0.949	4.974	4.098	4.077	20.286
SrHfO3	1.44	0.71	0.957	0.525	0.518	0.943	4.978	4.081	4.064	20.236
PrInO3	1.3	0.8	0.871	0.592	0.512	1.049	4.315	4.159	4.071	17.571
SrNbO3	1.44	0.68	0.971	0.503	0.489	0.927	4.994	4.031	4.023	20.094
SrTaO3	1.44	0.68	0.971	0.503	0.489	0.927	4.994	4.031	4.023	20.094
PrPdO3	1.3	0.76	0.888	0.562	0.473	1.026	4.308	4.092	4.019	17.317
SrWO3	1.44	0.66	0.981	0.488	0.470	0.917	5.006	3.997	3.996	20.009
PrAgO3	1.3	0.75	0.892	0.555	0.464	1.021	4.308	4.075	4.006	17.259
SrMoO3	1.44	0.65	0.986	0.481	0.461	0.911	5.013	3.980	3.982	19.968
SrTcO3	1.44	0.645	0.988	0.477	0.456	0.909	5.017	3.972	3.976	19.949
SrReO3	1.44	0.63	0.996	0.466	0.441	0.901	5.028	3.947	3.955	19.893
SrOsO3	1.44	0.63	0.996	0.466	0.441	0.901	5.028	3.947	3.955	19.893
SrIrO3	1.44	0.625	0.998	0.462	0.437	0.898	5.032	3.939	3.949	19.875
SrPtO3	1.44	0.625	0.998	0.462	0.437	0.898	5.032	3.939	3.949	19.875
PrNbO3	1.3	0.72	0.905	0.533	0.435	1.004	4.309	4.025	3.967	17.094
PrTaO3	1.3	0.72	0.905	0.533	0.435	1.004	4.309	4.025	3.967	17.094
SrRuO3	1.44	0.62	1.001	0.459	0.432	0.896	5.037	3.930	3.942	19.857
SrPdO3	1.44	0.615	1.003	0.455	0.427	0.893	5.041	3.922	3.935	19.840
SrTiO3	1.44	0.605	1.009	0.448	0.417	0.888	5.050	3.905	3.921	19.807
SrRhO3	1.44	0.6	1.011	0.444	0.413	0.885	5.055	3.897	3.915	19.791
PrMoO3	1.3	0.69	0.918	0.511	0.406	0.987	4.314	3.975	3.927	16.946
SrFeO3	1.44	0.585	1.019	0.433	0.398	0.878	5.069	3.872	3.894	19.745
PrRuO3	1.3	0.68	0.923	0.503	0.396	0.982	4.316	3.958	3.914	16.900
PrIrO3	1.3	0.68	0.923	0.503	0.396	0.982	4.316	3.958	3.914	16.900
SrVO3	1.44	0.58	1.022	0.429	0.393	0.875	5.074	3.863	3.888	19.730
PrTiO3	1.3	0.67	0.927	0.496	0.387	0.976	4.320	3.941	3.901	16.856
PrRhO3	1.3	0.665	0.929	0.492	0.382	0.974	4.321	3.933	3.895	16.834
SrCrO3	1.44	0.55	1.038	0.407	0.365	0.860	5.107	3.813	3.847	19.651
PrFeO3	1.3	0.645	0.939	0.477	0.363	0.963	4.329	3.899	3.869	16.752
PrVO3	1.3	0.64	0.941	0.474	0.358	0.960	4.331	3.891	3.862	16.733
SrMnO3	1.44	0.53	1.049	0.392	0.346	0.849	5.131	3.779	3.820	19.605
SrCoO3	1.44	0.53	1.049	0.392	0.346	0.849	5.131	3.779	3.820	19.605

PrGaO3	1.3	0.62	0.951	0.459	0.339	0.949	4.342	3.858	3.836	16.659
PrCrO3	1.3	0.615	0.953	0.455	0.334	0.947	4.345	3.849	3.830	16.642
PrCoO3	1.3	0.61	0.956	0.451	0.329	0.944	4.347	3.841	3.823	16.625
PrNiO3	1.3	0.61	0.956	0.451	0.329	0.944	4.347	3.841	3.823	16.625
SrNiO3	1.44	0.48	1.078	0.355	0.298	0.824	5.200	3.696	3.752	19.512
PrCuO3	1.3	0.54	0.991	0.4	0.262	0.907	4.400	3.724	3.732	16.425
PrMnO3	1.3	0.645	0.939	0.477	0.253	0.963	4.329	3.899	3.869	16.752

Table 5.15: The predicted migration energies for Pr-based oxide perovskites.

5.4 Double Halide Perovskite

compounds	a^{+2}(Å) [115, 116]	r_A(Å)	r_B^{+2}(Å)	r_X(Å)	t^{+2}	μ^{+2}
KNiF3	4.013	1.64	0.69	1.33	1.039	0.518
KMnF3	4.189	1.64	0.83	1.33	0.972	0.624
KGeF3	4.46	1.64	0.73	1.33	1.019	0.548
RbCoF3	4.141	1.72	0.745	1.33	1.039	0.560
RbMnF3	4.24	1.72	0.83	1.33	0.998	0.624
RbPdF3	4.298	1.72	0.86	1.33	0.984	0.646
RbGeF3	4.49	1.72	0.73	1.33	1.046	0.548
CsGeF3	4.56	1.88	0.73	1.33	1.101	0.548
CsGeCl3	5.35	1.88	0.73	1.81	1.027	0.403
CsSnCl3	5.56	1.88	1.1	1.81	0.896	0.607
CsPbCl3	5.605	1.88	1.19	1.81	0.869	0.657
CsSnBr3	5.804	1.88	1.1	1.96	0.887	0.561
CsSnI3	6.219	1.88	1.1	2.2	0.874	0.5
CsGeBr3	5.62	1.88	0.73	1.96	1.009	0.372
KGeBr3	5.55	1.64	0.73	1.96	0.946	0.372
RbGeBr3	5.57	1.72	0.73	1.96	0.967	0.372
CsPbBr3	5.874	1.88	1.19	1.96	0.861	0.607
KGeCl3	5.27	1.64	0.73	1.81	0.960	0.403
RbGeCl3	5.31	1.72	0.73	1.81	0.982	0.403
KCoF3	4.071	1.64	0.745	1.33	1.012	0.560
NaCoF3	3.9	1.39	0.745	1.33	0.926	0.560
KFeF3	4.121	1.64	0.78	1.33	0.995	0.586
RbFeF3	4.174	1.72	0.78	1.33	1.022	0.586
KVF3	4.1	1.64	0.79	1.33	0.990	0.593
NaVF3	3.94	1.39	0.79	1.33	0.907	0.593
RbVF3	4.17	1.72	0.79	1.33	1.017	0.593
RbPbF3	4.79	1.72	1.19	1.33	0.855	0.894

CsGeI3	5.983	1.88	0.73	2.2	0.984	0.331
CsPbI3	6.289	1.88	1.19	2.2	0.851	0.540
RbPbI3	6.375	1.72	1.19	2.2	0.817	0.540
compounds	a^{+4}(Å) [117]	r_A(Å)	r_B^{+4}(Å)	r_x(Å)	t^{+4}	μ^{+4}
Cs2SnBr6	10.77	1.88	0.69	1.96	1.024	0.352
Cs2GeCl6	10.23	1.88	0.53	1.81	1.115	0.292
Cs2SnCl6	10.355	1.88	0.69	1.81	1.043	0.381
Cs2PbCl6	10.416	1.88	0.775	1.81	1.009	0.428
K2NiF6	8.109	1.64	0.48	1.33	1.160	0.360
K2MnF6	8.221	1.64	0.53	1.33	1.129	0.398
K2GeF6	8.343	1.64	0.53	1.33	1.129	0.398
Rb2CoF6	8.462	1.72	0.53	1.33	1.159	0.398
Rb2MnF6	8.531	1.72	0.53	1.33	1.159	0.398
Rb2GeF6	8.583	1.72	0.53	1.33	1.159	0.398
Cs2GeF6	8.990	1.88	0.53	1.33	1.220	0.398
Rb2PdF6	8.570	1.72	0.615	1.33	1.108	0.462
Cs2SnI6	11.65	1.88	0.69	2.2	0.998	0.313
Cs2GeBr6	-	1.88	0.53	1.96	1.090	0.270
Cs2GeI6	-	1.88	0.53	2.2	1.056	0.240
Cs2PbBr6	-	1.88	0.775	1.96	0.992	0.395
Cs2PbI6	-	1.88	0.775	2.2	0.969	0.352
K2CoF6	-	1.64	0.53	1.33	1.129	0.398
K2FeF6	-	1.64	0.585	1.33	1.096	0.439
K2GeBr6	-	1.64	0.53	1.96	1.022	0.270
K2GeCl6	-	1.64	0.53	1.81	1.042	0.292
K2VF6	-	1.64	0.58	1.33	1.099	0.436
Na2CoF6	-	1.39	0.53	1.33	1.034	0.398
Na2VF6	-	1.39	0.58	1.33	1.006	0.436
Rb2FeF6	-	1.72	0.585	1.33	1.126	0.439
Rb2GeBr6	-	1.72	0.53	1.96	1.045	0.270
Rb2GeCl6	-	1.72	0.53	1.81	1.066	0.292
Rb2PbF6	-	1.72	0.775	1.33	1.024	0.582
Rb2PbI6	-	1.72	0.775	2.2	0.931	0.352
Rb2VF6	-	1.72	0.58	1.33	1.129	0.436

Table 5.16: Dataset of different ABX_3 and their related A_2BX_6 perovskites, The CN's of the ions in Table 1 for ABX_3 structure are 12, 6 and 6 for A^{+}, B^{+2}, X^{+}, respectively. Whereas for A_2BX_6 structures are 12, 6, and 6 for $A^{+}, B^{+4}, andX^{+}$, respectively

compounds	a_3(Å)	$a_3 * 2$(Å)	compounds)	a_6(Å)	$\Delta a\%$(Å)

KNiF3	4.013	8.026	K2NiF6	8.109	1.023
KMnF3	4.189	8.378	K2MnF6	8.221	-1.909
KGeF3	4.46	8.92	K2GeF6	8.343	-6.915
RbCoF3	4.141	8.282	Rb2CoF6	8.462	2.127
RbMnF3	4.24	8.48	Rb2MnF6	8.531	0.597
RbPdF3	4.298	8.596	Rb2PdF6	8.57	-0.303
RbGeF3	4.49	8.98	Rb2GeF6	8.583	-4.625
CsGeF3	4.56	9.12	Cs2GeF6	8.99	-1.446
CsGeCl3	5.35	10.7	Cs2GeCl6	10.23	-4.594
CsSnCl3	5.56	11.12	Cs2SnCl6	10.355	-7.387
CsPbCl3	5.605	11.21	Cs2PbCl6	10.416	-7.622
CsSnBr3	5.804	11.608	Cs2SnBr6	10.77	-7.780
CsSnI3	6.219	12.438	Cs2SnI6	11.65	-6.763

Table 5.17: The comparison of the lattice parameter of A_2BX_6 and double of the lattice parameter for ABX_3

compounds	r_A(Å)	r_B(Å)	r_X(Å)	E_A	E_B	E_X	a(Å) [117]	t	μ	τ
Rb2TeBr6	1.72	0.97	1.96	0.8	2.38	2.83	10.769	0.888	0.494	4.116
Rb2TeCl6	1.72	0.97	1.81	0.8	2.38	2.98	10.233	0.897	0.535	3.961
Cs2TeI6	1.88	0.97	2.2	0.77	2.38	2.76	11.7	0.910	0.440	4.196
Cs2PoI6	1.88	0.94	2.2	0.77	2.4	2.76	11.79	0.918	0.427	4.225
Cs2TeBr6	1.88	0.97	1.96	0.77	2.38	2.83	10.92	0.926	0.494	3.949
Cs2PoBr6	1.88	0.94	1.96	0.77	2.4	2.83	10.99	0.936	0.479	3.970
Cs2TeCl6	1.88	0.97	1.81	0.77	2.38	2.98	10.445	0.938	0.535	3.794
Rb2SnI6	1.72	0.71	2.2	0.8	1.88	2.76	11.62	0.952	0.322	4.836
Cs2UBr6	1.88	0.89	1.96	0.77	1.7	2.83	11.07	0.952	0.454	4.026
Cs2NpBr6	1.88	0.87	1.96	0.77	1.3	2.83	11.082	0.959	0.443	4.057
K2SnBr6	1.64	0.69	1.96	0.8	1.88	2.83	10.48	0.960	0.352	4.585
Rb2PbCl6	1.72	0.775	1.81	0.8	1.92	2.98	10.195	0.965	0.428	4.119
K2SnCl6	1.64	0.69	1.81	0.8	1.88	2.98	9.9877	0.975	0.381	4.368
K2TaCl6	1.64	0.68	1.81	0.8	1.94	2.98	9.9935	0.979	0.375	4.401
Rb2PtI6	1.72	0.625	2.2	0.8	1.91	2.76	11.217	0.981	0.284	5.238
Rb2SnBr6	1.72	0.69	1.96	0.8	1.88	2.83	10.58	0.981	0.352	4.569
K2OsBr6	1.64	0.63	1.96	0.8	1.85	2.83	10.3	0.982	0.321	4.832
K2ReBr6	1.64	0.63	1.96	0.8	2.06	2.83	10.385	0.982	0.321	4.832
Rb2PdI6	1.72	0.615	2.2	0.8	2.08	2.76	11.185	0.984	0.279	5.296
K2PtBr6	1.64	0.625	1.96	0.8	1.91	2.83	10.293	0.984	0.318	4.856
Rb2ZrCl6	1.72	0.72	1.81	0.8	1.7	2.98	10.178	0.986	0.397	4.257

K2WCl6	1.64	0.66	1.81	0.8	1.79	2.98	9.8223	0.987	0.364	4.472
Cs2HfI6	1.88	0.71	2.2	0.77	1.73	2.76	11.609	0.991	0.322	4.817
K2OsCl6	1.64	0.65	1.81	0.8	1.85	2.98	9.85	0.991	0.359	4.510
Rb2WBr6	1.72	0.66	1.96	0.8	1.79	2.83	10.489	0.993	0.336	4.690
K2TcCl6	1.64	0.645	1.81	0.8	2.18	2.98	9.83	0.993	0.356	4.530
K2SeBr6	1.64	0.6	1.96	0.8	2.54	2.83	10.384	0.994	0.306	4.984
Cs2SnI6	1.88	0.69	2.2	0.77	1.88	2.76	11.65	0.998	0.313	4.906
Rb2SnCl6	1.72	0.69	1.81	0.8	1.88	2.98	10.137	0.998	0.381	4.352
K2MoCl6	1.64	0.63	1.81	0.8	1.94	2.98	9.729	0.999	0.348	4.593
K2ReCl6	1.64	0.63	1.81	0.8	2.06	2.98	9.84	0.999	0.348	4.593
K2PtCl6	1.64	0.625	1.81	0.8	1.91	2.98	9.751	1.001	0.345	4.616
K2RuCl6	1.64	0.62	1.81	0.8	1.97	2.98	9.737	1.003	0.342	4.638
K2PdCl6	1.64	0.615	1.81	0.8	2.08	2.98	9.7097	1.005	0.339	4.661
Cs2PbCl6	1.88	0.775	1.81	0.77	1.92	2.98	10.416	1.009	0.428	4.072
K2TiCl6	1.64	0.605	1.81	0.8	1.86	2.98	9.792	1.010	0.334	4.710
Rb2WCl6	1.72	0.66	1.81	0.8	1.79	2.98	9.957	1.010	0.364	4.463
Cs2PtI6	1.88	0.625	2.2	0.77	1.91	2.76	11.367	1.021	0.284	5.251
Cs2SnBr6	1.88	0.69	1.96	0.77	1.88	2.83	10.77	1.024	0.352	4.558
Rb2PtCl6	1.72	0.625	1.81	0.8	1.91	2.98	9.884	1.025	0.345	4.614
Rb2PdCl6	1.72	0.615	1.81	0.8	2.08	2.98	9.99	1.029	0.339	4.662
Cs2ZrCl6	1.88	0.72	1.81	0.77	1.7	2.98	10.428	1.031	0.397	4.234
Rb2TiCl6	1.72	0.605	1.81	0.8	1.86	2.98	9.922	1.033	0.334	4.712
Cs2WBr6	1.88	0.66	1.96	0.77	1.79	2.83	10.733	1.036	0.336	4.690
Cs2PdI6	1.88	0.615	2.2	0.77	2.08	2.76	11.332	1.039	0.295	5.117
K2MnCl6	1.64	0.53	1.81	0.8	2.04	2.98	9.6445	1.042	0.292	5.154
Cs2SnCl6	1.88	0.69	1.81	0.77	1.88	2.98	10.3552	1.043	0.381	4.341
Cs2TaCl6	1.88	0.68	1.81	0.77	1.94	2.98	10.271	1.047	0.375	4.380
Cs2PtBr6	1.88	0.625	1.96	0.77	1.91	2.83	10.67	1.050	0.318	4.867
Cs2PdBr6	1.88	0.62	1.96	0.77	2.08	2.83	10.621	1.052	0.316	4.894
Cs2WCl6	1.88	0.66	1.81	0.77	1.79	2.98	10.245	1.056	0.364	4.463
Cs2MoCl6	1.88	0.65	1.81	0.77	1.94	2.98	10.2121	1.060	0.359	4.507
Rb2MnCl6	1.72	0.53	1.81	0.8	2.04	2.98	9.838	1.066	0.292	5.171
Cs2ReCl6	1.88	0.63	1.81	0.77	2.06	2.98	10.255	1.069	0.348	4.602
Cs2IrCl6	1.88	0.625	1.81	0.77	1.87	2.98	10.2119	1.071	0.345	4.627
Cs2PtCl6	1.88	0.625	1.81	0.77	1.91	2.98	10.192	1.071	0.345	4.627
Cs2TiCl6	1.88	0.605	1.81	0.77	1.86	2.98	10.219	1.080	0.334	4.732
Rb2SeCl6	1.72	0.5	1.81	0.8	2.54	2.98	9.978	1.080	0.276	5.404
Rb2PdF6	1.72	0.615	1.33	0.8	2.08	3.78	8.57	1.108	0.462	3.881
Cs2GeCl6	1.88	0.53	1.81	0.77	1.99	2.98	10.23	1.115	0.292	5.216
K2MnF6	1.64	0.53	1.33	0.8	2.04	3.78	8.221	1.129	0.398	4.248

Cs2SeCl6	1.88	0.5	1.81	0.77	2.54	2.98	10.26	1.129	0.276	5.458
Rb2CrF6	1.72	0.55	1.33	0.8	2	3.78	8.523	1.147	0.413	4.161
Rb2CoF6	1.72	0.53	1.33	0.8	1.72	3.78	8.4628	1.159	0.398	4.266
Rb2MnF6	1.72	0.53	1.33	0.8	2.04	3.78	8.531	1.159	0.398	4.266
Rb2GeF6	1.72	0.53	1.33	0.8	1.99	3.78	8.5825	1.159	0.398	4.266
K2NiF6	1.64	0.48	1.33	0.8	1.76	3.78	8.109	1.160	0.360	4.551
Cs2PtF6	1.88	0.625	1.33	0.77	1.91	3.78	9.05	1.161	0.469	3.859
Cs2PdF6	1.88	0.615	1.33	0.77	2.08	3.78	9.00	1.166	0.462	3.898
Rb2NiF6	1.72	0.48	1.33	0.8	1.76	3.78	8.462	1.191	0.360	4.578
Cs2CrF6	1.88	0.55	1.33	0.77	2	3.78	9.022	1.207	0.413	4.199
K2SiF6	1.64	0.4	1.33	0.8	1.98	3.78	8.1419	1.213	0.300	5.230
Cs2CoF6	1.88	0.53	1.33	0.77	1.72	3.78	8.914	1.220	0.398	4.310
Cs2GeF6	1.88	0.53	1.33	0.77	1.99	3.78	8.99	1.220	0.398	4.310
Cs2MnF6	1.88	0.53	1.33	0.77	2.04	3.78	8.972	1.220	0.398	4.310
Rb2SiF6	1.72	0.4	1.33	0.8	1.98	3.78	8.446	1.246	0.300	5.273
Cs2NiF6	1.88	0.48	1.33	0.77	1.76	3.78	8.938	1.254	0.360	4.639
Cs2SiF6	1.88	0.4	1.33	0.77	1.98	3.78	8.89	1.312	0.300	5.362

Table 5.18: The training dataset for double halide perovskites

compounds	a_0(Å)	$predicted"a"$(Å)	Δa(Å)	Other [117]	Other [118]	Other [119]	Other [120]	Other [121]
Cs2GeF6	8.990	8.855	0.135	8.855	8.885	8.983	-	8.976
Cs2MnF6	8.972	8.855	0.117	8.890	8.885	8.983	8.953	8.926
Cs2NiF6	8.938	8.815	0.123	8.814	8.849	8.941	8.925	-
Cs2PdF6	9.000	8.924	0.076	8.924	8.945	9.028	-	9.076
Cs2PtF6	9.050	8.932	0.118	8.934	8.952	9.030	-	-
Cs2SiF6	8.890	8.751	0.139	8.736	8.792	8.911	-	-
Rb2CrF6	8.523	8.530	-0.007	8.587	8.506	8.520	8.523	-
Rb2MnF6	8.531	8.514	0.017	8.576	8.492	8.496	8.531	8.511
Rb2NiF6	8.462	8.474	-0.012	8.500	8.457	8.442	8.463	-
Rb2PdF6	8.570	8.582	-0.012	8.610	8.553	8.587	-	8.675
Rb2GeF6	8.583	8.514	0.069	8.541	8.492	8.496	-	-
Rb2SiF6	8.446	8.410	0.036	8.422	8.400	8.185	8.446	-
K2MnF6	8.221	8.343	-0.122	8.419	8.296	8.253	8.198	8.318
K2NiF6	8.109	8.303	-0.194	8.343	8.260	8.193	-	-
K2SiF6	8.142	8.239	-0.097	8.265	8.204	8.185	-	8.210
Cs2GeCl6	10.230	10.265	-0.035	10.206	10.291	10.210	-	10.119
Cs2IrCl6	10.212	10.342	-0.130	10.285	10.358	10.206	-	10.193
Cs2MoCl6	10.212	10.362	-0.150	10.313	10.376	10.249	-	10.211
Cs2PbCl6	10.416	10.462	-0.046	10.463	10.465	10.469	-	-
Cs2PtCl6	10.192	10.342	-0.150	10.285	10.358	10.206	10.179	-
Cs2ReCl6	10.255	10.346	-0.091	10.313	10.362	10.214	-	10.218
Cs2SeCl6	10.260	10.241	0.019	10.136	10.270	10.271	10.228	10.207
Cs2SnCl6	10.355	10.394	-0.039	10.367	10.405	10.332	-	-
Cs2TaCl6	10.271	10.386	-0.115	10.392	10.397	10.311	-	10.322
Cs2TeCl6	10.445	10.618	-0.173	10.631	10.603	10.430	10.497	-
Cs2TiCl6	10.219	10.326	-0.107	10.320	10.344	10.187	10.199	-
Cs2WCl6	10.245	10.370	-0.125	10.357	10.383	10.269	-	-

Cs2ZrCl6	10.428	10.418	0.010	10.444	10.426	10.391	10.408	-
Rb2MnCl6	9.838	9.924	-0.086	9.927	9.898	9.876	9.745	9.789
Rb2PbCl6	10.195	10.120	0.075	10.148	10.072	10.249	10.184	-
Rb2PdCl6	9.990	9.992	-0.002	9.961	9.959	9.887	-	-
Rb2PtCl6	9.884	10.000	-0.116	9.971	9.966	9.907	9.877	-
Rb2SeCl6	9.978	9.900	0.078	9.822	9.877	9.939	9.993	-
Rb2SnCl6	10.137	10.052	0.085	10.053	10.012	10.077	10.074	-
Rb2TeCl6	10.233	10.277	-0.044	10.317	10.211	10.240	-	-
Rb2TiCl6	9.922	9.984	-0.062	10.006	9.952	9.878	9.895	-
Rb2WCl6	9.957	10.028	-0.071	10.043	9.991	9.994	-	-
Rb2ZrCl6	10.178	10.076	0.102	10.130	10.033	10.152	10.202	-
K2MnCl6	9.645	9.753	-0.109	9.770	9.702	9.726	-	-
K2MoCl6	9.729	9.833	-0.104	9.841	9.787	9.841	-	-
K2OsCl6	9.850	9.849	0.001	9.819	9.773	9.787	9.785	-
K2PdCl6	9.710	9.821	-0.112	9.804	9.763	9.753	-	-
K2PtCl6	9.751	9.829	-0.078	9.814	9.770	9.775	-	-
K2ReCl6	9.840	9.833	0.007	9.842	9.773	9.787	9.846	9.791
K2RuCl6	9.737	9.825	-0.088	9.809	9.766	9.763	-	-
K2SnCl6	9.988	9.881	0.106	9.896	9.816	9.961	9.987	-
K2TaCl6	9.994	9.873	0.120	9.921	9.809	9.931	9.982	9.920
K2TcCl6	9.830	9.845	-0.015	9.841	9.784	9.827	9.822	-
K2TiCl6	9.792	9.813	-0.021	9.849	9.755	9.743	9.808	-
K2WCl6	9.822	9.857	-0.035	9.886	9.794	9.871	9.916	-
Cs2PtBr6	10.670	10.782	-0.112	10.712	10.798	10.625	-	-
Cs2SnBr6	10.770	10.834	-0.064	10.794	10.844	10.792	10.785	-
Cs2TeBr6	10.920	11.059	-0.139	10.058	11.043	10.938	10.874	-
Cs2WBr6	10.733	10.810	-0.077	10.784	10.823	10.707	10.719	10.757
Rb2SnBr6	10.580	10.493	0.087	10.479	10.452	10.574	10.551	10.519
Rb2TeBr6	10.769	10.718	0.051	10.743	10.650	10.766	10.719	-
Rb2WBr6	10.489	10.469	0.020	10.470	10.430	-	-	-
K2OsBr6	10.300	10.274	0.026	10.245	10.213	10.283	10.293	10.302
K2PtBr6	10.293	10.270	0.023	10.240	10.209	10.270	10.290	-
K2ReBr6	10.385	10.274	0.111	10.268	10.213	10.283	10.394	-
K2SeBr6	10.384	10.250	0.134	10.091	10.120	10.327	10.367	-
K2SnBr6	10.480	10.322	0.158	10.322	-	-	10.536	-
Cs2HfI6	11.609	11.555	0.054	11.547	11.561	11.638	-	-
Cs2PdI6	11.332	11.127	0.205	11.386	11.494	11.363	-	-
Cs2PtI6	11.367	11.487	-0.120	11.395	11.501	11.382	-	-
Cs2SnI6	11.650	11.539	0.111	11.477	11.547	11.573	-	-
Cs2TeI6	11.700	11.764	-0.064	11.741	11.746	11.707	-	11.665
Rb2PdI6	11.185	11.138	0.047	11.071	11.101	11.184	11.269	-
Rb2PtI6	11.217	11.146	0.071	11.081	11.108	11.205	-	-
Rb2SnI6	11.620	11.214	0.406	11.163	-	-	11.589	-
Cs2NpBr6	11.082	10.979	0.103	11.020	10.972	11.062	-	-
Cs2PoBr6	10.990	11.035	-0.045	11.036	11.022	10.993	-	-
Cs2UBr6	11.070	10.995	0.075	11.009	10.986	11.053	11.075	-
Cs2PoI6	11.790	11.740	0.050	11.720	11.725	11.782	-	11.734

Table 5.19: The predicted lattice parameters along with those other authors

compounds	t	μ	τ	$t\&\tau$
Cs2CoF6	1.220	0.398	4.310	P
Cs2CrF6	1.207	0.413	4.199	P
Cs2GeCl6	1.115	0.292	5.216	NP

Cs2GeF6	1.220	0.398	4.310	P
Cs2HfI6	0.991	0.322	4.817	P
Cs2IrCl6	1.071	0.345	4.627	P
Cs2MnF6	1.220	0.398	4.310	P
Cs2MoCl6	1.060	0.359	4.507	P
Cs2NiF6	1.254	0.360	4.639	P
Cs2NpBr6	0.959	0.443	4.057	P
Cs2PbCl6	1.009	0.428	4.072	P
Cs2PdBr6	1.052	0.316	4.894	NP
Cs2PdF6	1.166	0.462	3.898	P
Cs2PdI6	1.039	0.295	5.117	P
Cs2PoBr6	0.936	0.479	3.970	P
Cs2PoI6	0.918	0.427	4.225	P
Cs2PtBr6	1.050	0.318	4.867	P
Cs2PtCl6	1.071	0.345	4.627	P
Cs2PtF6	1.161	0.469	3.859	P
Cs2PtI6	1.021	0.284	5.251	P
Cs2ReCl6	1.069	0.348	4.602	P
Cs2SeCl6	1.129	0.276	5.458	NP
Cs2SiF6	1.312	0.300	5.362	P
Cs2SnBr6	1.024	0.352	4.558	P
Cs2SnCl6	1.043	0.381	4.341	P
Cs2SnI6	0.998	0.313	4.906	P
Cs2TaCl6	1.047	0.375	4.380	P
Cs2TeBr6	0.926	0.494	3.949	P
Cs2TeCl6	0.938	0.535	3.794	P
Cs2TeI6	0.910	0.440	4.196	P
Cs2TiCl6	1.080	0.334	4.732	P
Cs2UBr6	0.952	0.454	4.026	P
Cs2WBr6	1.036	0.336	4.690	P
Cs2WCl6	1.056	0.364	4.463	P
Cs2ZrCl6	1.031	0.397	4.234	P
K2MnCl6	1.042	0.292	5.154	P
K2MnF6	1.129	0.398	4.248	P
K2MoCl6	0.999	0.348	4.593	P
K2NiF6	1.160	0.360	4.551	P
K2OsBr6	0.982	0.321	4.832	P
K2OsCl6	0.991	0.359	4.510	P
K2PdCl6	1.005	0.339	4.661	P
K2PtBr6	0.984	0.318	4.856	P

K2PtCl6	1.001	0.345	4.616	P
K2ReBr6	0.982	0.321	4.832	P
K2ReCl6	0.999	0.348	4.593	P
K2RuCl6	1.003	0.342	4.638	P
K2SeBr6	0.994	0.306	4.984	P
K2SiF6	1.213	0.300	5.230	P
K2SnBr6	0.960	0.352	4.585	P
K2SnCl6	0.975	0.381	4.368	P
K2TaCl6	0.979	0.375	4.401	P
K2TcCl6	0.993	0.356	4.530	P
K2TiCl6	1.010	0.334	4.710	P
K2WCl6	0.987	0.364	4.472	P
Rb2CoF6	1.159	0.398	4.266	P
Rb2CrF6	1.147	0.413	4.161	P
Rb2MnCl6	1.066	0.292	5.171	P
Rb2MnF6	1.159	0.398	4.266	P
Rb2NiF6	1.191	0.360	4.578	P
Rb2PbCl6	0.965	0.428	4.119	P
Rb2PdCl6	1.029	0.339	4.662	P
Rb2PdF6	1.108	0.462	3.881	P
Rb2PdI6	0.984	0.279	5.296	P
Rb2PtCl6	1.025	0.345	4.614	P
Rb2PtI6	0.981	0.284	5.238	P
Rb2SeCl6	1.080	0.276	5.404	P
Rb2SiF6	1.246	0.300	5.273	P
Rb2SnBr6	0.981	0.352	4.569	P
Rb2SnCl6	0.998	0.381	4.352	P
Rb2SnI6	0.952	0.322	4.836	P
Rb2TeBr6	0.888	0.494	4.116	P
Rb2TeCl6	0.897	0.535	3.961	P
Rb2TiCl6	1.033	0.334	4.712	P
Rb2WBr6	0.993	0.336	4.690	P
Rb2WCl6	1.010	0.364	4.463	P
Rb2ZrCl6	0.986	0.397	4.257	P
Rb2GeF6	1.159	0.398	4.266	P
Cs2CeCl6	0.973	0.480	3.884	P
Cs2HfF6	1.112	0.533	3.592	P
Cs2IrF6	1.161	0.469	3.859	P
Cs2SnF6	1.123	0.518	3.645	P
Cs2ThCl6	0.948	0.519	3.810	P

Cs2UCl6	0.966	0.491	3.858	P
Cs2VF6	1.188	0.436	4.049	P
Cs2ZrF6	1.107	0.541	3.567	P
K2GeF6	1.129	0.398	4.248	P
K2HfF6	1.029	0.533	3.632	P
K2IrF6	1.074	0.469	3.848	P
K2PdF6	1.079	0.462	3.881	P
K2PtI6	0.961	0.284	5.240	P
K2PuCl6	0.913	0.475	4.058	P
K2ReF6	1.071	0.473	3.832	P
K2ReI6	0.959	0.286	5.212	P
K2RhF6	1.088	0.451	3.934	P
K2SnI6	0.939	0.313	4.933	P
K2TcI6	0.954	0.293	5.135	P
K2TeBr6	0.956	0.357	4.551	P
K2TeI6	0.936	0.318	4.894	P
K2ThF6	0.925	0.706	3.549	P
K2TiF6	1.085	0.454	3.916	P
K2UF6	0.945	0.669	3.509	P
K2ZrF6	1.024	0.541	3.614	P
Na2GeF6	1.034	0.398	4.229	P
Na2IrCl6	0.929	0.345	4.678	P
Na2SiF6	1.111	0.300	5.114	P
Na2SnCl6	0.905	0.381	4.499	P
Na2SnF6	0.952	0.518	3.803	P
Na2TiF6	0.993	0.454	3.960	P
Na2UF6	0.866	0.669	3.997	P
Na2ZrF6	0.938	0.541	3.782	P
Rb2HfF6	1.057	0.533	3.611	P
Rb2IrF6	1.103	0.469	3.846	P
Rb2PtF6	1.103	0.469	3.846	P
Rb2PuCl6	0.934	0.475	3.990	P
Rb2RhF6	1.117	0.451	3.938	P
Rb2TeI6	0.955	0.318	4.876	P
Rb2UBr6	0.913	0.454	4.135	P
Rb2ZrF6	1.052	0.541	3.590	P

Table 5.20: The calculated tolerance "t" and modified tolerance "τ" factor along with $t\&\tau$ for the double halide perovskites of table5.18

compounds	ΔH	$predicted\Delta H$	$\Delta H + predicted\Delta H$
Rb2PdCl6	-10.580	-10.623	0.043
Cs2PtCl6	-11.410	-11.363	-0.047
Rb2SnBr6	-11.080	-10.720	-0.360
Rb2PdBr6	-8.900	-9.079	0.179
Cs2PtBr6	-9.630	-9.819	0.189
Rb2SnI6	-7.890	-8.250	0.360
Rb2PdI6	-6.830	-6.609	-0.221
Cs2PtI6	-7.490	-7.349	-0.141

Table 5.21: The training dataset and the predicted of the formation energies "ΔH" of double halide perovskites

compounds	ΔH	$(t+\mu)^{\eta}$
K2ThF6	-22.414	1.077
K2UF6	-21.320	1.076
Na2UF6	-20.506	1.070
Cs2TeCl6	-18.912	1.073
Rb2TeCl6	-18.391	1.067
Cs2ZrF6	-18.382	1.082
Cs2ThCl6	-18.256	1.069
Cs2HfF6	-18.163	1.082
Rb2ZrF6	-17.860	1.076
Cs2SnF6	-17.725	1.082
Rb2HfF6	-17.642	1.076
K2ZrF6	-17.600	1.073
K2HfF6	-17.381	1.073
Cs2TeBr6	-17.368	1.069
Cs2UCl6	-17.161	1.068
Rb2TeBr6	-16.847	1.063
Na2ZrF6	-16.786	1.066
Cs2CeCl6	-16.724	1.068
Cs2PoBr6	-16.712	1.067
K2TeBr6	-16.587	1.062
Cs2IrF6	-16.303	1.082
Cs2PtF6	-16.303	1.079
Na2SnF6	-16.129	1.066
Cs2PdF6	-16.084	1.080
Rb2PuCl6	-15.984	1.065

Rb2IrF6	-15.781	1.076
Rb2PtF6	-15.781	1.076
K2PuCl6	-15.723	1.063
K2ReF6	-15.630	1.073
Cs2UBr6	-15.618	1.064
Rb2PdF6	-15.563	1.076
K2IrF6	-15.521	1.073
Cs2VF6	-15.318	1.082
K2PdF6	-15.302	1.073
Rb2RhF6	-15.234	1.076
Cs2NpBr6	-15.180	1.063
Rb2UBr6	-15.096	1.062
K2TiF6	-15.083	1.073
K2RhF6	-14.974	1.073
Cs2TeI6	-14.898	1.063
Cs2CrF6	-14.661	1.078
Cs2PbCl6	-14.645	1.068
Rb2TeI6	-14.377	1.059
Na2TiF6	-14.269	1.064
Cs2PoI6	-14.242	1.061
Cs2CoF6	-14.224	1.081
Cs2MnF6	-14.224	1.079
Cs2GeF6	-14.224	1.079
Rb2CrF6	-14.140	1.076
Rb2PbCl6	-14.124	1.062
K2TeI6	-14.116	1.057
Rb2CoF6	-13.702	1.077
Rb2MnF6	-13.702	1.075
Rb2GeF6	-13.702	1.074
K2MnF6	-13.442	1.076
K2GeF6	-13.442	1.073
Cs2ZrCl6	-13.441	1.067
Cs2NiF6	-13.129	1.080
Rb2ZrCl6	-12.920	1.061
Cs2SnCl6	-12.785	1.067
Na2GeF6	-12.627	1.064
Rb2NiF6	-12.608	1.076
Cs2TaCl6	-12.566	1.069
K2NiF6	-12.348	1.078
Rb2SnCl6	-12.263	1.061

Cs2WCl6	-12.128	1.069
K2SnCl6	-12.003	1.059
Cs2MoCl6	-11.909	1.070
K2TaCl6	-11.784	1.058
Rb2WCl6	-11.607	1.064
Cs2ReCl6	-11.472	1.068
Cs2SiF6	-11.379	1.081
Cs2PtCl6	-11.362	1.070
Cs2IrCl6	-11.362	1.069
K2WCl6	-11.346	1.061
Cs2SnBr6	-11.241	1.065
Na2SnCl6	-11.189	1.054
K2OsCl6	-11.128	1.060
K2TcCl6	-11.018	1.060
Cs2TiCl6	-10.924	1.069
Rb2SiF6	-10.857	1.076
Rb2PtCl6	-10.841	1.064
Rb2SnBr6	-10.720	1.058
K2MoCl6	-10.690	1.062
K2ReCl6	-10.690	1.060
Rb2PdCl6	-10.622	1.062
K2SiF6	-10.597	1.076
Cs2WBr6	-10.584	1.065
K2PtCl6	-10.580	1.061
K2RuCl6	-10.471	1.062
K2SnBr6	-10.459	1.055
Rb2TiCl6	-10.403	1.063
K2PdCl6	-10.362	1.062
K2TiCl6	-10.143	1.060
Rb2WBr6	-10.063	1.059
Cs2PtBr6	-9.818	1.065
Na2SiF6	-9.783	1.063
Na2IrCl6	-9.766	1.053
Cs2PdBr6	-9.709	1.066
Cs2GeCl6	-9.283	1.067
Cs2HfI6	-9.208	1.058
K2OsBr6	-9.146	1.056
K2ReBr6	-9.146	1.055
K2PtBr6	-9.037	1.056
Cs2SnI6	-8.771	1.057

Rb2MnCl6	-8.762	1.063
Rb2SnI6	-8.687	1.049
Cs2SeCl6	-8.627	1.066
K2MnCl6	-8.501	1.061
K2SeBr6	-8.489	1.054
Cs2PdI6	-8.364	1.057
Rb2SeCl6	-8.105	1.060
K2SnI6	-7.989	1.052
Cs2PtI6	-7.348	1.060
K2TcI6	-7.004	1.052
Rb2PtI6	-6.827	1.053
K2ReI6	-6.676	1.052
Rb2PdI6	-6.608	1.053
K2PtI6	-6.566	1.051

Table 5.22: The predicted formation energies "ΔH" of the 119 double halide perovskites of table5.18.

compounds	a(Å)	ΔH	t	μ	$(t+\mu)^{\eta}$	τ	$t\&\tau$
Na2TeI6	10.718	-13.303	0.801	0.441	1.053	5.251	NP
Na2PoI6	10.694	-12.646	0.808	0.427	1.052	5.121	NP
Na2ThI6	10.694	-12.646	0.808	0.427	1.052	5.121	NP
Na2TeBr6	10.013	-15.773	0.808	0.495	1.059	5.004	NP
Na2TeCl6	9.572	-17.317	0.814	0.536	1.062	4.849	NP
Na2PoBr6	9.989	-15.116	0.817	0.480	1.058	4.865	NP
Na2ThBr6	9.989	-15.116	0.817	0.480	1.058	4.865	NP
Na2PaI6	10.662	-11.771	0.819	0.409	1.051	4.998	NP
Na2UI6	10.654	-11.552	0.822	0.405	1.051	4.975	NP
Na2PoCl6	9.548	-16.660	0.823	0.519	1.061	4.706	NP
Na2ThCl6	9.548	-16.660	0.823	0.519	1.061	4.706	NP
Na2CeI6	10.638	-11.114	0.827	0.395	1.050	4.939	NP
Na2NpI6	10.638	-11.114	0.827	0.395	1.050	4.939	NP
Na2PaBr6	9.957	-14.241	0.828	0.459	1.056	4.731	NP
Na2PuI6	10.630	-10.895	0.830	0.391	1.050	4.924	NP
Na2UBr6	9.949	-14.022	0.831	0.454	1.056	4.705	NP
Na2AmI6	10.622	-10.677	0.832	0.386	1.049	4.913	NP
Na2CmI6	10.622	-10.677	0.832	0.386	1.049	4.913	NP
Na2PrI6	10.622	-10.677	0.832	0.386	1.049	4.913	NP
Na2PaCl6	9.516	-15.785	0.835	0.497	1.060	4.564	NP
Na2TeF6	8.163	-22.257	0.836	0.729	1.073	4.354	NP

Na2CeBr6	9.933	-13.584	0.837	0.444	1.056	4.663	NP
Na2NpBr6	9.933	-13.584	0.837	0.444	1.056	4.663	NP
Na2BkI6	10.606	-10.239	0.838	0.377	1.049	4.898	NP
Na2UCl6	9.508	-15.566	0.838	0.492	1.060	4.537	NP
Na2PuBr6	9.925	-13.366	0.840	0.439	1.055	4.645	NP
Na2CfI6	10.598	-10.042	0.840	0.373	1.049	4.895	NP
Na2AmBr6	9.917	-13.147	0.843	0.434	1.055	4.631	NP
Na2CmBr6	9.917	-13.147	0.843	0.434	1.055	4.631	NP
Na2PrBr6	9.917	-13.147	0.843	0.434	1.055	4.631	NP
Na2CeCl6	9.492	-15.128	0.844	0.481	1.059	4.490	NP
Na2NpCl6	9.492	-15.128	0.844	0.481	1.059	4.490	NP
Na2PoF6	8.138	-21.601	0.847	0.707	1.072	4.195	NP
Na2ThF6	8.138	-21.601	0.847	0.707	1.072	4.195	NP
Na2PuCl6	9.484	-14.909	0.847	0.475	1.059	4.471	NP
Na2BkBr6	9.901	-12.709	0.849	0.423	1.055	4.609	NP
Na2AmCl6	9.476	-14.691	0.851	0.470	1.058	4.454	P
Na2CmCl6	9.476	-14.691	0.851	0.470	1.058	4.454	P
Na2PrCl6	9.476	-14.691	0.851	0.470	1.058	4.454	P
Na2CfBr6	9.893	-12.512	0.852	0.419	1.054	4.603	P
Na2PbI6	10.562	-9.035	0.853	0.352	1.047	4.909	P
K2TeI6	11.252	-14.117	0.857	0.441	1.058	4.488	P
Na2BkCl6	9.460	-14.253	0.857	0.459	1.058	4.429	P
Na2TbI6	10.549	-8.707	0.858	0.345	1.047	4.924	P
Na2CfCl6	9.453	-14.056	0.860	0.454	1.058	4.420	P
Na2PaF6	8.106	-20.725	0.862	0.677	1.071	4.031	P
K2PoI6	11.228	-13.460	0.865	0.427	1.057	4.475	P
K2ThI6	11.228	-13.460	0.865	0.427	1.057	4.475	P
Na2PbBr6	9.857	-11.505	0.866	0.395	1.053	4.599	P
Na2UF6	8.098	-20.506	0.866	0.669	1.071	3.997	P
K2TeBr6	10.547	-16.587	0.869	0.495	1.063	4.240	P
Na2ZrI6	10.517	-7.832	0.869	0.327	1.046	4.990	P
Na2TbBr6	9.845	-11.177	0.871	0.388	1.053	4.608	P
Na2HfI6	10.509	-7.613	0.872	0.323	1.046	5.013	P
Na2CeF6	8.082	-20.069	0.874	0.654	1.070	3.939	P
Na2NpF6	8.082	-20.069	0.874	0.654	1.070	3.939	P
Rb2TeI6	11.422	-14.378	0.874	0.441	1.059	4.364	P
Na2PbCl6	9.416	-13.049	0.875	0.428	1.057	4.406	P
K2PaI6	11.196	-12.585	0.876	0.409	1.056	4.481	P
K2TeCl6	10.106	-18.131	0.878	0.536	1.066	4.085	P
K2PoBr6	10.523	-15.931	0.878	0.480	1.062	4.220	P

K2ThBr6	10.523	-15.931	0.878	0.480	1.062	4.220	P
Na2PuF6	8.074	-19.850	0.878	0.647	1.070	3.913	P
Na2SnI6	10.493	-7.175	0.878	0.314	1.045	5.065	P
K2UI6	11.188	-12.366	0.879	0.405	1.056	4.487	P
Na2TbCl6	9.404	-12.721	0.880	0.420	1.056	4.411	P
Na2NbI6	10.485	-6.956	0.881	0.309	1.045	5.094	P
Na2TaI6	10.485	-6.956	0.881	0.309	1.045	5.094	P
Na2AmF6	8.066	-19.631	0.882	0.639	1.070	3.890	P
Na2CmF6	8.066	-19.631	0.882	0.639	1.070	3.890	P
Na2PrF6	8.066	-19.631	0.882	0.639	1.070	3.890	P
Rb2PoI6	11.398	-13.721	0.883	0.427	1.059	4.369	P
Rb2ThI6	11.398	-13.721	0.883	0.427	1.059	4.369	P
Na2ZrBr6	9.812	-10.302	0.884	0.367	1.052	4.657	P
K2CeI6	11.171	-11.929	0.884	0.395	1.056	4.502	P
K2NpI6	11.171	-11.929	0.884	0.395	1.056	4.502	P
K2PoCl6	10.082	-17.474	0.887	0.519	1.065	4.060	P
K2ThCl6	10.082	-17.474	0.887	0.519	1.065	4.060	P
Na2HfBr6	9.804	-10.083	0.887	0.362	1.052	4.675	P
K2PuI6	11.163	-11.710	0.887	0.391	1.056	4.512	P
Na2WI6	10.469	-6.518	0.888	0.300	1.045	5.161	P
Rb2TeBr6	10.718	-16.848	0.888	0.495	1.064	4.116	P
K2PaBr6	10.491	-15.055	0.890	0.459	1.061	4.215	P
K2AmI6	11.155	-11.491	0.890	0.386	1.055	4.524	P
K2CmI6	11.155	-11.491	0.890	0.386	1.055	4.524	P
K2PrI6	11.155	-11.491	0.890	0.386	1.055	4.524	P
Na2BkF6	8.050	-19.193	0.890	0.624	1.069	3.850	P
Na2MoI6	10.461	-6.300	0.891	0.295	1.044	5.198	P
Na2TcI6	10.457	-6.190	0.892	0.293	1.044	5.218	P
K2UBr6	10.483	-14.836	0.893	0.454	1.061	4.217	P
Na2SnBr6	9.788	-9.645	0.894	0.352	1.051	4.717	P
Rb2PaI6	11.366	-12.846	0.894	0.409	1.058	4.395	P
Na2CfF6	8.043	-18.996	0.894	0.617	1.069	3.835	P
Na2ZrCl6	9.372	-11.846	0.894	0.398	1.055	4.449	P
K2BkI6	11.139	-11.053	0.896	0.377	1.055	4.552	P
Na2OsI6	10.445	-5.862	0.897	0.286	1.044	5.280	P
Na2ReI6	10.445	-5.862	0.897	0.286	1.044	5.280	P
Rb2UI6	11.358	-12.627	0.897	0.405	1.058	4.405	P
Na2NbBr6	9.780	-9.426	0.897	0.347	1.051	4.741	P
Na2TaBr6	9.780	-9.426	0.897	0.347	1.051	4.741	P
Rb2PoBr6	10.693	-16.191	0.897	0.480	1.063	4.114	P

Rb2ThBr6	10.693	-16.191	0.897	0.480	1.063	4.114	P
Rb2TeCl6	10.277	-18.392	0.898	0.536	1.067	3.962	P
Na2HfCl6	9.364	-11.627	0.898	0.392	1.055	4.464	P
Na2IrI6	10.441	-5.753	0.899	0.284	1.044	5.302	P
Na2PtI6	10.441	-5.753	0.899	0.284	1.044	5.302	P
K2CfI6	11.132	-10.856	0.899	0.373	1.055	4.567	P
K2CeBr6	10.466	-14.399	0.899	0.444	1.061	4.226	P
K2NpBr6	10.466	-14.399	0.899	0.444	1.061	4.226	P
Na2RuI6	10.437	-5.643	0.900	0.282	1.044	5.325	P
K2PaCl6	10.050	-16.599	0.900	0.497	1.064	4.048	P
Na2PdI6	10.433	-5.534	0.902	0.280	1.044	5.349	P
K2PuBr6	10.458	-14.180	0.903	0.439	1.060	4.233	P
Rb2CeI6	11.342	-12.189	0.903	0.395	1.058	4.429	P
Rb2NpI6	11.342	-12.189	0.903	0.395	1.058	4.429	P
K2UCl6	10.042	-16.380	0.904	0.492	1.064	4.048	P
Na2WBr6	9.764	-8.989	0.904	0.337	1.051	4.797	P
Na2TiI6	10.425	-5.315	0.905	0.275	1.043	5.398	P
Na2SnCl6	9.348	-11.189	0.905	0.381	1.055	4.500	P
Rb2PuI6	11.334	-11.970	0.906	0.391	1.057	4.444	P
K2AmBr6	10.450	-13.961	0.906	0.434	1.060	4.242	P
K2CmBr6	10.450	-13.961	0.906	0.434	1.060	4.242	P
K2PrBr6	10.450	-13.961	0.906	0.434	1.060	4.242	P
Na2RhI6	10.421	-5.205	0.907	0.273	1.043	5.424	P
Na2MoBr6	9.756	-8.770	0.908	0.332	1.050	4.829	P
Rb2PoCl6	10.253	-17.735	0.908	0.519	1.066	3.954	P
Rb2ThCl6	10.253	-17.735	0.908	0.519	1.066	3.954	P
Na2NbCl6	9.340	-10.970	0.909	0.376	1.055	4.521	P
Na2TaCl6	9.340	-10.970	0.909	0.376	1.055	4.521	P
Rb2AmI6	11.326	-11.751	0.909	0.386	1.057	4.459	P
Rb2CmI6	11.326	-11.751	0.909	0.386	1.057	4.459	P
Rb2PrI6	11.326	-11.751	0.909	0.386	1.057	4.459	P
Na2TcBr6	9.752	-8.660	0.909	0.329	1.050	4.845	P
Rb2PaBr6	10.661	-15.316	0.910	0.459	1.063	4.128	P
Cs2TeI6	11.764	-14.899	0.910	0.441	1.062	4.197	P
K2CeCl6	10.026	-15.943	0.910	0.481	1.064	4.054	P
K2NpCl6	10.026	-15.943	0.910	0.481	1.064	4.054	P
Na2FeI6	10.409	-4.877	0.911	0.266	1.043	5.506	P
K2BkBr6	10.434	-13.523	0.912	0.423	1.060	4.263	P
K2PbI6	11.095	-9.849	0.913	0.352	1.054	4.662	P
Rb2UBr6	10.653	-15.097	0.913	0.454	1.063	4.135	P

K2TeF6	8.696	-23.071	0.913	0.729	1.078	3.591	P
Na2VI6	10.405	-4.768	0.913	0.264	1.043	5.535	P
K2PuCl6	10.018	-15.724	0.914	0.475	1.064	4.059	P
Na2PbF6	8.006	-17.990	0.914	0.583	1.068	3.786	P
Na2OsBr6	9.740	-8.332	0.915	0.321	1.050	4.899	P
Na2ReBr6	9.740	-8.332	0.915	0.321	1.050	4.899	P
Rb2BkI6	11.310	-11.314	0.915	0.377	1.057	4.495	P
K2CfBr6	10.427	-13.326	0.915	0.419	1.060	4.274	P
Na2WCl6	9.324	-10.533	0.916	0.365	1.054	4.570	P
Na2IrBr6	9.736	-8.223	0.916	0.319	1.050	4.918	P
Na2PtBr6	9.736	-8.223	0.916	0.319	1.050	4.918	P
K2AmCl6	10.010	-15.505	0.917	0.470	1.063	4.065	P
K2CmCl6	10.010	-15.505	0.917	0.470	1.063	4.065	P
K2PrCl6	10.010	-15.505	0.917	0.470	1.063	4.065	P
K2TbI6	11.083	-9.521	0.917	0.345	1.054	4.700	P
Rb2CfI6	11.303	-11.117	0.918	0.373	1.057	4.512	P
Na2RuBr6	9.732	-8.113	0.918	0.316	1.050	4.938	P
Cs2PoI6	11.740	-14.242	0.919	0.427	1.062	4.226	P
Cs2ThI6	11.740	-14.242	0.919	0.427	1.062	4.226	P
Rb2CeBr6	10.637	-14.659	0.919	0.444	1.062	4.153	P
Rb2NpBr6	10.637	-14.659	0.919	0.444	1.062	4.153	P
Na2MoCl6	9.316	-10.314	0.920	0.359	1.054	4.598	P
Na2PdBr6	9.728	-8.004	0.920	0.314	1.050	4.959	P
Na2TbF6	7.994	-17.661	0.920	0.571	1.067	3.779	P
Rb2PaCl6	10.221	-16.860	0.921	0.497	1.066	3.962	P
Na2TcCl6	9.312	-10.204	0.922	0.356	1.054	4.613	P
Rb2PuBr6	10.629	-14.440	0.923	0.439	1.062	4.164	P
Na2CrI6	10.381	-4.111	0.923	0.250	1.042	5.726	P
Na2TiBr6	9.720	-7.785	0.924	0.309	1.050	5.002	P
K2BkCl6	9.994	-15.067	0.924	0.459	1.063	4.082	P
Rb2UCl6	10.213	-16.641	0.924	0.492	1.066	3.967	P
K2PoF6	8.672	-22.415	0.925	0.707	1.078	3.550	P
K2ThF6	8.672	-22.415	0.925	0.707	1.078	3.550	P
Na2RhBr6	9.716	-7.676	0.925	0.306	1.049	5.024	P
Rb2AmBr6	10.621	-14.222	0.926	0.434	1.062	4.177	P
Rb2CmBr6	10.621	-14.222	0.926	0.434	1.062	4.177	P
Rb2PrBr6	10.621	-14.222	0.926	0.434	1.062	4.177	P
Cs2TeBr6	11.059	-17.369	0.927	0.495	1.067	3.950	P
K2CfCl6	9.987	-14.870	0.927	0.454	1.063	4.092	P
Na2OsCl6	9.300	-9.876	0.927	0.348	1.054	4.661	P

Na2ReCl6	9.300	-9.876	0.927	0.348	1.054	4.661	P
Na2IrCl6	9.296	-9.767	0.929	0.345	1.053	4.678	P
Na2PtCl6	9.296	-9.767	0.929	0.345	1.053	4.678	P
Na2CoI6	10.365	-3.674	0.930	0.241	1.042	5.871	P
Na2GeI6	10.365	-3.674	0.930	0.241	1.042	5.871	P
Na2MnI6	10.365	-3.674	0.930	0.241	1.042	5.871	P
K2ZrI6	11.051	-8.646	0.930	0.327	1.053	4.823	P
Cs2PaI6	11.708	-13.367	0.931	0.409	1.061	4.280	P
K2PbBr6	10.390	-12.320	0.931	0.395	1.059	4.352	P
Na2FeBr6	9.704	-7.347	0.931	0.298	1.049	5.096	P
Na2RuCl6	9.292	-9.657	0.931	0.343	1.053	4.696	P
Rb2CeCl6	10.197	-16.203	0.931	0.481	1.065	3.981	P
Rb2NpCl6	10.197	-16.203	0.931	0.481	1.065	3.981	P
Rb2PbI6	11.266	-10.110	0.932	0.352	1.056	4.623	P
Na2VBr6	9.700	-7.238	0.933	0.296	1.049	5.121	P
Rb2BkBr6	10.605	-13.784	0.933	0.423	1.062	4.205	P
K2HfI6	11.043	-8.427	0.933	0.323	1.053	4.858	P
Na2PdCl6	9.288	-9.548	0.933	0.340	1.053	4.715	P
Cs2UI6	11.700	-13.148	0.934	0.405	1.061	4.297	P
Rb2PuCl6	10.189	-15.984	0.935	0.475	1.065	3.990	P
Rb2CfBr6	10.598	-13.587	0.936	0.419	1.061	4.220	P
K2TbBr6	10.378	-11.991	0.936	0.388	1.059	4.385	P
Cs2PoBr6	11.035	-16.712	0.936	0.480	1.066	3.970	P
Cs2ThBr6	11.035	-16.712	0.936	0.480	1.066	3.970	P
Rb2TbI6	11.254	-9.782	0.936	0.345	1.056	4.666	P
Na2TiCl6	9.280	-9.329	0.937	0.334	1.053	4.754	P
Rb2TeF6	8.867	-23.332	0.938	0.729	1.080	3.467	P
Na2ZrF6	7.962	-16.786	0.938	0.541	1.067	3.782	P
Rb2AmCl6	10.181	-15.765	0.938	0.470	1.065	4.000	P
Rb2CmCl6	10.181	-15.765	0.938	0.470	1.065	4.000	P
Rb2PrCl6	10.181	-15.765	0.938	0.470	1.065	4.000	P
Cs2TeCl6	10.618	-18.913	0.939	0.536	1.070	3.795	P
Na2RhCl6	9.276	-9.219	0.939	0.331	1.053	4.774	P
K2SnI6	11.027	-7.989	0.940	0.314	1.053	4.934	P
Cs2CeI6	11.684	-12.710	0.940	0.395	1.061	4.333	P
Cs2NpI6	11.684	-12.710	0.940	0.395	1.061	4.333	P
Na2SeI6	10.341	-3.017	0.940	0.227	1.042	6.119	P
K2PaF6	8.640	-21.539	0.942	0.677	1.077	3.515	P
K2NbI6	11.019	-7.770	0.943	0.309	1.053	4.975	P
K2TaI6	11.019	-7.770	0.943	0.309	1.053	4.975	P

Na2HfF6	7.954	-16.567	0.943	0.534	1.066	3.787	P
Cs2PuI6	11.676	-12.491	0.943	0.391	1.061	4.353	P
K2PbCl6	9.950	-13.864	0.944	0.428	1.062	4.159	P
Na2CrBr6	9.676	-6.581	0.944	0.281	1.049	5.290	P
Na2FeCl6	9.263	-8.891	0.945	0.323	1.053	4.839	P
Rb2BkCl6	10.165	-15.328	0.945	0.459	1.065	4.025	P
Cs2AmI6	11.668	-12.273	0.946	0.386	1.061	4.375	P
Cs2CmI6	11.668	-12.273	0.946	0.386	1.061	4.375	P
Cs2PrI6	11.668	-12.273	0.946	0.386	1.061	4.375	P
K2UF6	8.632	-21.321	0.946	0.669	1.077	3.509	P
Na2VCl6	9.259	-8.782	0.947	0.320	1.053	4.863	P
Na2NiI6	10.325	-2.579	0.947	0.218	1.041	6.307	P
Rb2CfCl6	10.157	-15.131	0.949	0.454	1.065	4.037	P
Cs2PoCl6	10.594	-18.256	0.949	0.519	1.069	3.811	P
Cs2ThCl6	10.594	-18.256	0.949	0.519	1.069	3.811	P
K2TbCl6	9.938	-13.535	0.949	0.420	1.062	4.187	P
Rb2ZrI6	11.222	-8.906	0.949	0.327	1.055	4.799	P
K2WI6	11.003	-7.333	0.949	0.300	1.052	5.063	P
Cs2PaBr6	11.003	-15.837	0.949	0.459	1.066	4.014	P
K2ZrBr6	10.346	-11.116	0.950	0.367	1.058	4.489	P
Rb2PoF6	8.843	-22.675	0.950	0.707	1.080	3.443	P
Rb2ThF6	8.843	-22.675	0.950	0.707	1.080	3.443	P
Na2CoBr6	9.660	-6.144	0.951	0.270	1.048	5.418	P
Na2GeBr6	9.660	-6.144	0.951	0.270	1.048	5.418	P
Na2MnBr6	9.660	-6.144	0.951	0.270	1.048	5.418	P
Rb2PbBr6	10.561	-12.580	0.951	0.395	1.061	4.313	P
Na2SnF6	7.938	-16.129	0.952	0.519	1.066	3.804	P
Cs2BkI6	11.652	-11.835	0.952	0.377	1.060	4.421	P
Rb2HfI6	11.214	-8.688	0.953	0.323	1.055	4.836	P
Cs2UBr6	10.995	-15.618	0.953	0.454	1.066	4.027	P
K2HfBr6	10.338	-10.897	0.953	0.362	1.058	4.520	P
K2TcI6	10.991	-7.005	0.954	0.293	1.052	5.135	P
K2CeF6	8.616	-20.883	0.955	0.654	1.076	3.502	P
K2NpF6	8.616	-20.883	0.955	0.654	1.076	3.502	P
Cs2CfI6	11.644	-11.638	0.955	0.373	1.060	4.444	P
Rb2TbBr6	10.549	-12.252	0.957	0.388	1.061	4.350	P
Na2NbF6	7.930	-15.911	0.957	0.511	1.066	3.815	P
Na2TaF6	7.930	-15.911	0.957	0.511	1.066	3.815	P
Na2CrCl6	9.235	-8.125	0.959	0.304	1.052	5.017	P
K2PuF6	8.608	-20.664	0.959	0.647	1.076	3.501	P

Rb2SnI6	11.198	-8.250	0.959	0.314	1.055	4.918	P
Cs2CeBr6	10.979	-15.180	0.959	0.444	1.065	4.057	P
Cs2NpBr6	10.979	-15.180	0.959	0.444	1.065	4.057	P
K2MoI6	10.979	-6.676	0.959	0.286	1.052	5.213	P
K2OsI6	10.979	-6.676	0.959	0.286	1.052	5.213	P
K2ReI6	10.979	-6.676	0.959	0.286	1.052	5.213	P
K2SnBr6	10.322	-10.460	0.961	0.352	1.058	4.586	P
K2IrI6	10.975	-6.567	0.961	0.284	1.052	5.240	P
K2PtI6	10.975	-6.567	0.961	0.284	1.052	5.240	P
Rb2NbI6	11.190	-8.031	0.962	0.309	1.055	4.961	P
Rb2TaI6	11.190	-8.031	0.962	0.309	1.055	4.961	P
Cs2PaCl6	10.562	-17.381	0.963	0.497	1.069	3.847	P
K2RuI6	10.971	-6.457	0.963	0.282	1.052	5.268	P
Cs2PuBr6	10.971	-14.962	0.963	0.439	1.065	4.074	P
Na2SeBr6	9.636	-5.487	0.963	0.255	1.048	5.639	P
K2AmF6	8.600	-20.445	0.963	0.639	1.076	3.500	P
K2CmF6	8.600	-20.445	0.963	0.639	1.076	3.500	P
K2PrF6	8.600	-20.445	0.963	0.639	1.076	3.500	P
K2NbBr6	10.314	-10.241	0.964	0.347	1.058	4.622	P
K2TaBr6	10.314	-10.241	0.964	0.347	1.058	4.622	P
K2ZrCl6	9.905	-12.660	0.964	0.398	1.061	4.281	P
K2PdI6	10.967	-6.348	0.965	0.280	1.052	5.296	P
Rb2PbCl6	10.120	-14.124	0.966	0.428	1.064	4.119	P
Cs2AmBr6	10.963	-14.743	0.966	0.434	1.065	4.092	P
Cs2CmBr6	10.963	-14.743	0.966	0.434	1.065	4.092	P
Cs2PrBr6	10.963	-14.743	0.966	0.434	1.065	4.092	P
Cs2UCl6	10.554	-17.162	0.966	0.492	1.069	3.858	P
Na2WF6	7.914	-15.473	0.966	0.496	1.066	3.843	P
Na2CoCl6	9.219	-7.688	0.967	0.293	1.052	5.135	P
Na2GeCl6	9.219	-7.688	0.967	0.293	1.052	5.135	P
Na2MnCl6	9.219	-7.688	0.967	0.293	1.052	5.135	P
Rb2PaF6	8.811	-21.800	0.967	0.677	1.079	3.428	P
K2TiI6	10.959	-6.129	0.968	0.275	1.052	5.355	P
K2HfCl6	9.897	-12.441	0.968	0.392	1.061	4.308	P
Rb2WI6	11.174	-7.593	0.969	0.300	1.055	5.054	P
K2RhI6	10.955	-6.020	0.970	0.273	1.052	5.385	P
Cs2PbI6	11.608	-10.631	0.970	0.352	1.060	4.576	P
Na2NiBr6	9.620	-5.050	0.971	0.245	1.048	5.807	P
Rb2ZrBr6	10.517	-11.377	0.971	0.367	1.060	4.465	P
Rb2TbCl6	10.108	-13.796	0.971	0.420	1.064	4.152	P

Na2MoF6	7.906	-15.254	0.971	0.489	1.065	3.860	P
Rb2UF6	8.803	-21.581	0.971	0.669	1.079	3.428	P
K2WBr6	10.298	-9.803	0.972	0.337	1.058	4.700	P
K2BkF6	8.584	-20.008	0.972	0.624	1.075	3.504	P
Rb2MoI6	11.166	-7.375	0.973	0.295	1.055	5.104	P
Cs2BkBr6	10.947	-14.305	0.973	0.423	1.065	4.132	P
Cs2CeCl6	10.538	-16.724	0.974	0.481	1.069	3.885	P
Cs2NpCl6	10.538	-16.724	0.974	0.481	1.069	3.885	P
Na2TcF6	7.902	-15.145	0.974	0.485	1.065	3.869	P
Rb2TcI6	11.162	-7.265	0.974	0.293	1.054	5.130	P
Rb2HfBr6	10.509	-11.158	0.975	0.362	1.060	4.498	P
Cs2TbI6	11.595	-10.303	0.975	0.345	1.060	4.626	P
K2FeI6	10.943	-5.691	0.975	0.266	1.052	5.480	P
K2SnCl6	9.881	-12.003	0.976	0.381	1.061	4.369	P
K2CfF6	8.577	-19.811	0.976	0.617	1.075	3.507	P
Na2SiI6	10.261	-0.829	0.976	0.182	1.040	7.290	P
Cs2CfBr6	10.939	-14.108	0.976	0.419	1.065	4.151	P
K2VI6	10.939	-5.582	0.977	0.264	1.052	5.513	P
K2TcBr6	10.286	-9.475	0.977	0.329	1.057	4.763	P
Cs2PuCl6	10.530	-16.505	0.977	0.475	1.068	3.900	P
Rb2OsI6	11.150	-6.937	0.979	0.286	1.054	5.210	P
Rb2ReI6	11.150	-6.937	0.979	0.286	1.054	5.210	P
Na2SeCl6	9.195	-7.031	0.980	0.276	1.052	5.339	P
K2NbCl6	9.873	-11.785	0.980	0.376	1.061	4.401	P
K2TaCl6	9.873	-11.785	0.980	0.376	1.061	4.401	P
Rb2CeF6	8.787	-21.144	0.980	0.654	1.079	3.429	P
Rb2NpF6	8.787	-21.144	0.980	0.654	1.079	3.429	P
Cs2AmCl6	10.522	-16.287	0.981	0.470	1.068	3.916	P
Cs2CmCl6	10.522	-16.287	0.981	0.470	1.068	3.916	P
Cs2PrCl6	10.522	-16.287	0.981	0.470	1.068	3.916	P
Rb2IrI6	11.146	-6.827	0.981	0.284	1.054	5.238	P
Rb2PtI6	11.146	-6.827	0.981	0.284	1.054	5.238	P
Na2OsF6	7.890	-14.816	0.981	0.474	1.065	3.899	P
Na2ReF6	7.890	-14.816	0.981	0.474	1.065	3.899	P
Rb2SnBr6	10.493	-10.720	0.982	0.352	1.060	4.570	P
K2MoBr6	10.274	-9.146	0.983	0.321	1.057	4.832	P
K2OsBr6	10.274	-9.146	0.983	0.321	1.057	4.832	P
K2ReBr6	10.274	-9.146	0.983	0.321	1.057	4.832	P
Rb2RuI6	11.142	-6.718	0.983	0.282	1.054	5.267	P
Na2IrF6	7.886	-14.707	0.984	0.470	1.065	3.910	P

Na2PtF6	7.886	-14.707	0.984	0.470	1.065	3.910	P
Rb2PdI6	11.138	-6.609	0.985	0.280	1.054	5.297	P
K2IrBr6	10.270	-9.037	0.985	0.319	1.057	4.856	P
K2PtBr6	10.270	-9.037	0.985	0.319	1.057	4.856	P
Rb2PuF6	8.779	-20.925	0.985	0.647	1.078	3.432	P
Rb2NbBr6	10.485	-10.501	0.986	0.347	1.060	4.608	P
Rb2TaBr6	10.485	-10.501	0.986	0.347	1.060	4.608	P
Na2RuF6	7.882	-14.598	0.986	0.466	1.065	3.922	P
Rb2ZrCl6	10.076	-12.921	0.987	0.398	1.063	4.257	P
K2RuBr6	10.266	-8.928	0.987	0.316	1.057	4.881	P
Cs2TeF6	9.209	-23.853	0.987	0.729	1.085	3.300	P
K2CrI6	10.915	-4.926	0.987	0.250	1.051	5.729	P
K2WCl6	9.857	-11.347	0.988	0.365	1.061	4.472	P
Cs2ZrI6	11.563	-9.428	0.988	0.327	1.059	4.776	P
Na2NiCl6	9.179	-6.593	0.988	0.265	1.051	5.494	P
Rb2TiI6	11.130	-6.390	0.988	0.275	1.054	5.357	P
Cs2BkCl6	10.506	-15.849	0.988	0.459	1.068	3.951	P
K2PdBr6	10.262	-8.818	0.989	0.314	1.057	4.906	P
Na2PdF6	7.878	-14.488	0.989	0.462	1.065	3.934	P
Rb2AmF6	8.771	-20.706	0.989	0.639	1.078	3.436	P
Rb2CmF6	8.771	-20.706	0.989	0.639	1.078	3.436	P
Rb2PrF6	8.771	-20.706	0.989	0.639	1.078	3.436	P
Rb2RhI6	11.126	-6.280	0.990	0.273	1.054	5.389	P
Rb2HfCl6	10.068	-12.702	0.991	0.392	1.063	4.287	P
Cs2HfI6	11.555	-9.209	0.991	0.323	1.059	4.818	P
Cs2CfCl6	10.499	-15.652	0.992	0.454	1.068	3.969	P
K2TiBr6	10.254	-8.599	0.992	0.309	1.057	4.958	P
Cs2PbBr6	10.903	-13.101	0.993	0.395	1.064	4.266	P
Rb2WBr6	10.469	-10.064	0.993	0.337	1.060	4.690	P
K2TcCl6	9.845	-11.019	0.994	0.356	1.061	4.531	P
Na2TiF6	7.870	-14.269	0.994	0.455	1.065	3.960	P
K2RhBr6	10.250	-8.490	0.994	0.306	1.057	4.985	P
K2CoI6	10.899	-4.488	0.995	0.241	1.051	5.890	P
K2GeI6	10.899	-4.488	0.995	0.241	1.051	5.890	P
K2MnI6	10.899	-4.488	0.995	0.241	1.051	5.890	P
Rb2FeI6	11.113	-5.952	0.995	0.266	1.054	5.487	P
Na2RhF6	7.866	-14.160	0.997	0.451	1.065	3.974	P
Rb2MoBr6	10.461	-9.845	0.997	0.332	1.060	4.735	P
Rb2VI6	11.109	-5.843	0.997	0.264	1.054	5.521	P
K2PbF6	8.540	-18.804	0.998	0.583	1.075	3.539	P

Cs2SnI6	11.539	-8.771	0.998	0.314	1.059	4.907	P
Cs2TbBr6	10.891	-12.773	0.998	0.388	1.064	4.310	P
Rb2SnCl6	10.052	-12.264	0.998	0.381	1.063	4.352	P
Rb2BkF6	8.755	-20.268	0.998	0.624	1.078	3.446	P
Rb2TcBr6	10.457	-9.735	0.999	0.329	1.059	4.758	P
K2MoCl6	9.833	-10.690	1.000	0.348	1.060	4.594	P
K2OsCl6	9.833	-10.690	1.000	0.348	1.060	4.594	P
K2ReCl6	9.833	-10.690	1.000	0.348	1.060	4.594	P
Cs2PoF6	9.184	-23.197	1.000	0.707	1.085	3.300	P
Cs2ThF6	9.184	-23.197	1.000	0.707	1.085	3.300	P
K2FeBr6	10.238	-8.162	1.000	0.298	1.057	5.070	P
Cs2NbI6	11.531	-8.552	1.002	0.309	1.059	4.954	P
Cs2TaI6	11.531	-8.552	1.002	0.309	1.059	4.954	P
K2IrCl6	9.829	-10.581	1.002	0.345	1.060	4.616	P
K2PtCl6	9.829	-10.581	1.002	0.345	1.060	4.616	P
K2VBr6	10.234	-8.052	1.002	0.296	1.057	5.100	P
Rb2NbCl6	10.044	-12.045	1.002	0.376	1.063	4.387	P
Rb2TaCl6	10.044	-12.045	1.002	0.376	1.063	4.387	P
Rb2CfF6	8.747	-20.071	1.003	0.617	1.078	3.453	P
Na2SiBr6	9.556	-3.299	1.004	0.204	1.047	6.690	P
K2RuCl6	9.825	-10.471	1.004	0.343	1.060	4.639	P
Na2FeF6	7.854	-13.832	1.004	0.440	1.065	4.019	P
Rb2OsBr6	10.445	-9.407	1.005	0.321	1.059	4.829	P
Rb2ReBr6	10.445	-9.407	1.005	0.321	1.059	4.829	P
K2TbF6	8.528	-18.476	1.005	0.571	1.074	3.556	P
K2SeI6	10.874	-3.831	1.006	0.227	1.051	6.161	P
K2PdCl6	9.821	-10.362	1.006	0.340	1.060	4.662	P
Rb2IrBr6	10.441	-9.298	1.007	0.319	1.059	4.854	P
Rb2PtBr6	10.441	-9.298	1.007	0.319	1.059	4.854	P
Na2VF6	7.850	-13.722	1.007	0.436	1.064	4.035	P
Rb2CrI6	11.085	-5.186	1.008	0.250	1.054	5.743	P
Rb2RuBr6	10.437	-9.188	1.009	0.316	1.059	4.880	P
Cs2WI6	11.515	-8.115	1.009	0.300	1.059	5.055	P
Cs2PbCl6	10.462	-14.645	1.009	0.428	1.068	4.073	P
K2TiCl6	9.813	-10.143	1.010	0.334	1.060	4.710	P
Rb2PdBr6	10.433	-9.079	1.011	0.314	1.059	4.906	P
Rb2WCl6	10.028	-11.607	1.011	0.365	1.063	4.463	P
K2RhCl6	9.809	-10.034	1.012	0.331	1.060	4.735	P
Cs2MoI6	11.507	-7.896	1.012	0.295	1.059	5.108	P
K2NiI6	10.858	-3.394	1.013	0.218	1.051	6.364	P

Cs2ZrBr6	10.858	-11.898	1.013	0.367	1.064	4.443	P
Cs2TcI6	11.503	-7.786	1.014	0.293	1.059	5.135	P
K2CrBr6	10.210	-7.396	1.014	0.281	1.057	5.293	P
Rb2TiBr6	10.425	-8.860	1.014	0.309	1.059	4.961	P
Rb2MoCl6	10.020	-11.389	1.015	0.359	1.063	4.504	P
Cs2TbCl6	10.450	-14.317	1.015	0.420	1.068	4.113	P
Rb2CoI6	11.069	-4.748	1.015	0.241	1.054	5.908	P
Rb2GeI6	11.069	-4.748	1.015	0.241	1.054	5.908	P
Rb2MnI6	11.069	-4.748	1.015	0.241	1.054	5.908	P
Rb2RhBr6	10.421	-8.751	1.016	0.306	1.059	4.989	P
Rb2TcCl6	10.016	-11.279	1.017	0.356	1.063	4.525	P
Cs2HfBr6	10.850	-11.679	1.017	0.362	1.064	4.480	P
Cs2PaF6	9.152	-22.321	1.018	0.677	1.084	3.314	P
K2FeCl6	9.797	-9.706	1.019	0.323	1.060	4.814	P
Cs2OsI6	11.491	-7.458	1.019	0.286	1.059	5.222	P
Cs2ReI6	11.491	-7.458	1.019	0.286	1.059	5.222	P
K2VCl6	9.793	-9.596	1.021	0.320	1.060	4.841	P
Cs2IrI6	11.487	-7.349	1.021	0.284	1.059	5.251	P
Cs2PtI6	11.487	-7.349	1.021	0.284	1.059	5.251	P
K2CoBr6	10.194	-6.958	1.022	0.270	1.056	5.437	P
K2GeBr6	10.194	-6.958	1.022	0.270	1.056	5.437	P
K2MnBr6	10.194	-6.958	1.022	0.270	1.056	5.437	P
Cs2UF6	9.144	-22.102	1.022	0.669	1.084	3.319	P
Rb2FeBr6	10.409	-8.422	1.022	0.298	1.059	5.077	P
Rb2OsCl6	10.004	-10.951	1.023	0.348	1.063	4.591	P
Rb2ReCl6	10.004	-10.951	1.023	0.348	1.063	4.591	P
Cs2RuI6	11.483	-7.239	1.023	0.282	1.059	5.282	P
Na2CrF6	7.825	-13.066	1.023	0.414	1.064	4.144	P
Na2SiCl6	9.115	-4.843	1.024	0.221	1.051	6.315	P
K2ZrF6	8.496	-17.600	1.024	0.541	1.074	3.614	P
Rb2VBr6	10.405	-8.313	1.024	0.296	1.059	5.107	P
Rb2PbF6	8.711	-19.065	1.025	0.583	1.077	3.500	P
Cs2SnBr6	10.834	-11.241	1.025	0.352	1.064	4.559	P
Cs2PdI6	11.479	-7.130	1.025	0.280	1.059	5.313	P
Rb2IrCl6	10.000	-10.841	1.025	0.345	1.063	4.614	P
Rb2PtCl6	10.000	-10.841	1.025	0.345	1.063	4.614	P
Rb2SeI6	11.045	-4.092	1.027	0.227	1.054	6.184	P
Rb2RuCl6	9.996	-10.732	1.027	0.343	1.063	4.638	P
Cs2NbBr6	10.826	-11.022	1.029	0.347	1.064	4.601	P
Cs2TaBr6	10.826	-11.022	1.029	0.347	1.064	4.601	P

Cs2TiI6	11.471	-6.911	1.029	0.275	1.059	5.377	P
Rb2PdCl6	9.992	-10.623	1.029	0.340	1.063	4.662	P
K2HfF6	8.488	-17.381	1.029	0.534	1.074	3.632	P
Cs2RhI6	11.467	-6.801	1.030	0.273	1.059	5.410	P
Cs2ZrCl6	10.418	-13.442	1.031	0.398	1.067	4.234	P
Cs2CeF6	9.128	-21.665	1.032	0.654	1.084	3.333	P
Cs2NpF6	9.128	-21.665	1.032	0.654	1.084	3.333	P
Rb2TbF6	8.698	-18.736	1.032	0.571	1.077	3.521	P
Rb2TiCl6	9.984	-10.404	1.034	0.334	1.062	4.713	P
K2CrCl6	9.769	-8.940	1.034	0.304	1.060	5.020	P
Na2CoF6	7.809	-12.628	1.034	0.398	1.064	4.230	P
Na2GeF6	7.809	-12.628	1.034	0.398	1.064	4.230	P
Na2MnF6	7.809	-12.628	1.034	0.398	1.064	4.230	P
Rb2NiI6	11.029	-3.654	1.034	0.218	1.053	6.391	P
K2SeBr6	10.170	-6.301	1.035	0.255	1.056	5.681	P
Cs2HfCl6	10.410	-13.223	1.035	0.392	1.067	4.269	P
Rb2RhCl6	9.980	-10.294	1.036	0.331	1.062	4.739	P
Cs2FeI6	11.455	-6.473	1.036	0.266	1.058	5.513	P
Cs2WBr6	10.810	-10.585	1.036	0.337	1.064	4.691	P
Cs2PuF6	9.120	-21.446	1.036	0.647	1.084	3.342	P
Rb2CrBr6	10.380	-7.656	1.037	0.281	1.059	5.306	P
Cs2VI6	11.451	-6.364	1.038	0.264	1.058	5.549	P
K2SnF6	8.472	-16.944	1.040	0.519	1.074	3.673	P
Cs2MoBr6	10.802	-10.366	1.040	0.332	1.064	4.739	P
Cs2AmF6	9.112	-21.227	1.041	0.639	1.084	3.351	P
Cs2CmF6	9.112	-21.227	1.041	0.639	1.084	3.351	P
Cs2PrF6	9.112	-21.227	1.041	0.639	1.084	3.351	P
Rb2FeCl6	9.968	-9.966	1.042	0.323	1.062	4.820	P
Cs2TcBr6	10.798	-10.256	1.042	0.329	1.064	4.763	P
K2CoCl6	9.753	-8.502	1.043	0.293	1.060	5.154	P
K2GeCl6	9.753	-8.502	1.043	0.293	1.060	5.154	P
K2MnCl6	9.753	-8.502	1.043	0.293	1.060	5.154	P
K2NiBr6	10.153	-5.864	1.043	0.245	1.056	5.864	P
Cs2SnCl6	10.394	-12.785	1.044	0.381	1.067	4.341	P
K2SiI6	10.794	-1.643	1.044	0.182	1.051	7.406	NP
Rb2VCl6	9.964	-9.857	1.044	0.320	1.062	4.849	P
K2NbF6	8.463	-16.725	1.045	0.511	1.074	3.695	P
K2TaF6	8.463	-16.725	1.045	0.511	1.074	3.695	P
Rb2CoBr6	10.364	-7.219	1.045	0.270	1.059	5.455	P
Rb2GeBr6	10.364	-7.219	1.045	0.270	1.059	5.455	P

Rb2MnBr6	10.364	-7.219	1.045	0.270	1.059	5.455	P
Cs2NbCl6	10.386	-12.566	1.048	0.376	1.067	4.380	P
Cs2TaCl6	10.386	-12.566	1.048	0.376	1.067	4.380	P
Cs2OsBr6	10.786	-9.928	1.048	0.321	1.064	4.841	P
Cs2ReBr6	10.786	-9.928	1.048	0.321	1.064	4.841	P
Cs2CrI6	11.427	-5.707	1.049	0.250	1.058	5.781	NP
Cs2IrBr6	10.782	-9.819	1.050	0.319	1.064	4.867	P
Cs2PtBr6	10.782	-9.819	1.050	0.319	1.064	4.867	P
Cs2BkF6	9.096	-20.789	1.051	0.624	1.084	3.373	P
Na2SeF6	7.785	-11.971	1.051	0.376	1.064	4.379	P
Rb2ZrF6	8.666	-17.861	1.052	0.541	1.077	3.590	P
Cs2RuBr6	10.778	-9.709	1.052	0.316	1.064	4.895	NP
Cs2PdBr6	10.774	-9.600	1.054	0.314	1.064	4.923	NP
Cs2CfF6	9.089	-20.592	1.055	0.617	1.083	3.384	P
K2WF6	8.447	-16.287	1.055	0.496	1.073	3.745	P
K2SeCl6	9.729	-7.845	1.056	0.276	1.060	5.381	P
Cs2WCl6	10.370	-12.129	1.056	0.365	1.067	4.464	P
Cs2CoI6	11.411	-5.270	1.057	0.241	1.058	5.952	NP
Cs2GeI6	11.411	-5.270	1.057	0.241	1.058	5.952	NP
Cs2MnI6	11.411	-5.270	1.057	0.241	1.058	5.952	NP
Rb2HfF6	8.658	-17.642	1.057	0.534	1.077	3.611	P
Rb2CrCl6	9.940	-9.200	1.058	0.304	1.062	5.034	P
Rb2SeBr6	10.340	-6.562	1.058	0.255	1.059	5.704	NP
Cs2TiBr6	10.766	-9.381	1.059	0.309	1.064	4.980	NP
Cs2MoCl6	10.362	-11.910	1.061	0.359	1.067	4.508	P
Cs2RhBr6	10.762	-9.272	1.061	0.306	1.064	5.010	NP
Na2NiF6	7.769	-11.534	1.063	0.361	1.064	4.494	P
Cs2TcCl6	10.358	-11.800	1.063	0.356	1.067	4.531	P
K2TcF6	8.435	-15.959	1.063	0.485	1.073	3.787	P
K2NiCl6	9.713	-7.408	1.065	0.265	1.060	5.552	P
Rb2SiI6	10.965	-1.903	1.066	0.182	1.054	7.448	NP
Rb2NiBr6	10.324	-6.124	1.066	0.245	1.059	5.891	NP
Rb2CoCl6	9.924	-8.762	1.067	0.293	1.062	5.172	P
Rb2GeCl6	9.924	-8.762	1.067	0.293	1.062	5.172	P
Rb2MnCl6	9.924	-8.762	1.067	0.293	1.062	5.172	P
Cs2FeBr6	10.750	-8.943	1.067	0.298	1.064	5.103	NP
Rb2SnF6	8.642	-17.204	1.068	0.519	1.076	3.657	P
Cs2SeI6	11.387	-4.613	1.069	0.227	1.058	6.239	NP
Cs2VBr6	10.746	-8.834	1.069	0.296	1.064	5.136	NP
Cs2OsCl6	10.346	-11.472	1.069	0.348	1.067	4.602	P

Cs2ReCl6	10.346	-11.472	1.069	0.348	1.067	4.602	P
K2MoF6	8.423	-15.631	1.071	0.474	1.073	3.832	P
K2OsF6	8.423	-15.631	1.071	0.474	1.073	3.832	P
K2ReF6	8.423	-15.631	1.071	0.474	1.073	3.832	P
Cs2IrCl6	10.342	-11.363	1.072	0.345	1.067	4.627	P
Cs2PtCl6	10.342	-11.363	1.072	0.345	1.067	4.627	P
Rb2NbF6	8.634	-16.986	1.073	0.511	1.076	3.682	P
Rb2TaF6	8.634	-16.986	1.073	0.511	1.076	3.682	P
Cs2RuCl6	10.338	-11.253	1.074	0.343	1.067	4.653	P
K2IrF6	8.419	-15.521	1.074	0.470	1.073	3.848	P
K2PtF6	8.419	-15.521	1.074	0.470	1.073	3.848	P
Cs2PdCl6	10.334	-11.144	1.076	0.340	1.067	4.679	P
Cs2NiI6	11.371	-4.175	1.076	0.218	1.058	6.452	NP
K2RuF6	8.415	-15.412	1.077	0.466	1.073	3.864	P
Cs2PbF6	9.052	-19.586	1.078	0.583	1.083	3.454	P
K2SiBr6	10.089	-4.113	1.079	0.204	1.056	6.806	NP
K2PdF6	8.411	-15.302	1.080	0.462	1.073	3.881	P
Cs2TiCl6	10.326	-10.925	1.080	0.334	1.067	4.732	P
Rb2SeCl6	9.900	-8.106	1.081	0.276	1.062	5.404	P
Cs2CrBr6	10.722	-8.177	1.082	0.281	1.064	5.345	NP
Cs2RhCl6	10.322	-10.816	1.083	0.331	1.067	4.760	P
Rb2WF6	8.618	-16.548	1.084	0.496	1.076	3.736	P
K2TiF6	8.403	-15.084	1.085	0.455	1.073	3.917	P
Cs2TbF6	9.040	-19.257	1.086	0.571	1.083	3.481	P
K2RhF6	8.399	-14.974	1.088	0.451	1.073	3.935	P
Rb2MoF6	8.610	-16.329	1.089	0.489	1.076	3.765	P
Cs2FeCl6	10.309	-10.487	1.089	0.323	1.067	4.847	P
Rb2NiCl6	9.884	-7.668	1.090	0.265	1.062	5.578	P
Cs2CoBr6	10.706	-7.740	1.090	0.270	1.064	5.500	NP
Cs2GeBr6	10.706	-7.740	1.090	0.270	1.064	5.500	NP
Cs2MnBr6	10.706	-7.740	1.090	0.270	1.064	5.500	NP
Cs2VCl6	10.305	-10.378	1.092	0.320	1.067	4.877	P
Rb2TcF6	8.606	-16.220	1.092	0.485	1.076	3.781	P
K2FeF6	8.387	-14.646	1.097	0.440	1.073	3.993	P
K2VF6	8.383	-14.537	1.100	0.436	1.073	4.013	P
Rb2OsF6	8.594	-15.891	1.100	0.474	1.076	3.829	P
Rb2ReF6	8.594	-15.891	1.100	0.474	1.076	3.829	P
Rb2SiBr6	10.260	-4.374	1.103	0.204	1.059	6.848	NP
Rb2IrF6	8.590	-15.782	1.103	0.470	1.076	3.846	P
Rb2PtF6	8.590	-15.782	1.103	0.470	1.076	3.846	P

Cs2SeBr6	10.682	-7.083	1.104	0.255	1.064	5.759	P
K2SiCl6	9.649	-5.657	1.104	0.221	1.060	6.431	P
Cs2CrCl6	10.281	-9.721	1.106	0.304	1.067	5.072	P
Rb2RuF6	8.586	-15.672	1.106	0.466	1.076	3.864	P
Cs2ZrF6	9.008	-18.382	1.107	0.541	1.083	3.568	P
Rb2PdF6	8.582	-15.563	1.109	0.462	1.076	3.882	P
Cs2SiI6	11.307	-2.425	1.110	0.182	1.059	7.537	NP
Na2SiF6	7.705	-9.783	1.112	0.301	1.064	5.115	P
Cs2HfF6	9.000	-18.163	1.113	0.534	1.083	3.592	P
Cs2NiBr6	10.666	-6.646	1.113	0.245	1.064	5.952	NP
Rb2TiF6	8.574	-15.344	1.115	0.455	1.076	3.919	P
Cs2CoCl6	10.265	-9.284	1.115	0.293	1.067	5.217	NP
Cs2GeCl6	10.265	-9.284	1.115	0.293	1.067	5.217	NP
Cs2MnCl6	10.265	-9.284	1.115	0.293	1.067	5.217	NP
K2CrF6	8.359	-13.880	1.117	0.414	1.073	4.147	P
Rb2RhF6	8.570	-15.235	1.117	0.451	1.076	3.939	P
Cs2SnF6	8.984	-17.726	1.124	0.519	1.083	3.646	P
Rb2FeF6	8.558	-14.907	1.126	0.440	1.076	4.000	P
K2CoF6	8.343	-13.442	1.129	0.398	1.073	4.249	P
K2GeF6	8.343	-13.442	1.129	0.398	1.073	4.249	P
K2MnF6	8.343	-13.442	1.129	0.398	1.073	4.249	P
Rb2VF6	8.554	-14.797	1.129	0.436	1.076	4.021	P
Cs2NbF6	8.976	-17.507	1.129	0.511	1.083	3.675	P
Cs2TaF6	8.976	-17.507	1.129	0.511	1.083	3.675	P
Rb2SiCl6	9.819	-5.918	1.129	0.221	1.063	6.473	NP
Cs2SeCl6	10.241	-8.627	1.130	0.276	1.067	5.459	NP
Cs2NiCl6	10.225	-8.189	1.139	0.265	1.067	5.640	NP
Cs2WF6	8.960	-17.069	1.141	0.496	1.083	3.736	P
Cs2MoF6	8.952	-16.850	1.146	0.489	1.083	3.769	P
Rb2CrF6	8.530	-14.141	1.147	0.414	1.076	4.161	P
K2SeF6	8.319	-12.786	1.148	0.376	1.073	4.421	P
Cs2TcF6	8.948	-16.741	1.149	0.485	1.083	3.787	P
Cs2SiBr6	10.602	-4.895	1.151	0.204	1.064	6.937	NP
Cs2OsF6	8.936	-16.412	1.158	0.474	1.083	3.841	P
Cs2ReF6	8.936	-16.412	1.158	0.474	1.083	3.841	P
Rb2CoF6	8.514	-13.703	1.160	0.398	1.076	4.266	P
Rb2GeF6	8.514	-13.703	1.160	0.398	1.076	4.266	P
Rb2MnF6	8.514	-13.703	1.160	0.398	1.076	4.266	P
K2NiF6	8.303	-12.348	1.160	0.361	1.073	4.552	P
Cs2IrF6	8.932	-16.303	1.161	0.470	1.083	3.859	P

Cs2PtF6	8.932	-16.303	1.161	0.470	1.083	3.859	P
Cs2RuF6	8.928	-16.194	1.164	0.466	1.083	3.879	P
Cs2PdF6	8.924	-16.084	1.167	0.462	1.083	3.898	P
Cs2TiF6	8.916	-15.865	1.173	0.455	1.083	3.939	P
Cs2RhF6	8.912	-15.756	1.176	0.451	1.083	3.960	P
Rb2SeF6	8.490	-13.046	1.179	0.376	1.076	4.444	P
Cs2SiCl6	10.161	-6.439	1.181	0.221	1.068	6.562	NP
Cs2FeF6	8.900	-15.428	1.185	0.440	1.083	4.026	P
Cs2VF6	8.896	-15.318	1.188	0.436	1.083	4.049	P
Rb2NiF6	8.474	-12.609	1.192	0.361	1.077	4.578	P
Cs2CrF6	8.871	-14.662	1.207	0.414	1.083	4.199	P
K2SiF6	8.239	-10.597	1.214	0.301	1.074	5.231	P
Cs2CoF6	8.855	-14.224	1.220	0.398	1.083	4.311	P
Cs2GeF6	8.855	-14.224	1.220	0.398	1.083	4.311	P
Cs2MnF6	8.855	-14.224	1.220	0.398	1.083	4.311	P
Cs2SeF6	8.831	-13.568	1.240	0.376	1.084	4.499	P
Rb2SiF6	8.410	-10.858	1.247	0.301	1.078	5.273	P
Cs2NiF6	8.815	-13.130	1.254	0.361	1.084	4.640	P
Cs2SiF6	8.751	-11.379	1.312	0.301	1.085	5.362	NP

Table 5.23: The predicted formability of 640 double halide perovskites.

5.5 mechanical properities

compounds	r_A(Å)	r_B(Å)	r_X(Å)	t	μ	a(Å)	C_{11}(GPa)	C_{12}(GPa)	C_{44}(GPa)	B(GPa)	G(GPa)	B/G	C_P	H	K_{ic}
CsCaBr3 [122]	1.88	1	1.96	0.917	0.510	5.73	43.97	10.37	8.01	21.57	10.83	1.99	2.36	0.599	0.366
CsGeBr3 [123]	1.88	0.73	1.96	1.009	0.372	5.62	46.27	10.32	9.77	22.3	12.5	1.78	0.55	1.452	0.395
CsPbBr3 [124]	1.88	1.19	1.96	0.862	0.607	6.01	44.22	6.5	4.02	18.46	9.95	1.86	2.48	0.722	0.332
KGeBr3 [123]	1.64	0.73	1.96	0.946	0.372	5.55	46.25	10.72	2.86	22.57	6.56	3.44	7.86	-1.584	0.287
KPbBr3 [124]	1.64	1.19	1.96	0.808	0.607	5.97	45.3	5.96	2.95	18.39	9.64	1.91	3.01	0.536	0.325
NaPbBr3 [124]	1.39	1.19	1.96	0.752	0.607	5.95	46.05	5.68	2.29	18.57	9.45	1.97	3.39	0.376	0.323
RbGeBr3 [123]	1.72	0.73	1.96	0.967	0.372	5.57	46.54	10.44	7.44	22.48	10.7	2.10	3.00	0.357	0.366
RbPbBr3 [124]	1.72	1.19	1.96	0.826	0.607	5.98	45.43	6.27	3.31	18.56	9.81	1.89	2.96	0.607	0.330
CsCaCl3 [125]	1.88	1.00	1.81	0.929	0.552	5.47	56.9	9.69	10.23	23.64	14.4	1.76	-0.54	2.331	0.447
CsCdCl3 [126]	1.88	0.95	1.81	0.945	0.525	5.21	65.29	12.89	5.16	30.36	7.72	3.93	7.73	-1.323	0.378
CsGeCl3 [123]	1.88	0.73	1.81	1.027	0.403	5.35	51.88	13.1	10.63	26.02	13.56	1.92	2.47	1.288	0.435
CsPbCl3 [126]	1.88	1.19	1.81	0.870	0.657	5.61	52.94	11.7	4.8	25.44	9.02	1.23	6.90	-0.847	0.237
KGeCl3 [123]	1.64	0.73	1.81	0.960	0.403	5.27	56.74	11.19	7.77	26.37	12.17	2.17	3.42	0.492	0.412
RbCaCl3 [127]	1.72	1.00	1.81	0.888	0.552	5.42	40.32	21.89	6.01	26.08	7.14	3.93	15.88	-1.613	0.330
RbGeCl3 [123]	1.72	0.73	1.81	0.983	0.403	5.31	55.64	11.41	9.43	26.15	13.37	1.96	1.98	1.159	0.431
CsBaF3 [128]	1.88	1.35	1.33	0.847	1.015	4.97	98.99	15.13	40.73	42.93	41.2	1.04	-25.60	13.782	0.937
CsCaF3 [129]	1.88	1.00	1.33	0.974	0.752	4.57	99.87	23.56	25.04	50.92	29.64	1.65	-1.48	4.711	0.814
CsCdF3 [130]	1.88	0.95	1.33	0.996	0.714	4.47	110.99	37.95	20.61	53.27	25.91	2.40	17.34	2.777	0.849
CsGeF3 [123]	1.88	0.73	1.33	1.102	0.549	4.56	79.01	34.44	19.6	49.29	20.64	2.39	14.84	1.244	0.681
CsHgF3 [131]	1.88	1.02	1.33	0.966	0.767	4.68	83.21	33.74	13.37	49.24	17.14	2.92	20.37	0.067	0.634
CsPbF3 [132]	1.88	1.19	1.33	0.901	0.895	4.8	72.39	17.93	12.65	36.09	17.3	2.09	5.28	1.484	0.547
CsSrF3 [131]	1.88	1.18	1.33	0.904	0.887	4.81	81.3	16.09	14.26	38.97	19.99	1.89	1.83	2.282	0.603
KCaF3 [133]	1.64	1.00	1.33	0.901	0.752	4.41	116.64	18.8	15.19	49.58	24.83	2.07	3.61	2.830	0.750
KCdF3 [134]	1.64	0.95	1.33	0.921	0.714	4.38	146.13	22.08	19.77	63.43	31.92	1.98	2.31	3.792	0.940
KCoF3 [135]	1.64	0.745	1.33	1.012	0.560	4.04	116.8	24.83	40.53	83.04	42.64	1.37	-15.70	5.237	1.003
KFeF3 [135]	1.64	0.78	1.33	0.995	0.586	4.06	94.48	21.98	30.88	93.28	32.93	1.40	-8.90	1.568	0.785
KGeF3 [123]	1.64	0.73	1.33	1.019	0.549	4.46	80.67	35.57	5.96	50.61	10.52	4.81	29.61	-1.739	0.487
KMgF3 [136]	1.64	0.72	1.33	1.024	0.541	4.04	132.56	43.31	48.86	72.15	47.119	1.53	-5.55	8.571	1.172
KMnF3 [135]	1.64	0.83	1.33	0.972	0.624	4.19	69.26	23.57	8.36	70.1	13.08	2.97	15.21	-1.738	0.461
KNiF3 [135]	1.64	0.69	1.33	1.040	0.519	4.01	115.73	53.85	41.63	89.26	36.96	2.01	12.22	2.890	1.049
KZnF3 [137]	1.64	0.74	1.33	1.015	0.556	4.021	160.84	53.3	55.97	89.15	55.08	1.62	-2.67	8.880	1.405
NaMgF3 [138]	1.39	0.72	1.33	0.938	0.541	3.96	136.9	31.84	51.01	66.86	51.61	1.29	-19.17	11.840	1.166

NaZnF3 [138]	1.39	0.74	1.33	0.929	0.556	4.06	135.03	39.65	41.95	71.45	44.16	1.62	-2.30	7.444	1.133
RbCaF3 [133]	1.72	1.00	1.33	0.926	0.752	4.44	110.66	22.45	16.86	51.15	25.07	2.06	5.59	2.717	0.758
RbCdF3 [139]	1.72	0.95	1.33	0.946	0.714	4.5	117.2	33.6	17.4	53.36	24.98	2.46	16.20	2.407	0.831
RbCoF3 [140]	1.72	0.745	1.33	1.039	0.560	4.15	113.85	47.12	24.59	70.12	27.79	2.49	22.53	1.736	0.893
RbFeF3 [141]	1.72	0.78	1.33	1.022	0.586	4.08	116.2	65.3	31.4	81.33	28.9	2.90	33.90	1.265	0.994
RbGeF3 [123]	1.72	0.73	1.33	1.047	0.549	4.49	82.61	34.28	12.53	50.39	16.35	3.08	21.75	-0.252	0.608
RbMnF3 [142]	1.72	0.83	1.33	0.998	0.624	4.27	106.9	40.00	38.3	61.9	34.5	1.79	1.70	5.010	0.955
RbNiF3 [141]	1.72	0.69	1.33	1.068	0.519	4.11	104.9	69.2	30.5	72.78	24.6	3.30	38.70	0.661	0.906
CsGeI3 [143]	1.88	0.73	2.2	0.985	0.332	5.99	40.15	6.84	8.51	17.95	11.17	1.61	-1.67	1.711	0.347
KGeI3 [143]	1.64	0.73	2.2	0.927	0.332	5.94	42.26	6.08	6.95	18.14	10.31	1.76	-0.87	1.043	0.333
RbGeI3 [143]	1.72	0.73	2.2	0.946	0.332	5.97	41.01	6.31	8.46	17.9	11.34	1.58	-2.15	1.853	0.348
BaAmO3 [144]	1.61	0.85	1.35	0.951	0.630	4.416	220.18	67.53	49.59	119.18	58.49	2.04	17.94	6.399	1.755
BaBkO3 [145]	1.61	0.83	1.35	0.960	0.615	4.429	231	61.25	52.2	117.84	63.48	1.86	9.05	7.996	1.820
BaCfO3 [146]	1.61	0.821	1.35	0.964	0.608	4.33	209.6	66.21	39.47	114	50.28	2.27	26.74	4.593	1.575
BaCmO3 [147]	1.61	0.85	1.35	0.951	0.630	4.425	219	60.37	48.67	113.78	59.24	1.92	11.70	7.148	1.727
BaCrO3 [1]	1.61	0.55	1.35	1.102	0.407	3.957	173.2	133.16	118.3	146.45	59.36	2.47	14.86	4.580	1.855
BaFeO3 [148]	1.61	0.585	1.35	1.082	0.433	3.85	238.54	164.33	105.35	189.06	78.05	2.42	58.98	6.089	2.384
BaMoO3 [2]	1.61	0.65	1.35	1.047	0.481	4.01	253.67	111.54	81.63	158.92	77.23	2.06	29.91	7.932	2.218
BaNpO3 [4]	1.61	0.87	1.35	0.943	0.644	4.437	241.18	64.58	44.95	128.97	62.3	2.07	19.63	6.574	1.888
BaPaO3 [5]	1.61	0.9	1.35	0.930	0.667	4.51	205.6	67.58	29.94	114.59	42.14	2.72	37.64	2.536	1.476
BaPuO3 [7]	1.61	0.86	1.35	0.947	0.637	4.421	221.81	72.18	46.26	122.00	57.68	2.12	25.92	5.925	1.764
BaRuO3 [8]	1.61	0.62	1.35	1.062	0.459	4.005	234.7	174.2	93.9	194.4	59.71	3.26	80.30	2.498	2.156
BaThO3 [12]	1.61	0.94	1.35	0.914	0.696	4.555	216.2	76.39	38.6	119.57	49.07	2.44	37.79	3.880	1.635
BaTiO3 [3]	1.61	0.605	1.35	1.071	0.448	4.022	238.6	122.6	57.5	161.2	57.7	2.79	65.10	3.446	1.934
BaZrO3 [3]	1.61	0.72	1.35	1.011	0.533	4.226	252.00	107.9	71.5	155.9	71.72	2.17	36.40	6.819	2.174
CaCrO3 [1]	1.34	0.55	1.35	1.001	0.407	3.777	184.97	175.19	95.35	178.45	35.26	5.06	79.84	-0.589	1.542
CaMoO3 [2]	1.34	0.65	1.35	0.951	0.481	3.78	326.41	113.76	43.65	184.64	62.92	2.93	70.11	3.402	2.096
CaTaO3 [10]	1.34	0.68	1.35	0.937	0.504	3.975	404.32	86.24	16.65	192.27	49.78	3.86	69.59	1.047	1.951
CaZrO3 [16]	1.34	0.72	1.35	0.919	0.533	4.138	322.9	70.7	62.6	154.8	87.9	1.76	8.10	11.148	2.373
SrAmO3 [149]	1.44	0.85	1.35	0.897	0.630	4.373	220.00	67.00	46.00	117.00	56.00	2.09	21.00	5.899	1.693
SrCrO3 [1]	1.44	0.55	1.35	1.038	0.407	3.844	198.02	152.92	111.13	167.95	59.36	2.83	41.79	3.457	1.958
SrNbO3 [21]	1.44	0.68	1.35	0.972	0.504	4.073	282.45	118.97	56.75	173.46	56.75	3.06	62.22	2.746	2.002
SrPuO3 [22]	1.44	0.86	1.35	0.893	0.637	4.378	229.01	70.74	40.33	123.00	55.85	2.20	30.41	5.353	1.734
SrTaO3 [10]	1.44	0.68	1.35	0.972	0.504	4.007	285.56	74.48	34.48	144.84	55.05	2.63	40.00	3.727	1.787
SrThO3 [23]	1.44	0.94	1.35	0.861	0.696	4.53	209.64	72.33	32.18	120.17	68.65	1.75	40.15	9.330	1.933
SrTiO3 [21]	1.44	0.605	1.35	1.009	0.448	3.945	318.35	100.04	110.2	172.81	110.2	1.57	-10.16	15.497	2.741

SrUO3 [24]	1.44	0.89	1.35	0.881	0.659	4.376	258.91	70.68	94.34	133.43	94.25	1.42	-23.66	16.026	2.346
SrVO3 [21]	1.44	0.58	1.35	1.022	0.430	3.866	269.88	137.35	113.63	181.53	113.63	1.60	23.72	15.427	2.824
SrZrO3 [21]	1.44	0.72	1.35	0.953	0.533	4.179	309.71	71.96	73.78	151.21	73.78	2.05	-1.82	7.694	2.159

Table 5.24: Dataset for oxide and halide perovskites used included ionic radii r_A, r_B, r_X, lattice parameter (a), tolerance factor (t), octahedral factor (r_B/r_X)the elastic constant (C_{ij}), bulk modulus (B), shear modulus (G), Pugh ratio(B/G) Cauchy Pressure ($C_{12} + C_{44}$), Hardness (H), Facture Toughness (K_{ic}).

compounds	r_A(Å)	r_B(Å)	r_X(Å)	t	μ	a(Å)	C_{11}(GPa)	C_{12}(GPa)	C_{44}(GPa)	B(GPa)	G(GPa)	B/G	C_P	H	K_{ic}
AsNBa3 [45]	2.15	1.15	0.65	0.833	0.565	5.309	90.4	23.327	24.762	45.68	28.27	1.62	-1.435	5.058	0.828
BiNBa3 [45]	2.15	1.6	0.65	0.947	0.406	5.42	117.96	22.03	45.43	54.00	46.44	1.16	-23.4	12.832	1.166
SbNBa3 [45]	2.15	1.45	0.65	0.909	0.448	5.404	98.18	18.8	27.86	45.26	32.59	1.39	-9.06	7.455	0.893
BiNCa3 [46]	1.8	1.6	0.65	0.981	0.406	4.864	124.00	25.00	50.00	58.00	49.8	1.16	-25	13.461	1.185
GeNCa3 [46]	1.8	1.25	0.65	0.880	0.520	4.787	102.00	36.00	43.00	58.00	39.00	1.49	-7.00	7.719	1.041
PbNCa3 [46]	1.8	1.8	0.65	1.039	0.361	4.919	75.00	38.00	43.00	50.33	33.2	1.52	-5.00	6.539	0.907
PNCa3 [46]	1.8	1.00	0.65	0.808	0.650	4.703	151.00	23.00	48.00	65.66	54.4	1.21	-25.00	13.625	1.296
SbNCa3 [46]	1.8	1.45	0.65	0.938	0.448	4.854	113.04	26.57	43.82	55.39	43.58	1.27	-17.25	10.746	1.082
TlNCa3 [46]	1.8	1.9	0.65	1.068	0.342	4.949	82.2	30.3	37.1	47.6	32.64	1.46	-6.8	6.882	0.877
AgCNi3 [28]	1.35	1.6	0.7	1.018	0.438	3.825	312.00	104.00	57.00	173.33	75.8	2.29	47.00	6.558	2.242
AgNNi3 [50]	1.35	1.6	0.65	1.043	0.406	3.778	321.1	130.00	48.9	193.7	67.56	2.87	81.1	3.858	2.224
AlNNi3 [50]	1.35	1.25	0.65	0.919	0.520	3.779	431.4	96.1	48.00	207.86	95.86	2.17	48.1	8.668	2.744
CdCNi3 [29]	1.35	1.55	0.7	1.000	0.452	3.866	341.00	127.00	72.00	198.33	86.00	2.31	55.00	7.189	2.568
CdNNi3 [50]	1.35	1.55	0.65	1.025	0.419	3.852	324.4	119.2	38.1	187.6	63.9	2.94	81.1	3.457	2.149
CuNNi3 [50]	1.35	1.35	0.65	0.955	0.481	3.745	396.9	121.9	7.8	213.56	59.68	3.58	114.1	1.921	2.185
GaNNi3 [50]	1.35	1.3	0.65	0.937	0.500	3.788	336.8	134.3	34.9	201.8	61.44	3.28	99.4	2.534	2.167
InNNi3 [50]	1.35	1.55	0.65	1.025	0.419	3.845	303.5	132.5	111.4	189.5	101.04	1.88	21.1	11.260	2.713
MgCNi3 [28]	1.35	1.5	0.7	0.983	0.467	3.812	340.00	102.00	57.00	181.33	81.8	2.22	45.00	7.363	2.378
MgNNi3 [50]	1.35	1.5	0.65	1.008	0.433	3.815	319.9	108.6	96.9	179.03	100.4	1.78	11.7	12.071	2.620
PdNNi3 [50]	1.35	1.4	0.65	0.972	0.464	3.783	313.3	161.5	81.1	212.1	79.02	2.68	80.4	5.119	2.518
PtNNi3 [50]	1.35	1.35	0.65	0.955	0.481	3.782	316.9	197.7	50.5	237.43	54.14	4.39	147.2	0.664	2.205
SbNNi3 [50]	1.35	1.45	0.65	0.990	0.448	3.942	226.7	153.4	-8.6	177.83	9.5	18.72	162.00	-2.758	0.816
SnNNi3 [50]	1.35	1.45	0.65	0.990	0.448	3.91	239.9	153.5	2.2	182.3	18.6	9.80	151.3	-2.235	1.151
TcCNi3 [28]	1.35	1.35	0.7	0.931	0.519	3.825	357.00	148.00	76.00	217.66	87.4	2.49	72.00	6.401	2.697
ZnCNi3 [28]	1.35	1.35	0.7	0.931	0.519	3.793	344.00	110.00	64.00	188.00	85.2	2.21	46.00	7.671	2.465
ZnNNi3 [50]	1.35	1.35	0.65	0.955	0.481	3.77	381.6	116.5	17.9	204.86	63.76	3.21	98.6	2.802	2.219
ZrCNi3 [28]	1.35	1.55	0.7	1.000	0.452	3.915	312.00	110.00	69.00	177.33	81.8	2.17	41.00	7.637	2.383
AlCPd3 [110]	1.4	1.25	0.7	0.892	0.560	4.132	263.9	136.2	59.3	178.76	61.12	2.92	76.9	3.319	2.125
GeCPd3 [110]	1.4	1.25	0.7	0.892	0.560	4.183	286.8	89.3	68.5	155.13	80.6	1.92	20.8	9.121	2.287
InCPd3 [110]	1.4	1.55	0.7	0.993	0.452	4.206	211.9	148.6	22.2	169.7	25.98	6.53	126.4	-1.504	1.362
NbCPd3 [110]	1.4	1.45	0.7	0.960	0.483	4.189	236.6	165.1	12.00	188.93	21.5	8.79	153.1	-2.053	1.304
PbCPd3 [110]	1.4	1.8	0.7	1.077	0.389	4.293	284.3	74.5	57.7	144.43	76.58	1.89	16.8	9.046	2.179
ScCPd3 [110]	1.4	1.6	0.7	1.010	0.438	4.207	232.2	136.9	14.8	168.66	27.94	6.04	122.1	-1.288	1.408
YCPd3 [110]	1.4	1.85	0.7	1.094	0.378	4.292	288.6	93.3	108.4	158.4	104.1	1.52	-15.1	15.533	2.660

CdCPt3 [110]	1.35	1.55	0.7	1.000	0.452	4.231	101.5	245.8	100.5	197.7	31.44	6.29	145.3	-1.251	1.622
GaCPt3 [110]	1.35	1.3	0.7	0.914	0.538	4.198	302.6	141.6	116.5	195.26	102.1	1.91	25.1	11.023	2.893
MoCPt3 [110]	1.35	1.45	0.7	0.966	0.483	4.187	232.6	234.7	54.00	234.00	31.98	7.32	180.7	-1.521	1.770
NbCPt3 [110]	1.35	1.45	0.7	0.966	0.483	4.222	320.7	189.6	164.3	233.3	124.8	1.87	25.3	13.197	3.506
ScCPt3 [110]	1.35	1.6	0.7	1.018	0.438	4.242	324.2	136.1	39.4	198.8	61.26	3.25	96.7	2.602	2.273
SnCPt3 [110]	1.35	1.45	0.7	0.966	0.483	4.292	322.6	113.7	157.3	183.33	136.16	1.35	-43.6	22.021	3.273
YCPt3 [110]	1.35	1.85	0.7	1.104	0.378	4.322	159.4	197.4	154.00	184.73	84.8	2.18	43.4	7.802	2.602
LaCRh3 [40]	1.35	1.95	0.7	1.138	0.359	4.262	281.00	145.00	63.00	190.33	65.00	2.93	82.00	3.541	2.296
LuCRh3 [40]	1.35	1.75	0.7	1.069	0.400	4.147	354.00	150.00	81.00	218.00	89.4	2.44	69.00	6.764	2.843
ScCRh3 [40]	1.35	1.6	0.7	1.018	0.438	4.082	390.00	146.00	81.00	227.33	97.4	2.33	65.00	7.806	3.006
YCRh3 [40]	1.35	1.85	0.7	1.104	0.378	4.16	337.00	146.00	79.00	209.66	85.6	2.45	67.00	6.470	2.732
AlCSc3 [109]	1.6	1.25	0.7	0.876	0.560	4.51	220.00	40.00	79.00	100.00	83.4	1.20	-39.00	18.512	1.939
GaCSc3 [109]	1.6	1.3	0.7	0.892	0.538	4.48	227.00	35.00	76.00	99.00	84.00	1.18	-41.00	19.042	1.930
InCSc3 [109]	1.6	1.55	0.7	0.968	0.452	4.56	213.00	38.00	81.00	96.33	83.9	1.15	-43.00	19.711	1.920
TlCSc3 [109]	1.6	1.9	0.7	1.076	0.368	4.56	212.00	36.00	80.00	94.66	83.2	1.14	-44.00	19.842	1.895
AsNSr3 [43]	2.00	1.15	0.65	0.841	0.565	5.03	98.57	14.78	46.41	42.71	44.6	0.96	-31.63	16.404	0.979
BiNSr3 [43]	2.00	1.6	0.65	0.961	0.406	5.17	84.8	13.83	18.94	37.48	25.55	1.47	-5.11	5.505	0.704
SbNSr3 [43]	2.00	1.45	0.65	0.921	0.448	5.12	94.49	15.2	39.94	41.63	39.82	1.05	-24.74	13.387	0.921
AlCTi3 [38]	1.4	1.25	0.7	0.892	0.560	4.414	329.72	69.18	91.5	156.026	107.008	1.46	-22.32	16.798	2.715
AlNTi3 [111]	1.4	1.25	0.65	0.914	0.520	4.112	199.42	146.86	50.72	164.38	40.94	4.02	96.14	0.450	1.664
InCTi3 [111]	1.4	1.55	0.7	0.993	0.452	4.199	292.72	74.15	85.31	147.00	94.9	1.55	-11.16	14.194	2.420
InNTi3 [111]	1.4	1.55	0.65	1.018	0.419	4.195	137.69	161.35	38.54	153.46	18.39	8.34	122.81	-2.082	1.088
TlCTi3 [38]	1.4	1.9	0.7	1.111	0.368	4.209	279.3	82.92	72.76	148.38	82.932	1.79	10.16	10.424	2.276
TlNTi3 [111]	1.4	1.9	0.65	1.138	0.342	4.204	198.00	128.31	52.62	151.54	45.51	3.33	75.69	1.569	1.703

Table 5.25: Dataset for inverse perovskites used included ionic radii r_A, r_B, r_X,lattice parameter (a), tolerance factor (t), octahedral factor (r_B/r_X) the elastic constant (C_{ij}), bulk modulus (B), shear modulus (G), Pugh ratio (B/G) Cauchy Pressure ($C_{12} + C_{44}$), Hardness (H), Facture Toughness (K_{ic}).

compounds	t	μ	a()	B(GPa)	G(GPa)	B/G	C_P(GPa)	H	K_{ic}
CaZrO3	0.918	0.533	4.138	154.8	87.9	1.76	8.1	11.148	2.373
BaMoO3	1.046	0.481	4.01	158.92	77.23	2.06	29.91	7.932	2.218
BaZrO3	1.011	0.533	4.226	155.9	71.72	2.17	36.4	6.819	2.174
BaFeO3	1.081	0.433	3.85	189.06	78.05	2.42	58.98	6.089	2.384
SrNbO3	0.971	0.503	4.073	173.46	56.75	3.06	62.22	2.746	2.002
CaMoO3	0.951	0.481	3.78	184.64	62.92	2.93	70.11	3.402	2.096
BaRuO3	1.062	0.459	4.005	194.4	59.71	3.26	80.3	2.498	2.156
TlCTi3	1.111	0.368	4.209	148.38	82.932	1.79	10.16	10.424	2.276
MgNNi3	1.008	0.433	3.82	179.03	100.4	1.78	11.7	12.071	2.620
PbCPd3	1.077	0.389	4.293	144.43	76.58	1.89	16.8	9.046	2.179
GeCPd3	0.892	0.560	4.183	155.13	80.6	1.92	20.8	9.121	2.287
InNNi3	1.025	0.419	3.844	189.5	101.04	1.88	21.1	11.260	2.713
GaCPt3	0.914	0.538	4.198	195.26	102.1	1.91	25.1	11.023	2.893
NbCPt3	0.966	0.483	4.222	233.3	124.8	1.87	25.3	13.197	3.506
ZrCNi3	1.000	0.452	3.915	177.33	81.8	2.17	41	7.637	2.383
YCPt3	1.104	0.378	4.322	184.73	84.8	2.18	43.4	7.802	2.602
MgCNi3	0.983	0.467	3.812	181.33	81.8	2.22	45	7.363	2.378
ZnCNi3	0.931	0.519	3.793	188	85.2	2.21	46	7.671	2.465
AgCNi3	1.018	0.438	3.825	173.33	75.8	2.29	47	6.558	2.242
AlNNi3	0.919	0.520	3.779	207.86	95.86	2.17	48.1	8.668	2.744
CdCNi3	1.000	0.452	3.866	198.33	86	2.31	55	7.189	2.568
ScCRh3	1.018	0.438	4.082	227.33	97.4	2.33	65	7.806	3.006
YCRh3	1.104	0.378	4.16	209.66	85.6	2.45	67	6.470	2.732
LuCRh3	1.069	0.400	4.147	218	89.4	2.44	69	6.764	2.843
TcCNi3	0.931	0.519	3.825	217.66	87.4	2.49	72	6.401	2.697
AlCPd3	0.892	0.560	4.132	178.76	61.12	2.92	76.9	3.319	2.125
PdNNi3	0.972	0.464	3.783	212.1	79.02	2.68	80.4	5.119	2.518
CdNNi3	1.025	0.419	3.852	187.6	63.9	2.94	81.1	3.457	2.149
AgNNi3	1.043	0.406	3.778	193.7	67.56	2.87	81.1	3.858	2.224
LaCRh3	1.138	0.359	4.262	190.33	65	2.93	82	3.541	2.296
ScCPt3	1.018	0.438	4.242	198.8	61.26	3.25	96.7	2.602	2.273
ZnNNi3	0.955	0.481	3.77	204.86	63.76	3.21	98.6	2.802	2.219
GaNNi3	0.937	0.500	3.788	201.8	61.44	3.28	99.4	2.534	2.167

Table 5.26: The list of perovskites and inverse perovskites which satisfy the joint 5 conditions ($C_p > 0$, B/G>1.75, H>2, K_{ic}>2 and B>140).

compounds	t_A	t_B	μ_A	μ_B	Δa	ΔG	Q

CaZrO3/SrNbO3	0.918	0.971	0.533	0.503	0.065	31.15	4.643
CaZrO3/BaRuO3	0.918	1.062	0.533	0.459	0.133	28.19	5.236
CaZrO3/CaMoO3	0.918	0.951	0.533	0.481	0.358	24.98	6.037
CaZrO3/BaZrO3	0.918	1.011	0.533	0.533	-0.088	16.18	9.865
CaZrO3/BaMoO3	0.918	1.046	0.533	0.481	0.128	10.67	15.476
CaZrO3/BaFeO3	0.918	1.081	0.533	0.433	0.288	9.85	16.847
NbCPt3/AlCPd3	0.966	0.892	0.483	0.56	0.09	63.68	2.919
NbCPt3/ScCPt3	0.966	1.018	0.483	0.438	-0.02	63.54	2.928
NbCPt3/GaNNi3	0.966	0.937	0.483	0.5	0.434	63.36	2.939
NbCPt3/ZnNNi3	0.966	0.955	0.483	0.481	0.452	61.04	3.089
NbCPt3/CdNNi3	0.966	1.025	0.483	0.419	0.37	60.9	3.098
NbCPt3/LaCRh3	0.966	1.138	0.483	0.359	-0.04	59.8	3.173
NbCPt3/AgNNi3	0.966	1.043	0.483	0.406	0.444	57.24	3.360
NbCPt3/AgCNi3	0.966	1.018	0.483	0.438	0.397	49	4.093
NbCPt3/PbCPd3	0.966	1.077	0.483	0.389	-0.071	48.22	4.176
NbCPt3/PdNNi3	0.966	0.972	0.483	0.464	0.439	45.78	4.452
NbCPt3/GeCPd3	0.966	0.892	0.483	0.56	0.039	44.2	4.647
NbCPt3/ZrCNi3	0.966	1	0.483	0.452	0.307	43	4.804
NbCPt3/MgCNi3	0.966	0.983	0.483	0.467	0.41	43	4.804
NbCPt3/TlCTi3	0.966	1.111	0.483	0.368	0.013	41.87	4.961
NbCPt3/YCPt3	0.966	1.104	0.483	0.378	-0.1	40	5.24
NbCPt3/ZnCNi3	0.966	0.931	0.483	0.519	0.429	39.6	5.303
NbCPt3/YCRh3	0.966	1.104	0.483	0.378	0.062	39.2	5.367
NbCPt3/CdCNi3	0.966	1	0.483	0.452	0.356	38.8	5.432
NbCPt3/TcCNi3	0.966	0.931	0.483	0.519	0.397	37.4	5.673
NbCPt3/LuCRh3	0.966	1.069	0.483	0.4	0.075	35.4	6.050
NbCPt3/AlNNi3	0.966	0.919	0.483	0.52	0.443	28.94	7.624
NbCPt3/ScCRh3	0.966	1.018	0.483	0.438	0.14	27.4	8.109
NbCPt3/MgNNi3	0.966	1.008	0.483	0.433	0.402	24.4	9.229
NbCPt3/InNNi3	0.966	1.025	0.483	0.419	0.378	23.76	9.505
NbCPt3/GaCPt3	0.966	0.914	0.483	0.538	0.024	22.7	9.995

Table 5.27: The potential hard superlattices perovskites and inverse perovskites.

BIBLIOGRAPHY

[1] C.E. Hu, Z.Y. Zeng, C.Y. Kong, Y.T. Cui, L. Zhang,*"Equation of state and elastic properties of $ACrO_3$(A=Pb, Ca, Sr and Ba) perovskites under high pressure"*, Phys. B Condens. Matter.(2012).

[2] Somia, S. Mehmood, Z. Ali, I. Khan, F. Khan, I. Ahmad,*"First-Principles Study of Perovskite Molybdates $AMoO_3$ (A = Ca, Sr, Ba)"*, J. Electron. Mater. 48 (2019) 17301739.

[3] N. Iles, A. Kellou, K. Driss Khodja, B. Amrani, F. Lemoigno, D. Bourbie, H.Aourag,*"Atomistic study of structural, elastic, electronic and thermal properties of perovskites $Ba(Ti, Zr, Nb)O_3$"*,Comput. Mater.Sci. 39 (2007) 896902.

[4] S.A. Khandy, D.C. Gupta,*"Structural, elastic and magneto-electronic properties of half-metallic $BaNpO_3$ perovskite"*, Mater. Chem. Phys. 198 (2017) 380385.

[5] S.A. Khandy, D.C. Gupta,*"Understanding Ferromagnetic Phase Stability, Electronic and Transport Properties of $BaPaO_3$ and $BaNpO_3$ from Ab-Initio Calculations"*, J. Electron. Mater. 46 (2017) 55315539.

[6] Z. Ali, I. Ahmad, A.H. Reshak,*"GGA+U studies of the cubic perovskites $BaMO_3$(M=Pr, Th and U)"*, Phys. B Condens. Matter. 410 (2013) 217221.

[7] S.A. Dar, V. Srivastava, U.K. Sakalle, G. Pagare,*"Insight into Structural, Electronic,Magnetic, Mechanical, and Thermodynamic Properties of Actinide Perovskite $BaPuO_3$"*, J. Supercond. Nov. Magn. 31 (2018) 32013208.

[8] D.M. Han, X.J. Liu, S.H. Lv, H.P. Li, J. Meng,*"Elastic properties of cubic perovskite $BaRuO_3$ from first-principles calculations"*, Phys. B Condens. Matter. 405 (2010) 31173119.

[9] M.B. Saddique, M. Rashid, A. Afzal, S.M. Ramay, F. Aziz, A. Mahmood,*"Ground state opto-electronic and thermoelectric response of cubic $XSnO_3$ (X = Ba, Sr)compounds"*, Curr. Appl. Phys. 17 (2017) 10791086.

[10] Z. Ali, I. Khan, I. Ahmad, M.S. Khan, S.J. Asadabadi,*"Theoretical studies of the paramagnetic perovskites $MTaO_3$ (M = Ca, Sr and Ba)"*, Mater. Chem. Phys. 162 (2015) 308315.

[11] C. Ma, L. Ye, Z. Yang,*"Electronic structures of perovskite $BaTbO_3$ studied by the LSDA + U method"*, J. Phys. Condens. Matter. 17 (2005) 79637969.

[12] Y.B. Cherif, A. Labdelli, A. Boukortt, H. Abbassa, D. Aimouch, R. Hayn,*"Modified Becke-Johnson (mBJ) exchange potential investigation of the optoelectronic properties of $XThO_3$(X = Sa, Sr and Ba)"*, Int.J. Comput. Mater. Sci. Eng. 08 (2019) 1850029.

[13] G. Mustafa, N. ul Aarifeen, A. Afaq, M. Asif,*"Electronic and magnetic properties of $BaUO_3$ by modified BeckeJohnson (mBJ) functional"*, Mod. Phys. Lett. B. 32 (2018) 1850164.

[14] D. Cherrad, D. Maouche, M. Reffas, A. Benamrani,*"Structural, elastic, electronic and optical properties of the cubic perovskites $CaXO_3$ (X=Hf and Sn)"*, Solid State Commun. 150 (2010) 350355.

[15] X. Wu, Y. Dong, S. Qin, M. Abbas, Z. Wu,*"First-principles study of the pressureinduced phase transition in $CaTiO_3$"*, Solid State Commun. 136 (2005) 416420.

[16] Z.F. Hou,*"Ab initio calculations of elastic modulus and electronic structures of cubic $CaZrO_3$"*, Phys. B Condens. Matter. 403 (2008) 26242628.

[17] Z. Ali, I. Ahmad, B. Amin, M. Maqbool, G. Murtaza, I. Khan, M.J. Akhtar, F.Ghaffor,*"Theoretical studies of structural and magnetic properties of cubic perovskites $PrCoO_3$ and $NdCoO_3$"*, Phys. B Condens. Matter. 406 (2011) 38003804.

[18] M. Rezaiguia, W. Benstaali, A. Abbad, S. Bentata, B. Bouhafs,*"GGA + U Study of Electronic and Magnetic Properties of $Pr(Fe/Cr)O_3$ Cubic Perovskites"*, J.Supercond. Nov. Magn. 30 (2017) 25812590.

[19] B. Bouadjemi, S. Bentata, A. Abbad, W. Benstaali, B. Bouhafs,*"Half-metallic ferromagnetism in $PrMnO_3$ perovskite from first principles calculations"*,Solid State Commun. 168 (2013) 610.

[20] B. Sabir, G. Murtaza, Q. Mahmood, R. Ahmad, K.C. Bhamu,*"First principles investigations of electronics, magnetic, and thermoelectric properties of rare earth based $PrYO_3$ (Y=Cr, V) perovskites"*, Curr. Appl. Phys. 17 (2017) 15391546.

[21] I.R. Shein, V.L. Kozhevnikov, A.L. Ivanovskii,*"First-principles calculations of the elastic and electronic properties of the cubic perovskites $SrMO_3$ (M=Ti, V, Zr and Nb) in comparison with $SrSnO_3$"*, Solid State Sci. 10 (2008) 217225.

[22] S.A. Dar, V. Srivastava, U.K. Sakalle, A. Rashid, G. Pagare,*"First-principles investigation on electronic structure, magnetic, mechanical and thermodynamic properties of $SrPuO_3$ perovskite oxide"*, Mater. Res. Express. 5 (2018) 026106.

[23] Y. Benaissa Cherif, M. Rouaighia, A. Zaoui, A. Boukortt,*"Optoelectronic, Elastic and Thermal Properties of Cubic Perovskite-Type $SrThO_3$"*, Acta Phys. Pol. A. 131 (2017) 406414.

[24] B. Sahli, H. Bouafia, B. Abidri, A. Abdellaoui, S. Hiadsi, A. Akriche, N.Benkhettou, D. Rached, *"First-principles prediction of structural, elastic, electronic and thermodynamic properties of the cubic $SrUO_3$ -Perovskite"*, J. Alloys Compd. 635 (2015) 163172.

[25] T.T. Mayeshiba, D.D. Morgan,*"Factors controlling oxygen migration barriers in perovskites"*, Solid State Ionics. 296 (2016) 71-77.

[26] M. Islam,*"Computer modelling of defects and transport in perovskite oxides"*, Solid State Ionics.155(2002) 75-85.

[27] J. RICHTER, P. HOLTAPPELS, U. VOGT, T. GRAULE, L. GAUCKLER,*"Conduction behavior of $Pr_{1+x}Sr_xMn_{1+y}In_yO_{3+\sigma}$ perovskites"*, Solid State Ionics. 177(2006) 3105-3108.

[28] Bannikov, V. V, Shein, I. R. & Ivanovski, A. L.*"Band Structure , Elastic and Magnetic Properties, and Stability of Antiperovskites $MCNi_3$ (M = Y Ag) According to FPLAPW-GGA Calculations"*. Phys. Solid State 49, 17041714 (2007).

[29] Shein, I. R., Bannikov, V. V Ivanovskii, A. L.*"Structural , elastic and electronic properties of superconducting anti-perovskites $MgCNi_3$, $ZnCNi_3$ and $CdCNi_3$ from first principles"*. Phys. C 468, 16 (2008).

[30] Okoye, C. M. I.*"Theoretical investigation of electronic structure and optical properties of paramagnetic non-oxide perovskite $AlCNi_3$"*. Solid State Commun. 136, 605610 (2005).

[31] Sieberer, M., Mohn, P. Redinger, J.*"Role of carbon in $AlCNi_3$ and $GaCNi_3$: A density functional theory study"*. Phys. Rev. B 75, 16 (2007).

[32] Shein, I. R. Ivanovskii, A. L.*"Electronic and elastic properties of non-oxide anti-perovskites from first principles: Superconducting $CdCNi_3$ in comparison with magnetic $InCNi_3$"*. Phys. Rev., B 77, 104101 18 (2008).

[33] Shein, I. R. Ivanovskii, A. L.*"structural electronic and magnetic properties of $CaCNi_3$,$SrCNi_3$, and $BaCNi_3$ antiperovskites in comparison to superconducting $MgCNi_3$"*. J. Struct.Chem. 51, 176178 (2010).

[34] Cherrad, D., Maouche, D., Louail, L. Maamache, M.*"Ab initio comparative study of the structural, elastic and electronic properties of $SnAMn_3$ (A = N, C) antiperovskite cubic compounds"*. Solid State Commun. 150, 782787 (2010).

[35] Ennassiri, N., Tahiri, N., El Bounagui, O., Ez-Zahraouy, H. & Benyoussef, A. *"Magnetic, magnetocaloric and transport properties in $AlCMn_3$ antiperovskite compound"*. J. Alloys Compd. 741, 11961202 (2018).

[36] Shim, J. H., Kwon, S. K. Min, B. I.*"Electronic structure of metallic antiperovskite compound"*. Phys. Rev. B - Condens. Matter Mater. Phys. 66, 14 (2002).

[37] Suetin, D. V, Bannikov, V. V, Shein, I. R. Ivanovskii, A. L.*"Electronic and elastic properties basic solid state physics of perovskite-like $W3_NiC, W3_NiN$ and $Co3_WC$ from first-principles calculations"*. Phys. Status Solidi 1651, 16461651 (2009).

[38] Medkour, Y., Roumili, A., Boudissa, M. & Maouche, D. Structural, elastic and electronic properties of $ACTi_3$ (A = Al, In and Tl) antiperovskite". Solid State Commun. 149, 919922(2009).

[39] Ouyang, Y., Tang, M., Fang, J., Xiang, P. & Du, Y. The elastic constants for $Fe3_AlX$ (X = B ,C and N) with anti-perovskite structure". Phys. Scr. 80 055603,(2009).

[40] Bouhemadou, A.*"Elastic properties of mono and polycrystalline $RCRh_3$ (R=Sc,Y,La and Lu)under pressure effect"*. Solid State Commun. 149, 16581662 (2009).

[41] Suetin, D. V, Shein, I. R. & Ivanovskii, A. L.*"Structural , elastic , electronic and magnetic properties of perovskite-like $Co3_WC$, $Rh3_WC$ and $Ir3_WC$ from first principles calculations"*.Solid State Sci. 12, 814817 (2010).

[42] Medkour, Y., Roumili, A., Maouche, D., Reffas, M. & Saoudi, A.*"First principles study of structural , elastic and electronic properties of ACY_3 (A = Al , In and Tl)"*. Comput. Mater. Sci.47, 973976 (2010).

[43] Reshak, A. H. & Semari, F.*"FP-APW + lo study of the elastic , electronic and optical properties for the cubic antiperovskite $ANSr_3$ (A = As , Sb and Bi) under pressure effect"*. Phys. B Phys.Condens. Matter 405, 18941900 (2010).

[44] Amara, K., Zemouli, M., Elkeurti, M., Belfedal, A. & Saadaoui, F.*"First-principles study of $XNMg_3$ (X = P , As , Sb and Bi) antiperovskite compounds"*. J. Alloys Compd. 576, 398403(2013).

[45] Hichour, M. Rached, D. Rabah, M.*"Structural and elastic properties of antiperovskites $XNBa_3$ (X = As , Sb) under pressure effect"*. Phys. B Phys. Condens. Matter 404, 40344038 (2009).

[46] Ming Chern, P. Y., Vennos, D. A. DiSalvo, F. J.*"Synthesis, Structure, and Properties of Antiperovskite Nitrides A-f"*. J. Solid State Chem 96, 415425 (1992).

[47] Haddadi, K., Bouhemadou, A. Louail, L.*"Ab initio investigation of the structural, elastic and electronic properties of the anti-perovskite $TlNCa_3$"*. Solid State Commun. 150, 932937 (2010).

[48] Moreno-Armenta, M. G., Pz, W. L. Takeuchi, N.*"First-principles calculations of the structural and electronic properties of Cu_3MN compounds with M = Ni, Cu, Zn, Pd, Ag, and Cd"*.Solid State Sci. 9, 166172 (2007).

[49] Sieberer, M., Khmelevskyi, S. Mohn, P.*"Magnetic instability within the series TCu_3N (T=Pd,Rh, and Ru): A first-principles study"*. Phys. Rev. B Condens. Matter Mater. Phys. 74, 47(2006).

[50] Bannikov, V. V, Shein, I. R. Ivanovskii, A. L.*"Elastic properties of antiperovskite-type Ni-rich nitrides $MNNi_3$ (M = Zn , Cd , Mg , Al , Ga , In , Sn , Sb , Pd , Cu , Ag and Pt) as predicted from first-principles calculations"*. Phys. B Phys. Condens. Matter 405, 46154619 (2010).

[51] Bertaut, E. F., Fruchart, D., Bouchaud, J. P. Fruchart, R.*"Diffraction neutronique de Mn_3GaN"*.Solid State Commun. 6, 251256 (1968).

[52] Hua, L., Wang, L. Chen, L. F.*"First-principles investigation of Ge doping effects on the structural, electronic and magnetic properties in antiperovskite Mn_3CuN"*. J. Phys. Condens.Matter 22, (2010).

[53] Medkour, Y., Roumili, A., Maouche, D. Maamache, M.*"First-principles study of the structural,electronic, and magnetic properties of $InCCo_3$ and $InNCo_3$"*. Solid State Commun. 151, 19161919 (2011).

[54] Kuhnen, C. A. Dos Santos, A. V.*"Electronic and magnetic properties of $AlFe_3$ and $AlFe_3N$ nitride"*. J. Alloys Compd. 384, 8087 (2004).

[55] Wu, Z. Meng, J.*"Elastic and electronic properties of $CoFe_3N$, $RhFe_3N$, and $IrFe_3N$ from first principles"*. Appl. Phys. Lett. 90, 241901 (2007).

[56] Houben, A. Muller, P. Von Appen, J. Lueken, H.*"Synthesis, crystal structure, and magnetic properties of the semihard itinerant ferromagnet $RhFe_3N$"*. Angew. Chemie Int. Ed. 44, 72127215 (2005).

[57] Zhao, E.*"First-principles investigation on the elastic , magnetic and electronic properties of MFe_3N (M = Fe , Ru , Os)"*. Chem. Phys. Lett. 449, 96100 (2007).

[58] Rached, H., Rached, D., Rabah, M., Khenata, R. & Reshak, A. H.*"Full-potential calculation of the structural, elastic, electronic and magnetic properties of $XFeO_3$ (X=Sr and Ba) perovskite"*. Phys.B Condens. Matter 405, 35153519 (2010).

[59] Ghebouli, M. A., Ghebouli, B., Fatmi, M. & Bouhemadou, A.*"Calculation of physical properties of the cubic perovskite-type oxide $BiScO_3$ using the PP-PW method based on the DFT theory"*.Solid State Commun. 151 908915 (2011).

[60] Noor, N. A., Hassan, M., Rashid, M., Alay-e-Abbas, S. M. & Laref, A.*"Systematic study of elastic, electronic, optical and thermoelectric properties of cubic $BiBO_3$and $BiAlO_3$compounds at different pressure by using ab-initio calculations"*. Mater. Res. Bull. 97, 436443 (2018).

[61] Behram, R. B. Iqbal ,M.A, Alay-e-Abbas, S.M.*"Theoretical investigation of mechanical,optoelectronic and thermoelectric properties of $BiGaO_3$ and $BiInO_3$ compounds"*. Mater. Sci.Semicond. Process. 41, 297303 (2016).

[62] Piskunov, S., Heifets, E., Eglitis, R. I. & Borstel, G.*"Bulk properties and electronic structure of $SrTiO_3$, $BaTiO_3$, $PbTiO_3$ perovskites: An ab initio HF/DFT study"*. Comput. Mater. Sci. 29, 165178 (2004).

[63] Khandy, S. A. Gupta, D. C.*"Structural, elastic and thermo-electronic properties of paramagnetic perovskite $PbTaO_3$"*. RSC Adv. 6, 4800948015 (2016).

[64] Dar, S. A., Srivastava, V., Sakalle, U. K., Ahmad Khandy, S. & Gupta, D. C.*"A DFT Study on Structural, Electronic Mechanical and Thermodynamic Properties of 5f-Electron System $BaAmO_3$"*. J. Supercond. Nov. Magn. 31, 141149 (2018).

[65] Wu, S. Q., Hou, Z. F. & Zhu, Z. Z.*"Elastic properties and electronic structures of $CdCNi_3$: A comparative study with $MgCNi_3$"*. Solid State Sci. 11, 251258 (2009).

[66] Park, M. S. Giim, J. S.*"Physical properties of $ZnCNi_3$: Comparison with superconducting $MgCNi_3$"*. Supercond. Sci. Technol. 17, 274277 (2004).

[67] Dong, A. F. Che, G. C.*"Synthesis and physical properties of $AlCNi_3$"*. Phys. C Supercond. its Appl.422, 6569 (2005).

[68] Tong, P., Sun, Y. P., Zhu, X. B. & Song, W. H.*"Strong electron-electron correlation in the antiperovskite compound $GaCNi_3$"*. Phys. Rev. B Condens. Matter Mater. Phys. 73, 15 (2006).

[69] Takejiro Kaneko, T. K. and K. S.*"Pressure Effect on the Magnetic Transition Temperatures in the Intermetallic Compounds Mn_3MC (M=Ga,Zn and Sn)"*. Phys. Soc. japan 56, 40474055 (1987).

[70] Wang, C. Martin, P.*"Experimental Determination of Phase Equilibria in the Fe-Al-C System"*. J.Phase Equilibria Diffus. 36, 350356 (2015).

[71] Shishido, T. Ishizawa, Y. Ye, J.*"Hardness and oxidation resistance of the perovskite-type $RRh_3B_xC_{1+x}$ (R = Y, Sc)"*. J. Alloys Compd. 408412, 375378 (2006).

[72] Nowotny, V. H.*"Strukturchemie einiger Verbindungen der ergangsmetalle mit den elementen C, Si, Ge, Sn. Prog"*. Solid State Chem. 5, 2770 (1971).

[73] Haddadi, K., Bouhemadou, A., Louail, L., Rahal, F. & Maabed, S.*"Prediction study of the structural , elastic and electronic properties of $ANSr_3$ (A = As , Sb and Bi)"*. Comput. Mater. Sci.46, 881886 (2009).

[74] Belaroussi, T., Amrani, B., Benmessabih, T., Iles, N. & Hamdache, F.*"Structural and thermodynamic properties of antiperovskite $SbNMg_3$"*. Comput. Mater. Sci. 43, 938942 (2008).

[75] Belaroussi, T., Benmessabih, T., Hamdache, F. & Amrani, B.*"First-principles study of the structural and thermodynamic properties of $AsNMg_3$ antiperovskite"*. Phys. B 403, 26492653(2008).

[76] Jha, P. K. & Gupta, S. K.*"First principles lattice dynamical study of the cubic antiperovskite compounds"*. Solid State Commun. 150, 16501655 (2010).

[77] Beznosikov, B. V.*"Predicted nitrides with an antiperovskite structure"*. J. Struct. Chem. 44, 885888 (2003).

[78] Haddadi, K., Bouhemadou, A., Louail, L., Maabed, S. & Maouche, D.*"Structural and elastic properties under pressure effect of the cubic antiperovskite compounds $ANCa_3$ (A = P , As , Sb, and Bi)"*. Phys. Lett. A 373, 17771781 (2009).

[79] Haddadi, K., Bouhemadou, A., Louail, L. & Medkour, Y.*"Structural, elastic and electronic properties of $XNCa_3$ (X = Ge, Sn and Pb) compounds"*. Solid State Commun. 149, 619624(2009).

[80] Liu, L., Wu, X., Wang, R., Gan, L. & Wei, Q.*"Nonlinear elastic properties of superconducting antiperovskites $MNNi_3$ (M =Zn, Cd, Mg, Al, Ga, and In) from first principles"*. J. Supercond.Nov. Magn. 27, 18511859 (2014).

[81] Li, C., Chen, W. G., Wang, F., Li, S. F. & Sun, Q.*"First-principles investigation of mechanical and electronic properties of $MNNi_3$ (M = Zn , Mg , or Cd)"*. J. Appl. Phys. 3, 16 (2012).

[82] Cao, W. H. He, B. Liao, C. Z.*"Preparation and properties of antiperovskite-type nitrides: $InNNi_3$and $InNCo_3$"*. J. Solid State Chem. 182, 33533357 (2009).

[83] Helal, M. A. & Islam, A. K. M. A.*"Elastic, electronic, and optical properties of hypothetical $SnNNi_3$ and $CuNNi_3$ in comparison with superconducting $ZnNNi_3$"*. Phys. B Condens. Matter 406, 45644568 (2011).

[84] Ali, M. A.*"Ni-rich Nitrides $ANNi_3$ (A = Pt, Ag, Pd) in Comparison with Superconducting $ZnNNi_3$"*. J. Sci. Res. 4, 110 (2012).

[85] Ttnc, H. M. & Srivastava, G. P.*"Ground state ,phonon spectrum , and superconducting properties of the cubic inverse perovskite $CuNNi_3$"*. Phys. C 507, 1016 (2014).

[86] Dos Santos, A. V. & Kuhnen, C. A.*"Electronic structure and magnetic properties of $CoFe_3N, CrFe_3N$ and $TiFe_3N$"*. J. Alloys Compd. 321, 6066 (2001).

[87] Von Appen, J. & Dronskowski, R.*"Predicting new ferromagnetic nitrides from electronic structure theory: $IrFe_3N$ and $RhFe_3N$"*. Angew. Chemie Int. Ed. 44, 12051210 (2005).

[88] Puvaneswari, S., Priyanga, G. S., Rajeswarapalanichamy, R. & Santhosh, M.*"Structural,electronic, elastic and magnetic properties of $RuFe_3N$ and $OsFe_3N$: A first principle study"*. AIP Conf. Proc. 1665, 14 (2015).

[89] Terki, R., Feraoun, H., Bertrand, G. & Aourag, H.*"Full potential calculation of structural, elastic and electronic properties of $BaZrO_3$ and $SrZrO_3$"*. Phys. Status Solidi Basic Res. 242, 10541062(2005).

[90] Yamanaka, S.*"Thermochemical and thermophysical properties of alkaline-earth perovskites"*. J. Nucl. Mater. 344, 6166 (2005).

[91] Bouhemadou, A. & Haddadi, K. *"Structural, elastic, electronic and thermal properties of the cubic perovskite-type $BaSnO_3$"*. Solid State Sci. 12, 630636 (2010).

[92] Li, Z., Iitaka, T. & Tohyama, T.*"Pressure-induced ferromagnetism in cubic perovskite $SrFeO_3$ and $BaFeO_3$"*. Phys. Rev. B Condens. Matter Mater. Phys. 86, 36 (2012).

[93] Tariq, S., Mubarak, A. A., Saad, S., Imran Jamil, M. & M Sohail Gilani, S.*"Quantum density functional theory studies of structural, elastic, and opto-electronic properties of $ZMoO_3$ (Z = Ba and Sr) under pressure"*. Chinese Phys. B 28, (2019).

[94] Jacobson, A. J., Tofield, B. C. & Fender, B. E. F.*"The structures of $BaCeO_3$, $BaPrO_3$ and $BaTbO_3$ by neutron diffraction: lattice parameter relations and ionic radii in O-perovskites"*. Acta Crystallogr. Sect. B Struct. Crystallogr. Cryst. Chem. 28, 956961 (1972).

[95] Shein, I. R., Shein, K. I. & Ivanovskii, A. L.*"Elastic and electronic properties and stability of $SrThO_3$, $SrZrO_3$ and ThO_2 from first principles"*. J. Nucl. Mater. 361. 6977 (2007).

[96] Boudali, A. DrissKhodja, M. Amrani, B.*"First-principles study of structural, elastic, electronic,and thermal properties of $SrTiO_3$ perovskite cubic"*. Phys. Lett. Sect. A Solid State Phys. 373, 879884 (2009).

[97] Rey, M. J.*"Preparation and structure of the compounds $SrVO_3$ and Sr_2VO_4"*. J. Solid State Chem. 86, 101108 (1990).

[98] Turzhevsky, S. A., Novikov, D. L., Gubanov, V. A. & Freeman, A. J.*"Electronic structure and crystal chemistry of niobium oxide phases"*. Phys. Rev. B 50, 32003208 (1994).

[99] Wattiaux, A.*"A novel preparation method of the $SrFeO_3$ cubic perovskite by electrochemical means"*. Solid State Commun. 77, 489493 (1991).

[100] Zhu, Z. L., Gu, J. H., Jia, Y. & Hu, X.*"A comparative study of electronic structure and magnetic properties of $SrCrO_3$ and $SrMoO_3$"*. Phys. B Condens. Matter 407, 19901994 (2012).

[101] Gasperin, M.*"$CaTaO_3$: un nouveau compos type pvskite"* . Acta Crystallogr. 11, 739739(1958).

[102] Wang, H. Zhenye, Z. Wang, R.*"First-principles study of the cubic perovskites $BiMO_3$ (M=Al, Ga, In, and Sc)"*. Phys. Rev. B Condens. Matter Mater. Phys. 75, 19 (2007).

[103] Shirane, G., Pepinsky, R. & Frazer, B. C.*"X-ray and neutron diffraction study of ferroelectric $PbTiO_2$"* . Acta Crystallogr. 9, 131140 (1956).

[104] Russell, L. E., Harrison, J. D. L. & Brett, N. H.*"Perovskite-type compounds based on plutonium"*.J. Nucl. Mater. 2, 310320 (1960).

[105] Ghebouli, M. A.*"Structural, elastic and optoelectronic properties of Sr-based perovskite-type oxides $SrXO_3$ (M=Th, Zr) via first-principles calculations"*. Chinese J. Phys. 56, 15151524(2018).

[106] Verma, A. S. & Kumar, A.*"Bulk modulus of cubic perovskites"*. J. Alloys Compd. 541, 210214(2012).

[107] Haddadi, K., Bouhemadou, A., Louail, L. & Maamache, M.*"Density functional study of the structural , electronic , elastic and thermodynamic properties of $ACRu_3$ (A = V , Nb and Ta)compounds"*. Intermetallics 19, 476485 (2011).

[108] Wang, N. N., Shao, D. F., Lu, W. J. & Lu, H. Y.*"Mechanical and electronic properties of antiperovskite Ti-based compounds $AXTi_3$ (X = C, N): A first-principles investigation"*. J. Appl.Phys. 119, 044903 (2016).

[109] Haddadi, K., Bouhemadou, A., Zerarga, F. & Bin-omran, S.*"First-principles investigation of the ternary scandium based inverse-perovskite carbides Sc_3AC (A = Al , Ga , In and Tl)"*. Solid State Sci. 14, 11751185 (2012).

[110] Bannikov, V. V & Ivanovskii, A. L.*"Elastic and electronic properties of antiperovskite-type Pd and Pt-based ternary carbides from first-principles calculations"*. J. Alloys Compd. 577, 615621(2013).

[111] Cherrad, D., Selmani, L., Maouche, D. & Maamache, M.*"First principles calculations on elasticity, electronic structure and bonding properties of antiperovskites $ANTi_3$ (A = Al , In and Tl)"*. J.Alloys Compd. 509, 43574362 (2011).

[112] Zhao, H., Chang, A. & Wang, Y.*"Structural, elastic, and electronic properties of cubic perovskite $BaHfO_3$ obtained from first principles"*. Phys. B Condens. Matter 404, 21922196 (2009).

[113] Hou, Z. F.*"Elasticity, electronic structure, and dielectric property of cubic $SrHfO_3$ from first principles"*. Phys. Status Solidi Basic Res. 246, 135139 (2009).

[114] Ghebouli, B. Ghebouli,M.A. Chihi.T, Fatmi.M, Boucetta.S, Reffas.M.*"First-principles study of structural, elastic, electronic and optical properties of $SrMO_3$ (M=Ti and Sn)"*. Solid State Commun. 149, 22442249 (2009).

[115] L.Q. Jiang, J.K. Guo, H.B. Liu, M. Zhu, X. Zhou, P. Wu, C.H. Li, J. Phys. Chem. Solids., 2006, 67, 1531-1536.

[116] A.S. Verma, V.K. Jindal, J. Alloys Compd., 2009, 485, 514-518.

[117] M.G. Brik, I.V. Kityk, J. Phys. Chem. Solids., 2011, 72, 1256-1260.

[118] V. Sidey, J. Phys. Chem. Solids., 2019, 126, 310-313.

[119] W. Rahim, A. Cheng, C. Lyu, T. Shi, Z. Wang, D.O. Scanlon, R.G. Palgrave, Chem. Mater., 2020.

[120] M. Nait Amar, M.A. Ghriga, M.E.A. Ben Seghier, H. Ouaer, J. Phys. Chem. B., 2020, 124, 6037-6045.

[121] I.O. Alade, I.A. Olumegbon, A. Bagudu, J. Appl. Phys., 2020, 127, 015303.

[122] M.G. Brik.*"Comparative first-principles calculations of electronic. optical and elastic anisotropy properties of $CsXBr_3$(X=Ca.Ge.Sn) crystals"*. Solid State Commun. 151 (2011) 1733-1738.

[123] M. Houari. B. Bouadjemi. S. Haid. M. Matougui. T. Lantri. Z. Aziz. S. Bentata. B. Bouhafs. *"Semiconductor behavior of halide perovskites $AGeX_3$ (A = K. Rb and Cs; X = F. Cl and Br):first-principles calculations"*. Indian J. Phys. 94 (2020) 455-467.

[124] I. Bourachid. M. Caid. O. Cheref. D. Rached. H. Heireche. B. Abidri. H. Rached. N. Benkhettou.*"Insight into the structural. electronic. mechanical and optical properties of inorganic lead bromide perovskite $APbBr_3$ (A = Li. Na. K. Rb. and Cs)"*. Comput. Condens. Matter. 24 (2020) e00478.

[125] K. Ephraim Babu. N. Murali. K. Vijaya Babu. P. Taddesse Shibeshi. V. Veeraiah.*"Structural. Elastic. Electronic. and Optical Properties of Cubic Perovskite $CsCaCl_3$ Compound: An ab initio Study"*. Acta Phys. Pol. A. 125 (2014) 1179-1185.

[126] B.M. Ilyas. B.H. Elias.*"A theoretical study of perovskite $CsXCl_3$ (X=Pb. Cd) within first principles calculations"*. Phys. B Condens. Matter. 510 (2017) 60-73.

[127] A.A. Mubarak.*"The elastic. electronic and optical properties of $RbCaX_3$ (X = F . Cl) compounds"*. Int. J. Mod. Phys. B. 28 (2014) 1450192.

[128] M. Harmel. H. Khachai. A. Haddou. R. Khenata. G. Murtaza. B. Abbar. S. Bin Omran. M. Khalfa.*"Ab Initio Study of the Mechanical. Thermal and Optoelectronic Properties of the Cubic $CsBaF_3$"*. Acta Phys. Pol. A. 128 (2015) 34-42.

[129] A. Meziani. H. Belkhir.*"First-principles calculations of structural. elastic and electronic properties of $CsCaF_3$ compound"*. Comput. Mater. Sci. 61 (2012) 67-70.

[130] B. Salmankurt. S. Duman.*"Investigation of the structural. mechanical. dynamical and thermal properties of $CsCaF_3$ and $CsCdF_3$"*. Mater. Res. Express. 3 (2016) 045903.

[131] B. Ghebouli. M.A. Ghebouli. A. Bouhemadou. M. Fatmi. R. Khenata. D. Rached. T. Ouahrani. S. Bin-Omran. *"Theoretical prediction of the structural. elastic. electronic. optical and thermal properties of the cubic perovskites $CsXF_3$ (X = Ca. Sr and Hg) under pressure effect"*. Solid State Sci. 14 (2012) 903-913.

[132] C.G. Ma. M.G. Brik.*"Hybrid density-functional calculations of structural. elastic and electronic properties for a series of cubic perovskites $CsMF_3$ (M=Ca. Cd. Hg. and Pb)"*. Comput. Mater. Sci. 58 (2012) 101-112.

[133] K.E. Babu. N. Murali. K.V. Babu. B.K. Babu. V. Veeraiah.*"Structural. electronic and elastic properties of $KCaF_3$ and $RbCaF_3$for vacuum-ultraviolet-transparent lens materials"*. AIP Conf. Proc.. 2015: p. 100002.

[134] K.E. Babu. N. Murali. K.V. Babu. B.K. Babu. V. Veeraiah.*"Elastic and Optoelectronic Properties of $KCdF_3$: ab initio Calculations through LDA/GGA/TB-mBJ within FP-LAPW Method"*. Chinese Phys. Lett. 32 (2015) 016201.

[135] Hayatullah. G. Murtaza. R. Khenata. S. Muhammad. A.H. Reshak. K.M. Wong. S. Bin Omran. Z.A. Alahmed. *"Structural. chemical bonding. electronic and magnetic properties of KMF_3 (M=Mn. Fe. Co. Ni) compounds"*. Comput. Mater. Sci. 85 (2014) 402-408.

[136] G. Pilania. V. Sharma.*"First principles investigations of structural. electronic. elastic. and dielectric properties of $KMgF_3$"*. J. Mater. Sci. 48 (2013) 7635-7641.

[137] T. Seddik. R. Khenata. O. Merabiha. A. Bouhemadou. S. Bin-Omran. D. Rached.*"Elastic. electronic and thermodynamic properties of fluoro-perovskite $KZnF_3$ via first-principles calculations"*. Appl. Phys. A. 106 (2012) 645-653.

[138] R. Arar. T. Ouahrani. D. Varshney. R. Khenata. G. Murtaza. D. Rached. A. Bouhemadou. Y. Al-Douri. S. Bin Omran. A.H. Reshak.*"Structural. mechanical and electronic properties of sodium based fluoroperovskites $NaXF_3$ (X=Mg. Zn) from first-principle calculations"*. Mater. Sci. Semicond. Process. 33 (2015) 127-135.

[139] A. Cheriet. B. Lagoun. M. Halit. M. Zaabat. C. Abdelhakim. L. Hamza.*"First-Principles Study of Structural. Electronic. Optical and Elastic Properties of Cadmium Based Fluoro-Perovskite $MCdF_3$ (M= Rb. Tl)"*. Solid State Phenom. 297 (2019) 173-186.

[140] N. Erum. M.A. Iqbal.*"Elastomechanical and Magneto-Optoelectronic Investigation of $RbCoF_3$ An ab initio DFT Study"*. Acta Phys. Pol. A. 138 (2020) 509-517.

[141] A.A. Mubarak. S. Al-Omari.*"First-principles calculations of two cubic fluoropervskite compounds: $RbFeF_3$ and $RbNiF_3$"*. J. Magn. Magn. Mater. 382 (2015) 211-218.

[142] H.M. Huang. C.X. Yu. Z.Y. Jiang. S.J. Luo. Y.J. Hu.*"Effect of Strain on the Elastic. Electronic. and Magnetic Properties of Fluoro-Pervskite $RbMnF_3$ and $RbFeF_3$"*. J. Supercond. Nov. Magn. 32 (2019) 3811-3821.

[143] M. Houari. B. Bouadjemi. M. Matougui. S. Haid. T. Lantri. Z. Aziz. S. Bentata. B. Bouhafs. *"Optoelectronic properties of germanium iodide perovskites $AGeI_3$ (A = K. Rb and Cs): first principles investigations"*. Opt. Quantum Electron. 51 (2019) 234.

[144] S.A. Dar. V. Srivastava. U.K. Sakalle. S. Ahmad Khandy. D.C. Gupta.*"A DFT Study on Structural. Electronic Mechanical and Thermodynamic Properties of 5f-Electron System $BaAmO_3$"*. J. Supercond. Nov. Magn. 31 (2018) 141-149.

[145] K.A. Parrey. N. Devi. R. Khenata. S.A. Khandy.*"Investigating structure. magneto-electronic. elastic and thermoelectric properties of alkaline earth actinide perovskite oxide $BaBkO_3$ from first principle calculations"*. Comput. Condens. Matter. 17 (2018) e00340.

[146] S.A. Khandy. I. Islam. D.C. Gupta. R. Khenata. A. Laref. S. Rubab.*"DFT understandings of structural properties. mechanical stability and thermodynamic properties of $BaCfO_3$ perovskite"*. Mater. Res. Express. 5 (2018) 105702.

[147] S.A. Dar. V. Srivastava. U.K. Sakalle. V. Parey.*"Ferromagnetic Phase Stability. Magnetic. Electronic. Elasto-Mechanical and Thermodynamic Properties of $BaCmO_3$ Perovskite Oxide"*. J. Electron. Mater. 47 (2018) 3809-3816.

[148] H. Rached. D. Rached. M. Rabah. R. Khenata. A.H. Reshak.*"Full-potential calculation of the structural. elastic. electronic and magnetic properties of $XFeO_3$ (X=Sr and Ba) perovskite"*. Phys. B Condens. Matter. 405 (2010) 3515-3519.

[149] S.A. Dar. V. Srivastava. U.K. Sakalle.*"A First-Principles Calculation on Structural. Electronic. Magnetic. Mechanical. and Thermodynamic Properties of $SrAmO_3$"*. J. Supercond. Nov. Magn. 30 (2017) 3055-3063.

CHAPTER 6

CONCLUSION

As a conclusion, we present the main motivations for our work.

This work was done as part of the Materials Genome Project's global mission, which aims to build an infrastructure to speed up the discovery of novel materials. As a result, we have shown in this study that using datamining approaches and existing experimental or theoretical knowledge on inverse perovskite compounds, it is possible to forecast new ones with interesting features without performing any more tests or calculations.

This research has highlighted the need of using multivariate methodologies in conjunction with empirical rules to gain new insights into perovskite-structured ionic conductors. We've developed a new empirical relationship between ionic radii and the lattice constant, and we've demonstrated that different geometrical descriptor combinations are adequate for different search spaces and application contexts. Through a linear link between decomposition energies and descriptor $(t + \mu)^{\eta}$, we anticipated a thermodynamic stability trend of oxide perovskites.

We conclude from the data that the degree of distortion from the totally symmetric structure is the most crucial parameter influencing the oxide ion conductivity in perovskites, with a balance struck between empirical crystallographic requirements (the lattice tolerance factor,the lattice free volume,critical radius). On the other hand, we've discovered that the oxygen migration barrier and the oxygen vacancy formation energy are closely related, and that higher conductivity is associated with lower activation energies. We were able to forecast a significant number of potential ion conductor compounds by extending our existing modeling technique to additional 904 tested hypothetical ABO_3.

This research has highlighted the need of using multivariate methodologies in conjunction with empirical rules to gain new insights into double halide perovskites. We've developed a new

empirical relationship between ionic radii and the lattice constant, and we've demonstrated that different geometrical descriptor combinations are adequate for different search spaces and application contexts. Through a linear association between decomposition energies and descriptor $(t + \mu)^{\eta}$, we projected thermodynamic stability.

We conclude from the findings that the rules and tolerance and octahedral ranges employed for oxide perovskites are no longer valid for double halide perovskites. On the other hand, we've developed a new modified tolerance factor that appears to be more accurate in predicting the formability of these perovskites. We were able to forecast a huge number of probable perovskites by expanding our existing modeling effort to include another 640 tested hypothetical A_2BX_6.